UNIVERSITY OF

LIVERPOOL

Department of Chemistry

Water-dispersible Magnetic Nanoparticles for Biomedical applications: Synthesis and Characterisation

Thesis submitted in accordance with the requirements of the University of Liverpool for the degree of Doctor of Philosophy

By

Le Trong Lu

2011

I certify that all material in this thesis that is not my own work has been clearly identified and no material is included for which a degree has previously been *awarded*

Acknowledgements

I would like to thank my supervisor, Dr Nguyen TK Thanh, and co-supervisor Prof David G Fernig, for their support and guidance during this project. Special thanks to Prof. Mathias Brust for his supervision during my re-writing this thesis.

Thanks are due to Dr Le Duc Tung, Department of Physics, University of Liverpool, for his help with the SQUID measurements as well as the discussions and interpretation of the data. I would also like to thank Dr. Ian Prior and Ms Alison Backett and Ms Cornelia Muncke, Departments of Physiology, Dr. Pope Marion, School of Veterinary Science, University of Liverpool for their assistance with the transmission electron microscope (TEM), Dr Shinya Maenosono, School of Materials Science, Japan Advanced Institute of Science and technology for X-ray. Thanks also to Dr James Long, Iota nano solution Ltd, Liverpool for DLS measurements, Dr Donald Maclaren, Department of Physics and Astronomy, University of Glassgow, UK, Mr Ong Khac Quy, Department of Chemistry, Purdue University, USA for their HRTEM measurements.

My thanks also go to Professor Andy Cooper and Dr. Bien Tan for providing the water-dispersible polymers.

Special thanks to Dr Laura Parkes, Magnetic Resonance and Image Analysis Centre, University of Liverpool and Dr Xiaoting Meng, School of Medical Sciences, University of Aberdeen for their collaborative research and useful discussions

I am very grateful to my colleagues, Mr. Ian Robinson, Dr. Diane Ung and other past and current members of Nanomag Lab, Department of Chemistry and Lab D, School of Biological Science for their tremendous support during my work.

I would like to acknowledge the financial support which I have received from Vietnamese Government (322 project), Department of Chemistry - University of Liverpool, the Royal Society, the North West Cancer Research Fund and the Wellcome Trust.

Abstract

Magnetic nanoparticles have attracted a great attention due to their diverse potential applications in biology and technology and a substantial number of synthetic methods have been developed to produce these materials. Chemical synthesis approaches have been a particular focus of the field, because of their ability to tune the size, shape and composition, as well as surface of the nanoparticles. To produce magnetic nanoparticles for biomedical applications, one of the primary requirements is to make nanoparticles that are dispersible and stable in aqueous medium under physiological conditions. The focus of this thesis has been the development of methods to synthesise magnetic nanoparticles of different compositions and shape that are dispersible and stable in water.

Monodisperse water-dispersible magnetic Co nanoparticles were fabricated using a facile reduction method in water in the presence of hydrophilic polymers. The size and shape of the nanoparticles were both tunable by varying the conditions of synthesis. The size of the spherical nanoparticles would be tuned between 2–7.5 nm by changing the concentration of the polymer. The synthesis approach could also be used to produce nanorods of 15 x 36 nm. The spherical nanoparticles were superparamagnetic at room temperature and were stable in water and in electrolyte solutions of up to 0.23 mM NaCl. The preliminary use of the Co nanoparticles as a MRI contrast enhancer was tested and provided evidence that these materials have considerable potential in this application.

Using a similar method, water-dispersible and colloidal stable CoPt nanoparticles were prepared. The effect of structure, functional group and combinations of stabilising ligands on the morphology of the nanoparticles was investigated. It was found that multiple-thiol functional groups play a critical role in the formation of hollow nanoparticles. The size of hollow nanoparticles could be tuned in the range of 7-54 nm by changing the concentration and molecular weight of the ligands. The hollow nanoparticles were water-dispersible and superparamagnetic at room temperature. They were stable in wide range of pH from 1 to 12.5 and at electrolyte concentrations as high as 2 M NaCl. An experiment on tracking stem cells labelled with the CoPt hollow nanoparticles indicated that MRI can effectively detect low numbers of labelled cells due to the enhanced contrast provided by the nanoparticles. CoPt hollow nanoparticles may, thus, have potential applications in MRI.

CoFe and cobalt ferrite nanoparticles were synthesised by thermal decomposition in organic solvent to take advantage of the superior control over monodispersity and morphology of the nanoparticles afforded by solvent based syntheses. In the case of CoFe nanoparticles, a layer of Pt was also deposited on the nanoparticles to make core/shell structures. Varying reaction conditions, such as reaction time, had an insignificant effect on monodispersity, size and shape of CoFe nanoparticles. However, these parameters had a substantial impact on the cobalt ferrite nanoparticles. Cobalt ferrite nanoparticles with sizes in a broad range from 4 nm to over 30 nm and diverse shapes including spherical, cubic and star-like, were synthesised by changing surfactant concentration and reaction time.
Ligand exchange using hydrophilic silane and/or polymer ligands were demonstrated to be efficacious on CoFe, CoFe/Pt and cobalt ferrite nanoparticles. After ligand exchange, the nanoparticles were reasonably stable in water.

The work presented in this thesis demonstrates that chemical synthesis is an efficient route to the production of magnetic nanoparticles of diverse composition and shape and so magnetic properties. Moreover, these materials were found to be stable in aqueous solutions. However, it is clear that the application of such magnetic nanoparticles in biology and medicine will require substantial further effort in the development of ligand shells able to withstand the rigours of the biological environment. Given the success of chemical synthesis demonstrated in this thesis, the development of ligand shell systems is now a major challenge of the field.

List of publications

Meng, X.; Seton, H.; **Lu, L.T.**; Prior, I.A.; Thanh, N.T.K.; Song, B. Tracking transplanted neural progenitor cells in spinal cord slices by CoPt contrasting MRI. *Nanoscal 2011,* (FRONT COVER, RSC NEWS).

Lu, L.T.; Tung, L.D.; Long, J.; Fernig, D.G.; Thanh, N.T.K.; Facile synthesis of stable, water-soluble magnetic CoPt hollow nanostructures assisted by multi-thiol ligands. *J. Mater. Chem.* **2009**, 19, 6023-6028.

Parkes, L.M.; Hogson, R.; **Lu, L.T.**; Tung, L.D.; Robinson, I.; Fernig, D.G.; Thanh, N.T.K.; Cobalt nanoparticles as a novel magnetic resonance contrast agent relaxivities a 1.5 T and 3 Tesla. *Contrast Media & Molec. Imag.* **2008**, 3, 150-156

Lu, L.T.; Tung, L.D.; Robinson, I.; Ung, D.; Tan, B.; Long, J.; Cooper, A.I.; Fernig, D.G.; Thanh, N.T.K.; Size and shape control for water-soluble magnetic cobalt nanoparticles using polymer ligands. *J. Mater. Chem.* **2008**, 18, 2453-248.

Ronbinson, I.; Alexander, C.; **Lu, L.T.**; Tung, L.D.; Fernig, D.G.; Thanh, N.T.K.; One-step synthesis of monodisperse water-soluble 'dual-responsive' magnetic nanoparticles. *Chem. Commun.* **2007**, 44, 4602-4604.

In preparation

Lu, L.T.; Tung, L.D.; Maenosono, S.; Maclaren, D.; Fernig, D.G.; Thanh, N.T.K. Synthesis and characterisation of CoFe/Pt core/shell nanoparticles. *J. Phys. Chem. C.*

Lu, L.T.; Tung, L.D.; Quy, O.K.; Maenosono, S.; Fernig, D.G.; Thanh, N.T.K. Synthesis an characterisation of cobalt ferrite nanoparticles with controlled morphology and composition. *Chem. Mater.*

Conference Presentation

Nanoparticles 2009: Synthesis, Properties and Application of Nanoparticles, Liverpool, UK September 2009. **Oral** ''*Synthesis and characterisation of magnetic nanoparticles for bioapplications*''

Nanoparticles 2008: Synthesis, Properties and Application of Nanoparticles, Braford, UK Febuary 2008. **Poster** ''*Facile synthesis of stable water-soluble magnetic CoPt: solid, nanochains/wires and hollow nanoparticles*''

7th International Conference on the Scientific and Clinical application of Magnetic Carriers, Vancourver, Canada, April 2008. **Poster** ''*Stable water-soluble magnetic hollow CoPt nanoparticles*''.

MC8: advancing Materials by Chemical Design, London, UK, July 2008. **Poster** ''*Synthesis of monodisperse tunable size and shape water-soluble magnetic Co nanoparticles using a simple reductant method*''

16th Annual ISMRM-ESMRMB Meeting 2007, Berlin, Germany, May 2007: **Poster** " *Relaxivity of Cobalt Nanoparticles, a Novel MR Contrast Agent*"

Nanoparticls: New opportunities for colloidal Scientists, Warwich, March 2007. **Oral** ''*Fabrication of monodisperse, tunable morphology water-soluble magnetic Co nanoparticles using a simple reductant method in the presence of polymer ligands*''.

Table of Contents

List of Figures

List of Tables

Abbreviations

AFM : Atomic force microscopy

APS : 3-aminopropyltriethoxylane

CALNN : Cysteine-alanine-leucine-asparagine-asparagine

CCALNN : Cysteine-cysteine-alanine-leucine-asparagine-asparagine

CCVVVT : Cysteine-cysteine-valine-valine-valine-threonin

CVVVT : Cysteine-valine-valine-valine-threonin

$Co(acac)_2$: Cobalt (II) acetylacetonate

$Co_2(CO)_8$: Dicobalt octacarbonyl

$CoCl_2$: Cobalt (II) chloride

Co : Cobalt

CoFe : Cobalt iron

$CoFe_2O_4$: Cobalt ferrite

CoPt : Cobalt platinum

EDS : Energy dispersive x-ray spectroscopy

EELS : Electron energy loss spectroscopy

Fe_2O_3 : Magnemite

Fe_3O_4 : Magnetite

CTAB : Cethyltrimethylammonium bromide

DCB : 1,2-dichlorobenzene

DLS : Dynamic Light Scattering

DSC : Differential scanning calorimetry

FC : Field-cooled

$Fe(acac)_3$: Iron (III) acetylacetonate

$Fe(CO)_5$: Iron pentacarbonyl

FT-IR : Fourier transform infrared

H : Magnetic field

H_C : Coercivity

HDD : 1,2-hexadecanediol

HRTEM : High resolution transmission electron microscopy

HSAB : Hard and soft acids and bases

ICP-AES : Inductively coupled plasma atomic emission spectroscopy

M_R : Remanent magnetisation

MRI : Magnetic resonance imaging

M_S : Saturated magnetisation

$NaBH_4$: Sodium borohydride

NaOH : Sodium hydroxide

N_2H_4 : Hydrazine

NH_4OH : Ammonium hydroxide

NMR : Nuclear magnetic resonance

NNLACC : Asparagine-asparagine-leucine-alanine-cysteine-cysteine

NNLACCALNN : Asparagine-asparagine-leucine-alanine-cysteine-cysteine-alanine-leucine- asparagine-asparagine

NPs : Nanoparticles

OA : Oleic acid

OLA : Oleylamine

PAA-DDT : Poly(acrylic acid) dodecanethiolether

PEGA-DDT : Poly(ethylene glycol) monomethacrylate dodecanethiolether

PEG-COOH : Methoxypolyethylene glycol acetic acid

PEG-NH_2 : Methoxypolyethylene glycol amine

PEG-SH : O-[-(3-mercaptonpropionylamino)ethyl]-o'-methyl-polyethyleneglycol

PMAA-DDT : Poly(methyacrylic acid) dodecane thiolether

PMAA-PTMP: Poly-(methacrylicacid) pentaerythritol tetrakis (3-mercaptopropionate)

QDs : Quantum dots

Silane-NH_2 : N-[3-(trimethoxysilyl)-propyl]ethylenediamine

SQUID : Superconducting quantum interference device

STM : Scanning tunnelling microscopy

T_1 : Longitudinal relaxation time

T_2 : Transverse relaxation time

T_B : Blocking temperature

TEM : Transmission electron microscopy

TEOS : Tetraethylorthosilicate (TEOS)

TGA : Thermal gravimetric analysis

TMAOH : Tetramethylammonium hydroxide

TLVVN : Threonine-leucine -valine-valine- asparagine peptide

TOP : Trioctylphosphine

TOPO : Trioctylphosphine oxide

TTTPCCVTTT :Threonin-threonin-threonin-proline-cysteine-cysteine-valine-threonin-threonin-threonin

TTTTCCTTTT :Threonin-threonin-threonin-threonin-cysteine-cysteine-threonin-threonin-threonin- threonin

VPD-DDT : n-vinyl-pyrrolidine dodecanethiolether

XPS : X-ray photoelectron spectroscopy

XRD : Powder X-ray diffraction

ZFC : Zero field-cooled

Chapter 1
Introduction

1.1 Overview

Nanoparticles, generally defined as particles with a size of less than 100 nm,[1] have been studied for hundreds of years. Particularly, gold, silver or copper in particulate form have been fabricated by firing their metal salts or oxides in the glaze and they have been widely used to decorate ceramic objects by artisans in Europe since the 14th century and as dyes in stained glass windows of cathedrals and chinaware in the 17th and 18th century.[2] The iridescent effect of stained ceramic and glass objects, which is due to the presence of metal in colloidal form, was not understood until Faraday published his work on the ''experimental relations of gold (and other metals) to light'' in 1857,[3] and the physical mechanism of the colouration of the metal colloids as the result of absorption and scattering of light was established by Mie in 1908.[3] The area of nanomaterials virtually exploded after the discovery of scanning tunnelling microscopy (STM) and atomic force microscopy (AFM) in the 1980s.[4-6] Before this, transmission electron microscopy (TEM) was the only suitable technique available to characterise nanomaterials. Due to its high cost and maintenance, the access to TEM was restricted to a relatively small number of researchers. The discovery of STM and AFM has inspired intense research activity in the field as these techniques are cheaper and easier to use than TEM and have high resolution down to the atomic scale.[5]

The great interest in nanoparticles originates from the fact that new properties, unlike those of bulk materials, arise at the nanometre length scale. As the size of particles decreases to the nanometre range, surface and quantum confinement effects are dominant

in the materials and affect the chemical reactivity of materials as well as their mechanical, electronic, optical and magnetic properties.[7] For example, a 60 μm carbon microparticle has a mass of 0.3 μg and a surface area of 0.01 mm^2. The same mass of the material in the nanoparticulate form with particle size of 60 nm has total surface of 11.3 mm^2 and consists of 10^9 nanoparticles.[7] The ratio of surface to mass (or volume) increases more than 1000 times when particle size decreases from 60 μm to 60 nm. Hence, the reactivity of the material in nanoparticulate form is enhanced roughly 1000-fold.[7] With Au metal or noble metals in general, when the particle size is reduced to tens of nanometres, it shows an intense absorption in the UV-vis spectrum which is resulting from the collective oscillation of the electrons in the conduction band (plasmon absorption).[8] In semiconductors (e.g. CdSe, CdTe, InAs and GaAs), it is well known that the band gap energy is strongly influenced by the size of the crystals. As the size of the particles decreases below the Bohr radius of the electron-hole (exciton) the band gap increases causing a blue shift of absorption and emission bands. This is known as the quantum-size effect.[9]

In magnetic materials, when their size is below a few tens of nanometres, the particles are known to be a single domain and can become superparamagnetic at room temperature. Superparamagnetism is a unique property of the nanoscale material, which cannot occur in the analogous bulk material. When the superparamagnetic nanoparticles are placed in an external magnetic field (H), their magnetic moments align in the direction of the magnetic field and enhance the magnetic flux. When the external magnetic field is removed, thermal energy causes the moments to randomise and the magnetic nanoparticles have no magnetic remanence. This is illustrated in Figure 1.1.

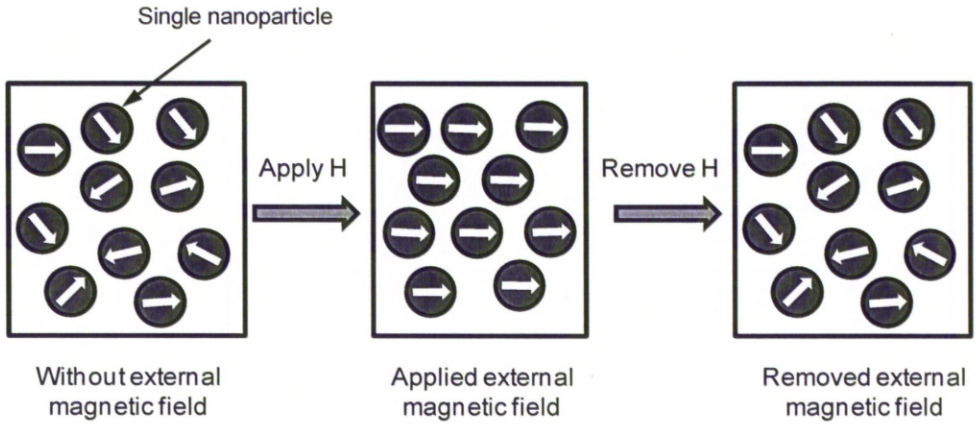

Figure 1.1: The behaviour of superparamagnetic nanoparticles with and without the presence of an applied magnetic field (H).

At the nanoscale, the physical properties of nanostructures depend not only on size, but also on their shape. The syntheses of nanoparticles by methods that allow the control of morphology have offered opportunities for new applications. For example, solid spherical Au nanoparticles exhibit a UV-vis spectrum at around 520 nm and the peak can be tuned only a few tens of nm by varying their size. However, rod shapes and hollow nanostructures allow the tuning of the plasmon band between 700 and 1200 nm, depending on the aspect ratios of the rods[10] or thickness and dimension of the nanocages[11,12] and nanoshells.[13] The red-shift from visible to infrared makes gold nanorods, nanocages and nanoshells extremely useful in many *in vivo* medical applications, as at these wavelengths biological tissues are relatively transparent.

With magnetic nanoparticles, the particle shape also has great effect on the magnetic properties due to the dominating effect of anisotropy in magnetism. Thus, synthesis methods which offer control over the size and shape of magnetic nanoparticles may offer many promising applications in diverse areas such as magnetic recording media,[14-16] catalysis[17-19] and biomedicine.[20, 21]

Nanoparticles with a core-shell structure have been studied extensively for the combined properties of cores and shells, which provide them with substantial potential applications in biomedicine and technology. The core consists of inorganic materials such as noble metals, semiconductors or magnetic materials, and the shell can be a ligand shell of organic molecules or an inorganic coating. At the nanoscale, nanoparticles tend to aggregate to minimise their surface energy associated with their high surface area to volume ratio. In addition, many uncoated nanoparticles are chemically highly active and extremely sensitive to oxygen. Therefore, coating them with an organic ligand shell or an inorganic layer is a critical requirement to protect the nanoparticles from aggregation and undesired chemical reaction.[22] Using organic molecules such as polymers or surfactants during the synthesis processes is a common and feasible way to restrict the development (control the size) and, in many cases, to control the shape of nanoparticles. In biomedicine, it is important that the protecting ligand shells can also be used for further functionalisation, for instance with other nanoparticles or biomolecules, depending on the desired application.[22] The alternative, coating nanoparticles with an inorganic layer of noble metals, silica or carbon, may provide for a more efficient protection of the core than an organic shell, for example, to protect cores such as Co, Fe or CoFe from oxidation. Moreover, the inorganic coating can provide a very effective platform for the attachment of molecules. For example, the surface of Au coated magnetic nanoparticles can easily be modified with thiol functionalised molecules, since the strong interaction between Au surface and thiols is well characterised. An overview of the inorganic coating of magnetic core/shell nanoparticles is described in Section 1.5.

For biomedical applications, nanoparticles have to be dispersible and colloidally stable in aqueous and physiological environments,[23] as well as being biocompatible and non-toxic. It is crucial that their size is appropriate for the envisaged applications and that the interaction of their surface with the complex macromolecular environment of biological

systems is predictable. In the case of magnetic nanoparticles, they should be superparamagnetic at room temperature. This will allow dispersion of the nanoparticles in a solution without aggregation after exposing them to a magnetic field.[24]

There are several approaches for making water-dispersible nanoparticles. In the simplest case, the nanoparticles are synthesised directly in aqueous solution utilising reduction or coprecipitation methods. In practically all of these methods, ligands such as polymers,[25-29] surfactants,[30,31] or peptides[32] are used to protect the nanoparticles from oxidation and aggregation and to provide functional groups at the surface of particles for subsequent biofunctionalisation.[23,33,34] In a second approach, the nanoparticles are prepared by a two-step method. Here, they are first synthesised in an organic solvent and then, to make them water-dispersible, the surface of the nanoparticles is modified by ligand exchange to replace the hydrophobic molecules, or by wrapping them with hydrophilic ones.

Amongst the various magnetic materials prepared for biomedical applications, magnetic nanoparticles of iron oxides (e.g. Fe_2O_3 and Fe_3O_4) have been generally chosen because of their ease of preparation, relatively oxidative stability, biocompatibility and lack of toxicity. However, these nanoparticles have relatively low saturation magnetisation. Contrary, magnetic systems based on Co and its alloys, such as CoPt or CoFe, are known to have higher saturation magnetisation. CoFe alloy is the material with the highest saturation magnetisation (245 $Am^2 kg^{-1}$) known. The saturation magnetisations of Co and Co_3Pt alloy are 161 $Am^2 kg^{-1}$ and 124 $Am^2 kg^{-1}$ respectively, compared, for instance with some iron oxides, Fe_3O_4 (90-92 $Am^2 kg^{-1}$) and γ-Fe_2O_3 (80 $Am^2 kg^{-1}$),[14,15,35] which could make the use of Co and its alloys advantageous in several *in vivo* applications such as MRI and hyperthermia treatment of cancer. Ferrite materials such as $CoFe_2O_4$, which have almost the same level of magnetic moment, but have a higher anisotropic energy than those of iron oxide nanoparticles,[36,37] have attracted attention due to potential uses for technological applications.[14-16]

1.2 Magnetism and magnetic materials

The magnetic moment of atoms originates from their electrons' magnetic moments. Each electron has a spin magnetic dipole moment which is an intrinsic property, the spinning around its own axis, and an orbital magnetic dipole moment.[38] In nature, all materials are magnetic to some extent. The magnetic properties of a material are determined by the electronic structure of the atoms creating the materials and varying from very weak magnetic for diamagnetic materials to permanent magnetic for ferromagnetic materials. A diamagnetic material is a substance composed of atoms which have no net spin magnetic dipole or orbital magnetic dipole. When a diamagnetic material is exposed to an external magnetic field, a weak induced magnetic field in the opposite direction is generated in that material (Figure 1.2a). The magnetic susceptibility value of diamagnetic materials, a ratio of magnetisation to magnetic field, is negative and common in the order of -10^{-6} to -10^{-5} cgs g^{-1}.[39] All materials that have filled electron shells are classified as purely diamagnetic. Materials that have partly filled electron shells display other forms of magnetism. Paramagnetic materials have partly filled electron shells. Thus, atoms constituting of materials possess a net magnetic moment.[38,40] However, in the absence of an external magnetic field, the atoms randomly align due to thermal energy resulting in zero net magnetic moment for the material. When exposed to an external magnetic field the magnetic moments of the atoms orientate in the direction of the magnetic field giving the material an induced magnetism (Figure 1.2b). Paramagnetic nanoparticles show magnetic susceptibility values in the range of 10^{-5} to 10^{-3} cgs g^{-1}.[39]

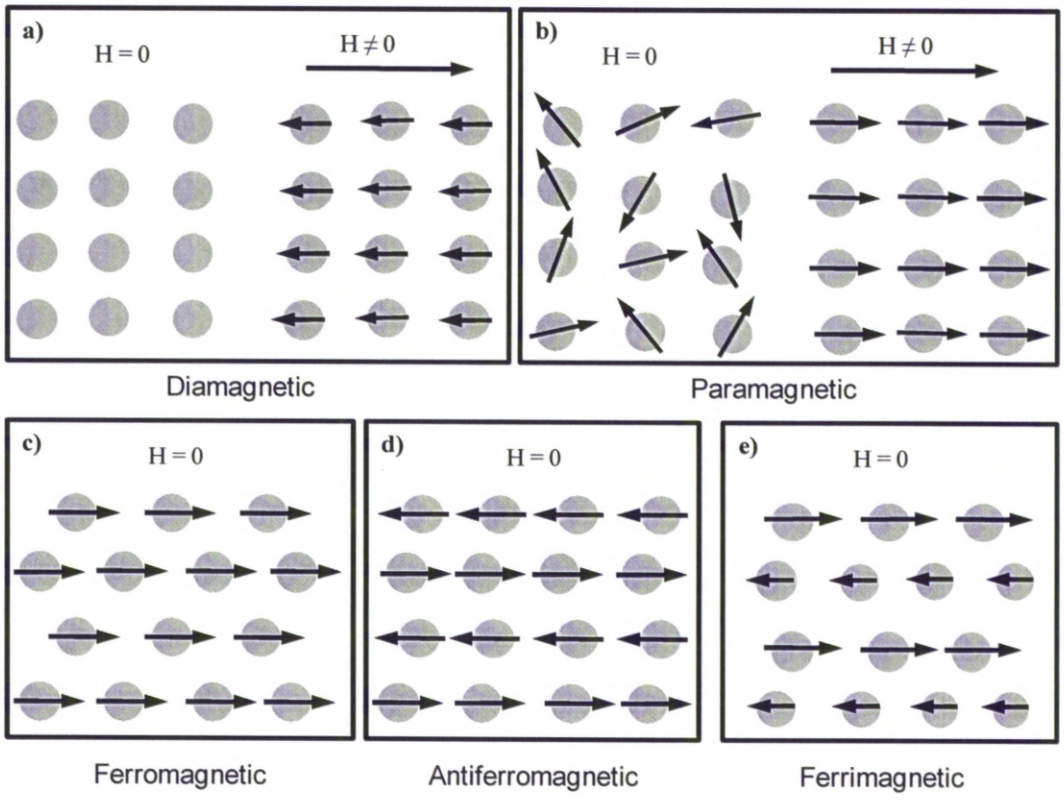

Figure 1.2: Types of magnetic behaviour in the absence or presence of external magnetic field (H) (adapted from ref.[41]).

Materials which are magnetic in the absence of an external magnetic field and exhibit ordered magnetic states are classified as ferromagnetic, ferrimagnetic and antiferromagnetic. In those materials the electrons of neighbouring atoms interact with one another via a process called exchange coupling. This exchange coupling interaction causes the magnetic moments of the atoms to align at room temperature in spite of the effect of thermal energy.[42] The magnetic moments of atoms can align parallel or antiparallel, depended on the coupling interaction (Figure 1.2c-e). In ferromagnetic materials the magnetic dipoles align in parallel, thus this alignment generates a large spontaneous magnetisation in the material even in the absence of an external magnetic field.[38] The most common ferromagnetic materials are zero-valent transition metals such as Fe, Co, Ni and their alloys. Antiferromagnetic materials are constituted by sublattices of atoms whose magnetic dipoles are equal in strength, but aligned in

opposite directions.[38] Thus, antiferromagnetic materials display a zero net magnetisation, e.g., CoO, NiO and FeO. If the magnetic dipoles of the sublattices are unequal in strength the material is described as ferrimagnetic. Ferrimagnetic materials can be classified as a subclass of antiferromagnetic materials.[38] Ferrimagnetic materials, like ferromagnetic materials, have spontaneous magnetisation, but lower value than that of ferromagnetic materials. Transition metal oxide such as Fe_3O_4 and mixed ferrite such as $CoFe_2O_4$ are typical examples of ferrimagnetic materials.[38]

The magnetic behaviours of ferro-, ferri- and antiferromagnetic materials are strongly temperature dependent. Above a critical temperature, called the Curie temperature for ferro- and ferrimagnetic materials and Neel temperature for antiferromagnetic material, the thermal energy is sufficient to disrupt the magnetic order and magnetic moments of atoms are free to move out of alignment and the materials are paramagnetic.[38] To minimise magnetic energy, magnetic materials like ferro- or ferrimagnetic ones tend to subdivide into domains. The domain size is in range of few tens to few hundreds of nanometres and is determined by the uniaxial anisotropy constant and the magnetic property of each material.[43] Within a domain, magnetic moments tend to align in a particular crystal direction called the easy axis of magnetisation.[38]

When particle size is reduced to below the size of a domain, magnetic nanoparticles are known to be a single domain and can become superparamagnetic at room temperature. Superparamagnetism is a unique property of the nanoscale material, which cannot occur in the same bulk material. Below a certain temperature called the blocking temperature, T_b, which is determined by the size of the nanoparticle and the anisotropic constant of the material (larger nanoparticles have higher blocking temperatures), the magnetic moment becomes blocked. Above the blocking temperature (but below the Curie temperature) magnetic nanoparticles are uniformly magnetised along an easy axis, but thermal energy causes the magnetisation to switch between equivalent easy axes. This phenomena was first described by Stoner in 1949.[44]

In the presence of an external magnetic field, the magnetic moments of super-paramagnetic nanoparticles align to the direction of the magnetic field and enhance the magnetic flux. Superparamagnetic nanoparticles exhibit paramagnetic behaviour, but have a much higher magnetic susceptibility. When the external magnetic field is removed, thermal energy causes the moment to randomise and the superparamagnetic nanoparticles have no magnetic remanence (Figure.1.1). Such superparamagnetic nanoparticles are greatly interesting, in particular, regarding potential biomedical applications.[20,45,46]

1.3 Bioapplications of magnetic nanoparticles

Magnetic nanoparticles offer a huge potential for applications in biomedicine, which can be divided according to their use outside (*in vitro*) or inside (*in vivo*) the living organism. The main *In vitro* use of magnetic nanoparticles is for separation and purification. As for *in vivo* applications, nanoparticles have been suggested to be useful materials in a range of areas including targeted drug delivery,[45,47-49] contrast enhancement in magnetic resonance imaging (MRI),[50-53] and hyperthermia cancer treatment.[54-57]

1.3.1 Magnetic purification and separation

The application of functionalised magnetic nanoparticles in combination with magnetic separation has received increasing attention in recent years as magnetic nanoparticles can be quickly separated by magnetic forces. It is possible to magnetically separate selected target entities out of mixtures and the biological solutions simply by attaching them to magnetic nanoparticles before applying a magnetic field.[58]

In magnetic separation, first the magnetic nanoparticles coated with biocompatible molecules have to be labelled with a desired biological entity by mixing with a sample containing the target entity, which can include proteins, DNA, RNA, and cells and, following an appropriate reaction. Once the target entity is attached to the magnetic

nanoparticles, the whole magnetic complex can be easily and quickly separated from the sample using a magnetic separator and washed with water. Finally, the isolated target entity can be eluted and used for further work.[59] Figure 1.3 shows a schematic strategy for magnetic separation and purifications using magnetic nanoparticles.

In comparison with other techniques such as centrifugation, chromatography or ultrafiltration, magnetic separation has advantages such as quick, simple handling of the sample and is easily automated.[60-65] Despite these advantages, it should be noted that this application is not yet a routine for biologists, which may reflect the fact that there are remaining issues with non-specific interactions of the magnetic nanoparticles still to be addressed.

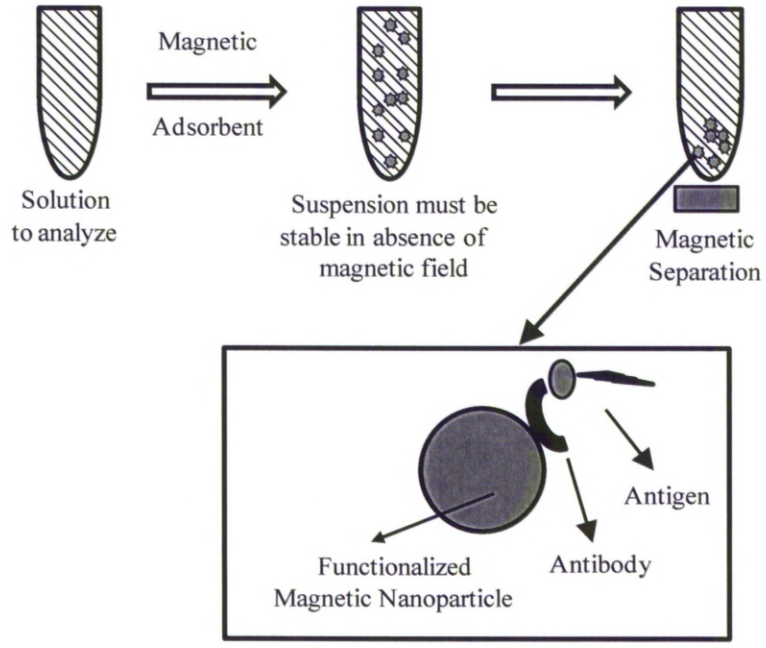

Figure 1.3: Schematic strategy for magnetic separation and purification using magnetic nanoparticles (Reprinted from ref [23]).

1.3.2 Magnetic drug delivery

Targeted drug delivery using a concept similar to that of magnetic separation involves the intravenous injection of nanoparticles into the patient. When the drug conjugated particles enter in blood stream, they are guided to specific target sites and are held there by an applied external magnetic field. Figure 1.4 shows a schematic strategy of magnetic targeted drug delivery using magnetic nanoparticles as carriers. When drug/carriers reach the desired sites, the drug can be released by enzymatic activity or by changing the physiological conditions such as pH, temperature.[20,45]

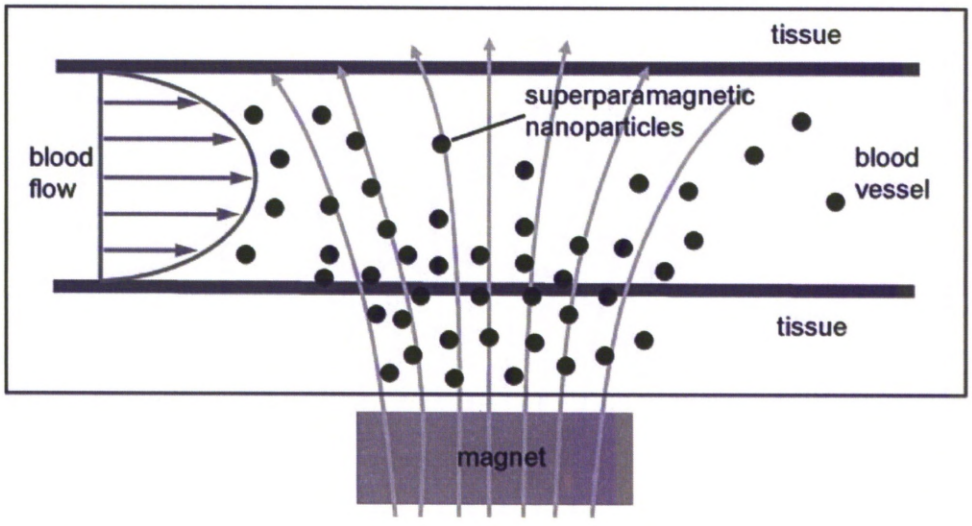

Figure 1.4: Schematic strategy for magnetic targeted drug delivery using magnetic nanoparticles as carriers. Drug conjugated magnetic nanoparticles are injected into the circulation system and are guided and held at targeted sites by an external magnetic field (Reprinted from ref.[41]).

This technique offers some advantages in comparison with standard, systemic drug delivery. For example, in cancer treatment many current chemotherapeutic agents are non-specific and tend to destroy normal healthy tissues, which results in unwanted side effects. However, if such treatments could be localised and the drug could be delivered to tumours, the global (but not local) dose could be reduced and so would the side effects. Moreover,

many drugs used in chemotherapy are poorly water-dispersible. Using them as conjugates with nanoparticles can significantly improve their solubility, resulting in an enhanced effectiveness of the treatment.

With magnetic drug delivery applications, magnetic field strength and gradient, size and magnetic properties of the nanoparticles are the physical parameters that determine the successfulness of the therapy. Others such as blood flow rate, particle concentration, infusion route and circulation time, as well as physiological factors such as tissue depth to the target site (i.e. distance from the magnetic field source), reversibility and strength of the drug/carrier binding (drug releaseability) and tumour volume are also important.[20,49]

1.3.3 MRI contrast agents

Magnetic resonance imaging (MRI) is based on relaxation signals of proton spins of water molecules in biological tissues excited by radiofrequency pulsed sequences under a strong static magnetic field (B_0).[51] Briefly, proton spins of water molecules will align with the applied magnetic field, B_o, but precess at a frequency and an angle dependent on the strength of field (Figure 1.5a). By applying a transversal radiofrequency pulse (RF pulse) of the same frequency, the spinning protons will be excited, which results in an alignment away from B_o (the projection of magnetic moment of protons on the direction of applied field , M_z is decreased and the projection of magnetic moment on the perpendicular plane xOy, M_{xy} is increased) (Figure 1.5b). After the RF pulse has ended the protons attempt to return to their original alignment and energy state through two independent relaxation processes, spin-lattice relaxation (T_1) and spin-spin relaxation (T_2).

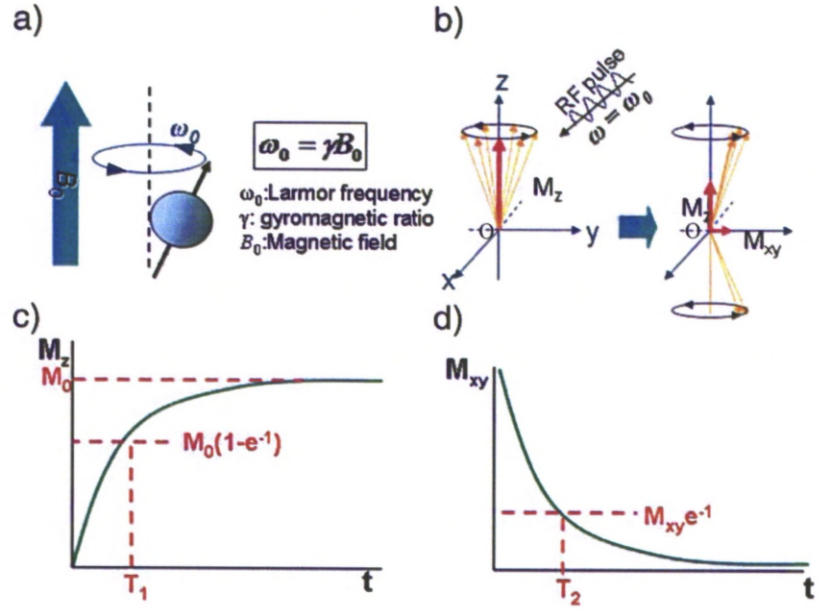

Figure 1.5: Principle of magnetic resonance imaging. a) spins align with the external magnetic field at an angle and precess under the Larmor frequency (ω_o). b) after applying of RF pulse magnetisation of spins changes. Excited spins return to their original alignment and energy state through c) T_1 relaxation and d) T_2 relaxation (Reprinted from ref [51]).

In longitudinal relaxation, the excited spins return to their original alignment by releasing the absorbed energy to the lattice.[50,66,67] The relaxation time T_1 is defined as the time duration that takes the M_z magnetisation to recovers to 63 % of initial state (Figure 1.5c). In transverse relaxation, the energy is dispersed between neighbouring nuclei due to the spin-spin interactions.[50,66,67] The transverse relaxation time T_2 is the time period that takes 63 % of M_{xy} magnetisation to disappear (Figure 1.5d). The time T_2 is usually shorter than T_1. These relaxation processes can be used to generate an image. Intensity of signal tends to increase with increasing inverse longitudinal relaxation time ($1/T_1$ or relaxation rate r_1) and decrease with increasing inverse transverse relaxation time ($1/T_2$ or relaxation rate r_2). The contrast in MR images, the signal differences between adjacent regions, arises from differences in the relaxation time of protons associated with the local environment of the tissue. The difference in the relaxation time between tissues or between lesions and

surrounding normal tissue is usually small. Thus, MRI is sometimes hindered by low contrast of the acquired images. By using contrast agents, the relaxation times T_1 and T_2 of the surrounding protons can be reduced, thus enhancing the contrast of the images. Small molecules consisting of complexes of the paramagnetic gadolinium ion are the most commonly used contrast agents. These decrease T_1 relaxation time (positive contrast agents). Superparamagnetic nanoparticles are used to decrease T_2 relaxation time (negative contrast agents).

1.3.4 Hyperthermia cancer treatment

Another interesting potential application of magnetic nanoparticles is hyperthermia treatment of cancer. The physical principle of magnetic induction hyperthermia is based on the fact that, when magnetic nanoparticles are exposed to a varying magnetic field, heat is generated by the hysteresis loss, Neel-relaxation (re-orientation of magnetisation) and Brown-relaxation (frictional forces).[22] Tumour cells are known to be more sensitive to a temperature increase than normal cells[57,68] and magnetic nanoparticles can be guided to tumours, as discussed before. Heating tumour cells to a temperature of 42 - 46 °C will fatally damage the cells via an apoptotic process, also called programmed cell death. At a temperature between 42 - 46 °C, the function of many structure and enzymatic proteins within the cells is changed, this change alters cell growth and differentiation which induces apoptosis.[57]

Moreover, hyperthermia seems to modify the surface of the cell, such that they are easier recognised by the immune system.[69] The conventional hyperthermia treatment of cancers involves using a device to heat tumour cells. However, the disadvantage of using devices is their damage to surrounding healthy tissue. Magnetic nanoparticle hyperthermia offers a potential solution to this problem. Generally, magnetic nanoparticles are directly injected into the target tumour tissue, which is subsequently followed by exposure to an

externally alternating magnetic field, causing the nanoparticles to heat up. In many cases, the nanoparticles are functionalised with an antibody to facilitate their selected cellular uptake by the tumour and then can be delivered to the target site via circulatory system (Figure 1.6).[57,70]

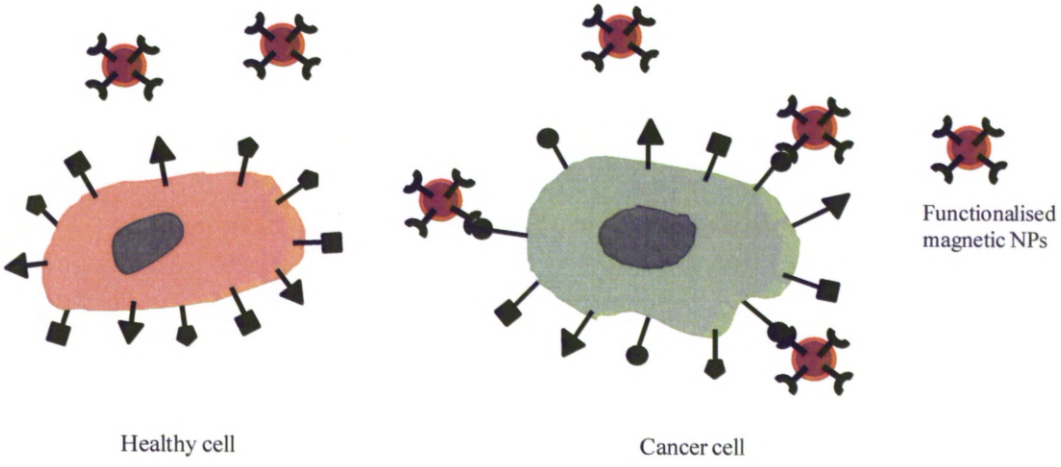

Figure 1.6: Selected targeting of cancer cells by functionalised magnetic nanoparticles (Adapted from ref.[71]).

1.4 Synthesis of magnetic nanoparticles

In terms of synthetic methodology, magnetic nanoparticles can be prepared by either ''top down'' or ''bottom up'' processes.[72] In ''top down'' methods, magnetic nanoparticles are obtained by breaking down raw powder materials using high energy mechanical milling, either under inert gas, or ambient conditions.[73-75] For example, Ponpandian and co-workers have prepared $NiFe_2O_4$ nanoparticles using planetary milling. By varying milling time, the particle size was controlled from 16 to 50 nm.[74] Horvath *et al.* fabricated iron nanoparticles by mechanical milling using a mixture of Fe_3O_4 and Al or Zn as raw materials. Iron nanoparticles of about 12 nm were formed by displacement reactions of Fe^{3+} with the more reactive metals of Al or Zn after 60 min of milling.[76]

The advantages of the mechanical milling methods are that they are very simple and easy to scale up for production of large quantities of magnetic nanoparticles. The disadvantages, however, are the contamination, broad size distribution and irregular shape of products.[77]

In the ''bottom up'' approach, nanostructures are built up from the ''atomic level'' forming either in gas phase (gas phase methods) or in liquid phase (wet chemical methods). In gas phase methods, the particles are formed on a non-wetting surface from a saturated vapour of atoms of the given metal.

In the following sections, three main routes to synthesise magnetic nanoparticles, including the preparation in aqueous solution, microemulsion or reverse micelles and preparation in organic solvents at high temperature as well the advantages and disadvantages of each will be discussed. Other methods such as hydrothermal synthesis and gas phase preparation will also be described. A detailed description of all available synthesis methods is beyond the scope of this thesis, since its focus is on wet chemical methods in aqueous solution or in organic solvents, without the use of complex apparatus.

1.4.1 Nucleation and growth

The formation of nanoparticles involves the processes of nucleation and growth from saturated solution or vapour. Understanding the nucleation and growth of nanoparticles as well as parameters governing these processes is important as it will allow us to develop the synthetic methods that can generate products with controllable monodispersibility, size and shape. For any given solvent, the solubility of any solute is limited. Addition of excess solute thus can lead to precipitation and formation of particles. Therefore, in case of nanoparticle formation, for nucleation to happen, the solution has to be supersaturated. The supersaturation is generally achieved either by directly dissolving the solute at high

temperature and then cooling to lower temperatures or by adding the necessary reactants to generate supersaturated solution during the reaction.[72,78]

Generally, there are two types of nucleation processes: homogeneous nucleation and heterogeneous nucleation. Homogeneous nucleation occurs in the absence of a seed. Heterogeneous nucleation happens in the presence of the surface of a foreign seed. In the case of homogeneous nucleation, according to classical nucleation theory,[79] for a supersaturated solution, the solute molecules or species (monomers) combine to generate clusters or nuclei. The overall Gibbs free energy change, ΔG, for formation of a nucleus with radius r from solution with saturation ratio S is the sum of free energy due to the formation of a new volume and the free energy due to new surface created:[78-80]

$$\Delta G = -\frac{4}{3V}\pi r^3 k_B T \ln(S) + 4\pi r^2 \gamma \qquad (1.1)$$

where V is the molecular volume of the nuclei, k_B is the Boltzmann constant, T is absolute temperature, S is saturation ratio ($S = C/C_{eq}$, C is solute concentration and C_{eq} is equilibrium solubility of solute at the temperature and pressure of the system) and γ is the surface energy per unit surface area. The growth of the nuclei to form stable particles depends on a competition between a decrease in bulk energy and an increase in surface energy, which favours shrinkage.[79] The dependence of surface and bulk energy terms as well as overall free energy ΔG on the nucleus size is shown in Figure 1.7a.

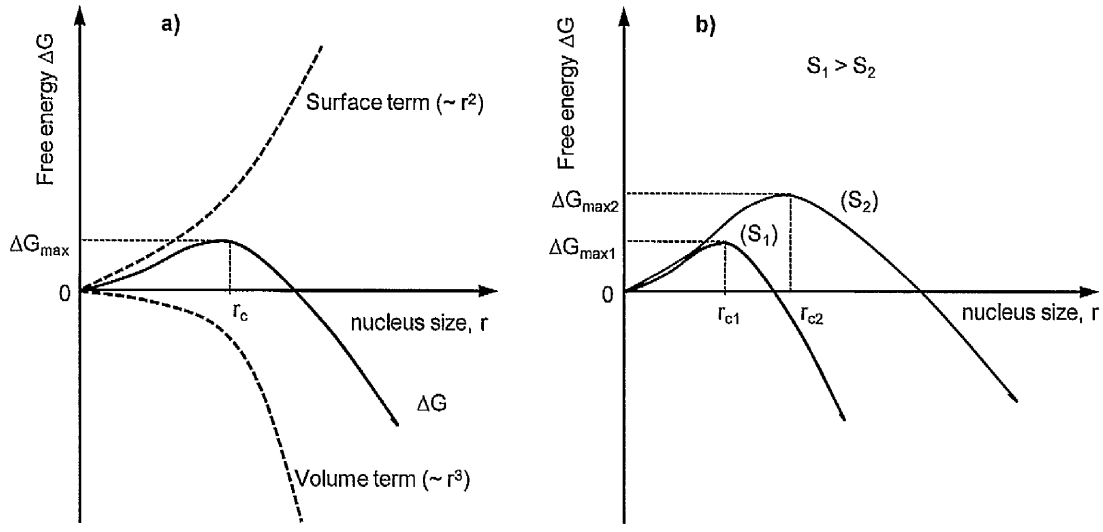

Figure 1.7: Free energy diagram for nucleation as function of nucleus size (a) and dependence of the critical size and the energy barrier on supersaturation ratio (reprinted from ref.[81])

It can be seen that the overall free energy has a positive maximum ΔG_{max}. This maximum value is the activation energy or energy barrier for nucleation. The value of r at which ΔG reaches a maximum is called critical size. The critical nucleus size r_c is obtained by setting $d\Delta G/dr = 0$:[78]

$$r_c = \frac{2V\gamma}{3k_BT\ln(S)} \qquad (1.2)$$

The maximum value of free energy is determined by inserting equation 1.2 into equation1.1:

$$\Delta G_{max} = \frac{16\pi V^2\gamma^3}{27(k_BT\ln S)^2} \qquad (1.3)$$

For the above equations, it can be seen that an increase in the supersaturation ratio, S, will lead to a decrease of activation energy and critical size r_c (Figure 1.7b). During the nucleation process, many tiny nuclei are continuously generated but then are quickly

shrunk or dissolved because of their high surface energy. Only nuclei larger than the critical size r_c can continue to grow to form particles due to the decrease their free energy.[80]

LaMer and his colleague, in the 1950s, first developed a model to explain the formation of uniform colloidal particles.[82] In their work, a short burst of nucleation, which generates all nuclei at virtually the same time, occurs from homogeneous solution when the concentration of solutes reaches a critical supersaturation level. These nuclei then grow uniformly to form particles by diffusion of surrounding solutes in the solution to their surface, and the growth process continues as long as the solution is saturated (Figure 1.8a).[23] According to LaMer, to obtain uniform particles, the nucleation period should be short so that no additional nucleation occurs during the growth step (the separation of nucleation and growth). Otherwise, polydisperse particles would be formed if the nucleation process occurred throughout the particle growth process.[72]

Based on the LaMer model, Murray *et al.* for the first time developed a ''hot injection'' method for the synthesis of monodisperse cadmium chalcogenide nanocrystals.[83] In their work, a high degree of supersaturation which results in a burst of nucleation was achieved by rapid injection of organometallic reactants into a hot surfactant solvent. During the nucleation stage, the monomer concentration in the solution rapidly drops and thus leads to a dramatic decrease of nucleation rate. This ''hot injection'' method has then been applied widely for the synthesis of various magnetic nanoparticles.[84-89]

In fact, the formation of monodisperse particles is complex process.[90-92] Numerous theoretical and experimental evidences indicated that LaMer's model is applicable in a limited number of cases and general to the initial stages of the particle formation when monomer concentration in the solution is still high.[93] In many cases, nucleation followed by growth via aggregation of small particles or multiple nucleation and growth by Ostwald ripening are involved in particle formation.[23] Ostwald ripening, which was first described

by Wilhelm Ostwald and then theoretically explained by Lifshitz, Slyozov and independently by Wagner (so-called LSW theory),[94] is the growth mechanism where large particles grow at the expense of smaller ones and generally occurs at the later stages of particle growth when the monomer or ion concentration is depleted. As the result of the Ostwald ripening, size distribution of the particles is usually broad. However, it can be narrowed by extending reaction time long enough to remove all small ones (Figure 1.8b).

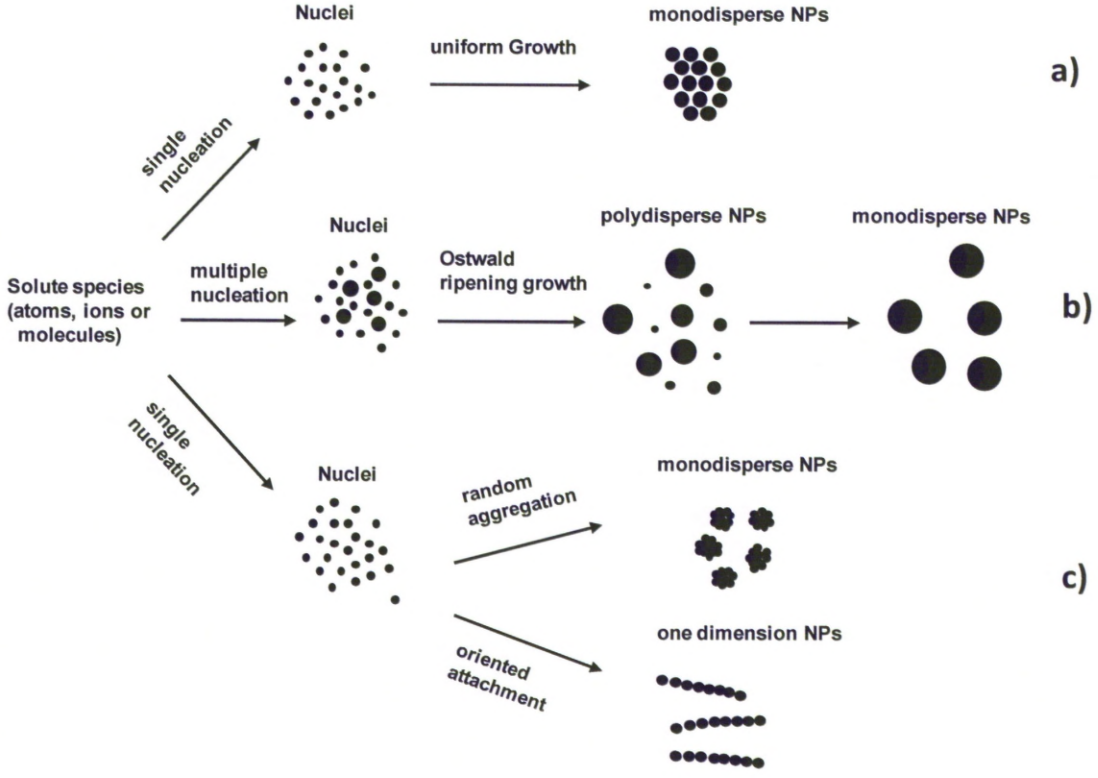

Figure 1.8: Mechanism of formation of uniform particles in solution: a) single nucleation and uniform growth by diffusion (classical model of LaMer and Dinegar), b) multiple nucleation events and Ostwald ripening growth, and c) nucleation and growth via aggregation of smaller subunits (Adapted from ref [23]).

Monodisperse particles can also be achieved as a result of aggregation of small ones. Because of their high surface energy, small particles tend to aggregate to decrease their surface energy. Depending on the surface chemistry of the particles, aggregation can occur

either randomly or by oriented attachment. Oriented attachment generally generates one dimensional structures or secondary particles with complex shapes whereas random attachment leads to the formation of polycrystalline or porous spherical particles.[95-97] Figure 1.8c presents the formation mechanism of monodisperse particles via aggregation growth. Growth by aggregation usually occurs when nucleation and growth are fast.[98] Recently, Zheng and co-workers have reported a direct observation of the growth of Pt particles using *in situ* TEM. The authors have observed that in addition to uniform growth the Pt particles are also formed via aggregation process. For the particles formed by means of monomer attachment, a continuous increase in size and invariation of nearly spherical shape is observed. The particles created by aggregation event shows both changes in size and shape and recrystallisation within the particles.[90]

Heterogeneous nucleation has also been used to synthesise uniform nanoparticles. Seeded growth is one of such approaches. In the seeded growth method, pre-formed nanoparticles are introduced into the reaction mixture as nuclei, and the growth of nanoparticles progresses by adsorption of solute species on the surface of the nuclei. In this method, it is obvious that the nucleation step is physically separated from the growth. However, the solute concentration has to be low during the growth process to avoid homogeneous nucleation.[72]

1.4.2 Stabilising ligands

Stabilisation or coating of magnetic nanoparticles using polymers or surfactants (stabilising ligands) plays a crucial role to obtain colloidal nanoparticles. The stabilising ligand can prevent the nanoparticles from aggregation, which allows them to disperse in a solvent, and enhance their chemical stability. The ligand also, in many cases, enables to control the particle size and shape. To stabilise or coat nanoparticles, it is essential that the ligand molecules attach/adsorb strongly to the particle surface. The attachment of a ligand

can be achieved via electrostatic interactions between the charged surface of the particles and the ligand molecules, or through chemical interactions (chelating, covalent bonding) to the particle surface via a functional group of the ligand molecules. The latter is more common in the synthesis of colloidal nanoparticles. Functional groups have different affinities to different materials. Therefore, the selection of the functional group of a stabilising ligand is important and depends on the kind of the material forming nanoparticles.

According to the acid-base concept and their classification in hard and soft acids and bases (HSAB) proposed by Pearson,[99, 100] the strength of bonds between Lewis acids and Lewis bases depends on their hardness and softness. Hard acids prefer to form strong bonds with hard bases and vice versa. Metal ions of small ionic radius and metal ions at high oxidation state, for example, Li^+, Na^+, Mg^{2+}, Fe^{3+}, Co^{3+} are hard acids. Metal atoms or metal ions of large size at low oxidation state, such as Ag^+, Au^+, Pd^{2+} or Pt^{2+} are soft acids. Likewise, hard bases are classified as electron donors of small size, low polarisability and high electronegativity. Soft bases are electron donors of large size, high polarisability and low electronegativity. Therefore, compounds containing O, N such as alcohols, ethers, carboxylates, amines and imines are hard bases, and thus, stabilising ligands containing these hard bases can strongly bind with surface metallic ions of oxides such as Fe_2O_3, $MnFe_2O_4$, Co_2O_3, $CoFe_2O_4$ and Mn_3O_4. On the contrary, the compounds of S, P such as thiol, thiolether or phosphine are considered as soft bases and, therefore, can effectively coordinate with metal such as Au, Pt, Pd, Ag or CdSe. Table 1.1 presents a list of some hard and soft Lewis acids and Lewis bases and some common stabilising ligands using for the synthesis of nanoparticles.

Table 1.1: Classification of some Lewis acids, Lewis bases and stabilising ligands

Lewis acids	Lewis bases	Stabilising ligands
Hard acids: Li^+, Na^+, K^+, Be^{2+}, Mg^{2+}, Mn^{2+}, Cr^{3+}, Fe^{3+}, Co^{3+}, Ti^{4+}..	Hard bases: OH^-, $RCOO^-$, ROH, NH_3, RNH_2, R_3PO	Ligands with hard Lewis base functional group: oleic acid (OA), oleylamine (OLA), trio-ctylphosphine oxide (TOPO), dopamine, polyvinylpyrrolidone (PVP), polyvinyl alcohol (PVA), polyethylene glycol acetic acid (PEG-COOH), polyethylene glycol amine (PEG-NH_2), dextran, etc.
Soft acids: Ag^+, Au^+, Pd^{2+}, Pt^{2+}, Ag, Au, Pd, Pt,..	Soft bases: RSH, RS^-, RSR, RNC, $(RO)_3P$, R_3P	Ligands with soft Lewis base functional group: Alkyl thiol, polyethylene glycol thiol (PEG-SH), triphenylphosphine (TPP), trioctylphosphine (TOP).
Borderlines:* Fe^{2+}, Co^{2+}, Ni^{2+}, Zn^{2+},..		

*These acids strongly bond to neither soft nor hard bases.

1.4.3 Preparation in aqueous solution

1.4.3.1 Co-precipitation

Among the chemical methods of synthesis of magnetic nanoparticles, co-precipitation has been used for a long time and is probably the simplest and most efficient technique to prepare magnetic colloids.[101] In this technique, the particles are frequently formed in aqueous solution under strong basic condition achieved by adding sodium hydroxide or ammonium hydroxide. This process is generally used for the synthesis of oxides and ferrites.[68,102-104] The overall chemical reaction of ferrite formation can be illustrated by equation 1.4:

$$M^{2+} + 2Fe^{3+} + 8OH^- \rightarrow MFe_2O_4 + 4H_2O \qquad (1.4)$$

where M are Fe, Co, Ni, Mn, Zn or Mg.

A summary of oxide and ferrite nanoparticles prepared by co-precipitation and reaction conditions is presented in table 1.2.

Table 1.2: Summary of some magnetic nanoparticles and synthetic conditions prepared by precipitation technique in aqueous solution

Materials	Precursors	stabilisers	Precipitating agent and reaction conditions	Particle size (nm)	Refs.
Fe_3O_4	$FeCl_2$ $FeCl_3$	H^+	NH_4OH, under N_2, at 30 – 90 °C	8.4 - 51	105
	$Fe(NO_3)_3$	No	NaOH / NH_4OH / $N(CH_3)_4OH$; in the presence of $NaNO_3$/ NH_4NO_3/$N(CH_3)_4NO_3$	1.5 - 12.5	106, 107
		Sodium oleate	NaOH, pH = 11.5 - 14	1.3 - 6	108
$MgFe_2O_4$	$MgCl_2$ $FeCl_3$	OH^-	NaOH, at 100 °C	7.6 - 13	112
$MnFe_2O_4$	$MnCl_2$ $FeCl_3$ $FeSO_4$	OH^-	NaOH, at 100 °C and pH = 4-13	5 - 25	113
$NiFe_2O_4$	$FeCl_2$ $Ni(NO_3)_2$	no	NaOH, annealing at 500-700 °C		114
$CoFe_2O_4$@Au	$CoCl_2$ $FeCl_3$	oligomer	NaOH, 100 °C	21 - 29	115
$Ni_{1-x}Zn_xFe_2O_4$	$NiSO_4$ $ZnSO_4$ $FeSO_4$	no	NaOH, annealing at 800 °C	-	116
$Co_{1-x}Ni_xMn_{0.1}$ $Fe_{1.9}O_4$	$Co(NO_3)_2$ $Ni(NO_3)_2$ $Mn(NO_3)_2$ $Fe(NO_3)_3$	no	NH_4OH, pH = 10, annealing at 500 °C	-	117
Fe_3O_4	$FeSO_4$ $FeCl_3$	PMAA-PTTM	NH_4OH, at 100 °C, pH = 6.5-11.3	4.8 - 8.5	103
$M_{1-x}Fe_xFe_2O_4$ (M = Ni, Mg and Mn)	$FeCl_3$ MCl_2 (M = Ni, Mg or Mn)	polyacrylamine	$(NH_2)_2CO$, 200 °C	15 - 230	118
Fe_3O_4	$FeCl_2$ $FeCl_3$	starch/sodium oleate/PEG	NaOH, at 60-95 °C, pH = 7.5-14	6-12	119-121
		dextran	NH_4OH, under N_2 at 80 °C,	16-2,764	122-124
Fe_2O_3	$FeCl_2$ $FeCl_3$	dextran	NaOH, under air at 70 °C	4-6	125

To prevent the aggregation of the nanoparticles, a stabilising ligand is generally included in the synthesis.[68,103,119-123,126-132] In many cases, the agglomeration of the particles can be avoided by adsorption of charged species, such as OH^- and H^+ ions to the surface of the particles at different pH conditions (electrostatic repulsion).[101,109] The control over size, shape, monodispersity and structure of the products can be achieved by adjusting the pH,[106] the ionic strength,[106,133] the temperature, the nature of precursors[106] as well as the concentration of the reagents.[22,104]

Vayssieres *et al.* reported the synthesis of Fe_3O_4 nanoparticles by co-precipitation of ferrous chloride and ferric nitrate under different pH conditions and ionic strength.[106] It was pointed out that the particle size can be tuned by varying the pH value and the ionic strength. In their work, particle size could be increased from 1.5 to 12.5 nm when the pH value and salt concentration (ionic strength, I) decreased from pH = 12 and I = 3 M to pH = 8.5 and I = 0.5 M, respectively. The nature of the electrolyte used to maintain the ionic strength also plays an important role in determining the particle size. With nitrate salts as precursors, at a given pH and ionic strength, the authors observed that the efficiency of the cation to reduce particle size increases through a sequence $[N(NH_3)_4]^+ < [NH_4]^+ < Na^+$.[106]

Tang and co-workers prepared $MnFe_2O_4$ nanoparticles by the simple co-precipitation of a mixture of iron and manganese salts in sodium hydroxide solution.[113] The size of the particles increased from 5 to 25 nm by increasing the concentration ratio of $[Fe^{3+} + Mn^{2+}]/[OH^-]$ from 0.01 to 0.33. The particle size can be also controlled in a wider range (20 – 180 nm) by replacing ferric salts with ferrous ones.

The reaction temperature also has a significant effect on the size of the particles. Liu *et al.* reported the synthesis of Fe_3O_4 nanoparticles by precipitating an aqueous solution of Fe^{3+} and Fe^{2+} with ammonium hydroxide. Increasing reaction temperature from 30 to 90 ^oC particle size could be tuned from 8.4 to 51 nm.[105]

The addition of a stabilising ligand such as polymers and surfactants during the synthesis of magnetic nanoparticles by co-precipitation is important. The presence of these ligands is not only to improve the colloidal stability of the nanoparticles, but can also control the size of nanoparticles.[103] In addition, functional groups of the ligands can be used to conjugate nanoparticles with biological molecules for bioapplications.[120,124]

Bergemann and co-workers developed a synthesis of stable and water-dispersible Fe_3O_4 nanoparticles by precipitating iron carbonates with hydroxide solution.[134] The particle size was varied from a few tens of nanometres to over one micrometer simply by increasing the reaction temperature from 5 to 100 °C. Colloidal stability of the nanoparticles could be achieved by modifying their surface with stabilising ligands, such as starch, polysaccharide, polyacrylate or polyvinalcohol polymers.

Li *et al.* reported the synthesis of stable and water-dispersible Fe_3O_4 nanoparticles by precipitation of Fe^{3+} and Fe^{2+} under concentrated ammonia solution in the presence of poly(methacrylic acid) pentaerythritol tetrakis (3-mercaptopropionate) (PMAA-PTTM) polymer.[103] In their work, the particle size could be changed from 4.5 to 6.1 nm by simply decreasing the proportion of COOH group in the polymer and precursor concentration from 3.4 to 0.7. Surface of nanoparticles then could be conjugated with glutamic acid molecules to produce fluorescent magnetic nanoparticles.

Using a similar approach, Paul *et al.* synthesised water-dispersible dextran coated Fe_3O_4 nanoparticles.[122] It was found that the molecular weight of the polymer has a great effect not only on the size but also on the magnetic properties of the nanoparticles. Increasing the polymer molecular weight from 1,000 to 70,000 g mol^{-1} decreases the particle size from 2.7 μm to 21 nm. The magnetic susceptibility of the nanoparticles increases more than 12 times from $1.9x10^{-3}$ to $2.5x10^{-2}$ cgs g^{-1}, respectively.

Preparation of magnetic nanoparticles by precipitation of metal salts in aqueous solution offers some advantages as this method is simple, uses inexpensive starting materials and is

easy to scale up. However, the control of the size, monodispersity and uniformity of the nanoparticles is still a challenge.

1.4.3.2 Reduction synthesis

In contrast to the co-precipitation process, which was used for the synthesis of oxide or ferrite nanoparticles, reduction methods are employed for the synthesis of magnetic metal or alloy nanoparticles using reductants such as alkali borohydrides[135-142] or hydrazine.[143-146] Sodium borohydride has first been described as an effective reducing agent for metal ions by Schlesinger in the 1950s and has been extensively studied for the synthesis of magnetic nanoparticles afterward.[147] The chemistry of the reaction of metal salts and $NaBH_4$ in aqueous solution is quite complex as the metal ions and/or forming particles act as catalysts for the oxidation of BH_4^- by water. Depending on pH, BH_4^-/metal ion ratio and concentration of reagents, metal or metal boride nanoparticles can be formed as final product.[138,148-150]

Linderoth *et al.* synthesised Fe boride nanoparticles by the reduction of Fe^{2+} by $NaBH_4$ in aqueous solution. The boron content incorporated into the iron lattice was indicated to be sensitive to the pH value of the solution. With pH between 4 and 8, Fe boride nanoparticles with a B content varying from around 9 to 28 % were obtained. At pH of 9, metal Fe nanoparticles could be produced.[138] Shen *et al.* prepared Fe, Co and Ni boride nanoparticles in aqueous solution using of KBH_4 as reductant. The authors observed that the boron content in the product decreased with increasing KBH_4 concentration.[148] Tong *et al.* reported the synthesis of shape controlled Fe nanoparticles by reducing iron (II) sulfate utilising $NaBH_4$. Control of the shape of the particles was achieved by varying reaction temperature and reductant concentration.[142]

Kobayashi and co-workers prepared silica coated CoPt alloy nanoparticles by adding a mixture of $CoCl_2$ and H_2PtCl_6 salts into $NaBH_4$ solution in the presence of citric acid as

stabiliser and then following the addition of tetraethoxysilane ethanolic solution. The sample was then annealed to increase the crystallinity. The size of the CoPt cores, determined by Scherrer's formula using the halfwidth of the strongest peak of the XRD spectrum, increases from 4 to 11 nm with increasing annealing temperature from 200 to 600 °C.[136] Using a similar approach monodisperse silica coated Co nanoparticles were synthesised. It was observed that there was no boron detected by EDX analysis and the formation of metallic cobalt nanoparticles was possible owing to the presence of dissolved oxygen in the aqueous medium which could convert Co borides into Co.[151]

Recently, several research groups have developed the synthesis of water-dispersible metallic and alloy magnetic nanoparticles by the reduction of metal ions utilising $NaBH_4$ in the presence of biomacromolecules as templates.[139,140,152-155] Using apoferritin as template, Galvez *et al.* reported the synthesis of Co, Ni and CoNi nanoparticles. In their work, the apoferritin solution was mixed with metal salt solution and incubating for 24 h at pH = 8 to increase the amount of metal ions per protein cage. The mixture was then passed through a G-25 Sephadex column to eliminate free metal ions before $NaBH_4$ was added.[139,140] CoPt nanoparticles could be produced by a similar approach. The protein encapsulated CoPt nanoparticles obtained were dispersible and stable in aqueous solution.[153]

When hydrazine is used as a reducing agent for the synthesis of magnetic nanoparticles, the reactions are generally carried out in a preheated and basic solution.[143-145] Ni nanoparticles were synthesised by reduction of Ni^{2+} using hydrazine at 70 °C in concentrated NaOH and in the presence of sodium citrate as a stabilising ligand. Nanowires could be formed by applying an external magnetic field during the synthesis.[145]

Using Pt seeds as catalysts for the reduction of Ni^{2+} with hydrazine, Grzelczak *et al.* reported the synthesis of water-dispersible cetyltrimethylammonium bromide coated Ni nanoparticles.[146] Control of the size of the particles was achieved simply by varying

amounts of platinum seed. Decreasing molar ratios of Pt^0/Ni^{2+} from 0.1 to 0.01, the particles size can be increased from 13 to 33 nm.

Zero-valent metal could be used as a reductant for the synthesis of magnetic nanoparticles. A metal with more negative reduction potential could be used to reduce metal ions of the elements with less negative ones. Zhang *et al.* reported the synthesis of Ni nanoparticles with different shapes by reduction of Ni^{2+} in aqueous solution at room temperature utilising Mn powders as reducing agent.[156] Here, nickel ions were reduced to nickel metal whilst Mn was oxidised into Mn^{+2} via replacement reaction $Ni^{2+} + Mn \rightarrow Ni + Mn^{2+}$. Increasing reaction time from 2 h to 5 days, different shapes of nanosheets and nanoscrolls were obtained.

Using simultaneous $NaBH_4$ and Co metal as reductants, Vasquez and co-workers developed the synthesis of CoPt hollow nanoparticles by reducing Pt^{4+} in $NaBH_4$ solution in the presence of pre-formed Co particles and poly(vinyl pyrrolidone) polymer.[157] The authors indicated that hollow structure was formed as the Co core is sacrificially dissolved due to its reaction with Pt ions. In the presence of BH_4^- in the reaction mixture, any Co that is oxidised during the platinum reduction will be reduced back to Co metal. This results in the formation of CoPt hollow structures.[157] Using a similar process, Co@Au yolk/shell nanoparticles were produced. By applying a weak external magnetic field during the synthesis, Co@Au yolk/shell nanochains could be produced.[158]

The advantages of the aqueous syntheses of magnetic nanoparticles by reduction methods are that they are simple and easy to scale up. In addition, the nanoparticles prepared by these methods are normally dispersible in water, which is a crucial requirement for bioapplications. However, it has been demonstrated that the control of size, shape and monodispersity of the nanoparticles is generally more difficult to achieve than with some of the other methods such as syntheses in organic media. In addition, the

nanoparticles prepared by reduction methods are normally amorphous and sometimes the final product is contaminated, particularly when borohydrides are used as reductants.

1.4.4 Hydrothermal synthesis

Hydrothermal synthesis of nanoparticles is based on the ability of water at elevated pressures and temperatures to hydrolyse and dehydrate metal salts. Chemical reactions are always carried out in autoclaves or high pressure reactors where water can be brought to temperatures above its boiling point by autogenous increase in pressure resulting from the heating.[102] When other solvents than water are used for synthesis, the process is called solvothermal synthesis. At elevated temperature, solubility and reactivity of the reactants increase. Many reactants which are not soluble in water at normal conditions can be used in hydrothermal syntheses. Parameters such as pressure, temperatures, reaction time, precursor concentration and pH can be used to control size, shape and crystallinity of the products.[159-165] Hydrothermal processes have been widely used for the synthesis of magnetic nanoparticles such as oxides,[160,166,167] ferrites[159,164,168,169] or alloys.[163,170]

Recently, some improvements of the hydrothermal syntheses have been proposed namely the ''continuous flow'' hydrothermal reactor. The syntheses involve a rapid heating of flowing solutions of precursors by contact with a stream of supercritical water preheated to 200 - 400 °C. The liquids are transported with pumps. The mixture is then cooled down by a water cooler and the final product can be collected as a colloidal suspension.[102,162] The continuous flow process is particularly suitable for large scale preparations or for the synthesis of nanoparticles with multiple components.

The hydrothermal process is environmentally friendly as it does not involve any organic solvent, and it does not require any postannealling treatments as the products are generally crystalline. The method can produce nanoparticles with good control of size and shape. In addition, multicomponent nanoparticles, which are not always easy to prepare by other wet

chemistry methods, can be synthesised by the hydrothermal process. Disadvantages of the methods are the need of autoclaves or high pressure reactors for handling high pressure and high temperature synthesis conditions.

4.4.5 Preparation in organic solvents

Thermal decomposition has proved to be one of the most successful methods for the synthesis of magnetic nanoparticles, giving a good control over the size and shape of the nanoparticles.[17,171-173] In general, monodisperse nanoparticles are prepared by thermal decomposition of organometallic in a high boiling organic solvent in the presence of surfactants(s). The synthesis can be performed either by rapid injection of precursor(s) into a hot surfactant solution, the process is known as hot injection method, or through heating a reaction mixture prepared at low temperature to high temperature to produce nanoparticles (heating up process).[174] Figure 1.9 shows a synthesis of monodisperse nanoparticles using hot injection method.

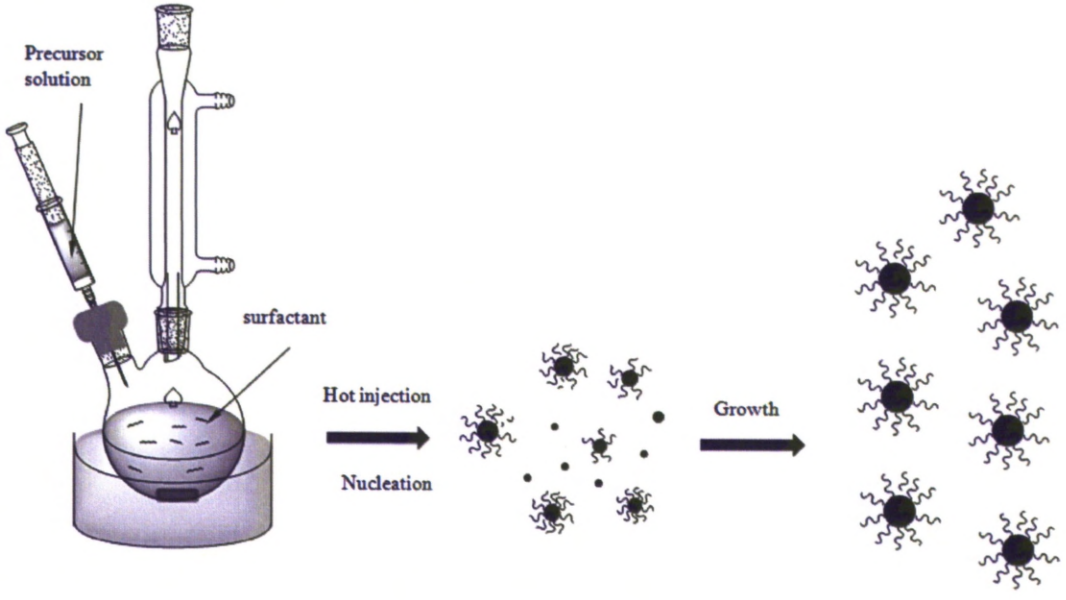

Figure 1.9: Synthesis of magnetic nanoparticles by hot injection method (Adapted from ref.[72]).

The organometallic compounds such as carbonyls,[87-89,175-177] acetylacetonates[178-183] and cupferrorates[184] are the most common precursors using in the synthesis. Though the inorganic metal salts of sulfate[17] or chlorides[173,185,186] have also been used. Fatty acids (FA),[89,187] oleylamine (OLA),[178,179,188] trioctylphosphine oxide (TOPO)[189] or a mixture of these[87,182,183,190-192] are widely used as surfactants. The structure of some common surfactants using in the synthesis of magnetic nanoparticles in organic media are shown in the Figure 1.10.

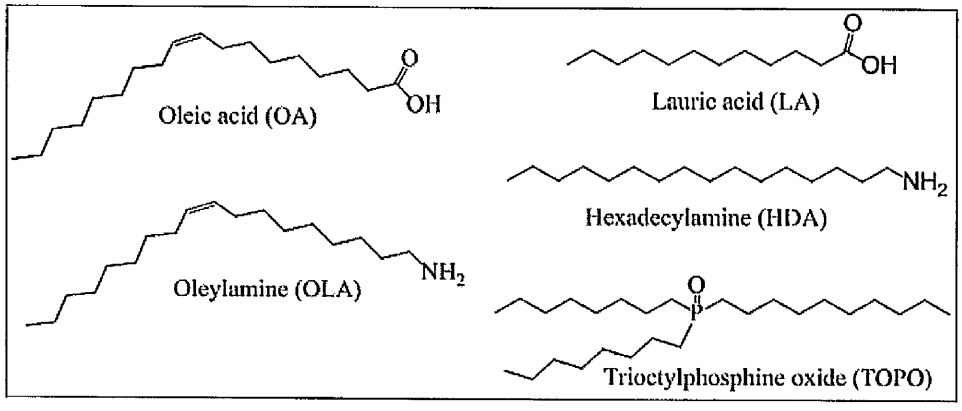

Figure 1.10: Structure of some common surfactants using in the synthesis of magnetic nanoparticles.

Tuning the ratio of metal precursors/surfactants and concentration of reagents is often used to control over the size and shape of nanoparticles.[192] A higher ratio of surfactant to precursor usually favours the formation of smaller.[193,194] Other reaction parameters, for instance, temperature and heating rate of the reaction,[183,195] as well as ageing time[180,183] can also play a critical role in the determination of the size, shape and monodispersity of the nanoparticles.

Synthesis at high temperatures offers some advantages over the other methods. Firstly, particles formed at high temperature are of high crystallinity. Secondly, the speed of nucleation and growth of nanoparticles can be readily controlled by tuning the temperature to that the nucleation or growth occurs. The growth of the nanoparticles can be stopped

rapidly by cooling the reaction, which is crucial in the determination of the morphology and size distribution of the products. For example, Puntes and co-workers have synthesised Co nanoparticles by injection of $Co_2(CO)_8$ into hot dichlorobenzene (182 °C) in the presence of oleic acid (OA) and trioctylphosphine oxide (TOPO).[84] Quenching the reaction at different times resulted in the formation of different shapes. Initially, Co nanodisks with tuneable size from 4x25 to 4x75 nm were obtained. As the reaction time increased, the nanodisks dissolved and spherical shapes of 8 nm with a narrow size distribution were formed as the final product. Shao *et al.* prepared Fe nanoparticles by thermal decomposition of iron carbonyl in kerosene in the presence of oleylamine.[196] The size and shape of the nanoparticles were tuned by varying reaction time and surfactant concentration. Using carbonyl compounds allows the production of high quality nanoparticles. These precursors, however, are very toxic, can cause environmental damage and are unstable. The preparations have to be carried on under a protective gas, for example in a glove box. Recently, in parallel with carbonyl precursors, metal acetyl-acetonate complexes have been extensively used for the synthesis of magnetic nanoparticles.[180,192,197-200] Using acetylacetonate complexes offers some advantages. They are non-toxic and stable so they can be handled on the bench. In addition, because of the low decomposition rate of acetylacetonate complexes, size and shape of the nanoparticles is more readily controlled.[180,192,197,198,200]

When metal carbonyl and acetylacetonate complexes were used together, alloy nanoparticles such as CoPt, FePt or FePd can be fabricated.[190,201-206] Using iron pentacar-bonyl in combination with Pt/Pd (II) acetylacetonate complexes, our group has successful synthesised FePt, FePd and FePtPd nanoparticles.[21] By controlling the synthesis conditions, e.g., nature and concentration of the precursors, reaction time, temperature and atmosphere, magnetic nanoparticles of size ranging from 5 to 50 nm and with a variety of

shapes including spheres, cubes, octopod-cubes, stars, rods, bilobes, tetrahedra, or multipods were produced.

Besides organometallic complexes, inorganic metal salts have been used in some instances as precursors.[17,173,185,186] Hyeon *et al.* have prepared multi-gram monodisperse iron oxide nanoparticles using $FeCl_2$ as the staring material. The size of nanoparticles was controlled from 5 to 22 nm by using solvents with different boiling points.[186]

1.4.6 Microemulsions

A microemulsion is a thermodynamically metastable isotropic dispersion of two immiscible liquids, consisting of nanosized domains of one or both liquids stabilised by an interfacial layer of surfactant molecules.[207,208] Microemulsions can be water-in-oil (reverse micelles) or oil-in-water (normal micelles). Figure1.11a shows a reverse micelle structure. In this structure, hydrophilic heads of surfactants orient toward the centre and hydrophobic tails direct outward. Common surfactants are used in the formation of reverse micelles, including Aerosol-OT, sodium bis(2-ethylhexyl) sulfosuccinate (AOT), Trixton X-100, sodium dodecyl sulfate (SDS), Igepal and cetyltrimethylammodium bromide (CTAB) (Figure 1.11b). Among these surfactants, Aerosol-OT, sodium bis(2-ethylhexyl) sulfosuccinate (AOT) is the most widely studied as its geometry makes it effective for forming reverse micelles in variety of nonpolar solvents, such as alkanes, aromatic solvents, halogenated alkanes.[209]

Reverse micelles have been successfully used to prepare magnetic nanoparticles. Aqueous solutions of metal salts containing elements that form the desired nanoparticles are added to the reverse micelle suspension. A reductant (e.g. $NaBH_4$ or N_2H_4) is added to the mixture and, once the nanoparticles are formed, the micelle solution is disrupted by the addition of an excess amount of polar solvent (e.g., methanol) and the nanoparticles are collected. Using the reverse micelle method, magnetic nanoparticles of various materials

such as Co,[210] Fe@Au,[211-213] Ni@Au[214] CoPt,[215] FePt,[216] Fe_3O_4[217] and $MnFe_2O_4$[218] have been successfully synthesised.

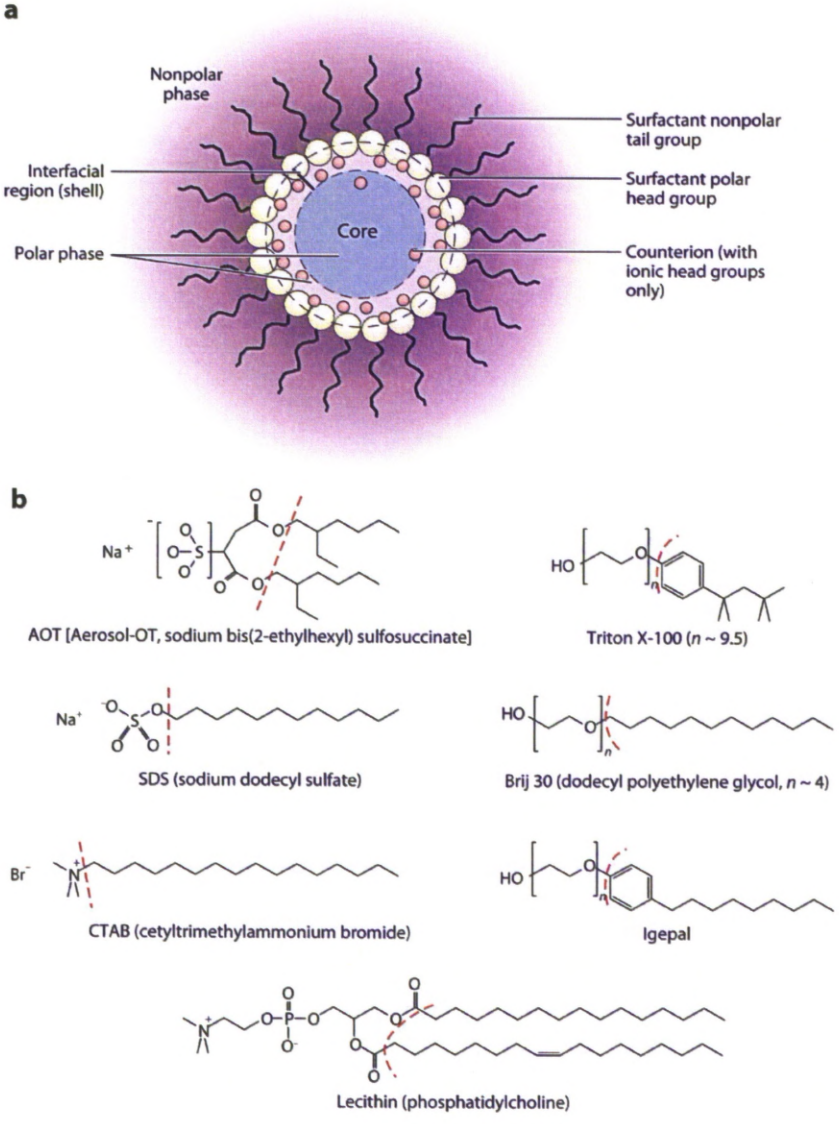

Figure 1.11: Reverse micelle structure (a) and common surfactants used in formation of reverse micelles. Each surfactant comprises a hydrophilic head group (left of red dashed) and hydrophobic tail (right of red dashed line) (Reprinted from ref. [209]).

Microemulsion methods are also useful techniques for making core/shell structures. The magnetic cores can be synthesised either directly using reverse micelles[213,219,220] or by thermal decomposition and are then transferred to micelles before coating.[221] An inorganic

shell of silica, gold or silver is frequently used for the system. However, control of the size and shape of the nanoparticles synthesised by these methods is difficult, as it reflects the interior of the micelle. Moreover, large amounts of solvents are necessary to synthesise appreciable amounts of materials. It is thus more expensive and difficult to scale-up.[22]

1.4.7 Gas-phase syntheses

Gas-phase syntheses of nanoparticles are based on homogeneous nucleation in gas or vapour phase followed by condensation and coagulation.[222] Precursors are generally evaporated and delivered by a gas flow to the reactor where the chemical decomposition and the particle formation occur. The precursors can be chemical compounds such as metal salts, metal carbonyls or they can be metals and alloys in solid form. Depending on the heating source, gas phase syntheses can be classified as hot-wall reactor, flame, plasma, laser and magnetron sputtering methods.

The hot-wall reactor method, which uses a furnace as the heat source to evaporate or decompose precursors, is probably the simplest technique for gas phase synthesis of nanoparticles. In this method, a flow of carrier gas is bubbled through a heated bubbling unit containing the precursor(s). The gas stream with precursors' vapour is then passed through a preheated furnace in which the precursors are decomposed and recombine to form small clusters or nanoparticles before cooling down by collision with a cold gas stream or impact on a cooled substrate.[223] A schematic diagram of a furnace system for the synthesis of nanoparticles was presented in Figure 1.12. In this system, the particles formed in the tubular furnace were expended into the low pressure working chamber to minimise further growth due to aggregation and are condensed out on the chiller, from which they can be scraped off and collected.[223,224]

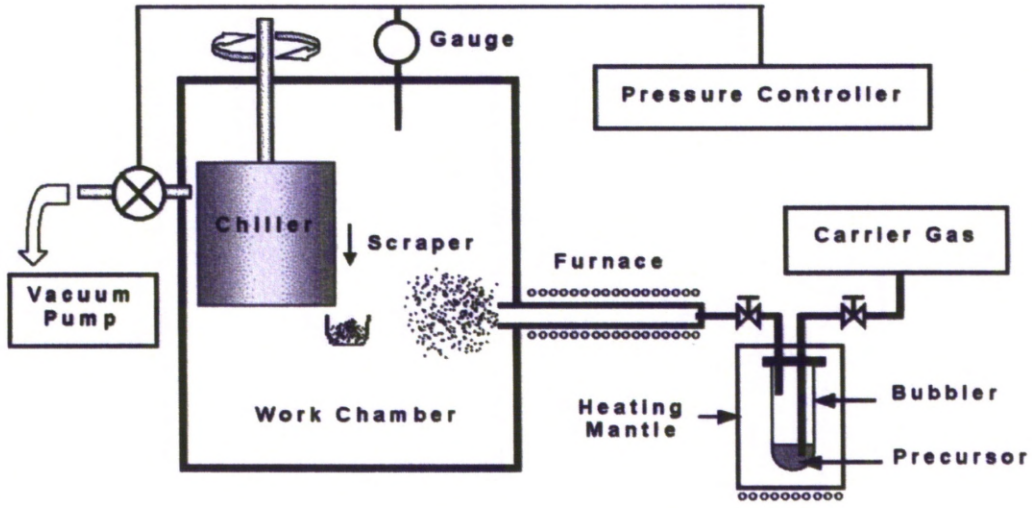

Figure 1.12: Schematic diagram of chemical vapour condensation system for the synthesis of magnetic nanoparticles (Reprinted from ref.[223]).

Kim *et al.* have extensively studied the synthesis of magnetic Co, Fe and CoFe nanoparticles by chemical vapour condensation processes using metal carbonyl precursors.[225-229] In their work, different carrier gases such as He, Ar or CO have been investigated. In case of CO as carrier gas, the authors showed that carbon coated magnetic nanoparticles core/shell structures could be produced.[225, 227] By varying the gas flow rate or decomposition temperature, the particle size and phase structure of the product could be changed.[225,227] Inorganic metal salts could be used as precursors for the synthesis. The metal salts are heated to vapour in evaporation unit and the vapour was carried by carrier gas to the reactor. To obtain metal or alloy nanoparticles, hydrogen is normally introduced to the reactor to reduce metal ions to metal.[52,230-232] The size of the particles could be tuned by varying the evaporation temperature or the carrier gas flow rate.[230,231]

The combustion flame process, annually producing millions of tons of carbon black and metal oxides, is the commercially most successful method for the synthesis of nanoparticles.[233] Instead of using an external heat source for the synthesis, the particle synthesis can be performed within a flame; therefore the energy needed for decomposition

or chemical reaction of precursors is produced *in situ* by the combustion reactions. The precursors supplied for the synthesis can be in the vapour phase (vapour-fed flame process)[233-237] or in liquid form (spray flame process).[233,238-247] Janzen and co-worker reported the synthesis of Fe_2O_3 nanoparticles by decomposition of $Fe(CO)_5$ in a prefixed H_2/O_2 flame. The $Fe(CO)_5$ vapour was delivered to the burner by Ar carrier gas.[234] The effect of the synthetic conditions such as precursor concentration, reactor pressure and H_2/O_2 ratio on the particle size was investigated. The evolution of the particles was investigated *in situ* by mass spectrometer. Kumfer *et al.* have developed the synthesis of Fe_3O_4 nanoparticles using a continuous, nonpremixed flame method.[237] In their work, CH_4 or C_2H_4 was used as carrier gas for an iron pentacarbonyl precursor. The flame was produced by injection of oxygen into a surrounding flow of fuel. The effect of flame temperature, ratio of oxygen to fuel and kind of fuel (CH_4 or C_2H_4) on the particle formation, Fe oxidation state and magnetic properties of nanoparticles was evaluated.

Vapour-fed flame synthesis normally involves the use of expensive and volatile metal carbonyl precursors and is generally carried out under inert gas. To overcome these complications, a spray flame process could be used. In the spray flame synthesis, precursors are dissolved in a solvent and sprayed into the flame. The precursors could be inorganic salts or metal carboxylates, which are inexpensive and less volatile than carbonyl compounds. Using the spray flame method, magnetic nanoparticles such as oxides, metals or core/shell structures have been synthesised.[238-247]

Thermal plasma can be used as a heat source in the gas phase synthesis of nanoparticles. In the thermal plasma process, the precursors in the gaseous, liquid or powder form are generally injected into the plasma flame. The gases such as hydrogen, nitrogen, argon or helium can be used to generate the plasma. Many plasma methods have been developed for nanoparticles synthesis including AC, DC, radio frequency (RF) plasma processes which use AC, DC or RF electric power sources,[248-259] and microwave or laser assisted plasma

ones.[260-263] By controlling the process parameters such as precursor concentration, quenching rate or gas pressure in the reactor, it is possible to control the size, monodispersity and aggregation of the products.[248,258,264] Wei *et al.* used an anodic arc plasma method to prepare Ni nanoparticles.[264] Nickel metal in the bulk form stored in a copper crucible was evaporated by arc discharge between a tungsten cathode and copper anode under argon atmosphere. The yield and size of the particles could be increased by increasing the gas pressure or the arc current intensity. Sergiienko and co-workers have developed a method for the synthesis of Co@C and FePt@C nanoparticles by DC arc discharge in ethanol solution assisted by ultra-sound.[249, 251] Co or FePt anodes were used as precursors to make magnetic cores and ethanol was used as carbon source for the graphite shell. Using a similar approach, Fe@C core/shell nanoparticles were prepared. The Fe@C core/shell structures were then coated with PEG polymer for bioapplications.[265] In comparison with conventional arc discharge plasma processes, which are generally equipped with an expensive vacuum system and require an electric discharge power of some tens kW, the arc discharge in liquid assisted by ultra-sound method offers some advantages. This method requires a much lower power of some tens of watts and can be operated without the vacuum equipment.[249] DC or AC plasma processes for synthesis nanoparticles often involved electrodes which are eroded or evaporated, thus may cause contamination of the products and require regular maintenance or replacement of the electrodes. To overcome these problems, RF plasma or microwave plasma methods are appropriate choices for the synthesis of nanoparticles, in which high temperatures are obtained by electroless radio frequency or microwave discharges.[258,266] It was shown that the process parameters such as concentration and nature of plasma generating gas,[257] feeding rate of precursors,[253,258] cooling rate,[253] carrier gas flow[259] or plasma-on time (for plasma discharge with a pulse operation of a square-wave on/off cycle)[252] had a great effect on magnetic properties, size and shape and efficiency of product formation.

Another way of heating precursors to induce reaction and homogeneous nucleation for forming nanoparticles is by absorption of laser energy. When organic metal compounds are used as precursors for the synthesis (laser pyrolysis method) heating is achieved by utilising an infrared laser such as a CO_2 laser, whose energy is absorbed by the precursors or by a photosensitiser. Photosensitisers such as ethylene or sulfur hexafluoride play the role of an energy transfer agent. They are excited by the absorption of laser radiation and transfer the absorbed energy by collision to the reactants.[224] Solid materials can also be used as precursors for the laser synthesis of nanoparticles (laser ablation method). However, this method is generally used to synthesise small amounts of products.[267]

Gas-phase syntheses are usually continuous processes and can produce a large amount of products, while liquid-based syntheses are often batch processes and are difficult to scale up. In addition, batch processes may result in product characteristics which vary from one batch to another.[222] Gas phase processes were also demonstrated to be relevant to the synthesis of carbon coated magnetic core/shell structures which are desired for many technological applications. However, these methods revealed disadvantages. The particles produced by gas phase methods are normally polydisperse and aggregated. Obtaining non-aggregated nanoparticles and good control over size and shape is still a challenge.

1.4.8 Other synthesis methods

Other approaches such as the polyol process and the sol-gel method have been developed and extensively utilised for the synthesis of magnetic nanoparticles. The polyol process, originally developed by Fievet *et al.*,[268] has been widely used for the synthesis of a variety of magnetic nanoparticles.[269-279] In this method, a suitable starting compound (precursor) is suspended in a liquid polyol. The system is then heated to a given temperature, normally the boiling point of the polyol. The polyols (usually polyethylene glycols) serve as solvent, reductant and as stabilising agent to control the growth and to

prevent the aggregation of the particles. The precursors can be hydroxides, inorganic salts, acetate and acetylacetonate compounds. Varying the experimental parameters such as precursor concentration, reaction temperature, pH and type of polyol allows to control the size, shape and aggregation of the particles.[269,275,276,278-280]

The polyol process can produce particles with good control of size and shape. Because the relatively high temperature of the synthesis, the particles produced by this method are normally of high crystallinity. The particles prepared by the polyol process can disperse in aqueous media as their surface is coated by hydrophilic polyol ligands.[277]

The sol-gel technique is based on the hydrolysis and condensation of precursors in aqueous or alcohol media under acidic or base conditions. This method is a suitable approach to synthesise oxide nanomaterials.[281-286] In the sol-gel method, a solution of precursors in the form of metal alkoxides or inorganic salts (a ''sol'') is initially hydrolysed in the presence of either water or alcohols, after which the precursors undergo condensation reactions followed by polymerisation reactions (gelation) to form a three-dimensional network of metal-oxide bonds. Final products are obtained by densification of the gel via removal of the solvent. The system parameters such as nature of the solvent, temperature, pH, precursor concentration and agitation strongly influence the structure and morphology of the final products.[286-288] For example, the solvent and the pH affect the kinetics and the hydrolysis and condensation reactions as well as isoelectric point and stability of the sol, thus govern the aggregation and size of particles. The advantage of this method is that it is a cheap and low temperature technique that allows to synthesise multiple component nanomaterials with good control over their chemical composition. However, the particles obtained by sol-gel processes are generally amorphous. Calcining may be required to improve the crystallinity of the sample. This step often leads to agglomerated particles.

1.5 Synthesis of core/shell structures

Core/shell nanoparticles with magnetic cores and an inorganic shell have attracted great attention for the combined functionalities of cores and shells, which provide them with substantial potential applications in biomedicine and technology. At the nanoscale, nanoparticles tend to aggregate to minimise their surface energy, associated with their high surface area to volume ratio. Therefore, coating them with an organic ligand shell is a critical requirement to protect the nanoparticles from aggregation. Many materials such as iron, cobalt, nickel and their alloys are extremely sensitive to oxygen. Solely encapsulation with organic molecules is possibly not enough to protect these materials from oxidation. Coating nanoparticles with an inorganic layer of noble metals, silica or carbon may provide more efficient protection of the core. Moreover, the inorganic coating can provide a very effective platform for attachment of molecules. For example, the surface of Au coated magnetic nanoparticles can easily be modified with thiolate-molecules, since the strong interaction between gold surfaces and thiol functional groups is well known and characterised. Figure 1.13 illustrated the structure of a core/shell nanoparticle.

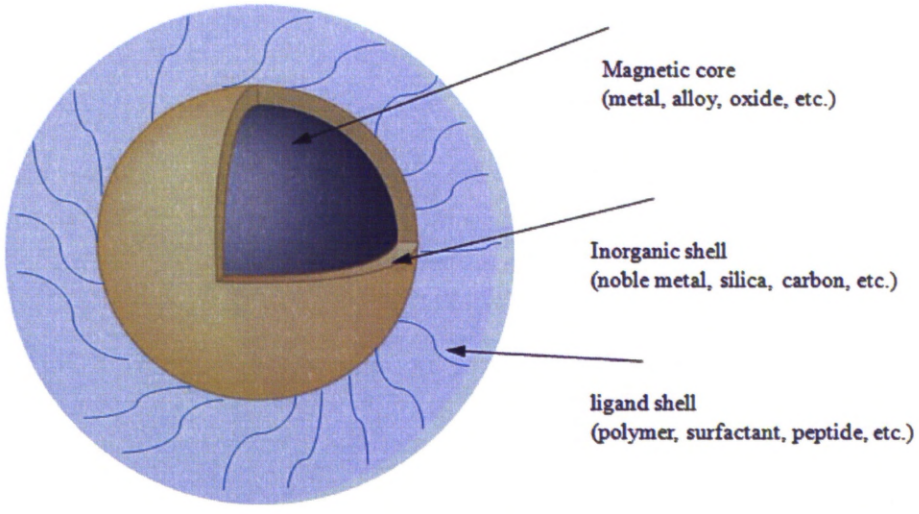

Figure 1.13: Illustration of a core/shell structure.

This section will focus on the synthesis of magnetic nanoparticles coated with silica, a noble metal or carbon. Other shells of materials such as quantum dots or oxides are also briefly mentioned. The advantages and disadvantages of each synthetic method are also discussed.

1.5.1 Core/shell structures with silica shell

Silica coating is one of the most popular techniques for the preparation of core/shell structures. The biocompatibility and the well characterised routes for surface modification have made silica a popular material for many biomedical applications. The coatings have generally been carried out through the Stober method[289,290] or the reverse micelle method,[291-293] and can be used for both hydrophilic and hydrophobic nanoparticles with a wide range of sizes, from a few nanometres to 100 nm. For example, using the Stober process, Ohmori and co-workers coated hematite spindles with silica by precipitation of tetraethyl orthosilicate (TEOS) onto hematite cores in the presence of ammonia. The shell thickness was controlled by varying precipitation times.[290] Chen *et al.* prepared 10 nm iron oxide nanoparticles and coated these with a silica shell of 20 nm thickness using the microemulsion method.[291] The surface of the particles was then modified with organic fluorescent molecules of N-1-(3-trimethoxysilypropyl)-N'-fluoresceyl-thiourea to form bifunctional optical and magnetic nanoparticles. These core/shell structures were successfully used for tracking human bone marrow stem cells. Kim *et al.* developed a procedure for the synthesis of silica coated magnetite nanoparticles using an "*in situ* reverse micelles" method.[294] The silica shell was formed by simply adding TEOS to the reverse micelle solution during the formation of the magnetite cores. The size of the magnetic core and the shell thickness were controlled by adjusting water/surfactant ratio and the amount of TEOS. The surface of the Fe_3O_4@silica core/shell structures was functionalised with NH_2 by mixing TEOS with 3-aminopropyltriethoxysilane (APS).[294] Using the reverse micelle

process, Yi *et al.* established a method to synthesise silica coated bifunctional optical and magnetic hybrid materials consisting of Fe_2O_3 and CdSe nanoparticles.[295] The maghemite nanoparticles and QDs were prepared separately in an organic solvent before adding to reverse micelles for silica coating.

Although substantial literatures exist for the silica coating of nanoparticles, the size of most silica coated nanoparticles is typically several tens of nanometres to micrometres. It is difficult to obtain core/shell structures with a shell that is just a few nm thick. Moreover, silica coating using the above processes is often used with dilute solutions of particles, less than 0.1 mg mL^{-1}, to prevent the particles from precipitation and aggregation, which makes the synthesis difficult to scale-up. To overcome these issues, Jana and co-authors developed a procedure to fabricate magnetic nanoparticles coated by a silica shell of just 2-5 nm thickness, which is easy to scale up to the multigram level.[296] In their work, instead of using the Stober or microemulsion methods involving TEOS, the authors used trimethoxysilanes as silica sources to coat hydrophobic pre-synthesised Fe_3O_4 nanoparticles and used toluene as the solvent. Both Fe_3O_4 nanoparticles and silanes disperse very well in toluene, enabling the use of a high concentration of the nanoparticles and the silanised nanoparticles (silica coated nanoparticles) were precipitated from this phase. The precipitation of the silanised nanoparticles restricted the growth of the silica shell and inhibited particle-particle cross-linking. In addition, the amine (NH_2) functional group of the silane molecules made the silanised nanoparticles water-dispersible and simple to conjugate with biomolecules such as antibodies.

Despite the common use of such silica coatings, most work has involved coating oxide,[291,294,295,297] ferrite[292] or alloy cores,[298-300] all of which are chemical stable. There are only a few reports on coating magnetic nanoparticles of Co or Fe transition metals with silica.[151] In addition, an amorphous silica shell is frequently formed as TEOS is deposited

on magnetic cores. Thus, in the cases of Co or Fe, the silica shell needs to be thick enough to protect the sensitive cores from oxidisation.[151]

1.5.2 Core/shell structure with noble metal shell

Recently, coating magnetic nanoparticles with a shell of noble metal has attracted considerable attention due to the combination of the novel combined properties from the magnetic and the optical components and the large knowledge base on forming ligand shells on noble metals such as Au. Coating a magnetic core with a noble metal shell improves not only the chemical stability, but will also potentially provide improved biocompatibility and catalytic activity alongside the magnetic properties of the magnetic nanoparticles. Among the noble metals Au, Ag and Pt, Au has received the most attention due to its unique optical properties. In addition, the chemical inertness of Au and its accepted biocompatibility (despite the fact that it binds many biomolecules) and ease of biofunctionalisation makes such core/shell nanoparticles extremely attractive for many biomedical applications. In order to make core/shell nanoparticles numerous synthetic techniques have been developed, including reverse micelle methods and seeding methods, which involve reducing Au salts by a mild reductant (e.g., hydroxylamine,[301] or sodium citrate[302] for synthesis in water or hexadecanediol,[303] oleylamine[304-306] for synthesis in organic media) in the presence of magnetic cores as seeds, and coating methods involved redox-transmetalation process.[214,307-309]

Reverse micelle methods have been widely used to coat Au over a variety of magnetic nanoparticles including alloys, (e.g. FePt,[310] Ni_3Au,[311] or FeNi[312]), oxides (e.g. Fe_3O_4)[313,314] and metals (e.g. Fe, Ni)[212-214] The magnetic cores can be either hydrophilic or hydrophobic and the shell thickness can be tuned by changing amount of Au salt. For example, Fu *et al.* have described a method for the synthesis of FePt@Au nanoparticles in the reverse micelles consisting of CTAB, n-butanol, heptane and water. A mixture of sodium

borohydride ($NaBH_4$) and hydrazine hydrate ($N_2H_4.H_2O$) was used as reductant.[310] Irudayaraj *et al.* reported the synthesis of Fe_3O_4@Au nanoparticles,[313] where the magnetite cores were first prepared in reverse micelles of CTAB using 1-butanol as co-surfactant and octane as the oil phase. A gold shell was achieved by successively adding $HAuCl_4$ and $NaBH_4$ reverse micelle solutions into pre-formed magnetite solutions. The core/shell nanoparticles were then bioconjugated with DNA and used in a DNA sensor.[313] Using the same procedure O'Connor[212] and Kauzlarich[213] reported the synthesis of Fe@Au nanoparticles. The growth mechanism and oxidation resistance of the core/shell nanoparticles were investigated. Interestingly, it was observed that whilst XRD could not detect the presence of an iron oxide phase, SQUID data showed a reduction of 50 % in magnetic moment after a 5 day exposure of the nanoparticles to air. The less effective oxidative resistance of Au shell was ascribed to the rough Au surfaces.[213]

One of the main issues in the reverse micelle methods is to control the shell homogeneity and consequent monodispersity of the core/shell nanoparticles. In some cases, the magnetic core is not in the centre of micelles, resulting in a heterogeneous shell, which could not protect the core from oxidation.[315]

Together with reverse micelle techniques, seeding methods have been intensively studied for the synthesis of core/shell nanoparticles. Here, pre-formed magnetic nanoparticles were used as seeds for the deposition of Au shell(s) and the coating could be carried out in either aqueous or organic media. To prevent the homogenous nucleation, which results in the formation of separated particles of the shell materials, a mild reductant has generally been used. For example, Williams *et al.* reported on the synthesis of water-dispersible Au coated Fe_3O_4 magnetic nanoparticles by reducing of Au^{3+} on the surface of Fe_3O_4 via iterative hydroxylamine seeding in water in the presence of citrate.[219] Using the same procedure, Chung and co-workers prepared Fe_2O_3@Au nanoparticles and used them as carriers for the immobilisation of hexa-arginine-targeted esterase (Arg_6-esterase).[316] The

immobilised Arg_6-esterase was reported to remain active after seven iterative uses. Krishnan *et al.* reported a successful synthesis of monodisperse Au coated Co nanoparticles by reducing an organo-gold compound with oleylamine in toluene.[85] The authors claimed that the use of a $[(C_6H_5)_3P]AuCl$ precursor, which exists as a stable complex in toluene, prevented the direct reaction of Au with the Co surface, was one of the key factors for the successful synthesis.

Sun *et al.* coated Au and Ag on the surface of Fe_3O_4 nanoparticles by reducing $HAuCl_4$ in a chloroform solution using oleylamine as reductant.[305] The obtained core/shell nanoparticles were transferred to water by a mixture of sodium citrate and CTAB and used as seeds for further coating with Ag or Au. Zhong *et al.* synthesised Fe_3O_4@Au core/shell nanoparticles by reduction of Au acetate using hexadecanediol in the presence of pre-synthesised Fe_3O_4 nanoparticles in phenyl ether.[303] Using a hetero-interparticle coalescence process, the same group prepared Au coated Fe_2O_3 nanoparticles. The core/shell nanoparticles were prepared by mixing pre-formed 4.4 nm Fe_2O_3 and 2 nm Au nanoparticles in toluene at 149 - 160 °C. Particle size was controlled in the range of 5 to 100 nm by varying the ratio of Au to Fe_2O_3 nanoparticles or changing capping ligands. The hydrophobic Au coated Fe_2O_3 nanoparticles were then transferred to water by ligand exchange with mercaptoundercanoic acid (MUA) and used for protein separation.[317]

Recently, a synthesis technique involving a redox-transmetalation process has been reported to prepare core/shell nanoparticles. In this method, pre-formed magnetic cores were used as both reductant and seed or template for coating.[308,318] This method offers some advantages, such as its simplicity, its independence from additional reductants and the production of monodispersed core/shell nanoparticles. In addition, the reduction process occurs on the surface of core templates, avoiding homogenous nucleation, which would result in the production of undesired new nanoparticles. Using the transmetalation process, Cheon and co-workers have synthesised magnetic Co nanoparticles coated with a

variety of metals including Au, Pt, Pd and Cu. Magnetic Co cores were prepared by thermal decomposition of $Co_2(CO)_8$ in toluene. Monodisperse core/shell nanoparticles were produced by reducing metal ions of Au, Pt, Pd and Cu on the Co surface at high temperatures.[308, 319] With a combination of reverse micelle and transmetalation approaches, Chen *et al.* prepared Ni@Au core/shell nanoparticles.[214,307] The diameters of the core/shell nanoparticles (core diameter and shell thickness) were tuned from 5-21 nm for core diameter and 3-10 nm for shell thickness by changing the size of droplets and the amount of Au precursors, respectively.

The redox-transmetalation method does have its own drawbacks. The gaps or cavities at the interface between the core and the shell are prone to produce defects. As the ions of the core materials diffuse out of the structure, in many cases, hollow structures are formed instead of core/shell nanoparticles.[157,320,321] Furthermore, the decrease in the size of the magnetic core due to the diffusion will lead to an undesired reduction in magnetic properties.

1.5.3 Core/shell structure with carbon shell

More recently, carbon coated magnetic nanoparticles have received increasing attention due to their potential for high chemical stability and biocompatibility.[22] In comparison with silica coatings, which have been most successfully applied to oxide and ferrite systems, carbon coatings are generally applied to metal or alloy magnetic nanoparticles, and thus have higher magnetic moment than those of oxides or ferrites.[52,243,246,322,323]

Dai and co-workers reported the preparation of single layer carbon coated CoFe nanoparticles with excellent magnetic properties and r_1 and r_2 relaxivities utilising scalable chemical vapour deposition (CVD).[52] The particles could be dispersed in water by surface modification with phospholipid molecules before loading into mesenchymal stem cells and showing high negative contrast enhancement in magnetic resonance imaging (MRI). Stark

and co-workers prepared highly stable, non-aggregated Co nanoparticles coated with a carbon shell using an one step flame spray process.[246] The carbon surface could be covalently functionalised with different functional groups. The obtained Co@C core/shell nanoparticles showed high stability in harsh conditions (e.g. pH 0-14). Guo *et al.* developed a method for carbon coating Fe_3O_4 nanoparticles that uses a gas-liquid interfacial reaction to prepare magnetic cores before employing a hydrothermal process to coat carbon shells. The Fe_3O_4@C nanoparticles indicated excellent cycling and rate performances as anode material for lithium-iron batteries.[324]

Although advantageous properties of carbon coated magnetic nanoparticles and numerous synthetic methods have been developed for carbon coatings. It still lacks an effective synthetic technique. Thus the magnetic@carbon core/shell nanoparticles obtained by the aforementioned methods are often in polydispersed and aggregated forms.[243,324,325] The synthesis of monodispersed and isolated carbon coated magnetic nanoparticles is still a challenge.

1.5.4 Core/shell structure with other shells

Although less studied than silica, gold or carbon coatings, oxide coatings for magnetic nanoparticles have attracted attention because of the simplicity of the synthesis, since one of the simplest techniques to coat magnetic nanoparticles is to passivate them with an oxide shell. With a pure metal core, passivation with an oxide layer, which could be obtained by controlled oxidation, could protect the sensitive core from further oxidation. For instance, Bonnemann *et al.* have developed Co@CoO core/shell nanoparticles by smoothly oxidising the as-prepared Co nanoparticles. The stable CoO outer shell could protect the inner Co core from further oxidation.[326] The same group have extended their method for passivation of Fe and CoFe alloy nanoparticles. In their report the authors indicated that reaction time and oxygen content were crucial factors for the formation of a

stable oxide shell.[327] Peng and co-workers have developed a method to prepare Co@CoO nanoparticles by oxidising gas-phase forming Co nanoparticles in a plasma-gas apparatus. The obtained nanoparticles were monodisperse with a uniform CoO shell.[328]

In many cases, coating magnetic cores with oxide shells such as iron oxides or ferrites not only protects the core from oxidation, but also provides a platform for further functionalisation. Moreover, as these oxide and ferrite shells are magnetic materials, the magnetic moments of the core/shell structures could be significantly enhanced when compared with those of magnetic@silica or Au core/shell nanoparticles. For instance, Xu and co-workers have developed a procedure for the synthesis of iron oxide coated Co and SmCo nanoparticles via a seeding process.[329] The iron oxide surface of nanoparticles was then functionalised with nitrilotriacetic acid molecules utilising dopamine as robust linker. Using a seeding method, Sun *et al.* synthesised Co nanoparticles coated with a ferrite shell (Fe_3O_4 or $MnFe_2O_4$).[330] In their synthesis, Co@ferrite core/shell structures were prepared by heating a mixture of pre-formed and purified Co nanoparticles and $Fe(acac)_3$ in the presence of oleic acid surfactant and 1,2-hexadecanediol as accelerating decomposition agent (Figure 1.14). Both Co and Co@ferrite core/shell nanoparticles could be transferred from organic medium to water by ligand exchange with PEGylated phospholipids.[330] Whilst hydrophilic Co nanoparticles were not stable, as they were quickly oxidised and aggregated in buffer solution, Co@ferrite core/shell nanoparticles retained a high magnetic moment and exhibited enhanced colloidal stability in buffer solution.

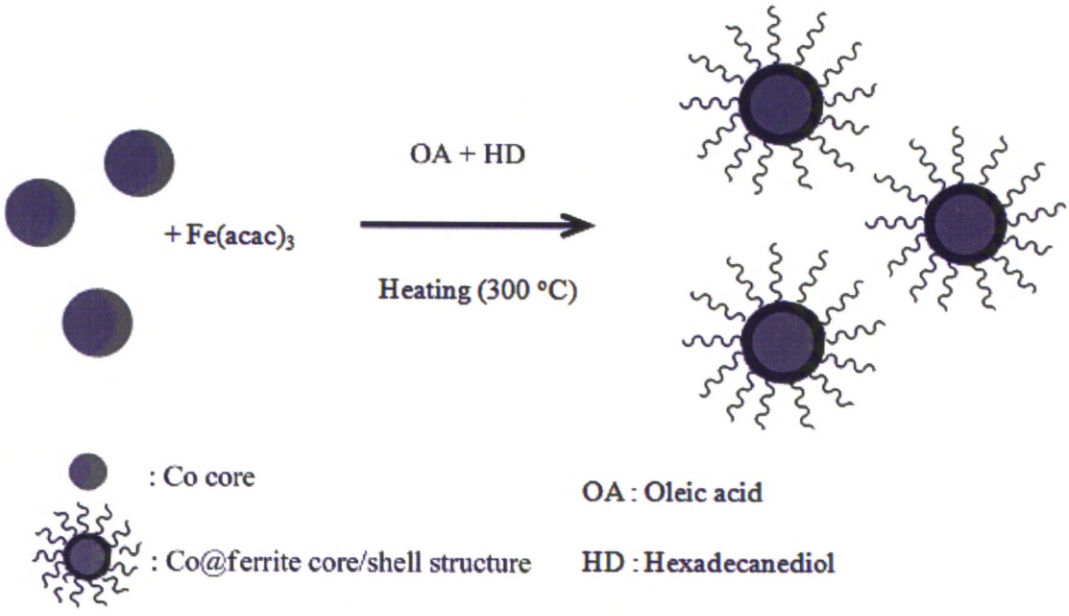

Figure 1.14: Scheme of the synthesis of Co@ferrite core/shell structure by thermal decomposition of $Fe(acac)_3$ in the presence of Co cores.

Coating magnetic nanoparticles with a semiconducting layer (quantum dots) has also received great interest, since the core/shell structures possess combined magnetic and fluorescent properties. For example, Klimov *et al.* have reported the synthesis of Co@CdSe core/shell nanoparticles by controlled CdSe decomposition onto pre-formed Co nanoparticles. The core/shell structures were shown to retain the magnetic properties of the Co core, while revealing the luminescent optical properties of the CdSe shell.[331] Xu and co-workers have developed a method for the synthesis of FePt coated CdSe or CdS. By changing reaction conditions such as precursor addition sequence, temperature or reaction time the authors were able to tune the morphology (core/shell spheres, nanosponges or heterodimer structures). These hybrid structures exhibit both the magnetic and the optical properties of their individual components.[332]

Besides the novel combined magnetic and fluorescent properties of QD coated magnetic nanoparticles, the well understood surface chemistry in the synthesis and biofuntionalisation of quantum dots gives these core/shell structures advantages in potential biomedical applications. However, there is still a challenge related to the cytotoxicity of the quantum dot shell, which needs to overcome.

1.6 Surface modifications and bioconjugations

In the section 5, the coating of magnetic nanoparticles with an inorganic shell has been discussed mainly in terms of chemical synthesis methods that improve the chemical stability, biocompatibility or physical properties of the core/shell structures. In this section, the focus is on the surface modification of the nanoparticles using organic molecules, with particular regard to water-dispersibility, colloidal stability and bioconjugation of magnetic nanoparticles.

For biomedical applications, one of the critical requirements for magnetic nanoparticles, as continually reiterated in the literature, is that they are both dispersible and colloidally stable in aqueous and physiological environments.[23] In addition, the surface of the nanoparticles should have specific sites for biofunctionalisation by the attachment of various bioactive molecules.[23,33,34] For these purposes, post-synthesis surface modification of the nanoparticles is often used. There are several existing methods for such modifications, of which ligand exchange reaction and wrapping/encapsulation around hydrophobic nanoparticles with a hydrophilic layer are the most common and versatile routes.[333] A list of common hydrophilic surfactant agents utilising for the surface modification of magnetic nanoparticles is shown in Table 1.3.

Table 1.3: The common hydrophilic surfactant agents for the surface modification of nanoparticles

Materials	Surfactant agents	Reference
Fe_3O_4	Dopamine ($(OH)_2C_6H_3CH_2CH_2NH_2$)	329, 334, 335
$CoFe_2O_4$, Fe_3O_4@Au	mercaptoundecanoic acid ($HSC_{11}H_{22}CO_2H$,), mercaptohexadecanoic acid ($HSC_{15}H_{30}CO_2H$) and L-aspartic acid ($HO_2CCH(NH_2)CH_2CO_2H$)	303, 313, 316, 336-339
Fe_3O_4, Co@SiO_2 Fe_3O_4@SiO_2, Fe_2O_3@CdSe	(3-aminopropyl)triethoxysilane ($NH_2(CH2)_3Si(OC_2H_5)_3$)	296, 340-345
Fe_3O_4 Fe_3O_4@SiO_2	Trimethoxyl polyethylene glycol (HN_2, SH, COOH)-$CH_2(CH_2OCH_2)$nCH2-Si$(OMe)_3$	345, 346
Fe_3O_4	dimercaptosuccinic acid ($SH(CH)(SH)CO_2H$)	308, 347-352
FePt	dopamine terminated PEG ($(OH)_2C_6H_3CH_2CH_2NH_2(CO)$-$CH_2CH_2(CO)(C_2H_4O)_nOH$), thiolated nitrilotriacetic acid ($(SH(CH_2)_n(CO)NH(CH_2)_4(HO_2C)CHN(CH_2CO_2H)_2$)	353, 354

With ligand exchange methods, the ligands on the surface of the nanoparticles such as the polymer or surfactant used during the synthesis are replaced. The new ligand molecules have to impart the properties described above to the nanoparticles. Consequently, they need to be chosen carefully for every nanoparticle material. For example, carboxylate and phosphate have been shown to bind well to oxide sufaces.[355-357] Thiols are known to bind strongly to the surfaces of noble metals such as Au and Pt.[358,359] Thus, hydrophilic ligands with carboxylate, phosphate, or thiol groups are suitable for ligand exchange processes of oxides, or noble metal nanoparticles, respectively. Cheon and co-workers have prepared monodisperse Fe_3O_4 nanoparticles with controllable size (4-12 nm). Hydrophobic Fe_3O_4 nanoparticles were transferred to water by ligand exchange using dimercaptosuccinic acid (DMSA). Here, the DMSA molecules were bound to the surface of the nanoparticles through their carboxylic group and a stable, hydrophilic ligand shell was attained via disulfide cross-linkages between the ligands. The attachment of biomolecules such as

antibodies could be obtained through the remaining free thiol or carboxylic groups.[351,360] Turro *et al.* have recently designed a ''universal ligand'' for ligand exchange of Fe_2O_3 nanoparticles. Their ligands, at one terminus, contain either a phosphate or a carboxylate functional group, which serves as a strong anchor to the surface of the nanoparticles, and azide or alkyne groups at the other end, provide functionality for further surface modification through a so-called ''click'' chemistry reaction.[361]

Peng *et al.* have designed a new class of ligands, poly(ethylene glycol) (PEG) terminated organic dendrons, with a hydroxamic acid group for ligand exchange on hydrophobic Fe_3O_4 nanoparticles.[362] The hydroxamic acid group of ligands are known to bind strongly to oxides and so provide a robust anchor to attach ligands to the particle surface, whilst the multiple PEG oligomer branches keep the nanoparticles dispersed in water dispersing and stabilise them from aggregation.

Recently, dopamine derived molecules have been successfully used for ligand exchange of hydrophobic nanoparticles of oxide materials. Two hydroxyl groups on the dopamine molecules have been shown to bind strongly to oxide materials.[329,363,364] Therefore, they served as robust anchors for the attachment of the molecules to the surface of nanoparticles.

Xu and co-worker reported, for the first time, the ligand exchange of Fe_2O_3 coated Co and SmCo core/shell nanoparticles utilising dopamine ligands. By immobilising functional molecules such as nitrilotriacetic acid (NTA) on the surface, the nanoparticles could be easily conjugated to proteins for magnetic separation.[329] Sun *et al.* have developed anticancer agents consisting of conjugated Fe_3O_4 nanoparticles for drug delivery. Monodisperse hydrophobic Fe_3O_4 nanoparticles were synthesised in an organic medium and transferred to water by ligand exchange utilising dopamine modified PEG and then were conjugated to anticancer agents such as 6-hydroxy-chromone-3-carbaldehyde. The authors reported that water solubility of the chromone was increased from less than 2.5 μg

mL^{-1} for the free agent up to 633 μg mL^{-1} when conjugated to the nanoparticles.[365] The structure of some common hydrophilic ligands using to stabilise magnetic nanoparticles in aqueous solution is shown in Figure 1.15.

Besides carboxylic, phosphonic, hydroxamic or dopamine functionalised ligands, thiol-derived molecules have also been extensively used for ligand exchange.[317,354,366,367] Thiol groups strongly bind to noble metals such as Au and the chemistry of thiol-Au bonding is well understood. Therefore, magnetic nanoparticles coated with noble metal shells, or alloy nanoparticles such as FePt, CoPt nanoparticles are suitable for these ligands.[302,304,306,308,313,316,317,338,354,368-370]

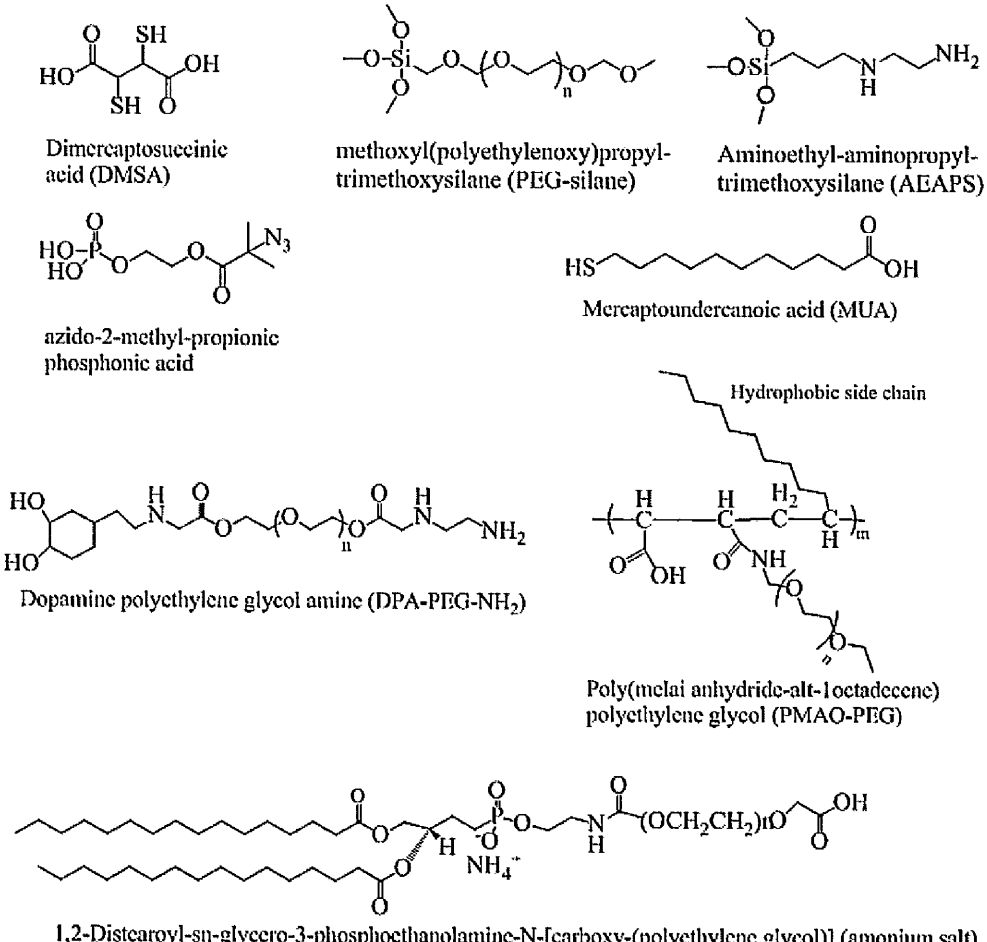

Figure 1.15: Structure of some common hydrophilic ligands using for the surface modification of magnetic nanoparticles.

Although ligand exchange methods are direct and fairly simple, there are certain disadvantages of this approach. The ligand molecules have to be able to strongly coordinate to the surface of inorganic nanoparticles. This means each ligand molecule with a specific functional group has to be individually chosen for each nanoparticle material. Thus, it lacks a general protocol that works for all materials. In addition, there are many materials to which no ligand could strongly coordinate.[333] Finally, the effects of any ligands that have not been exchanged and defects in ligand shells has not yet been the subject to any serious investigation.

In contrast to the above methods involving ligand exchange on the surface of nanoparticles, encapsulation methods are based on the addition of an extra layer around the hydrophobic surfactant layer formed during synthesis in organic solvents. To accomplish this, amphiphilic molecules are often used. The hydrophobic part of the ligand coordinates to the hydrophobic surfactant layer on the nanoparticles via hydrophobic interactions, whereas their hydrophilic part points outward into the solution to facilitate water dispersibility.[333,371-373] For example, Parak *et al.* have designed an amphiphilic polymer, poly(isobutylene-alt-maleic anhydride) modified with alkyl chains, to encapsulate hydrophobic nanoparticles. Hydrophobic nanoparticles of different types: Au, Fe_3O_4 and CdSe@ZnS have been coated with this polymer by hydrophobic interaction between the alkyl chains of the polymer and the surfactant molecules on the particles. The hydrophilic backbone part of the polymer provided not only water-dispersibility for the nanoparticles, but also a platform for bioconjugation.[371] Colvin and co-workers have successfully transferred monodisperse Fe_3O_4 nanoparticles to water utilising poly(maleic anhydride-alt-1octandecene) (PMAO) modified with polyethylene glycol, amphiphilic polymer. The PMAO-PEG modified nanoparticles were extremely stable in water and physiological buffers and exhibited negligible cytotoxicity to human breast cancer cells and human dermal fibroblast cells (see Figure 1.15 for structure of the polymer).[373] Other amphiphilic

molecules, such as block copolypeptide (poly(EG_2-Lys)100-b-poly(asp)$_{30}$), distearoyl phospholipid modified polyethylene glycol or poly (styrene$_{250}$-block-acrylic acid$_{13}$) have been used to transfer hydrophobic magnetic nanoparticles into water (see Figure 1.15 for structure of the polymer).[374-377]

The advantage of the encapsulation method is its generality, as the same procedure can be applied to almost any nanoparticles, regardless of the core material. However, this approach has disadvantage. In particular, the final size of the nanoparticles after coating is rather large due to the extra ligand layer, which may interfere in some biological applications.[333]

Although there has been substantial progress in transferring magnetic nanoparticles to water, the major successes have been attained with oxides or FePt alloy nanoparticles, i.e. materials which do not suffer from oxidation. With pure metal nanoparticles such as Fe, Co, Ni or alloys of these, which are easily oxidised, it is still a major challenge to obtain stable and water-dispersible nanoparticles.

1.7 Characterisation techniques of nanoparticles

Characterisation techniques using in the thesis

1.7.1 Transmission electron microscopy

Transmission electron microscopy (TEM) is probably the most important technique to characterise nanomaterials.[378] In TEM, electrons are emitted from a field-emission or thermionic electron gun and accelerated by a voltage between 100 - 400 kV and then passed through a condenser electron lens system until they interact with the sample at the objective lens system.[378] After penetrating the sample, the electrons travel through a series of additional magnetic lenses to a viewing 'screen' or a CCD camera.[378,379] The electron

lens, which usually consists of coils of copper wires surrounding soft iron pole pieces with a hole drilled through them, is one of the most important components in a TEM. Electron lenses act in a way emulating that of glass lenses in an optical microscope.[378] By varying the current passing through the coils, the focusing of the beam or magnification of an image can be controlled. In comparison with an optical microscope, TEM offers much better resolution. Theoretically, the imaging resolution δ of a microscope is determined:[378]

$$\delta \approx 0.61\lambda/\mu\sin\beta \qquad (1.5)$$

where λ is the wavelength of the radiation, μ is the refractive index of the viewing medium, and β is the semi-angle of collection of the magnifying lens which is determined by the ratio of the focal length to the diameter of a lens. For a light microscope, the wavelength of light is in the region of 400-700 nm, and thus the resolution of a good optical microscope is the range of 200-400 nm.[378,380] In a TEM, the wavelength λ of an electron accelerated at voltage V is described by expression: [378,381]

$$\lambda = h/(2m_0eV)^{1/2} \qquad (1.6)$$

where h is Planck's constant, m_0 is the rest mass of an electron, e is the electron charge and V is the accelerating voltage. With accelerating voltages of 100 - 400 kV, the wavelength of radiation is in a range of 0.037 to 0.016 Å. The theoretical image resolution of a TEM can be up to 0.02 Å. However, as the imperfection of the electron lenses and the divergent of the electron beam, the actual resolution of the best HRTEM is about 0.5 Å.[378,381]

With a TEM, a variety of data can be obtained including images, diffraction patterns and spectra. These data can disclose information about the size, shape, crystallinity and chemical composition of the analysing samples.[379,382,383] This section will discuss about imaging technique, a brief discussion of the TEM based electron diffraction and spectroscopy techniques will be presented in the section 1.7.6.

TEM imaging is based on the contrast within a sample, which arises from scattering of the incident electrons beam with the sample. The contrast is usually comprised of either mass-thickness contrast or diffraction contrast.[379]

Mass-thickness contrast occurs when incident electrons interacting with high or low atomic number (Z) elements and going through thick or thin samples. High Z elements scatter electrons stronger than low Z elements, so high Z (electron dense) elements appear darker than the low Z ones.[379] Thickness of the sample also affects the contrast. Thicker sections of the sample will scatter more electrons resulting in stronger contrast than the thinner section.

Diffraction contrast occurs when the incident electron beam interacts with a crystalline specimen.[379] Electrons interacting with specific lattice planes will be coherently elastically scattered. As a result, some regions will appear darker than the others depending on the orientation of the crystal to incident beam. TEM images are constructed relying on the mass-thickness contrast. Strongly scattered electrons are filtered by using apertures and only weakly scattered or un-scattered electrons are received by a CCD camera and processed by computer software or recorded on film. The higher contrast within the sample, the sharper images are obtained. This imaging technique is used to study the size and morphology of the sample.

In this work, TEM images of the samples were obtained using a FEI Tecnai G^2 120 kV TEM, operated at 100 kV and visualised using analySIS software. The diameter (d) of the nanoparticles and their size distribution were taken as the mean of minimum 200 nanoparticles measured from enlarged photographs using Bersoft Image Measurement 1.0 software. HRTEM images and electron diffraction were obtained using a Titan 80/300 (FEI, 300 kV) operated at 300 kV.

Preparations of specimens for TEM

Specimens of Co nanoparticles for inspection by TEM were prepared by casting a drop (5 μL) of a dilute solution of nanoparticles on a TEM grid and letting it to dry under ambient condition for at least one.

Specimens of CoPt nanoparticles for inspection by TEM were prepared analogously. Before the preparation of TEM samples, purification of CoPt nanoparticles was carried out by centrifugation at 6,000-12,000 rpm for 10 minutes. The supernatant was discarded, and the sediment was redispersed in water under sonication. The procedure was repeated at least two times before preparing samples for TEM.

Specimens of cobalt iron alloy and cobalt ferrite nanoparticles for inspection by TEM were prepared in the same way after purification. In a typical purification process, 0.5 mL solution of as-prepared nanoparticles was mixed with 0.5 mL ethanol. The nanoparticles were collected using a magnetic bar, and the supernatant was discarded. The nanoparticles were then dissolved in 0.5 mL hexane and further precipitated by adding 0.5 mL of ethanol. The precipitation-redispersion procedure was repeated 2 more times, and the nanoparticles were finally dissolved in 1 mL hexane or toluene before preparing for TEM.

1.7.2 X-ray powder diffraction (XRD)

After the discovery of X-rays by Rontgen in 1895 and the first diffraction experiments from a single crystal by Laue in 1912 and from a powder sample by Friedrich in 1913, X-ray diffraction (XRD) has become a useful tool in the characterisation of crystal structure and phase composition of different materials.

X-ray diffraction exploits the wave nature of X-rays and their interaction with a crystalline sample. In a X-ray diffractometer, X-ray radiation is generated within a vacuum tube from the impact of high energy electrons with a metal target, usually Cu or Co, and exits through a window composed of a light element, normally beryllium.[384,385] Inside the

X-ray tube, electrons are emitted from a cathode via electrical heating of a filament (usually tungsten). These electrons are then accelerated towards the anode by a high electric field.[384] If the accelerating voltage is high enough (30-60 kV), the incoming electrons have sufficient energy to eject electrons from the K shell of the Cu or Co anode, a characteristic X-ray spectrum of the target metal with sharp intense peaks is generated.[384, 385] When a beam of X-rays strikes a crystal sample, it is diffracted by electrons of atoms. The diffracted rays interfere with each other. The interferences can be either destructive or constructive. The constructive interference, which results in a signal, occurs only when the incident beam interacts with the sample at a specific angle (θ_B). The angle θ_B, known as Bragg angle, relates to the wavelength of the x-ray radiation and interplanar spacing d of the crystal by Bragg condition:

$$n\lambda = 2d_{hkl} \sin(\theta_B)$$

where n is an integer. The spacing d of various parallel atomic planes in a crystal can be calculated by using X-rays of known wavelength and measuring the theta angle. The spacing d described in Figure 1.16 is generally defined using Miller index hkl notation. A single atomic plane or a set of parallel planes is characterised by its Miller indices (hkl). These indices are determined by the inverses of intercepts on the axes of the plane and then reduce to three integers having the same ratio, usually the smallest integers.[384,386] For example, a plane whose intercepts are 2,2,3, the reciprocals are 1/2, 1/2 and 1/3, having the Miller indices are (332). A plane, which is parallel to an axe, having the corresponding index is zero.

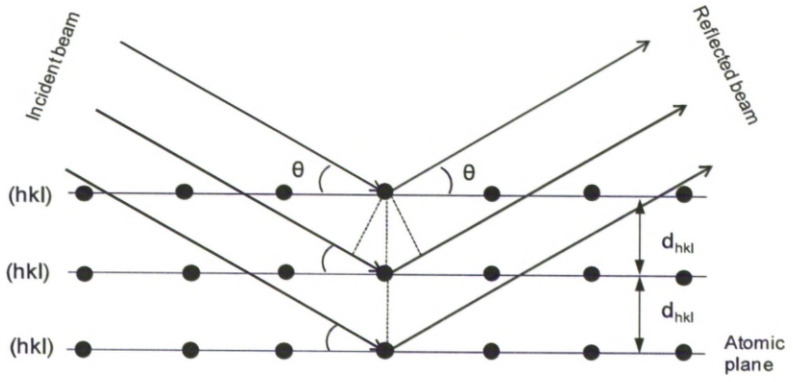

Figure 1.16: Geometrical illustration of Bragg's law (Adapted from ref.[384]).

With an X-ray diffractometer, to acquire the diffraction pattern, a sample is placed on a sample holder made of low X-ray absorption material and is rotated to vary the angle of incident beam (θ). Diffracted X-rays from the sample are collected at detector whose angular position is 2θ. This operation is generally called θ-2θ scanning regime (Figure1.17). There are, however, some configurations where sample was kept fixed during the scan whilst both X-ray source and detector are simultaneously rotated by the same angle of θ.

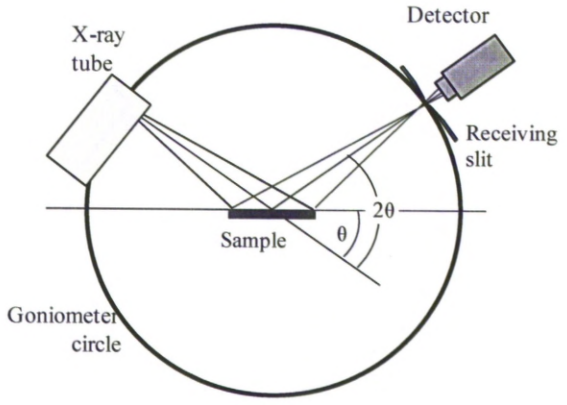

Figure 1.17: schematic configuration of an X-ray diffractometer operates at θ/2θ scanning mode (Bragg-Brentano geometry) (Adapted from ref.[384]).

The collected diffraction data is generally displayed on computer where the diffraction peaks are compared to database of known crystal structures to identify the unknown structures and phases of the investigating sample.

At a nanoscale, the size of crystallites can be determined from diffraction peaks by using the Scherrer equation (equation 1.8):[385,387]

$$t = \frac{K\lambda}{\beta\cos\theta} \qquad (1.8)$$

where t is the crystallite size (angstrom), K is a constant (K = 0.9, typically), λ is the wavelength of the X-ray radiation (angstrom), β is the full width at half maximum of a diffraction peak (radians) and θ is the diffraction angle (radians).

All X-ray diffraction (XRD) patterns of the sample in this work were obtained utilising a Rigaku RINT-2500 diffractometer (Cu $K\alpha$ radiation line λ =1.5408 Å; 40 kV/100 mA) and were recorded at angles between 20° and 90°, with a scan rate of 0.015°/min. The XRD patterns were also analyzed using MDI JADE7 software. Nanoparticle samples were dispersed in hexane, and then a colloidal solution of nanoparticles was deposited on Si (100) substrate followed by the nature evaporation of the solvent.

1.7.3 Superconducting Quantum Interference Device (SQUID)

There are different techniques for measuring the magnetic properties of magnetic materials. The superconducting Quantum Interference Device (SQUID) magnetometer is, the preferred method because of its precision and sensitivity.[38] The basic components of a SQUID magnetometer are its sensing superconducting coils which are separated by thin insulating layers (about 3 nm). These insulating layers are called the Josephson junctions after Brian Josephson who indicated theoretically that coherent Cooper electron pairs in

two superconductors can tunnel through a thin insulating layer between them.[388] The schematic structure of a dc-SQUID sensing device which has two Josephson junctions connected in parallel is shown in Figure 1.18. When there is no magnetic sample present, a Cooper electron pairs in the superconductors tunnelled through the Josephson junctions is not interfered. However, when a magnetised sample goes through the sensing coils of the SQUID, the magnetic flux changes the interference (phase shifts) of the Cooper pairs. The total current going through the superconducting loops changes as the result of changing of magnetic flux.[389] By measuring the current change, the magnetisation of the sample can be determined.

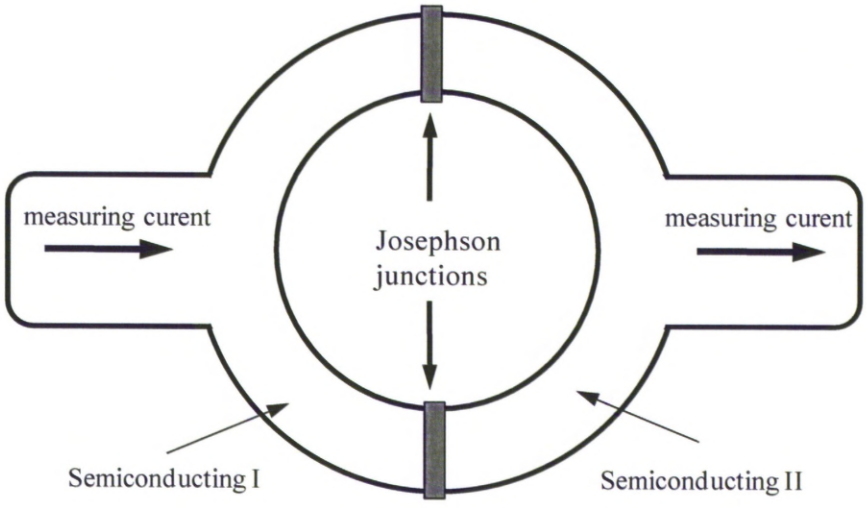

Figure 1.18: The schematic structure of a SQUID sensing device (Adapted from ref.[38])

With the SQUID magnetometer, one can measure the temperature and field dependence of the magnetisation. In the temperature dependence, the zero-field-cooled (ZFC), field-cooled (FC) magnetisation can be measured from which the blocking temperature (T_B) of the magnetic nanoparticles can be determined. At the blocking temperature, the magnetic nanoparticles transform from the ferromagnetic blocked state to the superparamagnetic state upon increasing temperature. In the ZFC measurement, the sample is cooled in zero

magnetic field. A magnetic field is then applied and measurement is conducted with warming. On the other hand, in the FC measurement, the sample is cooled in an applied magnetic field. Here, the FC measurement can be conducted either upon cooling or warming. In the field dependence, one can obtain the hysteresis loop to determine the coercivity (H_C) and remanent magnetisation (M_R) at a certain temperature.

For magnetic nanomaterials, SQUID data provide rich information about magnetic properties of a sample such as phase transformation temperature (blocking temperature), saturation magnetisation, coercivity and remanent magnetisation. In addition, particle size and size distribution, in many cases, can be estimated.[108,390] SQUID is also an effective analytical technique in the investigation of surface oxidisation of magnetic nanoparticles, particularly, those of transition metals such as Fe, Co and Ni. When the ferromagnetic Fe, Co or Ni nanoparticles are oxidised, usually it forms an antiferromagnetic phase (FeO, CoO or NiO) on the surface of the nanoparticles.[326,328] The formation of oxide phase will result in a decrease of the saturation magnetisation because of low magnetisation value of the oxide phase and a shift of the hysteresis loop due to the exchange bias between ferromagnetic and antiferromagnetic phases. Thus, by measuring the hysteresis loop of the sample before and after exposing to the air at different time will tell us that if the sample is oxidised or not and how fast is the oxidisation.[328] This measurement is particularly useful for studying the oxidation stability of the core/shell structure as the oxidisation of the core is difficult to detect by other common analytical techniques such as XPS or XRD.[213]

All magnetic property measurements of the samples in this work were carried out on an RF Quantum Design Magnetic Property Measurement System (MPMS) XL SQUID magneto-meter. Samples were prepared either in powder or in liquid form. 0.5 to 5 mg dried sample or 50-150 µl liquid sample was put into a gel-cap or sealed glass tube, respectively.

1.7.4 Dynamic light scattering

Dynamic light scattering (DLS), also referred to as photon correlation spectroscopy, is a popular method for particle sizing in the colloidal suspensions. This technique is based on the measurement of intensity fluctuations of the scattered light by particles in solution.[391,392] In the colloidal suspensions, particles are in continuous and random movement due to their bombardment with the surrounding solvent molecules. This is known as Brownian motion. The velocity of the Brownian motion or diffusion of the particles relates to the size of the particles. Larger particles move slower, smaller ones move faster. When the sample is illuminated by a laser beam, the particles scatter light. Because of the Brownian motion, the phase relation of the scattered light from different particles and the number of particles in the scattering volume will be changed continuously, which leads to a fluctuation in scattered light intensity.[391] Analysis of this the intensity fluctuation yields information on diffusion processes, and thus particle size can be calculated.[391, 392] The relation between the size of a particle and the diffusion coefficient is described by Stokes-Einstein equation:[391,392]

$$d_H = kT/(3\pi D\eta) \qquad (1.9)$$

where d_H is the hydrodynamic diameter of the particle, k is the Boltzmann's constant, T is the absolute temperature, η is the viscosity of solution and D is the diffusion coefficient of the particles in the solution.

In this work, the hydrodynamic size of nanoparticles was measured using dynamic light scattering, Zeta-sizer Nano S, Malvern Instrument Ltd UK. The optical configuration of the instrument is shown in Figure 1.19. In this configuration, a monochromatic laser beam goes through an attenuator, which allows to control the beam intensity, to the sample cell. Scattered light by the particles is collected using a detector positioned at an angle of 173 degrees to the direction of the incident beam. The signal is then passed to a correlator, where the scattering intensity at successive time intervals is compared to deduce the rate of

the fluctuation of the intensity. Output data of the correlator are further processed by the analytical software to generate information about particle size.

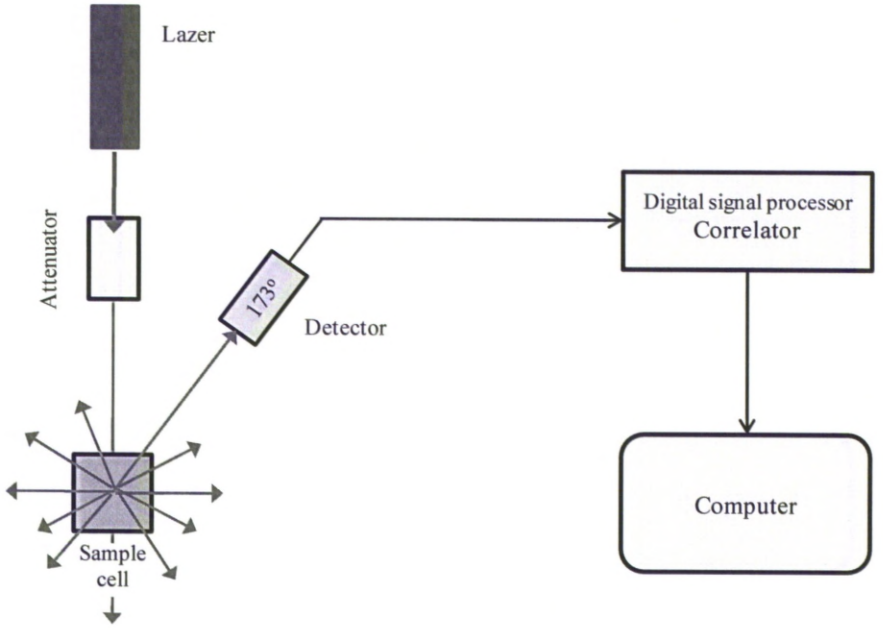

Figure 1.19: Optical configuration of a DLS instrument (Adapted from ref.[392])

DLS is a popular and effective technique for particle sizing in colloidal suspensions. It is also useful to study the colloidal stability of particles, as any aggregation within the sample can be easily detected. Particle size can be sensitive to pH and ionic strength of the solution as well as to the concentration of the particles. It should be also noted that particle size obtained by DLS is dynamic size (the core plus ligand shell).

1.7.5 Elemental analysis

Inductively coupled plasma atomic emission spectrometry (ICP-AES) is one of the most common techniques in the quantitative and qualitative analysis of elemental composition of a sample.[393, 394] ICP-AES relies on the physical principle that excited atoms or ions of an element will emit a spectrum of electromagnetic radiation characteristic for the element. In

the ICP-AES, the sample in liquid form is introduced to radiofrequency plasma torch using a nebuliser. Inside the plasma torch, the sample is atomised, excited and ionised by the plasma. The emitted radiation is recorded by a spectrometer or by a charge-coupled device (CCD).[393] There are many different excitation sources in the elemental analysis techniques, including flames, furnaces, DC arcs and AC sparks. However, inductively coupled plasma is preferably used due to its high temperature (6000-10000 °C), and non-contamination from electrodes. The high temperature of the inductively coupled plasma is a benefit of the technique as it can completely decompose the sample into free atoms or ions and excite them to high energy states, and thus achieve high sensitivity of detection. In addition, the use of a CCD detector enables the analysis of multiple elements simultaneously.[393-395] This technique is particularly useful for trace element analysis.

The chemical composition of the synthesised nanoparticles in this work was analysed using an inductively coupled plasma atomic emission spectroscopy (ICP-AES) (Spectro CirosCCD). Analytical specimens were prepared by digesting 1 to 3 mg of nanoparticles into 10 mL of a HNO_3 : HCl (4 : 1) mixture. A 0.25 mL of the digested sample was then diluted to 10 mL with a 2% HNO_3 solution before using for ICP-AES analysis.

Further characterisation techniques

1.7.6 TEM based analysis techniques

In a TEM, accompanying with images constructed using elastic scattering electrons, electron diffraction patterns and two types of spectroscopy, electron energy loss spectroscopy (EELS) and energy dispersive X-ray spectroscopy (EDX) could be used to analyse the sample.[383] EELS is a technique that takes advantage of inelastically scattered electrons to provide information about vibrational modes and other states of the sample in particular, ionisation energies. EDX analyses the x-rays emitted from the sample under

electron bombardment. Both techniques give information on the elemental composition of the sample.[383]

Electron diffraction

Electron diffraction could be used in studying the crystallinity of the sample. In diffraction patterns, the intense spots or rings are formed by the constructive interference of electrons, while the dark regions are the result of the destructive interference of electrons.[382] Diffraction provides information about arrangement of atoms in a lattice. It can be used to determine if a sample is amorphous or crystalline. If a sample is crystalline, the crystal structure and lattice parameters of the specimen can be determined by the analysis the diffraction patterns. With a crystalline sample, electron diffraction is controlled by Bragg's condition which is similar to x-ray diffraction:

$$n\lambda = 2d_{hkl} \sin(\theta_B) \qquad (1.7)$$

where n is an integer, λ is wavelength of the electron beam d_{hkl} is the spacing between atomic planes and θ_B is the Bragg angle (the angle between the incident electron beam and atomic plane).

Electron Energy Loss Spectroscopy (EELS)

When electrons interact with a sample they lose a certain amount of energy depending on the element and the energy level of the electron with which they interact.[378] These energy loss electrons are recorded by a magnetic prism spectrometer located under the viewing screen, which is moved whenever the spectrometer is in use.[378] As energy loss electrons enter the spectrometer, they are deflected or bent at different angles depending on the amount of energy lost. Trajectories of electrons with a significant energy loss are bent more than those of electrons with little or no energy loss. If an incident electron interacts with an atom within the sample with sufficient energy to eject an inner shell electron, the

resulting atom becomes ionised. The incident electron after interaction will lose a specific amount of energy depending on the inner shell location of the electron that was ejected.[378] Since ionisation happens at specific energies, the ionisation edges of a spectrum are sharp. So electrons that lose energy because of core ionisation are used in the analysis the elemental composition of a sample. EELS is particularly useful technique in the mapping elemental distribution in a sample.[157]

Energy Dispersive X-ray Spectroscopy (EDX or EDS)

Energy dispersive X-ray spectroscopy (EDX or EDS) is another technique to determine the elemental composition of the sample by analysing X-rays emitted from the sample under electron bombardment. Since each element emits X-rays with specific energy, the EDX spectrum can be used to identify the chemical composition in the sample. In TEM, an EDX spectrometer is placed near the sample to maximise the X-ray signal reaching the detector. The advantages of EDX are the speed of collecting data and simultaneous display of X-ray data from a wide range of energy. However, a disadvantage of EDX is its relatively poor energy resolution (some tens of eV compared to 1 eV of EELS) which makes the technique not suitable for analysis of low atomic number elements ($Z < 11$).

Microscopic analysis is the most important technique for the characterisation of nanomaterials. It can provide rich information on size, shape, crystallinity, phase structure, chemical composition and elemental distribution of a sample. Nevertheless, this technique has some disadvantages. Its biggest drawback is that one only looks at a small part of a specimen at any time. Thus, for a polydisperse sample, the results reported may not necessarily represent the entire sample. In addition, preparations of specimens for TEM such as drying and purification sometimes alter the morphology of a sample when compared to that in suspension. Another disadvantage of TEM analysis is that it can cause

degradation or other damage to the sample due to the interactions between the high energy electron beam and the sample.

1.7.7 BET technique

The BET technique is based on the principle of physical adsorption of a gas on a solid surface. It was theoretically developed by Stephen Brunauer, Paul Hugh Emmett, and Edward Teller in 1938 and is possibly the most widely-used method for the determination of the surface area of powders and porous materials.[396] This method can be used to determine the average particle size of non-porous powders. In a gas adsorption experiment, the sample is heated and degassed by vacuum to remove all adsorbed foreign molecules.

To determine the surface area of a powder sample, a gas, usually nitrogen, because it is relatively cheap and inert, is introduced into the measurement tube containing the sample. The tube is maintained at a certain temperature, generally liquid nitrogen temperature, 77 K. At this temperature, gas molecules are adsorbed onto the surface of the powders to form a monolayer or multilayer of nitrogen molecules depending on the gas pressure. The amount of adsorbed gas (V) at relative pressure p/p_o is determined by BET equation:[396,397]

$$\frac{p}{V(p_o - p)} = \frac{1}{V_m C} + \frac{C-1}{V_m C} \cdot \frac{p}{p_o} \qquad (1.10)$$

where p and p_o are the equilibrium and saturation pressures of the gas, respectively, V_m is the adsorbed gas volume for one monolayer and C is a constant. By measuring the amount of adsorbed gas on the surface of the powder at different values of relative pressure, the dependence of $p/V(p_o - p)$ vs relative pressure (p/p_o) of BET equation can be plotted. The adsorption graph, also called adsorption isotherm, for a non-porous powder sample, usually has form as shown in Figure 1.20.

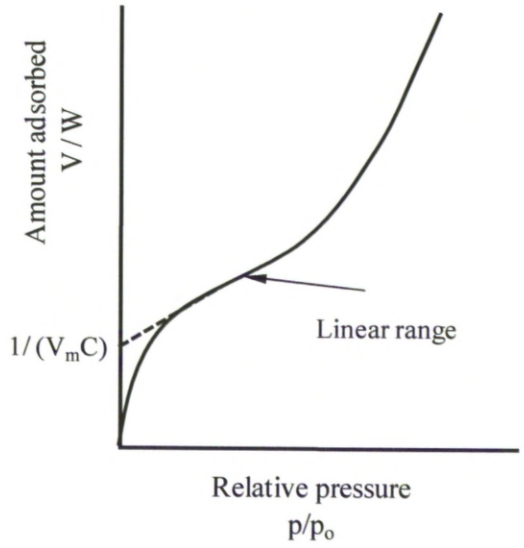

Figure 1.20: Adsorption isotherm of a non-porous powder sample (Reprinted from ref.[397])

The actual measurement of the adsorbed gas is usually carried out for the linear region of the adsorption isotherm where the relative gas pressure p/p_o is in the range of 0.05 and 0.35. From the BET adsorption isotherm, the amount of gas needed to form a monolayer, V_m, can be determined and, assuming the cross-sectional area of the gas molecule and the mass of the sample are known, the specific surface area of the powder sample (the surface area of a unit mass of sample) can be calculated.[396] For a spherical particle, the average particle diameter can be determined:[398]

$$d = 6000/ (S_{sp}.\rho_a) \qquad (1.11)$$

where S_{sp} is the specific surface area per unit mass ($m^2\ g^{-1}$) and ρ_a is solid density of the sample ($g\ cm^{-3}$). The particle diameter has the unit of nanometre.

The BET method is a relative accurate, fast and simple technique for the determination of the surface area, pore volume and particle size.[399] To obtain the correct result, gas adsorption has to be carried on the clean surface of the particles. In fact, however, many nanoparticles have been stabilised by organic molecules which bind strongly to particle surface. This interferes with gas adsorption. In addition, the aggregation and non-spherical

shape of the particles will result in a significant error in the calculation of the particle size.[398]

1.7.8 FT-IR spectroscopy

Fourier transform infrared (FT-IR) spectroscopy is one of the most extensively used and relatively inexpensive analytical techniques for characterising materials. It is particularly useful for the identification of the configurations and structures of organic substances. The FT-IR method is based on the principle that when electromagnetic radiation in infrared (IR) region, wavelength in the range of 0.7 - 1000 μm, interacts with a sample, it will be absorbed by molecules of the sample if the frequency of the incoming radiation matches the frequency of the vibration of the molecules. Each molecule has vibration modes which correspond to the molecular structure. Therefore, the absorption (or transmission) spectrum can be used to identify the chemical structure of the substances. FT-IR technique can be also utilised for quantitative analysis of components in a sample.

An FT-IR spectrometer consists of three basic components: IR radiation source, interferometer and detector.[400] Figure 1.21 illustrates schematically a typical FT-IR instrument. In an FT-IR spectrometer, a continuous radiation from the IR source, usual a filament made of silicon carbide or rare-earth oxides heated electrically to 800 - 1800 °C, is directed to the interferometer where the beam is split into two identical beams, which are recombined after travelling different path length, to generate an interference pattern. The resulting beam then passes through the sample and finally is focused on the detector.[400] The raw data are then converted into the spectrum by a Fourier Transform algorithm. The obtained FT-IR spectra are usually expressed in wavenumbers which are reciprocal of wavelengths and have unit of cm^{-1}.

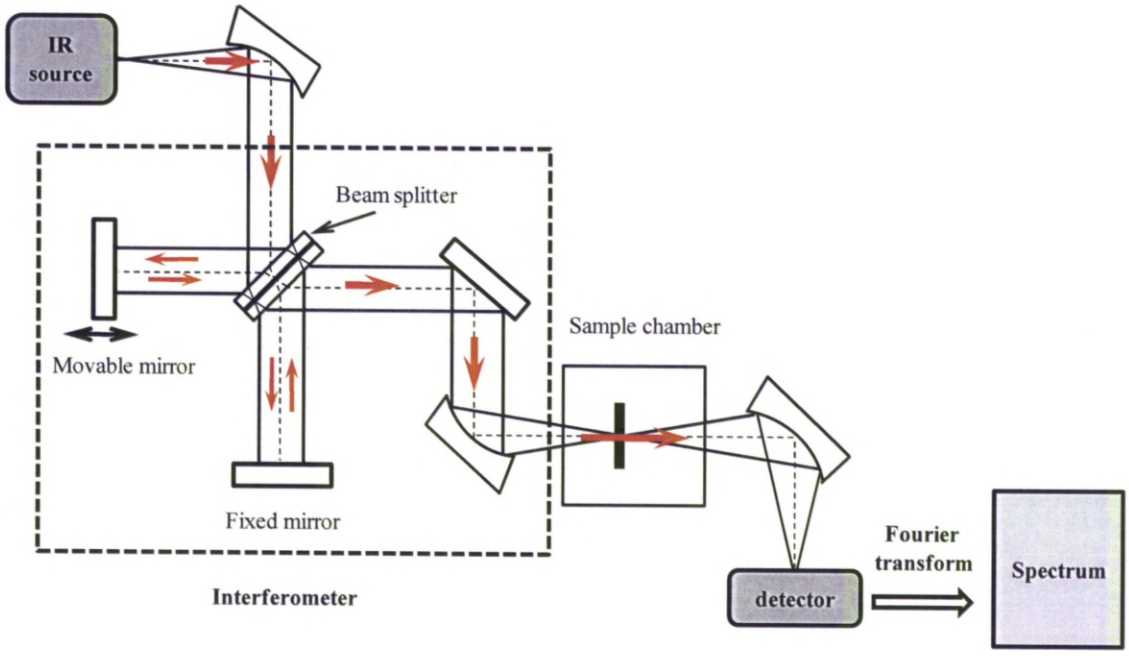

Figure 1.21: Schematic structure of a typical FT-IR spectrometer (Adapted from ref [401]).

Different forms of sample such as solid, liquid or gas can be investigated by FT-IR method. Commonly, solids are finely ground (particle size of about 2 μm) to minimise the scattering of radiation and are either mixed with KBr and pressed into a transparent pillet or dispersed in a suitable solution and held in IR cell before conducting the measurement.[400]

In FT-IR spectroscopy, spectrum of the sample often contains some background signal. To obtain the signal derived only from sample, it is necessary to carry out a background measurement, and the background spectrum is usually removed by subtraction from the sample spectrum. Background and sample measurements are always conducted under the sample conditions.[395]

FT-IR spectroscopy offers an effective, relatively inexpensive method for the investigation of chemical structure as it is easy to operate and fast in data acquisition. However, the interpretation of spectra of molecules with multiple functional groups or

unknown compound is sometime complex. Thus, in many cases, it has to combine with analytical data from other methods such as NMR or mass spectrometry.

1.7.9 Raman spectroscopy

Raman scattering, named after the Indian physicist C.V. Raman, is an important technique based on the excitation of vibrational modes within molecules.[402] Raman spectroscopy uses inelastic scattering of monochromatic light, usually from a laser, in which incident photons are scattered from a sample and shifted in frequency by the energy of characteristic vibrational modes of the molecules in the sample.

As light passes through a sample, there are different possible types of interactions between an incident light and the molecules within the sample (Figure 1.22). Firstly, as mentioned earlier, the IR absorption can occur if the energy of the photons is equal to the energy gap between the ground state of the molecule and other higher vibrational modes. As the result of the IR absorption, the molecule will be promoted to a higher vibrational energy state.[402]

Besides IR absorption, the incident photons can be scattered from the molecules. Scattering is the result of the interaction between the incident photon and electron cloud of the molecule. In the scattering process, the molecules are promoted to virtual energy states via the interaction with incident photons. These molecules will emit photon as they return to normal state. The energy of the emitted photon can be the same or differs from that of incident photon. The majority of light is scattered by Rayleigh scattering, which is an elastic scattering process. In Rayleigh scattering, the incident and emitted photons have exactly the same energy and there is no net energy transfer between matter and photons. However, there is small probability, about one in every10^6-10^8 photons that the incident photon is scattered with a slight energy shift due to inelastic interaction.[402,403] This is the Raman effect.

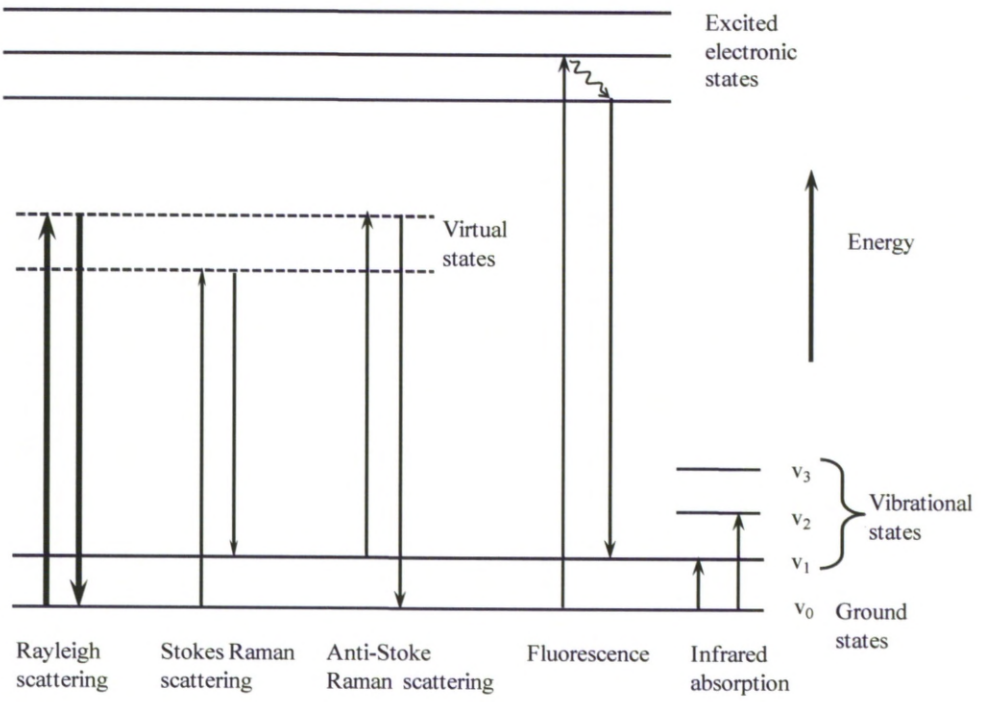

Figure 1.22: Interactions of light with matter (Adapted from ref.[404]).

In Raman scattering, molecules are excited from the ground state to a virtual state due to the interactions with incident light. As the molecule emits a photon it relaxes into a vibrational state different from the initial one. The difference in energy between the original state and this new state results in a shift in frequency of the emitted photon. If the final vibrational energy state of the molecule is higher than the initial one, energy is transferred from the incident photon to the molecule, the emitted photon will be shifted to a lower frequency (red-shift). This process is referred to as Stokes Raman scattering. If the final vibrational energy state of the molecule is lower than the initial state, energy is transferred from the molecule to incident photon, the emitted photon will be shifted to a higher frequency (blue-shift), This is known as Anti-Stokes Raman shift.[403] Generally, a Raman spectrum is recorded at room temperature in the Stokes scattering mode. This is because at room temperature Stokes scattering intensity is significantly stronger than the

Anti-Stokes scattering. The intensity of the signal is usually plotted as a function of the shift in frequency.[402]

The other inelastic process that often occurs during the interaction of incident light with a sample is fluorescence. In fluorescence the molecule is excited from the ground state to an electronically excited state by the absorption of an incident photon, and subsequently emits a photon with longer wavelength. This process may interfere with the Raman signal.

Raman spectroscopy provides an effective and flexible method for the investigation of the chemical structure of the sample. It is easy in operation, fast in data acquisition and simple in sample preparation. Raman spectroscopy can be performed on a sample of solid, liquid or gas, and it is not required a special holder like FT-IR does. As the signal from Raman scattering is quite weak, it is necessary to use either a high power laser or a laser with short wavelength. This possibly leads to either a degradation of sample or fluorescene.[403,405]

1.7.10 NMR spectroscopy

Nuclear magnetic resonance (NMR) spectroscopy is another important analytical technique in the quantitative and structure determination of compounds and materials. Since its discovery in 1945 by research groups at Stanford and M.I.T., NMR has become irreplaceable in many research areas such as chemistry, bio-chemistry and medicine.[395] NMR spectrometry is based on the NMR phenomenon exhibited by nuclei that possess non-zero spin when placed in strong static magnetic field, which causes a small energy difference between ''spin-up'' and ''spin-down'' states. Transitions between these states can be probed by electromagnetic radiation in the radio wave range.

The energy difference between the states is proportional to the field B_0. The magnetic moment of the nuclei in the high spin states is oriented against the external field. The

nuclear magnetic moment of the nuclei in the low spin states is aligned with the applied field (Figure 1.23a).

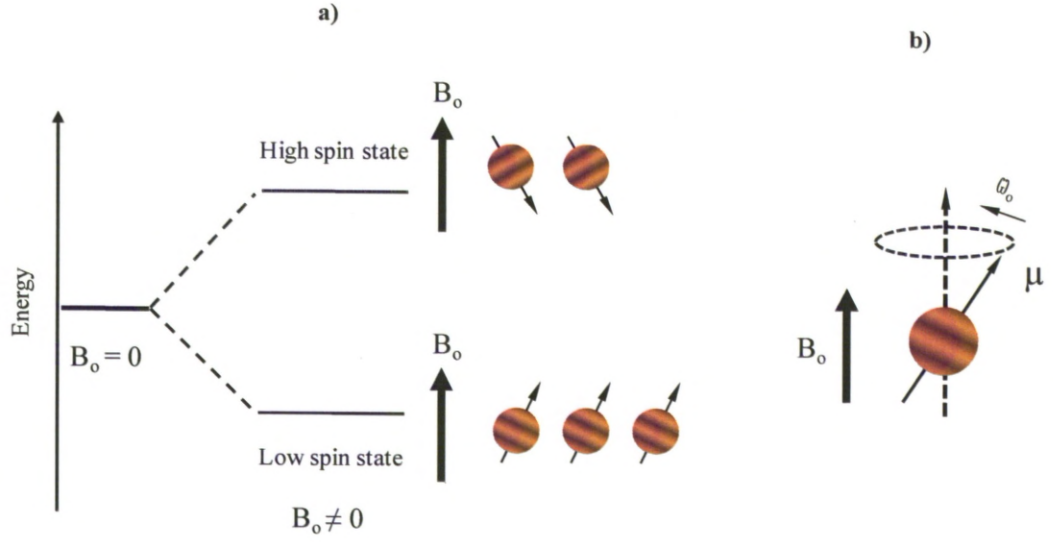

Figure 1.23: The responding of nuclei with spin quantum number I = 1/2 to the static magnetic field B_o: a) the energy state split and the alignment of magnetic moment of nuclei in the applied field and b) the precession of an nucleus spin around the direction of the applied field B_o.

At room temperature, the number of nuclei in low energy level is slightly in. The ratio of population distribution of nuclei in each spin is given by the Boltzmann distribution:[395, 406]

$$N_\beta/N_\alpha = \exp(-\gamma B_o/kT) \qquad (1.12)$$

where N_β is the number of nuclei in high energy state, N_α is the nuclei number in low energy state, k is the Boltzmann constant and T is the absolute temperature. In the presence of the applied magnetic field B_o, nuclear spins will precess around the applied field with an angular frequency which is determined by the strength of the magnetic field B_o and the gyromagnetic constant γ related to the ratio of the angular magnetic moment μ to the spin number I for a specific nucleus, as described by the expression:[395]

$$\omega_o = \gamma B_o. \qquad (1.13)$$

where ω_o is the Larmor frequency.

If a sample is irradiated with radio frequency waves that have energy equal to the energy difference between the two energy levels in the nuclei, and have propagation direction perpendicular to the field B_o, the nuclei of atoms in the sample will absorb the energy and be promoted to high energy level. This energy absorption is called resonance. The NMR signal is recorded as the excited nuclei return to initial state. The signal intensity is proportional to the population difference of the nuclei between the two energy levels. By increasing field intensity B_o, the difference between the two population can be increased, and thus, the NMR signal or sensitivity is increased.[395]

Each nucleus of an atom in a molecule is associated with electrons. In the presence of external field B_o, the circulation of electrons around the nucleus induces a small magnetic field, opposite to the applied field. Thus the actual magnetic field B_{eff} that causes the energy state split of a nucleus is:[395]

$$B_{eff} = B_o(1 - \sigma) \qquad (1.14)$$

where σ is called the shielding constant. The shielding constant varies with the chemical group or surrounding molecular environment of the atoms investigated. A variation in the magnetic field at the site of the nucleus due to the shielding effect generates a shift in the resonance frequency. This phenomenon is called a chemical shift. The chemical shift is expressed:[395]

$$\delta_i = \frac{\nu_i - \nu_{ref}}{\nu_{app}} \times 10^6 \qquad (1.15)$$

where δ_i is the chemical shift corresponding to a signal of frequency ν_i. The unit of the chemical shift is parts per million (ppm). ν_{ref} is the frequency of a reference compound (usually tetramethyl silane, TMS) and ν_{app} is the frequency of the instrument.

NMR spectroscopy has been extensively used for chemical structure determination in different research fields of organic and inorganic chemistry, biochemistry and medicine. In the area of nanostructured materials, NMR spectroscopy is usually utilised to investigate the interactions or coordination between ligand and surface of diamagnetic or anti-ferromagnetic nanoparticles.[407-411]NMR, however, is not suitable for the characterisation of nanoparticles of ferro- or ferrimagnetic materials, as the large saturation magnetisation of the materials causes both variations in local magnetic field which lead to shifts of the signal frequency and dramatic decreases in relaxation times which results in significant broadening of the signal peaks.[366,395,411,412] Thus far, there are only few reports on the characterisation of magnetic nanoparticles using this method.[412-414]

1.7.11 X-ray photoelectron spectroscopy (XPS)

X-ray photoelectron spectroscopy (XPS) is the most widely used analytical technique for surface chemical analysis. The underlying physical principle of XPS is the photoelectric effect. When the atoms comprising the surface of a sample are irradiated with an X-ray beam, if the energy of the X-rays is sufficiently high, core electrons (electrons are close to nucleus) in the atoms can be ejected. These emitted electrons are called photoelectrons. The energy of an emitted photoelectron is related to the frequency of the exciting radiation and the binding energy of the electron in the atom, and can be described by Einstein's equation:[415]

$$E_B = h\nu - E_{kin} + \Delta\phi \qquad (1.16)$$

where E_B is the binding energy of the electron within the atom, $h\nu$ is the energy of x-ray radiation, E_{kin} is the kinetic energy of the emitted photoelectron and $\Delta\phi$ is the 'work function' of the sample. The Binding energy E_B of an electron in an atom depends on the type of element and surrounding chemical environment. With energy of the incident x-ray radiation is known and work function $\Delta\phi$ is obtained from the energy calibration of the

instrument, the binding energy E_B can be determined through the measurement of kinetic energy of the emitted photoelectron. In a XPS spectrometer, monochromatic x-ray radiation generated by bombarding an anode (usually Mg, Al or Si) with a high energy electron beam is used as the exciting radiation source to eject electrons from the sample. The emitted electrons from the sample are then passed through an energy analyser where they are separated according to their energy before impinging on a detector. The electric signal generated at the detector is then analysed by a computer. The resultant XPS spectrum is usually comprised of sharp and intense peaks which reflect the discrete binding energies of the electrons in the sample. These peaks can be used to identify oxidative or chemical states, molecular functional groups, electronic structure and composition of a sample.[415]

XPS is a powerful and effective analytical technique. It can be used to identify most elements in the periodic table. For nanomaterials, XPS has been extensively used and demonstrated useful, particularly in the investigation of oxidative stability, ligand exchange reactions and surface functionalisation of nanoparticles as well as core/shell structures.[338,416-420] However, as the emitted electrons have to travel from the sample through the analyser to the detector, to avoid energy loss due to the collision between emitted electrons and gas molecules, the analysis has to be carried out under ultra high vacuum conditions (usually 10^{-9} - 10^{-10} torr).

1.7.12 Thermal analysis (TGA and DSC)

Thermal analyses are techniques utilised in the study of thermally-induced processes of materials.[421] Among many thermal analytical methods, thermal gravimetric analysis (TGA) and differential scanning calorimetry (DSC) are widely used for the study of a variety of thermodynamic processes and material properties such as phase transformations, thermal decompositions, and oxidative and thermal stabilities of a sample.[421,422] The basic principle

of TGA is based on the precision measurement of the amount and rate of change in weight of the sample with temperature over time.[421] In TGA, the sample is generally heated from ambient temperature to around 1000 °C at a constant rate and under controlled atmosphere (usually N_2, H_2 or O_2). The changes in weight are precisely measured utilising a thermobalance. These changes usually occur as weight loss in the sample due to desorption, dehydration or decomposition processes. In some cases, a gain in weight can be obtained as a sample becomes oxidised under oxygen atmosphere.[423] DSC relies on the measurement of the heat absorbed or released by the sample as compared with a reference, when both the sample and the reference are heated and maintained at the same temperature throughout the experiment. When a sample is heated it can undergo thermal-induced transition processes such as desorption, desolvation, de-composition, melting, crystallisation, oxidation, etc. These transitions can release or absorb heat. Therefore, at the transition points, the amount of heat energy required to increase the temperature of the sample is different to that required to increase the temperature of the reference.

TGA and DSC are particularly useful and widely utilised in various research and industry areas such as polymer,[424] biochemistry and pharmaceuticals,[421,425] and food[426] as these methods provide simple and effective tools for the investigation of thermal stability, thermodynamic processes and kinetic parameters of materials. For nanomaterials, thermal analyses have be typically applied in the studies of thermal decompositions of precursors and ligand shell,[427-429] interactions between organic molecules and particles,[430-432] and oxidative and thermal stability of the nanoparticles.[431,433]

The characterisation methods described above are only some of the most common analytical techniques in the characterisation of magnetic nanomaterials. Many other useful methods, including Mossbauer spectroscopy, neuron diffraction, mass spectroscopy, ultraviolet-visible spectroscopy (UV-vis), Auger electron spectroscopy (AES), X-ray absorption near edge structure (XANES), etc. have been also widely used for analysing

nanomaterials. A list of these techniques and their applications can be found in the literatures.[434]

1.8 Objectives

The core aim of this thesis is to prepare water-dispersible, stable and high saturation magnetisation nanoparticles including Co, CoPt, CoFe alloy, cobalt ferrite and CoFe@Pt core/shell structures, with the longer-term aim of using the new materials in bioapplications.

For Co and CoPt nanoparticles, the synthesis will be directly carried out in water and the research will focus on the exploring the effect of some water-dispersible polymer and peptide ligands on the morphology and colloidal stability of the nanoparticles.

CoFe alloy nanoparticles will be synthesised in organic solvent. Coating nanoparticles with an inorganic shell is particularly interesting. Ligand exchange will be conducted on both CoFe and core/shell nanoparticles to transfer them into water.

Cobalt ferrite nanoparticles will be synthesised in organic solvents. Utilising the advantages of high temperature synthesis in controlling the size, shape and monodispersity of the nanoparticles, the synthesis of nanoparticles with controlled size and shape will be explored.

The results of the experimental work are divided into four chapters, with a final summary chapter. Common characterisation techniques are briefly described in the introduction chapter.

Chapter 2 describes the research approach in the synthesis of water-dispersible and stable Co magnetic nanoparticles using a direct reduction method. The effects of polymer and peptide ligands (structures, functional group and length or molecular weight) as well as reaction conditions on the colloidal stability and morphology of the Co nanoparticles will be explored. Characterisation of polymer or peptide stabilised Co nanoparticles is provided

in terms of morphology, magnetic properties and colloidal stability. The ability of using Co nanoparticles as MRI contrast agents will also be assessed.

Chapter 3 describes a simple and general synthetic approach for fabrication of water-dispersible and chemically stable CoPt nanoparticles with controlled morphology and composition. The effect of precursor concentration, polymer and peptide ligands (structure, functional group) on the morphology and composition of CoPt nanoparticles will be investigated. The magnetic properties, morphology and colloidal stability in water and under physiological conditions will be characterised and presented. The cytotoxicity and the possibility of using these CoPt nanoparticles for stem cell tracking are also explored.

Chapter 4 will present the synthesis of high saturation magnetisation of CoFe alloy magnetic nanoparticles and CoFe@Pt core/shell structures using thermal decomposition approach. Ligand exchange reactions using amino-silane molecules and polyethylene glycol polymer to transfer hydrophobic CoFe and CoFe@Pt core/shell nanoparticles into water are also described. Characterisation of the obtained nanoparticles is provided in term of morphology, crystallinity, and magnetic properties.

Chapter 5 presents the study of the synthesis of monodisperse cobalt ferrite nanoparticles with controlled size and shape. The effect of surfactant concentration and precursor ratio on the morphology and composition of particles will be investigated. The morphology evolution with reaction time is also evaluated. Morphology, crystal structure and magnetic properties of the particles will be characterised and presented utilising TEM, HRTEM, XRD and SQUID. This chapter will also explore the ligand exchange using polymer ligand to transfer nanoparticles to water.

Chapter 6 presents a summary consideration on the achievements of the thesis. The future work and prospective applications of the research is also outlined.

Reference

1. http://www.nanotec.org.uk/report/chapter3.pdf.
2. Erhardt, D. *Nature Mater.* **2003,** 2, (8), 509-510.
3. Kerker, M. *J. Colloid&Interface Sci.* **1985,** 105, (2), 297-314.
4. Binnig, G.; Rohrer, H. *Helvetica Physica Acta* **1982,** 55, (6), 726-735.
5. Binnig, G.; Quate, C. F.; Gerber, C. *Phys. Rev. Lett.* **1986,** 56, (9), 930-933.
6. Binnig, G.; Rohrer, H. *IBM J. Res.& Dev.* **1986,** 30, (4), 355-369.
7. Buzea, C.; Pacheco, I. I.; Robbie, K. *Biointerphases* **2007,** 2, (4), 17-71.
8. Bohren, C. F.; Huffman, D. R., *Absorption and Scattering of Light by Small Particles*. Wiley Intersci.,: New York., 1983.
9. El-Sayed, M. A. *Account. Chem. Res.* **2001,** 34, (4), 257-264.
10. Nikoobakht, B.; El-Sayed, M. A. *Chem. Mater.* **2003,** 15, (10), 1957-1962.
11. Sun, Y. G.; Xia, Y. N. *JACS* **2004,** 126, (12), 3892-3901.
12. Skrabalak, S. E.; Au, L.; Lu, X. M.; Li, X. D.; Xia, Y. N. *Nanomed.* **2007,** 2, (5), 657-668.
13. West, J. L.; Halas, N. J. *Annual Rev. Biomed. Eng.* **2003,** 5, 285-292.
14. Weller, D.; Moser, A.; Folks, L.; Best, M. E.; Lee, W.; Toney, M. F.; Schwickert, M.; Thiele, J. U.; Doerner, M. F. *IEEE Trans. Mag.* **2000,** 36, (1), 10-15.
15. Weller, D.; Moser, A. *IEEE Trans. Mag.* **1999,** 35, (6), 4423-4439.
16. Pillai, V.; Shah, D. O. *J. Mag. Mag. Mater.* **1996,** 163, (1-2), 243-248.
17. Chen, Y. X.; Chen, S. P.; Zhou, Z. Y.; Tian, N.; Jiang, Y. X.; Sun, S. G.; Ding, Y.; Wang, Z. L. *JACS* **2009,** 131, (31), 10860-10861.
18. Muller, J. L.; Klankermayer, J.; Leitner, W. *Chem. Commun.* **2007,** (19), 1939-1941.
19. Hu, L. H.; Peng, Q.; Li, Y. D. *JACS* **2008,** 130, (48), 16136-16137.
20. Pankhurst, Q. A.; Connolly, J.; Jones, S. K.; Dobson, J. *J. Phys. D-Appl. Phys.* **2003,** 36, (13), R167-R181.
21. Ung, D.; Tung, L.; Caruntu, G.; Delapotas, D.; Alexandreu, I.; Prior, I.; Thanh, N. *Cryst. Eng. Commun.* **2009,** 11, 1309-1316.
22. Lu, A. H.; Salabas, E. L.; Schuth, F. *Angew. Chemie-Inter. Ed.* **2007,** 46, (8), 1222-1244.
23. Tartaj, P.; Morales, M. D.; Veintemillas-Verdaguer, S.; Gonzalez-Carreno, T.; Serna, C. J. *J. Phys. D-Appl. Phys.* **2003,** 36, (13), R182-R197.
24. Rye, P. D. *Bio-Techno.* **1996,** 14, (2), 155-157.

25. Hussain, I.; Graham, S.; Wang, Z. X.; Tan, B.; Sherrington, D. C.; Rannard, S. P.; Cooper, A. I.; Brust, M. *JACS* **2005,** 127, (47), 16398-16399.
26. Wang, Z. X.; Tan, B. E.; Hussain, I.; Schaeffer, N.; Wyatt, M. F.; Brust, M.; Cooper, A. I. *Langmuir* **2007,** 23, (2), 885-895.
27. Teranishi, T.; Miyake, M. *Chem. Mater.* **1998,** 10, (2), 594-600.
28. Teranishi, T.; Hosoe, M.; Tanaka, T.; Miyake, M. *J. Phys. Chem. B* **1999,** 103, (19), 3818-3827.
29. Ahmadi, T. S.; Wang, Z. L.; Green, T. C.; Henglein, A.; ElSayed, M. A. *Science* **1996,** 272, (5270), 1924-1926.
30. Shen, L. F.; Laibinis, P. E.; Hatton, T. A. *Langmuir* **1999,** 15, (2), 447-453.
31. Brown, K. R.; Walter, D. G.; Natan, M. J. *Chem. Mater.* **2000,** 12, (2), 306-313.
32. Doty, R. C.; Tshikhudo, T. R.; Brust, M.; Fernig, D. G. *Chem. Mater.* **2005,** 17, (18), 4630-4635.
33. Denizot, B.; Tanguy, G.; Hindre, F.; Rump, E.; Le Jeune, J. J.; Jallet, P. *J. Colloid& Interface Sci.* **1999,** 209, (1), 66-71.
34. Schutt, W.; Gruttner, C.; Hafeli, U.; Zborowski, M.; Teller, J.; Putzar, H.; Schumichen, C. *Hybridoma* **1997,** 16, (1), 109-117.
35. Clark, D. J.; ed., *Magnetic oxides*. Wiley: New York, **1972.**
36. Valenzuela, R., *Magnetic ceramics*. Cambrid. Uni. Press,: Cambridge, **1994**; p 312.
37. Jun, Y. W.; Lee, J. H.; Cheon, J. *Angew. Chemie-Inter. Ed.* **2008,** 47, (28), 5122-5135.
38. Cullity, B. D.; Graham, C. D., *Introduction to Magnetic Materials*. Second Ed.; Wiley: **2008**; p 537.
39. Jakubovics, J. P., *Magnetism and Magnetic Materials*. Maney Pub.: **1994**; p 175.
40. Kittel, C., *Introduction to Solid State Physics*. John Wiley & Son, Inc.: New York, **1986.**
41. Jeong, U.; Teng, X. W.; Wang, Y.; Yang, H.; Xia, Y. N. *Adv. Mater.* **2007,** 19, (1), 33-60.
42. Halliday, D.; Resnick, R.; Walker, J., *Fundamentals of Physics*: Extended. John Wiley & Son, Inc.: New York, **1997**; p 1232.
43. O'handley, R. C., Modern Magnetic Materials: Principles and Applications. John Wiley & Son, Inc.: New York, 2000; p 768.
44. Stoner, E. C.; Rhodes, P. *Philosoph. Magazine* **1949,** 40, (304), 481-522.

45. Alexiou, C.; Arnold, W.; Klein, R. J.; Parak, F. G.; Hulin, P.; Bergemann, C.; Erhardt, W.; Wagenpfeil, S.; Lubbe, A. S. *Cancer Res.* **2000,** 60, (23), 6641-6648.
46. Berry, C. C.; Curtis, A. S. G. *J. Phys. D-Appl. Phys.* **2003,** 36, (13), R198-R206.
47. Lubbe, A. S.; Alexiou, C.; Bergemann, C. *J. Surg. Res.* **2001,** 95, (2), 200-206.
48. Alexiou, C.; Jurgons, R.; Schmid, R. J.; Bergemann, C.; Henke, J.; Erhardt, W.; Huenges, E.; Parak, F. *J. Drug Targ.* **2003,** 11, (3), 139-149.
49. Lubbe, A. S.; Bergemann, C.; Brock, J.; McClure, D. G. *J. Mag. Mag. Mater.* **1999,** 194, (1-3), 149-155.
50. Matson, M. L.; Wilson, L. J. *Fut. Med. Chem.* **2010,** 2, (3), 491-502.
51. Na, H. B.; Song, I. C.; Hyeon, T. *Adv. Mater.* **2009,** 21, (21), 2133-2148.
52. Seo, W. S.; Lee, J. H.; Sun, X. M.; Suzuki, Y.; Mann, D.; Liu, Z.; Terashima, M.; Yang, P. C.; McConnell, M. V.; Nishimura, D. G.; Dai, H. J. *Nature Mater.* **2006,** 5, (12), 971-976.
53. Lee, J. H.; Huh, Y. M.; Jun, Y.; Seo, J.; Jang, J.; Song, H. T.; Kim, S.; Cho, E. J.; Yoon, H. G.; Suh, J. S.; Cheon, J. *Nature Med.* **2007,** 13, (1), 95-99.
54. Johannsen, M.; Gneveckow, U.; Eckelt, L.; Feussner, A.; Waldofner, N.; Scholz, R.; Deger, S.; Wust, P.; Loening, S. A.; Jordan, A. *Inter. J. Hyperthermia* **2005,** 21, (7), 637-647.
55. Jordan, A.; Scholz, R.; Wust, P.; Fahling, H.; Felix, R. *J. Mag. Mag. Mater.* **1999,** 201, 413-419.
56. Hergt, R.; Dutz, S.; Muller, R.; Zeisberger, M. *J. Phys.-Condens. Matter* **2006,** 18, (38), S2919-S2934.
57. Moroz, P.; Jones, S. K.; Gray, B. N. *Inter. J. Hyperthermia* **2002,** 18, (4), 267-284.
58. Franzreb, M.; Siemann-Herzberg, M.; Hobley, T. J.; Thomas, O. R. T. *Appl. Microbio. Biotechno.* **2006,** 70, (5), 505-516.
59. Safarik, I.; Safarikova, M. *BioMag. Res. Techno.* **2004,** 2, (1), 1-17.
60. Safarik, I.; Safarikova, M. *BioMag. Res. Techno.* **2004,** 2, 17.
61. Alche, J. D.; Dickinson, K. *Protein Express. Purif.* **1998,** 12, (1), 138-143.
62. Yavuz, C. T.; Prakash, A.; Mayo, J. T.; Colvin, V. L. *Chem. Eng. Sci.* **2009,** 64, (10), 2510-2521.
63. Azevedo, A. M.; Rosa, P. A. J.; Ferreira, I. F.; Aires-Barros, M. R. *Trends in Biotech.* **2009,** 27, (4), 240-247.
64. Vlassiouk, I.; Krasnoslobodtsev, A.; Smirnov, S.; Germann, M. *Langmuir* **2004,** 20, (23), 9913-9915.

65. Saxena, A.; Tripathi, B. P.; Kumar, M.; Shahi, V. K. *Adv. Colloid & Interface Sci.* **2009,** 145, (1-2), 1-22.

66. Brown, M. A.; Semelka, R. C., *MRI: Basic Principles and Applications*. 3rd Ed.; Wiley-Liss, New Jersey: 2003; p 210.

67. Fang, C.; Zhang, M. Q. *J. Mater. Chem.* **2009,** 19, (35), 6258-6266.

68. Laurent, S.; Forge, D.; Port, M.; Roch, A.; Robic, C.; Elst, L. V.; Muller, R. N. *Chem. Rev.* **2008,** 108, (6), 2064-2110.

69. Neuberger, T.; Schopf, B.; Hofmann, H.; Hofmann, M.; von Rechenberg, B. *J. Mag. Mag. Mater.* **2005,** 293, (1), 483-496.

70. Suzuki, M.; Shinkai, M.; Kamihira, M.; Kobayashi, T. *Biotech.&Appl. Biochem.* **1995,** 21, 335-345.

71. MNneil, S. E. *J. Leukocyte Biology* **2005,** 78, (3), 585-594.

72. Park, J.; Joo, J.; Kwon, S. G.; Jang, Y.; Hyeon, T. *Angew. Chemie-Inter. Ed.* **2007,** 46, (25), 4630-4660.

73. Kerekes, L.; Hakl, J.; Meszaros, S.; Vad, K.; Gurin, P.; Kis-Varga, I.; Uzonyi, I.; Szabo, S.; Beke, D. L. *Czechoslov. J. Phys.* **2002,** 52, A89-A92.

74. Ponpandian, N.; Narayanasamy, A.; Chinnasamy, C. N.; Sivakumar, N.; Greneche, J. M.; Chattopadhyay, K.; Shinoda, K.; Jeyadevan, B.; Tohji, K. *Appl. Phys. Lett.* **2005,** 86, (19), 3512-3514.

75. Chinnasamy, C. N.; Narayanasamy, A.; Ponpandian, N.; Chattopadhyay, K.; Guerault, H.; Greneche, J. M. *J. Phys.-Condens. Matter* **2000,** 12, (35), 7795-7805.

76. Pardavihorvath, M.; Takacs, L. *Scripta Metallurg. Mater.* **1995,** 33, (10-11), 1731-1740.

77. Huber, D. L. *Small* **2005,** 1, (5), 482-501.

78. Burda, C.; Chen, X. B.; Narayanan, R.; El-Sayed, M. A. *Chem. Rev.* **2005,** 105, (4), 1025-1102.

79. Mullin, J. W., *Crystallization*. 4th Ed.; Reed Elsevierplc group: 2001; p 610.

80. Dirksen, J. A.; Ring, T. A. *Chem. Eng. Sci.* **1991,** 46, (10), 2389-2427.

81. Cozzoli, P. D., *Advanced Wet-Chemical Synthetic Approaches to Inorganic Nanostructures*. Transworld Research Network: 2008; p 407.

82. Lamer, V. K.; Dinegar, R. H. *JACS* **1950,** 72, (11), 4847-4854.

83. Murray, C. B.; Norris, D. J.; Bawendi, M. G. *JACS* **1993,** 115, (19), 8706-8715.

84. Puntes, V. F.; Krishnan, K. M.; Alivisatos, A. P. *Science* **2001,** 291, (5511), 2115-2117.

85. Bao, Y. P.; Calderon, H.; Krishnan, K. M. *J. Phys. Chem. C* **2007,** 111, (5), 1941-1944.
86. Yin, J. S.; Wang, Z. L. *Phys. Rev. Lett.* **1997,** 79, (13), 2570-2573.
87. Samia, A. C. S.; Hyzer, K.; Schlueter, J. A.; Qin, C. J.; Jiang, J. S.; Bader, S. D.; Lin, X. M. *JACS* **2005,** 127, (12), 4126-4127.
88. Peng, S.; Wang, C.; Xie, J.; Sun, S. H. *JACS* **2006,** 128, (33), 10676-10677.
89. Lu, Y.; Lu, X. M.; Mayers, B. T.; Herricks, T.; Xia, Y. N. *J. Solid State Chem.* **2008,** 181, (7), 1530-1538.
90. Zheng, H. M.; Smith, R. K.; Jun, Y. W.; Kisielowski, C.; Dahmen, U.; Alivisatos, A. P. *Science* **2009,** 324, (5932), 1309-1312.
91. Morales, M. P.; Gonzalezcarreno, T.; Serna, C. J. *J. Mater. Res.* **1992,** 7, (9), 2538-2545.
92. Ocana, M.; Rodriguezclemente, R.; Serna, C. J. *Adv. Mater.* **1995,** 7, (2), 212-216.
93. Matijevic, E. *Chem. Mater.* **1993,** 5, (4), 412-426.
94. Lifshitz, I. M.; Slyozov, V. V. *J. Phys. & Chem. Solid.* **1961,** 19, (1-2), 35-50.
95. Niederberger, M.; Colfen, H. *Phys. Chem. Chem. Phys.* **2006,** 8, (28), 3271-3287.
96. Zhang, Q.; Liu, S. J.; Yu, S. H. *J. Mater. Chem.* **2009,** 19, (2), 191-207.
97. Wang, L. Y.; Bao, J.; Wang, L.; Zhang, F.; Li, Y. D. *Chem.-A Europ. J.* **2006,** 12, (24), 6341-6347.
98. Oskam, G.; Hu, Z. S.; Penn, R. L.; Pesika, N.; Searson, P. C. *Phys. Rev. E* **2002,** 66, (1), 2115-2124.
99. Pearson, R. G. *JACS* **1963,** 85, (22), 3533-3534.
100. Pearson, R. G. *J. Chem. Edu.* **1968,** 45, (9), 581-582.
101. Massart, R. *IEEE Trans. Mag.* **1981,** 17, (2), 1247-1248.
102. Cushing, B. L.; Kolesnichenko, V. L.; O'Connor, C. J. *Chem. Rev.* **2004,** 104, (9), 3893-3946.
103. Li, Z.; Tan, B.; Allix, M.; Cooper, A. I.; Rosseinsky, M. J. *Small* **2008,** 4, (2), 231-239.
104. Chinnasamy, C. N.; Jeyadevan, B.; Perales-Perez, O.; Shinoda, K.; Tohji, K.; Kasuya, A. *IEEE Trans. Mag.* **2002,** 38, (5), 2640-2642.
105. Liu, Z. L.; Liu, Y. J.; Yao, K. L.; Ding, Z. H.; Tao, J.; Wang, X. *J. Mater. Synth. & Process.* **2002,** 10, (2), 83-87.
106. Vayssieres, L.; Chaneac, C.; Tronc, E.; Jolivet, J. P. *J. Colloid & Interface Sci.* **1998,** 205, (2), 205-212.

107. Kang, Y. S.; Risbud, S.; Rabolt, J. F.; Stroeve, P. *Chem. Mater.* **1996,** 8, (9), 2209-2215.

108. Kim, D. K.; Zhang, Y.; Voit, W.; Rao, K. V.; Muhammed, M. *J. Mag. Mag. Mater.* **2001,** 225, (1-2), 30-36.

109. Li, J.; Dai, D. L.; Zhao, B. G.; Lin, Y. Q.; Liu, C. Y. *J. Nano. Res.* **2002,** 4, (3), 261-264.

110. Ayyappan, S.; Mahadevan, S.; Chandramohan, P.; Srinivasan, M. P.; Philip, J.; Raj, B. *J. Phys. Chem.* C **2010,** 114, (14), 6334-6341.

111. Chen, Y.; Ruan, M.; Jiang, Y. F.; Cheng, S. G.; Li, W. *J. Alloys & Compounds* **2010,** 493, (1-2), L36-L38.

112. Chen, Q.; Rondinone, A. J.; Chakoumakos, B. C.; Zhang, Z. J. *J. Mag. Mag. Mater.* **1999,** 194, (1-3), 1-7.

113. Tang, Z. X.; Sorensen, C. M.; Klabunde, K. J.; Hadjipanayis, G. C. *J. Colloid & Interface Sci.* **1991,** 146, (1), 38-52.

114. Wu, Y.; Shi, C. H.; Yang, W. *Rare Metals* **2010,** 29, (4), 385-389.

115. Pita, M.; Abad, J. M.; Vaz-Dominguez, C.; Briones, C.; Mateo-Marti, E.; Martin-Gago, J. A.; Morales, M. D. P.; Fernandez, V. M. *J. Colloid & Interface Sci.* **2008,** 321, (2), 484-492.

116. Jadhav, S. S.; Shirsath, S. E.; Toksha, B. G.; Patange, S. M.; Shengule, D. R.; Jadhav, K. M. *Phys. B-Condens. Matter* **2010,** 405, (12), 2610-2614.

117. Shaikh, P. A.; Kambale, R. C.; Rao, A. V.; Kolekar, Y. D. *J. Alloys & Compounds* **2010,** 492, (1-2), 590-596.

118. Cheng, W.; Tang, K. B.; Sheng, J. *Chem.-A Europ. J.* **2010,** 16, (12), 3608-3612.

119. Kim, D. K.; Mikhaylova, M.; Zhang, Y.; Muhammed, M. *Chem. Mater.* **2003,** 15, (8), 1617-1627.

120. Tamaura, Y.; Takahashi, K.; Kodera, Y.; Saito, Y.; Inada, Y. *Biotech. Lett.* **1986,** 8, (12), 877-880.

121. Kim, D. K.; Mikhaylova, M.; Wang, F. H.; Kehr, J.; Bjelke, B.; Zhang, Y.; Tsakalakos, T.; Muhammed, M. *Chem. Mater.* **2003,** 15, (23), 4343-4351.

122. Paul, K. G.; Frigo, T. B.; Groman, J. Y.; Groman, E. V. *Bioconj. Chem.* **2004,** 15, (2), 394-401.

123. Lawaczeck, R.; Menzel, M.; Pietsch, H. *Appl. Organometal. Chem.* **2004,** 18, (10), 506-513.

124. Hogemann-Savellano, D.; Bos, E.; Blondet, C.; Sato, F.; Abe, T.; Josephson, L.; Weissleder, R.; Gaudet, J.; Sgroi, D.; Peters, P. J.; Basilion, J. P. *Neoplasia* **2003,** 5, (6), 495-506.

125. Papisov, M. I.; Bogdanov, A.; Schaffer, B.; Nossiff, N.; Shen, T.; Weissleder, R.; Brady, T. J. *J. Mag. Mag. Mater.* **1993,** 122, (1-3), 383-386.

126. Fauconnier, N.; Bee, A.; Roger, J.; Pons, J. N. *J. Molec. Liquid.* **1999,** 83, (1-3), 233-242.

127. Portet, D.; Denizot, B.; Rump, E.; Hindre, F.; Le Jeune, J. J.; Jallet, P. *Drug Dev. Res.* **2001,** 54, (4), 173-181.

128. Mornet, S.; Vasseur, S.; Grasset, F.; Duguet, E. *J. Mater. Chem.* **2004,** 14, (14), 2161-2175.

129. Kroll, E.; Winnik, F. M.; Ziolo, R. F. *Chem. Mater.* **1996,** 8, (8), 1594-&.

130. Bahadur, R.; Bhattarai, S. R.; Aryal, S.; Bhattarai, N.; Lee, B. M.; Kim, H. Y. *Polymer Inter.* **2007,** 56, (4), 518-524.

131. Josephson, L.; Tung, C. H.; Moore, A.; Weissleder, R. *Bioconj. Chem.* **1999,** 10, (2), 186-191.

132. Skoutelas, A. P.; Karakassides, M. A.; Petridis, D. *Chem. Mater.* **1999,** 11, (10), 2754-2759.

133. Jolivet, J. P.; Froidefond, C.; Pottier, A.; Chaneac, C.; Cassaignon, S.; Tronc, E.; Euzen, P. *J. Mater. Chem.* **2004,** 14, (21), 3281-3288.

134. Bergemann, C.; Muller-Schulte, D.; Oster, J.; a Brassard, L.; Lubbe, A. S. *J. Mag. Mag. Mater.* **1999,** 194, (1-3), 45-52.

135. Oppegard, A. L.; Miller, H. C.; Darnell, F. J. *J. Appl. Phys.* **1961,** 32, (3), S184-187.

136. Kobayashi, Y.; Horie, M.; Nagao, D.; Ando, Y.; Miyazaki, T.; Konno, M. *Mater. Lett.* **2006,** 60, (16), 2046-2049.

137. Gibot, P.; Tronc, E.; Chaneac, C.; Jolivet, J. P.; Fiorani, D.; Testa, A. M. *J. Mag. Mag. Mater.* **2005,** 290, 555-558.

138. Linderoth, S.; Morup, S. *J. Appl. Phys.* **1990,** 67, (9), 4472-4474.

139. Galvez, N.; Sanchez, P.; Dominguez-Vera, J. M.; Soriano-Portillo, A.; Clemente-Leon, M.; Coronado, E. *J. Mater. Chem.* **2006,** 16, (26), 2757-2761.

140. Galvez, N.; Valero, E.; Ceolin, M.; Trasobares, S.; Lopez-Haro, M.; Calvino, J. J.; Dominguez-Vera, J. M. *Inorg. Chem.* **2010,** 49, (4), 1705-1711.

141. Linderoth, S.; Morup, S. *J. Appl. Phys.* **1991,** 69, (8), 5256-5261.

142. Tong, G. X.; Guan, J. G.; Xiao, Z. D.; Mou, F. Z.; Wang, W.; Yan, G. Q. *Chem. Mater.* **2008,** 20, (10), 3535-3539.
143. Chen, D. H.; Hsieh, C. H. *J. Mater. Chem.* **2002,** 12, (8), 2412-2415.
144. Wang, H. Z.; Li, J. G.; Kou, X. L.; Zhang, L. *J. Cryst. Growth* **2008,** 310, (12), 3072-3076.
145. Ji, R. P.; Jiang, J. S.; Hu, M. *J. Phys. Chem. C* **2010,** 114, (28), 12090-12094.
146. Grzelczak, M.; Perez-Juste, J.; Rodriguez-Gonzalez, B.; Spasova, M.; Barsukov, I.; Farle, M.; Liz-Marzan, L. M. *Chem. Mater.* **2008,** 20, (16), 5399-5405.
147. Schlesinger, H. I.; Brown, H. C.; Finholt, A. E.; Gilbreath, J. R.; Hoekstra, H. R.; Hyde, E. K. *JACS* **1953,** 75, (1), 215-219.
148. Shen, J. Y.; Li, Z. Y.; Yan, Q. J.; Chen, Y. *J. Phys. Chem.* **1993,** 97, (32), 8504-8511.
149. Linderoth, S.; Morup, S.; Bentzon, M. D. *J. Mag. Mag. Mater.* **1990,** 83, (1-3), 457-459.
150. Wells, S.; Charles, S. W.; Morup, S.; Linderoth, S.; Vanwonterghem, J.; Larsen, J.; Madsen, M. B. *J. Phys.-Condens. Matter* **1989,** 1, (43), 8199-8208.
151. Kobayashi, Y.; Horie, M.; Konno, M.; Rodriguez-Golzalez, B.; Liz-Marzan, L. M. *J. Phys. Chem. B* **2003,** 107, 7420-7425.
152. Warne, B.; Kasyutich, O. I.; Mayes, E. L.; Wiggins, J. A. L.; Wong, K. K. W. *IEEE Trans. Mag.* **2000,** 36, (5), 3009-3011.
153. Klem, M. T.; Willits, D.; Solis, D. J.; Belcher, A. M.; Young, M.; Douglas, T. *Adv. Funct. Mater.* **2005,** 15, (9), 1489-1494.
154. Mao, C. B.; Solis, D. J.; Reiss, B. D.; Kottmann, S. T.; Sweeney, R. Y.; Hayhurst, A.; Georgiou, G.; Iverson, B.; Belcher, A. M. *Science* **2004,** 303, (5655), 213-217.
155. Reiss, B. D.; Mao, C. B.; Solis, D. J.; Ryan, K. S.; Thomson, T.; Belcher, A. M. *Nano Lett.* **2004,** 4, (6), 1127-1132.
156. Zhang, G. X.; Sun, S. H.; Li, R. Y.; Zhang, Y.; Cai, M.; Sun, X. L. *Chem. Mater.* **2010,** 22, (16), 4721-4727.
157. Vasquez, Y.; Sra, A. K.; Schaak, R. E. *JACS* **2005,** 127, (36), 12504-12505.
158. Lu, Y.; Zhao, Y.; Yu, L.; Dong, L.; Shi, C.; Hu, M. J.; Xu, Y. J.; Wen, L. P.; Yu, S. H. *Adv. Mater.* **2010,** 22, (12), 1407-+.
159. Zhao, D.; Wu, X.; Guan, H.; Han, E. *J. Supercrit. Fluids* **2007,** 42, (2), 226-233.
160. Xu, C. B.; Teja, A. S. *J. Supercrit. Fluids* **2008,** 44, (1), 85-91.
161. Sue, K.; Suzuki, M.; Arai, K.; Ohashi, T.; Ura, H.; Matsui, K.; Hakuta, Y.; Hayashi, H.; Watanabe, M.; Hiaki, T. *Green Chem.* **2006,** 8, (7), 634-638.

162. Teja, A. S.; Koh, P. Y. *Progress in Cryst. Growth & CharacT. Mater.* **2009,** 55, (1-2), 22-45.

163. Zhou, X. M.; Wei, X. W. *Cryst. Growth & Design* **2009,** 9, (1), 7-12.

164. Ge, S.; Shi, X. Y.; Sun, K.; Li, C. P.; Uher, C.; Baker, J. R.; Holl, M. M. B.; Orr, B. G. *J. Phys. Chem. C* **2009,** 113, (31), 13593-13599.

165. Salazar-Alvarez, G.; Muhammed, M.; Zagorodni, A. A. *Chem. Eng. Sci.* **2006,** 61, (14), 4625-4633.

166. Takami, S.; Sato, T.; Mousavand, T.; Ohara, S.; Umetsu, M.; Adschiri, T. *Mater. Lett.* **2007,** 61, (26), 4769-4772.

167. Sreeja, V.; Joy, P. A. *Mater. Res. Bull.* **2007,** 42, (8), 1570-1576.

168. Chen, D.; Xu, R. *Mater. Res. Bull.* **1998,** 33, (7), 1015-1021.

169. Zhang, Z. J.; Chen, X. Y.; Wang, B. N.; Shi, C. W. *J. Cryst. Growth* **2008,** 310, (24), 5453-5457.

170. Liao, Q. L.; Tannenbaum, R.; Wang, Z. L. *J. Phys. Chem. B* **2006,** 110, (29), 14262-14265.

171. Park, J.; Lee, E.; Hwang, N. M.; Kang, M. S.; Kim, S. C.; Hwang, Y.; Park, J. G.; Noh, H. J.; Kini, J. Y.; Park, J. H.; Hyeon, T. *Angew. Chemie-Inter. Ed.* **2005,** 44, (19), 2872-2877.

172. Ung, D.; Tung, L. D.; Caruntu, G.; Delaportas, D.; Alexandrou, I.; Prior, I. A.; Thanh, N. T. K. *Cryst. eng. comm.* **2009,** 11, (7), 1309-1316.

173. Jana, N. R.; Chen, Y. F.; Peng, X. G. *Chem. Mater.* **2004,** 16, (20), 3931-3935.

174. Kwon, S. G.; Piao, Y.; Park, J.; Angappane, S.; Jo, Y.; Hwang, N. M.; Park, J. G.; Hyeon, T. *JACS* **2007,** 129, (41), 12571-12584.

175. Hyeon, T.; Lee, S. S.; Park, J.; Chung, Y.; Bin Na, H. *JACS* **2001,** 123, (51), 12798-12801.

176. Puntes, V. F.; Krishnan, K. M.; Alivisatos, P. *Appl. Phys. Lett.* **2001,** 78, (15), 2187-2189.

177. Wang, C.; Peng, S.; Lacroix, L. M.; Sun, S. H. *Nano Res.* **2009,** 2, (5), 380-385.

178. Seo, W. S.; Shim, J. H.; Oh, S. J.; Lee, E. K.; Hur, N. H.; Park, J. T. *JACS* **2005,** 127, (17), 6188-6189.

179. Xu, Z. C.; Shen, C. M.; Hou, Y. L.; Gao, H. J.; Sun, S. S. *Chem. Mater.* **2009,** 21, (9), 1778-1780.

180. Kim, D.; Lee, N.; Park, M.; Kim, B. H.; An, K.; Hyeon, T. *JACS* **2009,** 131, (2), 454-455.

181. Chaubey, G. S.; Barcena, C.; Poudyal, N.; Rong, C. B.; Gao, J. M.; Sun, S. H.; Liu, J. P. *JACS* **2007,** 129, (23), 7214-7215.
182. Song, O.; Zhang, Z. J. *JACS* **2004,** 126, (19), 6164-6168.
183. Yang, H. T.; Ogawa, T.; Hasegawa, D.; Takahashi, M. *J. Appl. Phys.* **2008,** 103, (7).
184. Rockenberger, J.; Scher, E. C.; Alivisatos, A. P. *JACS* **1999,** 121, (49), 11595-11596.
185. Kovalenko, M. V.; Bodnarchuk, M. I.; Lechner, R. T.; Hesser, G.; Schaffler, F.; Heiss, W. *JACS* **2007,** 129, (20), 6352-6352.
186. Park, J.; An, K. J.; Hwang, Y. S.; Park, J. G.; Noh, H. J.; Kim, J. Y.; Park, J. H.; Hwang, N. M.; Hyeon, T. *Nature Mater.* **2004,** 3, (12), 891-895.
187. Salazar-Alvarez, G.; Qin, J.; Sepelak, V.; Bergmann, I.; Vasilakaki, M.; Trohidou, K. N.; Ardisson, J. D.; Macedo, W. A. A.; Mikhaylova, M.; Muhammed, M.; Baro, M. D.; Nogues, J. *JACS* **2008,** 130, (40), 13234-13239.
188. Ren, J. T.; Tilley, R. D. *JACS* **2007,** 129, (11), 3287-3291.
189. An, K.; Kwon, S. G.; Park, M.; Bin Na, H.; Baik, S. I.; Yu, J. H.; Kim, D.; Son, J. S.; Kim, Y. W.; Song, I. C.; Moon, W. K.; Park, H. M.; Hyeon, T. *Nano Lett.* **2008,** 8, (12), 4252-4258.
190. Sun, S. H.; Murray, C. B.; Weller, D.; Folks, L.; Moser, A. *Science* **2000,** 287, (5460), 1989-1992.
191. Farrell, D.; Majetich, S. A.; Wilcoxon, J. P. *J. Phys Chem. B* **2003,** 107, (40), 11022-11030.
192. Zeng, H.; Rice, P. M.; Wang, S. X.; Sun, S. H. *JACS* **2004,** 126, (37), 11458-11459.
193. Murray, C. B.; Sun, S. H.; Gaschler, W.; Doyle, H.; Betley, T. A.; Kagan, C. R. *IBM J. Res. Dev.* **2001,** 45, (1), 47-56.
194. Sun, S.; Murray, C. B.; Doyle, H. *Adv. Hard & Soft Mag. Mater.* **1999,** 577, 385-398.
195. Kovalenko, M. V.; Bodnarchuk, M. I.; Lechner, R. T.; Hesser, G.; Schaffler, F.; Heiss, W. *JACS* **2007,** 129, (20), 6352-6353.
196. Shao, H. P.; Lee, H.; Huang, Y. Q.; Ko, I. Y.; Kim, C. *IEEE Trans. Mag.* **2005,** 41, (10), 3388-3390.
197. Hou, Y. L.; Xu, Z. C.; Sun, S. H. *Angew. Chemie-Inter. Ed.* **2007,** 46, (33), 6329-6332.
198. Yang, H. T.; Ogawa, T.; Hasegawa, D.; Takahashi, M. *J. Appl. Phys.* **2008,** 103, (7), 5421-5424.

199. Sun, S. H.; Zeng, H.; Robinson, D. B.; Raoux, S.; Rice, P. M.; Wang, S. X.; Li, G. X. *JACS* **2004,** 126, (1), 273-279.
200. Sun, S. H.; Zeng, H. *JACS* **2002,** 124, (28), 8204-8205.
201. Shevchenko, E. V.; Talapin, D. V.; Rogach, A. L.; Kornowski, A.; Haase, M.; Weller, H. *JACS* **2002,** 124, (38), 11480-11485.
202. Nandwana, V.; Elkins, K. E.; Poudyal, N.; Chaubey, G. S.; Yano, K.; Liu, J. P. *J. Phys. Chem. C* **2007,** 111, (11), 4185-4189.
203. Chen, M.; Kim, J.; Liu, J. P.; Fan, H. Y.; Sun, S. H. *JACS* **2006,** 128, (22), 7132-7133.
204. Shevchenko, E. V.; Talapin, D. V.; Schnablegger, H.; Kornowski, A.; Festin, O.; Svedlindh, P.; Haase, M.; Weller, H. *JACS* **2003,** 125, (30), 9090-9101.
205. Hou, Y. L.; Kondoh, H.; Kogure, T.; Ohta, T. *Chem. Mater.* **2004,** 16, (24), 5149-5152.
206. Chen, M.; Nikles, D. E. *J. Appl. Phys.* **2002,** 91, (10), 8477-8479.
207. Langevin, D. *Annual Rev. Phys. Chem.* **1992,** 43, 341-369.
208. Chhabra, V.; Pillai, V.; Mishra, B. K.; Morrone, A.; Shah, D. O. *Langmuir* **1995,** 11, (9), 3307-3311.
209. Levinger, N. E.; Swafford, L. A. *Annual Rev. Phys. Chem.* **2009,** 60, 385-406.
210. Zhang, X. H.; Ho, K. M.; Wu, A. H.; Wong, K. H.; Li, P. *Langmuir* **2010,** 26, (8), 6009-6014.
211. Carpenter, E. E.; Sangregorio, C.; O'Connor, C. J. *IEEE Trans. Mag.* **1999,** 35, (5), 3496-3498.
212. Lin, J.; Zhou, W. L.; Kumbhar, A.; Wiemann, J.; Fang, J. Y.; Carpenter, E. E.; O'Connor, C. J. *J. Solid State Chem.* **2001,** 159, (1), 26-31.
213. Cho, S. J.; Idrobo, J. C.; Olamit, J.; Liu, K.; Browning, N. D.; Kauzlarich, S. M. *Chem. Mater.* **2005,** 17, (12), 3181-3186.
214. Chen, D.; Liu, S.; Li, J. J.; Zhao, N. Q.; Shi, C. S.; Du, X. W.; Sheng, J. *J. Alloys & Compounds* **2009,** 475, (1-2), 494-500.
215. He, Q. G.; Mukerjee, S. *Electrochimica Acta* **2010,** 55, (5), 1709-1719.
216. Gao, Y.; Zhang, X. W.; Yin, Z. G.; Qu, S.; You, J. B.; Chen, N. F. *Nanoscale Res. Lett.* **2010,** 5, (1), 1-6.
217. Ervithayasuporn, V.; Kawakami, Y. *J. Colloid & Interface Sci.* **2009,** 332, (2), 389-393.

218. Bellusci, M.; La Barbera, A.; Seralessandri, L.; Padella, F.; Piozzi, A.; Varsano, F. *Polymer Inter.* **2009,** 58, (10), 1142-1147.
219. Lyon, J. L.; Fleming, D. A.; Stone, M. B.; Schiffer, P.; Williams, M. E. *Nano Lett.* **2004,** 4, (4), 719-723.
220. Cho, S. J.; Shahin, A. M.; Long, G. J.; Davies, J. E.; Liu, K.; Grandjean, F.; Kauzlarich, S. M. *Chem. Mater.* **2006,** 18, (4), 960-967.
221. Kim, J.; Kim, H. S.; Lee, N.; Kim, T.; Kim, H.; Yu, T.; Song, I. C.; Moon, W. K.; Hyeon, T. *Angew. Chemie-Inter. Ed.* **2008,** 47, (44), 8438-8441.
222. Kruis, F. E.; Fissan, H.; Peled, A. *J. Aerosol Sci.* **1998,** 29, (5-6), 511-535.
223. Dong, X. L.; Choi, C. J.; Kim, B. K. *J. Appl. Phys.* **2002,** 92, (9), 5380-5385.
224. Tavakoli, A.; Sohrabi, M.; Kargari, A. *Chem. Paper.* **2007,** 61, (3), 151-170.
225. Wang, Z. H.; Zhang, Z. D.; Choi, C. J.; Kim, B. K. *J. Alloys & Compounds* **2003,** 361, (1-2), 289-293.
226. Choi, C. J.; Tojochko, O.; Kim, B. K. *Mater. Lett.* **2002,** 56, (3), 289-294.
227. Wang, Z. H.; Choi, C. J.; Kim, B. K.; Kim, J. C.; Zhang, Z. D. *Carbon* **2003,** 41, (9), 1751-1758.
228. Wang, Z. H.; Choi, C. J.; Kim, J. C.; Kim, B. K.; Zhang, Z. D. *Mater. Lett.* **2003,** 57, (22-23), 3560-3564.
229. Dong, X. L.; Choi, C. J.; Kim, B. K. *Scripta Mater.* **2002,** 47, (12), 857-861.
230. Suh, Y. J.; Jang, H. D.; Chang, H.; Kim, W. B.; Kim, H. C. *Powder Techno.* **2006,** 161, (3), 196-201.
231. Jang, H. D.; Hwang, D. W.; Kim, D. P.; Kim, H. C.; Lee, B. Y.; Jeong, I. B. *Mater. Res. Bull.* **2004,** 39, (1), 63-70.
232. Zhang, D.; Wei, S. Y.; Kaila, C.; Su, X.; Wu, J.; Karki, A. B.; Young, D. P.; Guo, Z. H. *Nanoscale* **2010,** 2, (6), 917-919.
233. Strobel, R.; Pratsinis, S. E. *J. Mater. Chem.* **2007,** 17, (45), 4743-4756.
234. Janzen, C.; Roth, P. *Combust. & Flame* **2001,** 125, (3), 1150-1161.
235. Guo, B.; Kennedy, I. M. *Aerosol Sci. & Tech.* **2007,** 41, (10), 944-951.
236. Buyukhatipoglu, K.; Clyne, A. M. *J. Nano. Res.* **2010,** 12, (4), 1495-1508.
237. Kumfer, B. M.; Shinoda, K.; Jeyadevan, B.; Kennedy, I. M. *J. Aerosol Sci.* **2010,** 41, (3), 257-265.
238. Li, D.; Teoh, W. Y.; Selomulya, C.; Woodward, R. C.; Amal, R.; Rosche, B. *Chem. Mater.* **2006,** 18, (26), 6403-6413.
239. Grass, R. N.; Stark, W. J. *J. Mater. Chem.* **2006,** 16, (19), 1825-1830.

240. Strobel, R.; Pratsinis, S. E. *Adv. Powder Tech.* **2009,** 20, (2), 190-194.
241. Dosev, D.; Nichkova, M.; Dumas, R. K.; Gee, S. J.; Hammock, B. D.; Liu, K.; Kennedy, I. M. *Nanotech.* **2007,** 18, (5), 7613-7617.
242. Zhao, N.; Gao, M. Y. *Adv. Mater.* **2009,** 21, (2), 184-185.
243. Herrmann, I. K.; Grass, R. N.; Mazunin, D.; Stark, W. J. *Chem. Mater.* **2009,** 21, (14), 3275-3281.
244. Li, D.; Teoh, W. Y.; Woodward, R. C.; Cashion, J. D.; Selomulya, C.; Amal, R. *J. Phys. Chem. C* **2009,** 113, (28), 12040-12047.
245. Li, D.; Teoh, W. Y.; Selomulya, C.; Woodward, R. C.; Munroe, P.; Amal, R. *J. Mater. Chem.* **2007,** 17, (46), 4876-4884.
246. Grass, R. N.; Athanassiou, E. K.; Stark, W. J. *Angew. Chemie-Inter. Ed.* **2007,** 46, (26), 4909-4912.
247. Herrmann, I. K.; Urner, M.; Koehler, F. M.; Hasler, M.; Roth-Z'Graggen, B.; Grass, R. N.; Ziegler, U.; Beck-Schimmer, B.; Stark, W. J. *Small* **2010,** 6, (13), 1388-1392.
248. Vollath, D. *Kona-Powder & Particle* **2007,** 25, 39-55.
249. Sergiienko, R.; Shibata, E.; Zentaro, A.; Shindo, D.; Nakamura, T.; Qin, G. W. *Acta Mater.* **2007,** 55, (11), 3671-3680.
250. Sergiienko, R.; Shibata, E.; Kim, S.; Kinota, T.; Nakamura, T. *Carbon* **2009,** 47, (4), 1056-1065.
251. Sergiienko, R.; Kim, S.; Shibata, E.; Nakamura, T. *J. Nano. Res.* **2010,** 12, (2), 481-491.
252. Matsui, I. *J. Nano. Res.* **2006,** 8, (3-4), 429-443.
253. Bai, L. Y.; Fan, J. M.; Hu, P.; Yuan, F. L.; Li, J. L.; Tang, Q. *J. Alloys & Compounds* **2009,** 481, (1-2), 563-567.
254. Son, S.; Taheri, M.; Carpenter, E.; Harris, V. G.; McHenry, M. E. *J. Appl. Phys.* **2002,** 91, (10), 7589-7591.
255. Subramanian, V.; Baskaran, R.; Krishnan, H. *Aerosol & Air Quality Res.* **2009,** 9, (2), 172-186.
256. Turgut, Z.; Scott, J. H.; Huang, M. Q.; Majetich, S. A.; McHenry, M. E. *J. Appl. Phys.* **1998,** 83, (11), 6468-6470.
257. Bystrzejewski, M.; Karoly, Z.; Szepvolgyi, J.; Kaszuwara, W.; Huczko, A.; Lange, H. *Carbon* **2009,** 47, (8), 2040-2048.
258. Girshick, S. L.; Chiu, C. P.; Muno, R.; Wu, C. Y.; Yang, L.; Singh, S. K.; Mcmurry, P. H. *J. Aerosol Sci.* **1993,** 24, (3), 367-382.

259. Bystrzejewski, M.; Huczko, A.; Lange, H.; Baranowski, P.; Cota-Sanchez, G.; Soucy, G.; Szczytko, J.; Twardowski, A. *Nanotech.* **2007,** 18, (14), 8312-8317.
260. Chau, J. L. H.; Hsu, M. K.; Kao, C. C. *Mater. Lett.* **2006,** 60, (7), 947-951.
261. Srikanth, H.; Hajndl, R.; Chirinos, C.; Sanders, J.; Sampath, A.; Sudarshan, T. S. *Appl. Phys. Lett.* **2001,** 79, (21), 3503-3505.
262. Hojati-Talemi, P.; Azadmanjiri, J.; Simon, G. P. *Mater. Lett.* **2010,** 64, (15), 1684-1687.
263. Fujita, T.; Hayashi, Y.; Tokunaga, T.; Butler, T.; Rupesinghe, N. L.; Teo, K. B. K.; Amaratunga, G. A. J. *Appl. Phys. Lett.* **2007,** 90, (13), 3744-3746.
264. Wei, Z. Q.; Xia, T. D.; Bai, L. F.; Wang, J.; Wu, Z. G.; Yan, P. X. *Mater. Lett.* **2006,** 60, (6), 766-770.
265. Kim, S.; Sergiienko, R.; Shibata, E.; Nakamura, T. *Mater. Chem. & Phys.* **2010,** 122, (1), 164-168.
266. Gutsch, A.; Kramer, M.; Michael, G. *KONA* **2002,** No20, 24-37.
267. Swihart, M. T. *Current Opinion in Colloid & Interface Sci.* **2003,** 8, (1), 127-133.
268. Fievet, F.; Lagier, J. P.; Blin, B.; Beaudoin, B.; Figlarz, M. *Solid State Ionics* **1989,** 32-3, 198-205.
269. Ung, D.; Soumare, Y.; Chakroune, N.; Viau, G.; Vaulay, M. J.; Richard, V.; Fievet, F. *Chem. Mater.* **2007,** 19, (8), 2084-2094.
270. Joseyphus, R. J.; Shinoda, K.; Kodama, D.; Jeyadevan, B. *Mater. Chem. & Phys.* **2010,** 123, (2-3), 487-493.
271. Sicard, L.; Le Meins, J. M.; Methivier, C.; Herbst, F.; Ammar, S. *J. Mag. Mag. Mater.* **2010,** 322, (18), 2634-2640.
272. Altincekic, T. G.; Boz, I.; Baykal, A.; Kazan, S.; Topkaya, R.; Toprak, M. S. *J. Alloys & Compounds* **2010,** 493, (1-2), 493-498.
273. Kamal, S. S. K.; Sahoo, P. K.; Premkumar, M.; Rao, N. V. R.; Kumar, T. J.; Sreedhar, B.; Singh, A. K.; Ram, S.; Sekhar, K. C. *J. Alloys & Compounds* **2009,** 474, (1-2), 214-218.
274. Bai, L. Y.; Fan, J. M.; Cao, Y. B.; Yuan, F. L.; Zuo, A.; Tang, Q. *J. Cryst. Growth* **2009,** 311, (8), 2474-2479.
275. Wang, N.; Cao, X.; Kong, D. S.; Chen, W. M.; Guo, L.; Chen, C. P. *J. Phys. Chem. C* **2008,** 112, (17), 6613-6619.
276. Joseyphus, R. J.; Kodama, D.; Matsumoto, T.; Sato, Y.; Jeyadevan, B.; Tohji, K. *J. Mag. Mag. Mater.* **2007,** 310, (2), 2393-2395.

277. Cai, W.; Wan, J. Q. *J. Colloid & Interface Sci.* **2007,** 305, (2), 366-370.
278. Kodama, D.; Shinoda, K.; Sato, K.; Konno, Y.; Joseyphus, R. J.; Motomiya, K.; Takahashi, H.; Matsumoto, T.; Sato, Y.; Tohji, K.; Jeyadevan, B. *Adv. Mater.* **2006,** 18, (23), 3154-3155.
279. Ung, D.; Viau, G.; Ricolleau, C.; Warmont, F.; Gredin, P.; Fievet, F. F. *Adv. Mater.* **2005,** 17, (3), 338-339.
280. Chakroune, N.; Viau, G.; Ricolleau, C.; Fievet-Vincent, F.; Fievet, F. *J. Mater. Chem.* **2003,** 13, (2), 312-318.
281. Livage, J.; Henry, M.; Sanchez, C. *Progress in Solid State Chem.* **1988,** 18, (4), 259-341.
282. Ari, M.; Miller, K. J.; Marinkovic, B. A.; Jardim, P. M.; Avillez, R.; Rizzo, F.; White, M. A. *J. Sol-Gel Sci. Tech.* **2010,** DOI 10.1007/s10971-010-2364-9.
283. Gnanam, S.; Rajendram, V. *J. Sol-Gel Sci. Tech.* **2010,** DOI 10.1007/s10971-010-2356-9.
284. Prakash, I.; Nallamuthu, N.; Muralidharan, P.; Venkateswarlu, M.; Misra, M.; Mohanty, A.; Satyanarayana, N. *J. Sol-Gel Sci. Tech.* **2010,** DOI 10.1007/s10971-010-2350-2.
285. Gedam, N. N.; Padole, P. R.; Rithe, S. K.; Chaudhari, G. N. *J. Sol-Gel Sci. Tech.* **2009,** 50, (3), 296-300.
286. Brinker, C. J.; Scherer, G. W., *Sol–Gel Science: The Physics and Chemistry of Sol–Gel Processing*. Academic Press: Boston, 1990.
287. Cannas, C.; Gatteschi, D.; Musinu, A.; Piccaluga, G.; Sangregorio, C. *J. Phys. Chem. B* **1998,** 102, (40), 7721-7726.
288. Ennas, G.; Musinu, A.; Piccaluga, G.; Zedda, D.; Gatteschi, D.; Sangregorio, C.; Stanger, J. L.; Concas, G.; Spano, G. *Chem. Mater.* **1998,** 10, (2), 495-502.
289. Stober, W.; Fink, A.; Bohn, E. *J. Colloid & Interface Sci.* **1968,** 26, (1), 62-67.
290. Ohmori, M.; Matijevic, E. *J. Colloid & Interface Sci.* **1992,** 150, (2), 594-598.
291. Lu, C. W.; Hung, Y.; Hsiao, J. K.; Yao, M.; Chung, T. H.; Lin, Y. S.; Wu, S. H.; Hsu, S. C.; Liu, H. M.; Mou, C. Y.; Yang, C. S.; Huang, D. M.; Chen, Y. C. *Nano Lett.* **2007,** 7, (1), 149-154.
292. Vestal, C. R.; Zhang, Z. J. *Nano Lett.* **2003,** 3, (12), 1739-1743.
293. Tago, T.; Hatsuta, T.; Miyajima, K.; Kishida, M.; Tashiro, S.; Wakabayashi, K. *J. Amer. Ceram. Soc.* **2002,** 85, (9), 2188-2194.

294. Lee, J. S.; Lee, Y. J.; Youn, J. K.; Na, H. B.; Yu, T.; Kim, H.; Lee, S. M.; Koo, Y. M.; Kwak, J. H.; Park, H. G.; Chang, H. N.; Hwang, M.; Park, J. G.; Kim, J. B.; Hyeon, T. *Small* **2008,** 4, (1), 143-152.

295. Yi, D. K.; Selvan, T.; Lee, S. S.; Papaefthymiou, G. C.; Kundaliya, D.; Ying, J. Y. *JACS* **2005,** 127, (14), 4990-4991.

296. Jana, N. R.; Earhart, C.; Ying, J. Y. *Chem. Mater.* **2007,** 19, (21), 5074-5082.

297. Palani, A.; Lee, J. S.; Huh, J.; Kim, S.; Lee, Y. J.; Chang, J. H.; Lee, K.; Lee, S. W. *J. PROTEOME RES.* **2008,** 7, (8), 3591-3596.

298. Lee, D. C.; MiKulec, F. V.; Pelaez, J. M.; Koo, B.; Korgel, B. A. *J.Phys.Chem.B* **2006,** 110, 11160-11166.

299. Li, Y.; Zhang, X. L.; Qiu, R.; Qiao, R.; Kang, Y. S. *J. Phys. Chem. C* **2007,** 111, (29), 10747-10750.

300. Kobayashi, Y.; Kakinuma, H.; Nagao, D.; Ando, Y.; Miyazaki, T.; Konno, M. *J. Sol-Gel Sci. Tech.* **2008,** 47, 16-22.

301. Wang, L. Y.; Bai, J. W.; Li, Y. J.; Huang, Y. *Angew. Chemie-Inter. Ed.* **2008,** 47, (13), 2439-2442.

302. Lo, C. K.; Xiao, D.; Choi, M. M. F. *J. Mater. Chem.* **2007,** 17, (23), 2418-2427.

303. Wang, L. Y.; Luo, J.; Fan, Q.; Suzuki, M.; Suzuki, I. S.; Engelhard, M. H.; Lin, Y. H.; Kim, N.; Wang, J. Q.; Zhong, C. J. *J. Phys. Chem. B* **2005,** 109, (46), 21593-21601.

304. Wang, L. Y.; Park, H. Y.; Lim, S. I. I.; Schadt, M. J.; Mott, D.; Luo, J.; Wang, X.; Zhong, C. J. *J. Mater. Chem.* **2008,** 18, (23), 2629-2635.

305. Xu, Z. C.; Hou, Y. L.; Sun, S. H. *JACS* **2007,** 129, (28), 8698-8699.

306. Liu, H. L.; Sonn, C. H.; Wu, J. H.; Lee, K. M.; Kim, Y. K. *Biomater.* **2008,** 29, (29), 4003-4011.

307. Chen, D.; Li, J. J.; Shi, C. S.; Du, X. W.; Zhao, N. Q.; Sheng, J.; Liu, S. *Chem. Mater.* **2007,** 19, (14), 3399-3405.

308. Jun, Y. W.; Huh, Y. M.; Choi, J. S.; Lee, J. H.; Song, H. T.; Kim, S.; Yoon, S.; Kim, K. S.; Shin, J. S.; Suh, J. S.; Cheon, J. *JACS* **2005,** 127, (16), 5732-5733.

309. Jun, C. H.; Park, Y. J.; Yeon, Y. R.; Choi, J. R.; Lee, W. R.; Ko, S. J.; Cheon, J. *Chem. Commun.* **2006,** (15), 1619-1621.

310. Fu, Y. Z.; Xiang, X. D. *J. Dispers. Sci. & Tech.* **2008,** 29, (6), 861-865.

311. Chiu, H. K.; Chiang, I. C.; Chen, D. H. *J. Nano. Res.* **2009,** 11, (5), 1137-1144.

312. Cushing, B. L.; Golub, V. O.; Henry, M.; Oliva, B. L.; Cook, E.; Holmes, C. W.; O'Connor, C. J. *Nanotech.* **2005,** 16, (9), 1701-1706.
313. Kouassi, G. K.; Wang, P.; Sreevatan, S.; Irudayaraj, J. *Biotech. Progress* **2007,** 23, (5), 1239-1244.
314. Mikhaylova, M.; Kim, D. K.; Bobrysheva, N.; Osmolowsky, M.; Semenov, V.; Tsakalakos, T.; Muhammed, M. *Langmuir* **2004,** 20, (6), 2472-2477.
315. Ravel, B.; Carpenter, E. E.; Harris, V. G. *J. Appl. Phys.* **2002,** 91, (10), 8195-8197.
316. Jeong, J.; Ha, T. H.; Chung, B. H. *Analyt. Chim. Acta* **2006,** 569, (1-2), 203-209.
317. Park, H. Y.; Schadt, M. J.; Wang, L.; Lim, I. I. S.; Njoki, P. N.; Kim, S. H.; Jang, M. Y.; Luo, J.; Zhong, C. J. *Langmuir* **2007,** 23, (17), 9050-9056.
318. Ban, Z. H.; Barnakov, Y. A.; Golub, V. O.; O'Connor, C. J. *J. Mater. Chem.* **2005,** 15, (43), 4660-4662.
319. Park, J. I.; Cheon, J. *JACS* **2001,** 123, (24), 5743-5746.
320. Liang, H. P.; Wan, L. J.; Bai, C. L.; Jiang, L. *J. Phys. Chem. B* **2005,** 109, (16), 7795-7800.
321. Schwartzberg, A. M.; Olson, T. Y.; Talley, C. E.; Zhang, J. Z. *J. Phys. Chem. B* **2006,** 110, (40), 19935-19944.
322. Sun, X. C.; Nava, N. *Nano Lett.* **2002,** 2, (7), 765-769.
323. Tsang, S. C.; Caps, V.; Paraskevas, I.; Chadwick, D.; Thompsett, D. *Angew. Chemie-Inter. Ed.* **2004,** 43, (42), 5645-5649.
324. Cui, Z. M.; Hang, L. Y.; Song, W. G.; Guo, Y. G. *Chem. Mater.* **2009,** 21, (6), 1162-1166.
325. Nikitenko, S. I.; Koltypin, Y.; Palchik, O.; Felner, I.; Xu, X. N.; Gedanken, A. *Angew. Chemie-Inter. Ed.* **2001,** 40, (23), 4447-4448.
326. Bonnemann, H.; Brijoux, W.; Brinkmann, R.; Matoussevitch, N.; Waldofner, N.; Palina, N.; Modrow, H. *Inorg. Chim. Acta* **2003,** 350, 617-624.
327. Bonnemann, H.; Brand, R. A.; Brijoux, W.; Hofstadt, H. W.; Frerichs, M.; Kempter, V.; Maus-Friedrichs, W.; Matoussevitch, N.; Nagabhushana, K. S.; Voigts, F.; Caps, V. *Appl. Organometal. Chem.* **2005,** 19, (6), 790-796.
328. Peng, D. L.; Sumiyama, K.; Hihara, T.; Yamamuro, S.; Konno, T. J. *Phys. Rev. B* **2000,** 61, (4), 3103-3109.
329. Xu, C. J.; Xu, K. M.; Gu, H. W.; Zheng, R. K.; Liu, H.; Zhang, X. X.; Guo, Z. H.; Xu, B. *JACS* **2004,** 126, (32), 9938-9939.
330. Peng, S.; Xie, J.; Sun, S. H. *J. Solid State Chem.* **2008,** 181, (7), 1560-1564.

331. Kim, H.; Achermann, M.; Balet, L. P.; Hollingsworth, J. A.; Klimov, V. I. *JACS* **2005,** 127, (2), 544-546.

332. Gao, J. H.; Zhang, B.; Gao, Y.; Pan, Y.; Zhang, X. X.; Xu, B. *JACS* **2007,** 129, (39), 11928-11935.

333. Pellegrino, T.; Kudera, S.; Liedl, T.; Javier, A. M.; Manna, L.; Parak, W. J. *Small* **2005,** 1, (1), 48-63.

334. Gu, H. W.; Xu, K. M.; Xu, C. J.; Xu, B. *Chem. Commun.* **2006,** (9), 941-949.

335. Xie, J.; Chen, K.; Lee, H. Y.; Xu, C. J.; Hsu, A. R.; Peng, S.; Chen, X. Y.; Sun, S. H. *JACS* **2008,** 130, (24), 7542-7543.

336. Kim, D. H.; Nikles, D. E.; Johnson, D. T.; Brazel, C. S. *J. Mag. Mag. Mater.* **2008,** 320, (19), 2390-2396.

337. Wang, L. Y.; Luo, J.; Maye, M. M.; Fan, Q.; Qiang, R. D.; Engelhard, M. H.; Wang, C. M.; Lin, Y. H.; Zhong, C. J. *J. Mater. Chem.* **2005,** 15, (18), 1821-1832.

338. Zhao, X. L.; Cai, Y. Q.; Wang, T.; Shi, Y. L.; Jiang, G. B. *Analyt. Chem.* **2008,** 80, (23), 9091-9096.

339. Lim, I. I. S.; Njoki, P. N.; Park, H. Y.; Wang, X.; Wang, L. Y.; Mott, D.; Zhong, C. J. *Nanotech.* **2008,** 19, (30), 5371-5376.

340. Kang, K.; Choi, J.; Nam, J. H.; Lee, S. C.; Kim, K. J.; Lee, S. W.; Chang, J. H. *J. Phys. Chem. B* **2009,** 113, (2), 536-543.

341. Yamaura, M.; Camilo, R. L.; Sampaio, L. C.; Macedo, M. A.; Nakamura, M.; Toma, H. E. *J. Mag. Mag. Mater.* **2004,** 279, (2-3), 210-217.

342. Chen, F. H.; Gao, Q.; Ni, J. Z. *Nanotechnology* **2008,** 19, (16), 2161-2166.

343. Shen, X. C.; Fang, X. Z.; Zhou, Y. H.; Liang, H. *Chem. Lett.* **2004,** 33, (11), 1468-1469.

344. Bruce, I. J.; Sen, T. *Langmuir* **2005,** 21, (15), 7029-7035.

345. De Palma, R.; Peeters, S.; Van Bael, M. J.; Van den Rul, H.; Bonroy, K.; Laureyn, W.; Mullens, J.; Borghs, G.; Maes, G. *Chem. Mater.* **2007,** 19, (7), 1821-1831.

346. Piao, Y.; Kim, J.; Bin Na, H.; Kim, D.; Baek, J. S.; Ko, M. K.; Lee, J. H.; Shokouhimehr, M.; Hyeon, T. *Nature Mater.* **2008,** 7, (3), 242-247.

347. Mejias, R.; Perez-Yague, S.; Roca, A. G.; Perez, N.; Villanueva, A.; Canete, M.; Manes, S.; Ruiz-Cabello, J.; Benito, M.; Labarta, A.; Batlle, X.; Veintemillas-Verdaguer, S.; Morales, M. P.; Barber, D. F.; Serna, C. J. *Nanomed.* **2010,** 5, (3), 397-408.

348. Dilnawaz, F.; Singh, A.; Mohanty, C.; Sahoo, S. K. *Biomater.* **2010,** 31, (13), 3694-3706.

349. Valois, C. R. A.; Braz, J. M.; Nunes, E. S.; Vinolo, M. A. R.; Lima, E. C. D.; Curi, R.; Kuebler, W. M.; Azevedo, R. B. *Biomater.* **2010,** 31, (2), 366-374.

350. Fauconnier, N.; Pons, J. N.; Roger, J.; Bee, A. *J. Colloid & Interface Sci.* **1997,** 194, (2), 427-433.

351. Huh, Y. M.; Jun, Y. W.; Song, H. T.; Kim, S.; Choi, J. S.; Lee, J. H.; Yoon, S.; Kim, K. S.; Shin, J. S.; Suh, J. S.; Cheon, J. *JACS* **2005,** 127, (35), 12387-12391.

352. Lai, C. W.; Wang, Y. H.; Uttam, B. P.; Chen, Y. C.; Hsiao, J. K.; Liu, C. L.; Liu, H. M.; Chen, C. Y.; Chou, P. T. *Chem. Commun.* **2008,** (42), 5342-5344.

353. Hong, R.; Fischer, N. O.; Emrick, T.; Rotello, V. M. *Chem. Mater.* **2005,** 17, (18), 4617-4621.

354. Xu, C. J.; Xu, K. M.; Gu, H. W.; Zhong, X. F.; Guo, Z. H.; Zheng, R. K.; Zhang, X. X.; Xu, B. *JACS* **2004,** 126, (11), 3392-3393.

355. Kreller, D. I.; Gibson, G.; Novak, W.; Van Loon, G. W.; Horton, J. H. *Colloids & Surfaces A-Physicochem. & Eng. Aspect.* **2003,** 212, (2-3), 249-264.

356. Mutin, P. H.; Guerrero, G.; Vioux, A. *J. Mater. Chem.* **2005,** 15, (35-36), 3761-3768.

357. Sahoo, Y.; Pizem, H.; Fried, T.; Golodnitsky, D.; Burstein, L.; Sukenik, C. N.; Markovich, G. *Langmuir* **2001,** 17, (25), 7907-7911.

358. Brust, M.; Walker, M.; Bethell, D.; Schiffrin, D. J.; Whyman, R. *JACS* **1994,** (7), 801-802.

359. Fu, X. Y.; Wang, Y.; Wu, N. Z.; Gui, L. L.; Tang, Y. Q. *J. Colloid & Interf. Sci.* **2001,** 243, 326-330.

360. Jun, Y. W.; Hub, Y. M.; Choi, J. S.; Lee, J. H.; Song, H. T.; Kim, S. J.; Yoon, S.; Kim, K. S.; Shin, J. S.; Suh, J. S.; Cheon, J. *JACS* **2005,** 127, 5732-5733.

361. White, M. A.; Johnson, J. A.; Koberstein, J. T.; Turro, N. J. *JACS* **2006,** 128, (35), 11356-11357.

362. Kim, M.; Chen, Y. F.; Liu, Y. C.; Peng, X. G. *Adv. Mater.* **2005,** 17, (11), 1429-1430.

363. Chen, L. X.; Liu, T.; Thurnauer, M. C.; Csencsits, R.; Rajh, T. *J. Phys. Chem. B* **2002,** 106, (34), 8539-8546.

364. Rajh, T.; Chen, L. X.; Lukas, K.; Liu, T.; Thurnauer, M. C.; Tiede, D. M. *J. Phys. Chem. B* **2002,** 106, (41), 10543-10552.

365. Wang, B. D.; Xu, C. J.; Xie, J.; Yang, Z. Y.; Sun, S. L. *JACS* **2008,** 130, (44), 14436-14437.

366. Latham, A. H.; Williams, M. E. *Langmuir* **2006,** 22, (9), 4319-4326.

367. Gao, J. H.; Zhang, W.; Huang, P. B.; Zhang, B.; Zhang, X. X.; Xu, B. *JACS* **2008,** 130, (12), 3710-3711.

368. Srivastava, S.; Samanta, B.; Arumugam, P.; Han, G.; Rotello, V. M. *J. Mater. Chem.* **2007,** 17, (1), 52-55.

369. Gu, H. W.; Ho, P. L.; Tsang, K. W. T.; Yu, C. W.; Xu, B. *Chem. Commun.* **2003,** (15), 1966-1967.

370. Bagaria, H. G.; Ada, E. T.; Shamsuzzoha, M.; Nikles, D. E.; Johnson, D. T. *Langmuir* **2006,** 22, (18), 7732-7737.

371. Lin, C. A. J.; Sperling, R. A.; Li, J. K.; Yang, T. Y.; Li, P. Y.; Zanella, M.; Chang, W. H.; Parak, W. G. J. *Small* **2008,** 4, (3), 334-341.

372. Pellegrino, T.; Manna, L.; Kudera, S.; Liedl, T.; Koktysh, D.; Rogach, A. L.; Keller, S.; Radler, J.; Natile, G.; Parak, W. J. *Nano Lett.* **2004,** 4, (4), 703-707.

373. Yu, W. W.; Chang, E.; Sayes, C. M.; Drezek, R.; Colvin, V. L. *Nanotech.* **2006,** 17, (17), 4483-4487.

374. Euliss, L. E.; Grancharov, S. G.; O'Brien, S.; Deming, T. J.; Stucky, G. D.; Murray, C. B.; Held, G. A. *Nano Lett.* **2003,** 3, (11), 1489-1493.

375. Grancharov, S. G.; Zeng, H.; Sun, S. H.; Wang, S. X.; O'Brien, S.; Murray, C. B.; Kirtley, J. R.; Held, G. A. *J. Phys. Chem. B* **2005,** 109, (26), 13030-13035.

376. Kim, B. S.; Qiu, J. M.; Wang, J. P.; Taton, T. A. *Nano Lett.* **2005,** 5, (10), 1987-1991.

377. Lim, Y. T.; Lee, K. Y.; Lee, K.; Chung, B. H. *Biochem. & Biophys. Res. Commun.* **2006,** 344, (3), 926-930.

378. Williams, D. B.; Carter, C. B., *Transmission Electron Microscopy: Basics I.* Plenum Press: NY, 1996; p 193.

379. Williams, D. B.; Carter, C. B., *Transmission Electron Microscopy: Imaging III.* Plenum Press: NY, 1996; p 198.

380. http://en.wikipedia.org/wiki/Transmission_electron_microscopy.

381. http://en.wikipedia.org/wiki/High-resolution_transmission_electron_microscopy.

382. Williams, D. B.; Carter, C. B., *Transmission Electron Microscopy: Diffraction II.* Plenum Press: NY, 1996; p 170.

383. Williams, D. B.; Carter, C. B., *Transmission Electron Microscopy: Spectrometry IV.* Plenum Press: NY, 1996; p 166.
384. Pecharsky, V. K.; and Zavalij, P. Y., *Fundamentals of Powder Diffraction and Structural Characterization of materials.* Springer: 2005; p 713.
385. Cullity, B. D., *Elemental of X-ray Diffraction.* Wesley Pub. Comp. Inc.: Massachusetts, 1956; p 531.
386. Kittel, C., *Introduction to Solid State Physics.* John Wiley@Son Inc.: New York, 1996; p 692.
387. Borchert, H.; Shevehenko, E. V.; Robert, A.; Mekis, I.; Kornowski, A.; Grubel, G.; Weller, H. *Langmuir* **2005,** 21, (5), 1931-1936.
388. Josephson, B. D. *Phys. Lett.* **1962,** 1, (7), 251-253.
389. Ibach, H.; Luth, H., *Solid-State Physics: An Introduction to Principles of Materials Science.* Springer: NY, 2003; p 501.
390. Chantrell, R. W.; Popplewell, J.; Charles, S. W. *IEEE Trans. Mag.* **1978,** 14, (5), 975-977.
391. Urban, C. PhD thesis: "*Development of Fiber Optic Based Dynamic Light Scattering for a Characterization of Turbid Suspensions*". University of Karlsruhe, Karlsruhe, 1999.
392. http://www.malvern.com/common/downloads/campaign/MRK656-01.pdf.
393. Boss, C. B.; Fredeen, K. J., Concepts, *Instrumentation and Techniques in Inductively Coupled Plasma Optical Emission Spectrometry.* Perkin Elmer: 1997; p 125.
394. Ebdon, L.; Evans, E. H.; Fisher, A.; Hill, S. J., *An Introduction to Analytical Atomic Spectrometry.* John Wiley and Son Inc.: NJ, 1998; p 225.
395. Rouessac, F.; Rouessac, A., *Chemical Analysis: Modern Instrumetation Methods and Techniques.* John Wiley & Son Inc.: NY, 2000; p 464.
396. Brunauer, S.; Emmett, P. H.; Teller, E. *JACS* **1938,** 60, 309-319.
397. Kaye, B. H., *Characterization of Powders and Aerosols.* Wiley-VCH: 1999; p 314.
398. Wang, H. Z.; Kou, X. L.; Mang, B.; Li, J. L. *Bull. Mater. Sci.* **2008,** 31, (1), 97-100.
399. Groen, J. C.; Peffer, L. A. A.; Perez-Ramirez, J. *Microporous & Mesoporous Mater.* **2003,** 60, (1-3), 1-17.
400. Settle, F., *Handbook of Instrumental Techniques for Analytical Chemistry.* Prentice Hall Inc.: NJ, 1997; p 995.
401. www.jasco.hu/konyvtar/FT-IR-Grundl.-Seminar.pdf.

402. Smidth, E.; and Dent, G., *Modern Raman Spectroscopy: A Practical approach*. John Wiley & Son Ltd.: West Sussex, 2005; p 210.
403. Bakeev, K. A., *Process Analytical Technology: Spectroscopic Tools and Implementation Strategies for the Chemical and Pharmaceutical Industries*, Second Ed. John Wiley & Son Ltd.: 2010; p 576.
404. http://en.wikipedia.org/wiki/Raman_spectroscopy.
405. McCREERY, R. L., *Raman Spectroscopy for Chemical Analysis*. John Wiley & Son Inc.: NY, 2000; p 448.
406. http://www.cis.rit.edu/htbooks/nmr/inside.htm.
407. Sachleben, J. R.; Colvin, V.; Emsley, L.; Wooten, E. W.; Alivisatos, A. P. *J. Phys. Chem. B* **1998,** 102, (50), 10117-10128.
408. Ladizhansky, V.; Hodes, G.; Vega, S. *J. Phys. Chem. B* **1998,** 102, (43), 8505-8509.
409. Becerra, L. R.; Murray, C. B.; Griffin, R. G.; Bawendi, M. G. *J. Chem. Phys.* **1994,** 100, (4), 3297-3300.
410. Tomaselli, M.; Yarger, J. L.; Bruchez, M.; Havlin, R. H.; deGraw, D.; Pines, A.; Alivisatos, A. P. *J. Chem. Phys.* **1999,** 110, (18), 8861-8864.
411. Schladt, T. D.; Graf, T.; Tremel, W. *Chem. Mater.* **2009,** 21, (14), 3183-3190.
412. Hensen, E. J. M.; Zhu, Q.; Hendrix, M. M. R. M.; Overweg, A. R.; Kooyman, P. J.; Sychev, M. V.; van Santen, R. A. *J. Catalys.* **2004,** 221, (2), 560-574.
413. Willis, A. L.; Turro, N. J.; O'Brien, S. *Chem. Mater.* **2005,** 17, (24), 5970-5975.
414. Cannas, C.; Musinu, A.; Ardu, A.; Orru, F.; Peddis, D.; Casu, M.; Sanna, R.; Angius, F.; Diaz, G.; Piccaluga, G. *Chem. Mater.* **2010,** 22, (11), 3353-3361.
415. Vickerman, J. C., *Surface Analysis: The Principle Techniques*. John Wiley & Son Inc.: NY, 1998; p 472.
416. Robinson, D. B.; Persson, H. H. J.; Zeng, H.; Li, G. X.; Pourmand, N.; Sun, S. H.; Wang, S. X. *Langmuir* **2005,** 21, (7), 3096-3103.
417. Gehl, B.; Aleksandrovic, V.; Erbacher, M.; Juergens, B.; Schurenberg, M.; Kornowski, A.; Weller, H.; Baumer, M. *Chem. phys. chem.* **2008,** 9, (6), 821-825.
418. Zhang, X. B.; Yan, J. M.; Han, S.; Shioyama, H.; Xu, Q. *JACS* **2009,** 131, (8), 2778-2779.
419. Wang, D. L.; Xin, H. L.; Yu, Y. C.; Wang, H. S.; Rus, E.; Muller, D. A.; Abruna, H. D. *JACS* **2010,** 132, (50), 17664-17666.
420. Naumkin, A. V.; Vasil'kov, A. Y.; Volkov, I. O.; Smirnov, V. V.; Nikolaev, S. A. *Inorg. Mater.* **2007,** 43, (4), 381-385.

421. Cammenga, H. K.; Epple, M. *Angew. Chemie-Inter. Ed.* **1995,** 34, (11), 1171-1187.
422. Gabbott, P., *Principles and Applications of Thermal Analysis*. Blackwell Pub.: Oxford, 2008; p 464.
423. Brown, M. E., *Introduction to Thermal Analysis: techniques and applications*. Chapman & Hall Ltd.: NY, 1988; p 222.
424. Wunderlich, B., *Thermal Analysis for Polymer Materials*. Springer: Berlin, 2005; p 894.
425. Clas, S. D.; Dalton, C. R.; Hancock, B. C. *Pharmaceut. Sci. & Tech. Today* **1999,** 2, (8), 311-320.
426. Biliaderis, C. G. *Food Chem.* **1983,** 10, (4), 239-265.
427. Bao, N. Z.; Shen, L. M.; An, W.; Padhan, P.; Turner, C. H.; Gupta, A. *Chem. Mater.* **2009,** 21, (14), 3458-3468.
428. Luo, J.; Han, L.; Kariuki, N. N.; Wang, L. Y.; Mott, D.; Zhong, C. J.; He, T. *Chem. Mater.* **2005,** 17, (21), 5282-5290.
429. Di, H. W.; Luo, Y. L.; Xu, F.; Chen, Y. S.; Nan, Y. F. *J. Biomater. Sci.-Polymer Ed.* **2011,** 22, (4-6), 557-576.
430. Cohen, H.; Gedanken, A.; Zhong, Z. Y. *J. Phys. Chem. C* **2008,** 112, (39), 15429-15438.
431. Kataby, G.; Prozorov, T.; Koltypin, Y.; Cohen, H.; Sukenik, C. N.; Ulman, A.; Gedanken, A. *Langmuir* **1997,** 13, (23), 6151-6158.
432. Wada, H.; Takada, K.; Sasaki, T. *Solid State Ionics* **2004,** 172, (1-4), 421-424.
433. Yin, X. J.; Peng, K.; Hu, A. P.; Zhou, L. P.; Chen, J. H.; Du, Y. W. *J. Alloys & Compounds* **2009,** 479, (1-2), 372-375.
434. Willard, M. A.; Kurihara, L. K.; Carpenter, E. E.; Calvin, S.; Harris, V. G. *Inter. Mater. Rev.* **2004,** 49, (3-4), 125-170.

Chapter 2
Synthesis and characterisation of water-dispersible magnetic Co nanoparticles

2.1 Introduction

Magnetic nanoparticles are of great interest because of their substantial potential in magnetic separation and purification of biomolecules and cells[1-6] and applications in fields such as targeted drug delivery, hyperthermia treatment for solid tumours and magnetic resonance imaging (MRI) as described in Section 1.3.[7-13] In order to make use of the magnetic nanoparticles it is essential that their surface chemistry is tailored to enable biological stability. This includes the need for nanoparticle stability, dispersibility in aqueous solutions of electrolytes and colloidal stability and biology-specific properties, such as biocompatibility, non-toxicity and specific biorecognition. In addition, it is also very important that the magnetic properties of the nanoparticles can be fine tuned for particular applications.

A lot of effort has been made in the field to obtain good biological stability. This has largely focused on surface modification of the nanoparticles, by creating a polymer and/or an inorganic shell, with the aims of improving colloidal stability and of protecting the nanoparticles from oxidation and aggregation. These types of coating also provide functional groups at the surface for subsequent biofunctionalization.

In terms of water-dispersibility, nanoparticles are either synthesised directly in water (Section 1.4.3) or in organic medium (Section1.4.5) and then transferred into water using

ligand exchange reactions (Section 1.6). The former is generally applied to oxide materials (Fe_2O_3, Fe_3O_4).[14-19] However, there is very little literature on the direct synthesis of stable water-dispersible Co nanoparticles. Likewise, the transfer of hydrophobic nanoparticles into aqueous medium has proved successful only in systems of oxides (Fe_2O_3, Fe_3O_4),[20-26] ferrites ($CoFe_2O_4$, $MnFe_2O_4$)[26-29] or alloys ($CoPt_3$, FePt).[22,25,30-32] Thus, the synthesis of water-dispersible, high saturation magnetisation nanoparticles of Co is still a challenge. The importance of high saturation magnetisation is that it provides advantages in several applications, such as magnetic separation and MRI. Compared to magnetic oxide systems such as iron oxides (Fe_2O_3, Fe_3O_4), Co is known to have the saturation magnetization nearly 2.5 times higher.

In this chapter, magnetic Co nanoparticles were directly synthesised in aqueous solution by reduction of Co salt in the presence of water-dispersible peptide or polymer with sonication. Nine peptide sequences and different polymers such as poly(methacrylic acid) dodecanethioether (PMAA-DDT), poly(acrylic acid) dodecanethioether (PAA-DDT), poly-(ethylene glycol) monomethacrylate (PEGA-DDT) and n-vinylpyrrolidine dodecanethiol ether (VPD-DDT) were investigated. In this way it was possible to cover at least some of the potential variation in the structure of the peptides and polymers that might affect synthesis. The synthesised nanoparticles were characterised using TEM, SQUID, ICP-AES and zeta potential measurements. Other analytical methods, such as XPS, FTIR, TGA and DSC which have been extensively used in the literatures for the characterisation of the oxidative stability of nanoparticles (XPS) or for studying of the interactions between stabilising ligands and the surface of nanoparticles are also discussed.

2.2 Experimental

2.2.1 Materials

The following chemicals were used: cobalt (II) chloride hydrous ($CoCl_2.6H_2O$) 97 % purity was purchased from Aldrich Ltd, UK. Sodium borohydride ($NaBH_4$) was obtained from VWR Ltd, UK. CALNN, CCALNN, NNLACC, CVVVT, TLVVN, CCVVVT, NNLACCALNN, TTTPCCVTTT and TTTTCCTTTT peptides were purchased from Pepsyn Ltd, Liverpool, UK. The structure of the peptides is shown in Table 2.1. Water-dispersible polymers including poly(methacrylic acid) dodecanethioether (PMAA-DDT) of different molecular weight, poly(acrylic acid) dodecanethioether (PAA-DDT) of 2,430 g mol^{-1}, poly(ethylene glycol) monomethacrylate (PEGA-DDT) of 3,470 g mol^{-1} and n-vinylpyrrolidine (VPD-DDT) of 37,320 g mol^{-1}, with alkyl thioether end-functional group (dodecanethiol) were synthesised by Professor Andy Cooper's group at Liverpool.[33, 34] The structure of the polymers is shown in Table 2.1.

The peptides and polymers were chosen because some of these ligands have been shown to be very effective stabilisers of Au nanoparticles.[34, 35] Although bonding to Co is different to Au, the thiols (peptides) and thiol ethers (polymers) were considered to be suitable for bonding to Co. According to the acid-base concept and their classification in hard and soft acids and bases (HSAB) proposed by Pearson,[36, 37] thiol or thiol ether is a soft base and Co metal is soft acid, and thus thiol or thiol ether should prefer to form strong bonds with Co metal. The sequence of the peptides CALNN and CCALNN was varied to allow for a small exploration of the potential sequence space so that more suitable peptides could be designed in the future. For example, NNLACC has a carboxylic acid adjacent to the terminal thiol, TLVVN has no thiol and three peptides, NNLACCALNN, TTTPCCVTTT and TTTTCCTTTT, have central thiols. The latters could test for the

potential of the peptides to adopt a conformation which leads to the N and C termini being exposed to the solvent so that the nanoparticles have no net charge.

Table 2.1: The structure of peptide and polymer ligands

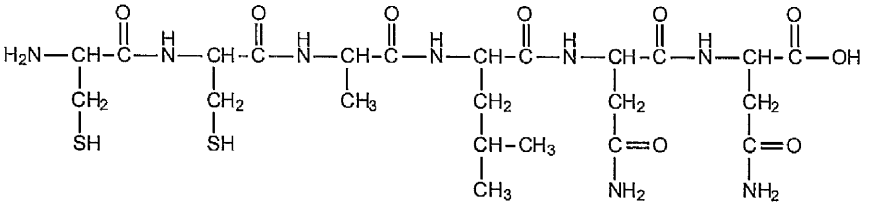 C C A L N N
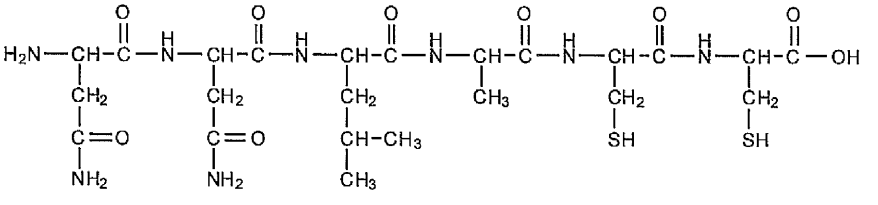 N N L A C C
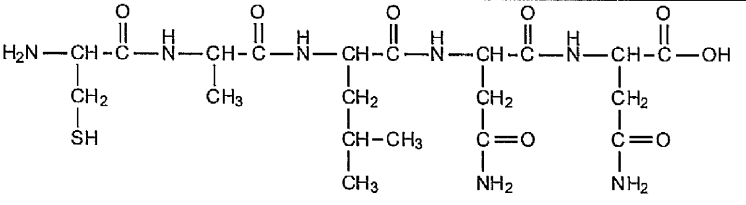 C A L N N
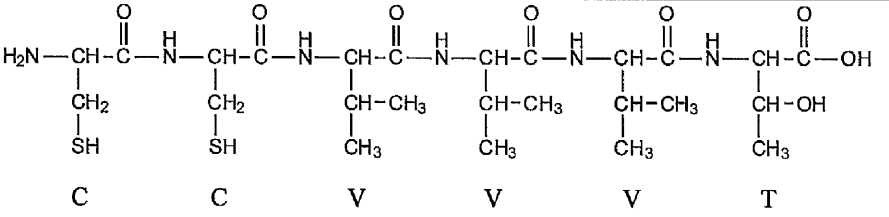 C C V V V T
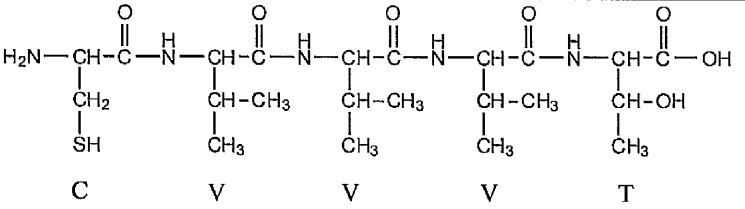 C V V V T

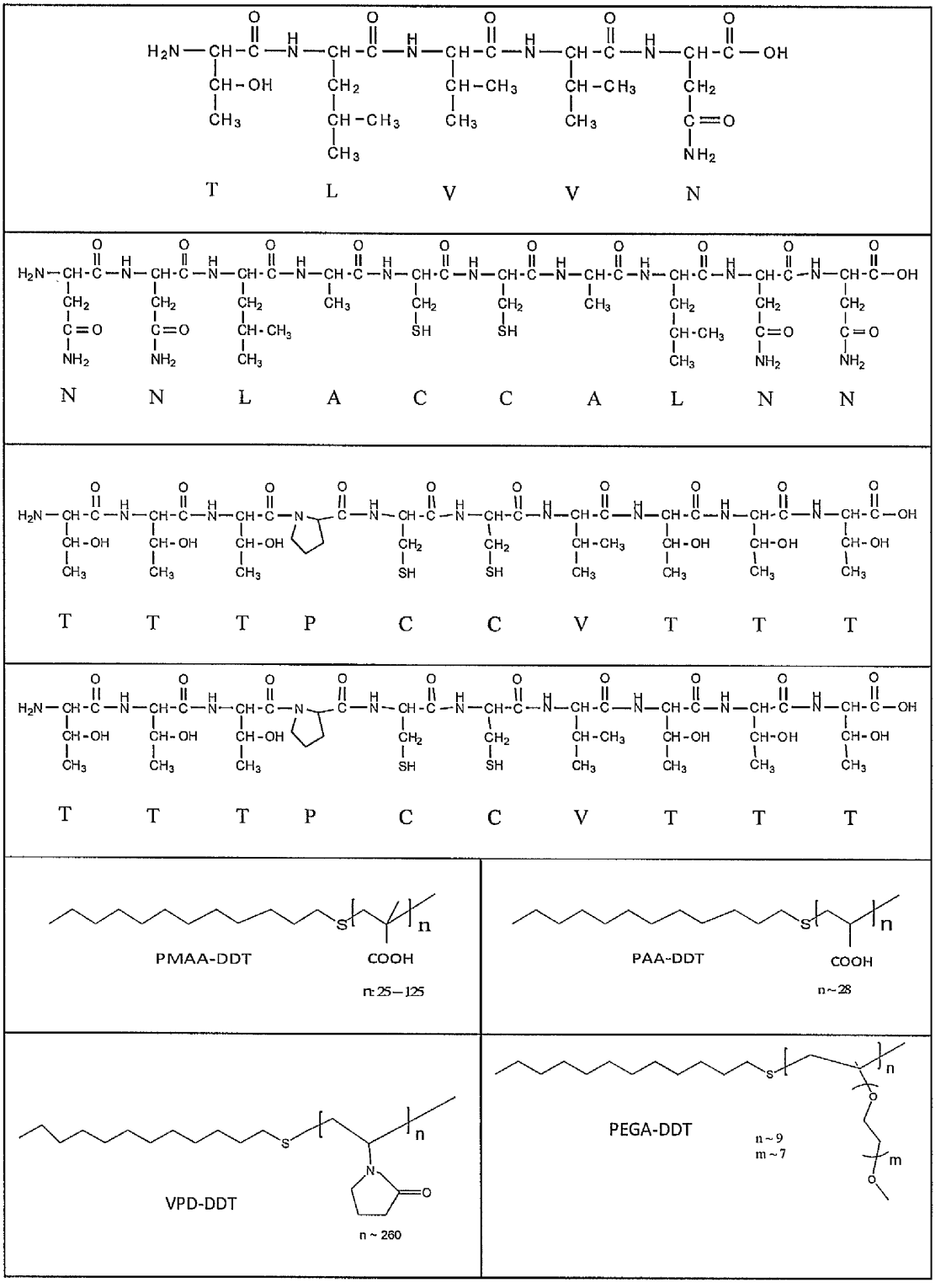
T L V V N
N N L A C C A L N N
T T T P C C V T T T
T T T P C C V T T T
PMAA-DDT
COOH
n: 25—125
PAA-DDT
COOH
n~28
VPD-DDT
n ~ 260
PEGA-DDT
n ~ 9
m ~ 7

2.2.2 Synthesis of Co nanoparticles

2.2.2.1 Synthesis of peptide stabilised Co nanoparticles

Peptide stabilised Co nanoparticles were prepared by reduction of Co^{2+} in water in the presence of a peptide ligand (Table 2.1). In a typical procedure the reductant, $NaBH_4$, and a peptide were stored in a 250 mL two-neck flask which was then de-gassed by purging with N_2 for 30 min and then placing under a vacuum mechanical pump for at least 15 min. To this flask, degassed and de-ionised water (49 mL) was added and the mixture was sonicated for 5 min using a U 300 Ultrawave sonic bath (Ultrawave Ltd, UK) to dissolve the reagents. $CoCl_2$ solution was freshly prepared by dissolving 13 mg (0.1 mmol) of $CoCl_2$ in 1 mL degassed water and then quickly injected into the reaction flask under sonication. The final concentrations of $NaBH_4$, $CoCl_2$ and peptide in the reaction flask were 20 mM, 2 mM and 4 mM. Sonication was continued for 3 min after the injection. During this time, the solution changed rapidly to a grey with significant H_2 gas evolution. After 1 h, five 1 mL fractions were withdrawn and stored in degassed small glass vials for visual observation of the stability of the nanoparticles.

2.2.2.2 Synthesis of polymer stabilised Co nanoparticles

Polymer stabilised Co nanoparticles were similarly prepared as peptide stabilised Co nanoparticles, but using different concentrations of the reagents. In a typical procedure the reductant, $NaBH_4$, and the polymer were added to a 250 mL two-neck flask which was then de-gassed by purging with N_2 for 30 min and placed under vacuum mechanical pump for at least 15 min. To this flask, degassed and de-ionised water (49 mL) was added and the mixture was sonicated for 7-12 min in a U300 Ultrawave sonic bath (Ultrawave Ltd, UK) to dissolve the polymer and the reductant. $CoCl_2$ solution was freshly prepared by dissolving 65 mg (0.5 mmol) of $CoCl_2$ in degassed water (1 mL). This solution was rapidly injected into the reaction flask under sonication. The final concentrations of $NaBH_4$ and

$CoCl_2$ in the reaction flask were 100 mM and 10 mM, respectively. Sonication was continued for 3 min after the injection. During this time, the solution changed rapidly to a near black colour with significant H_2 gas evolution. After 1 h, five 1 mL fractions were withdrawn and stored in degassed small glass vials for visual observation of the stability of the nanoparticles and as material for TEM. The effects of polymer structure (PAA-DDT, PEGA-DDT and VPD-DDT) and synthesis conditions such as speed and order of adding of reaction agents on the particle size were also studied.

2.3 Results and discussion

Sodium borohydride has been widely used as reductant for the synthesis of magnetic nanoparticles. As discussed in Section 1.4.3.2, the chemical reaction of Co salt and $NaBH_4$ in aqueous solution is quite complex.[38, 39] Depending on the pH and the presence of oxygen in the solution, metal and/or metal boride nanoparticles can be formed as final product. Generally, in aqueous solution, there exist possible chemical reactions described as follows:[38-41]

$$NaBH_4 + 2H_2O \rightarrow NaBO_2 + 4H_2\uparrow \quad (2.1)$$

$$NaBO_2 + H_2O \rightleftharpoons BO_2H + NaOH \quad (2.2)$$

under high pH (pH $\geq$ 9):

$$CoCl_2 + 2NaBH_4 + 6H_2O \rightarrow Co + 2NaH_2BO_3 + 2HCl + 7H_2\uparrow \quad (2.3)$$

under pH of 4 to 8 and in the presence of low oxygen content:

$$CoCl_2 + 4NaBH_4 + 9H_2O \rightarrow Co_2B + 3B(OH)_3 + NaCl + 12.5\ H_2\uparrow \quad (2.4)$$

$$4Co_2B + 3O_2 \rightarrow 8Co + 2B_2O_3 \quad (2.5)$$

In this work, $NaBH_4$ and polymer are dissolved in water prior to $CoCl_2$ solution added $NaBH_4$ slowly reacts with water through reactions 2.1 and 2.2. This is confirmed by the observed generation of hydrogen gas (bubbling). In the absence of $CoCl_2$, the pH of the

$NaBH_4$ solution increases due to the formation of NaOH. In the current study, a pH value of 9.5 of the $NaBH_4$ and polymer solution was measured after 3 min sonication (the longer sonication time, the higher pH is). As high pH of the $NaBH_4$ solution, when $CoCl_2$ is added to the reaction solution. Co^{2+} is quickly reduced by remaining $NaBH_4$ to form Co metal possibly via the reaction (2.3). Elemental analysis of some samples of PMAA-DDT coated Co nanoparticles shows that the sample is mainly composed of Co, no B content was detected in the analysed samples. This result is in agreement with that pure metal nanoparticles were achieved under synthesis condition of pH = 9.[40]

2.3.1 Peptide stabilised Co nanoparticles

Peptides are well known stabilisers for Au nanoparticles,[35] but they have rarely been used for magnetic nanoparticles.[42] In this study, the performance of peptides as stabilising ligands for the Co nanoparticles has been investigated. Nine different peptides (Table 2.1) were used. Visual inspection of the nanoparticles synthesised in the presence of peptides showed that the nanoparticles were stable for just a short time. After one or two days, the colour of the solutions began to change, indicative of the oxidation of the nanoparticles. Moreover, precipitation was apparent and the materials lost their magnetic properties (Table 2.2). It was hypothesised that the nanoparticles were unstable because the Co is sensitive to oxidation and the peptides failed to protect the Co core, either due to the peptide ligands being too short, or not forming an effective monolayer on the metal surface. To overcome this problem, longer ligands with fewer functional groups, such as the aforementioned polymers, were used in an attempt to improve the stability of the nanoparticles.

Table 2.2: Stability of the peptide coated Co nanoparticles

Sample	Peptides	Stability	
PeCo-1	TLVVN	change colour, clump and sediment after 24 h	no response to magnet
PeCo-2	CVVVT	change colour, clump and sediment after 24 h	response to magnet
PeCo-3	NNLACC	change colour after 24 h	sediment after 96 h
PeCo-4	TTTPCCVTTT	change colour after 48 h	no response to magnet, clump, sediment
PeCo-5	TTTTCCTTTT	change colour after 72 h	no response to magnet, clump, sediment,
PeCo-6	NNLACCALNN	change colour after 48 h	response to magnet sediment after 24 h
PeCo-7	CCVVVT	change colour after 72 h	clump and sediment after 96 h
PeCo-8	CCALNN	change colour after 72 h	response to magnet
PeCo-9	CALNN	sediment, change colour after 48 h	no response to magnet

2.3.2 Polymer stabilised Co nanoparticles

Four water- dispersible polymers of different structure, poly(acrylic acid) (PAA-DDT), poly(ethylene glycol) monomethacrylate (PEGA-DDT), n-vinylpyrrolidine (VPD-DDT) and poly(methacrylic acid) (PMAA-DDT) with alkyl thioether end-functional group (dodecanethiol) were used as stabilising ligands for synthesis of the Co nanoparticles. Whilst PEGA-DDT stabilised Co nanoparticles are stable in water for a week, nanoparticles stabilised by PAA-DDT deteriorated and lost their magnetic properties after two days. VPD-DDT stabilised Co nanoparticles were found to be stable in water up to one week. TEM images of the PEGA-DDT stabilised Co nanoparticles with narrow size distribution are presented in Figure 2.1. PMAA-DDT was found to be superior to the other polymers and was the subject of considerable further experimentation, which aimed to identify some of the parameters that might control the stability, size and morphology of the nanoparticles.

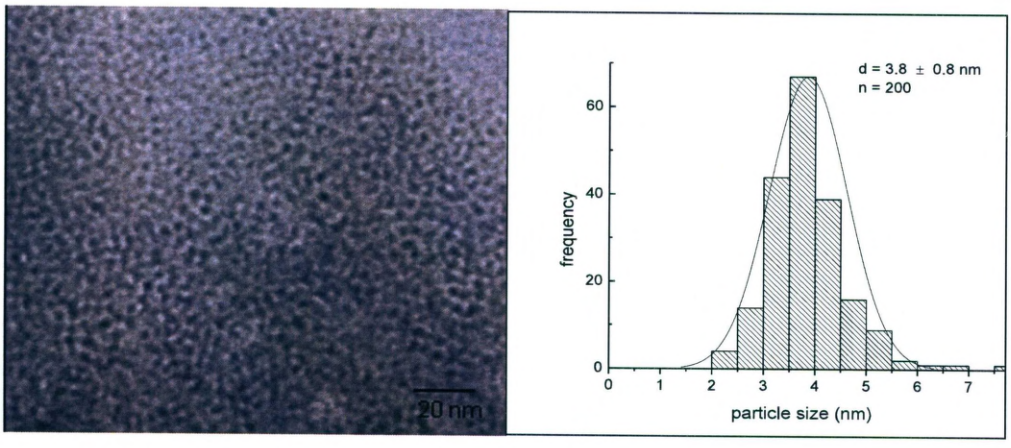

Figure 2.1: TEM image and size distribution of the PEGA-DDT (Mw = 3470) stabilised Co nanoparticles at 0.18 mM polymer concentration.

2.3.2.1 The effect of polymer molecular weight on the particle size

The effect of varying the molecular weight of the PMAA-DDT polymer (M_w = 2,500 - 13,500 g mol^{-1}) was investigated in syntheses where its concentration was fixed at 0.12 mM. TEM images were used to construct size distribution histograms of the Co nanoparticles. These show that small monodisperse nanoparticles were obtained ranging from 2.4 ± 0.2 nm to 3.8 ± 0.5 nm (Figure 2.2). Although the window in which the size of the nanoparticles can be tuned is quite narrow (1.4 nm), the particle size increases with increasing PMAA-DDT polymer molecular weight. Earlier, a similar relationship between the particle size and the polymer molecular weight was reported for Au nanoparticles in which heteroatom containing polymers were believed to act as a ''net'' to assist particle nucleation and thus they play an important role in determining the particle size.[34] The larger the polymer's molecular weight, the more rapidly atoms are to be supplied to growing clusters of metal atoms, resulting in larger nanoparticles. Furthermore, with the higher polymer molecular weight, more time is required for their diffusion and for the passivation of the growing nanoparticles and, as a result, this also leads to an increase in the particle size.[43] The present data show that the effect of polymer molecular weight on

the nanoparticle size is limited, in agreement with the previous data obtained with Au nanoparticles.

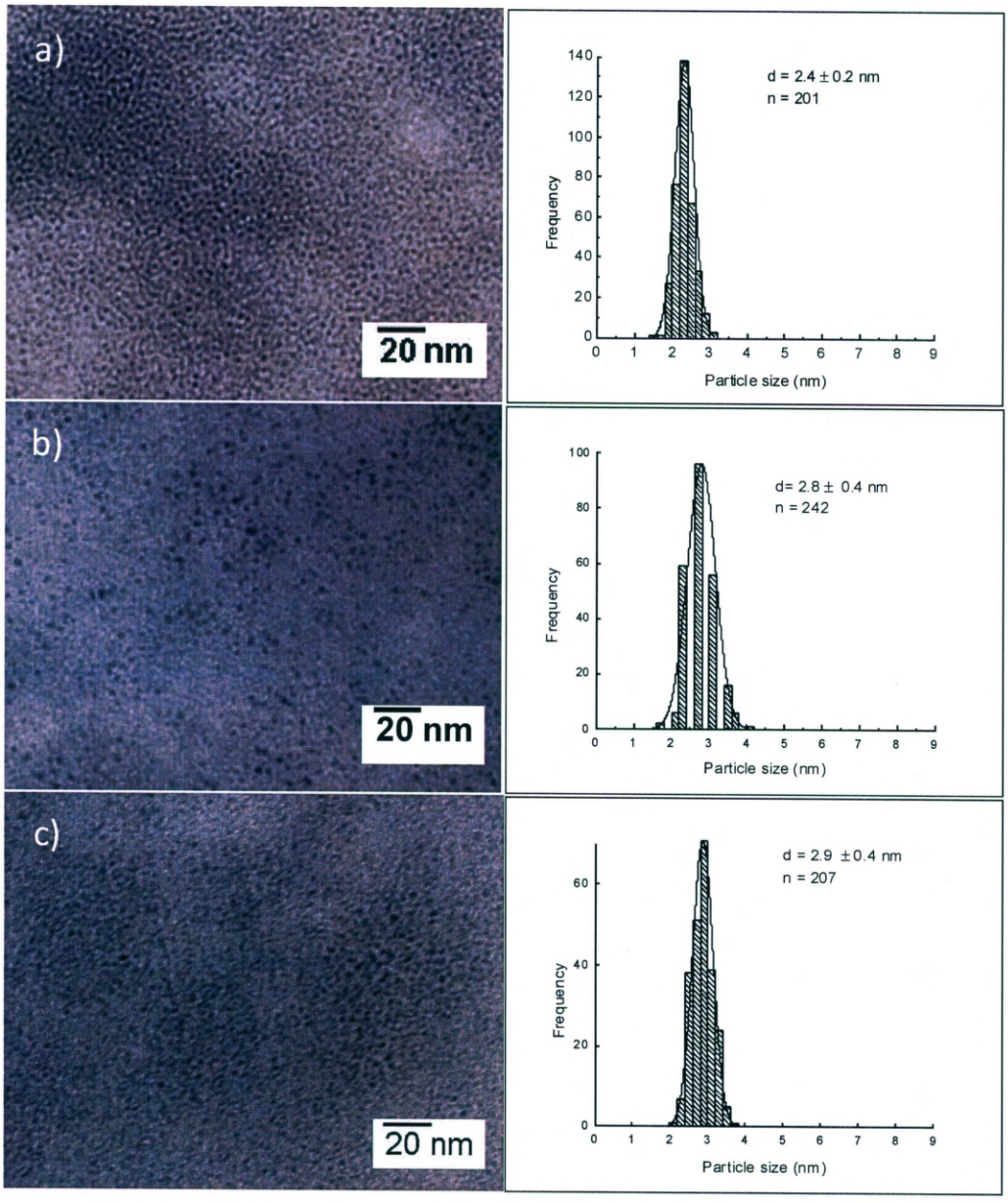

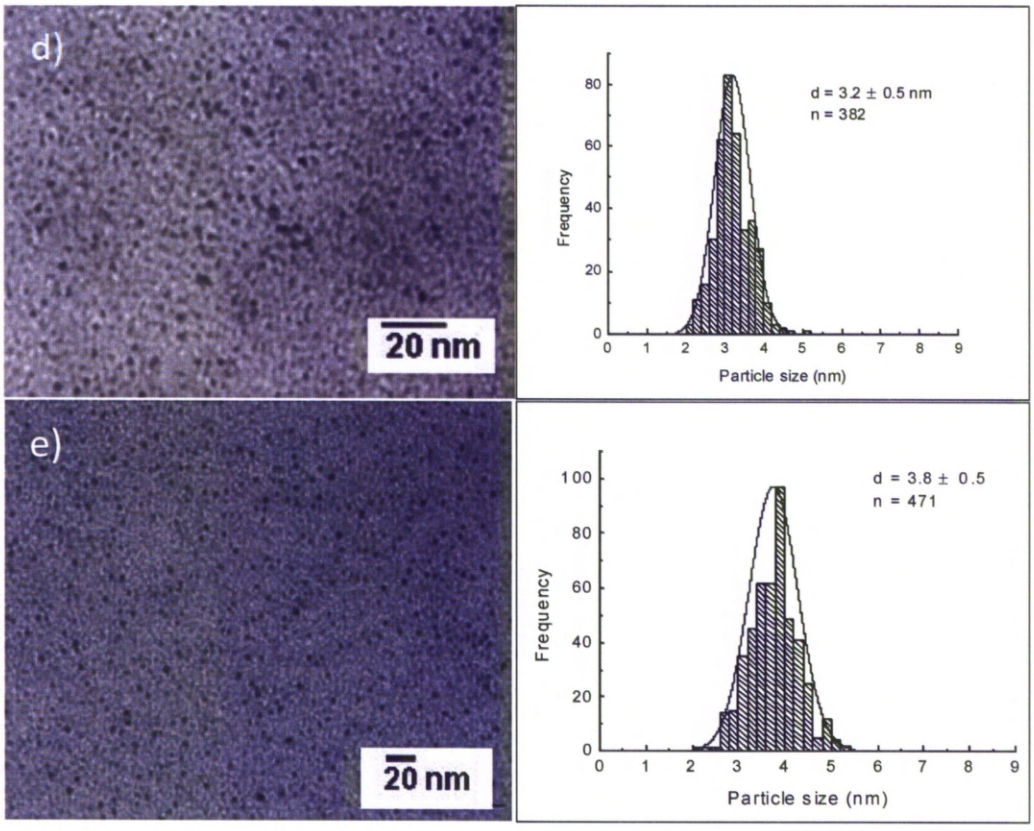

Figure 2.2: TEM images of PMAA-DDT stabilised Co nanoparticles (left panels) and the corresponding histograms of the particle size distribution (right panels) obtained when 0.12 mM polymer was used: a) M_w = 2,500; b) M_w = 3,640; c) M_w = 7,000; d) M_w = 8,610; and e) M_w = 13,500 g mol^{-1}. The corresponding particle sizes are 2.4 nm, 2.8 nm, 2.9 nm, 3.2 nm and 3.8 nm.

.

2.3.2.2 Effect of polymer concentration on the particle size and shape

In order to extend the range of nanoparticle size, the PMAA-DDT polymer with molecular weight M_w = 13,500 g mol^{-1}, which produced the largest Co nanoparticles (average diameter 3.8 nm), was chosen. By varying the polymer concentration, it was found that the size of the Co nanoparticles could be controlled to a greater extent. It can be seen that the average particle size increases with decreasing polymer concentration. With the polymer concentration in the range of 0.006 mM to 0.48 mM, the average particle size

can be tuned between 7.5 ± 0.7 and 2.1 ± 0.2 nm, as indicated by TEM images and size distribution histograms of the Co nanoparticles stabilised by PMAA-DDT (Figure 2.3). The fact that the size of the Co nanoparticles could be tuned over a broader range by varying the polymer concentration rather than the polymer molecular weight is comparable with results obtained for Au nanoparticles prepared using these polymer ligands.[34]

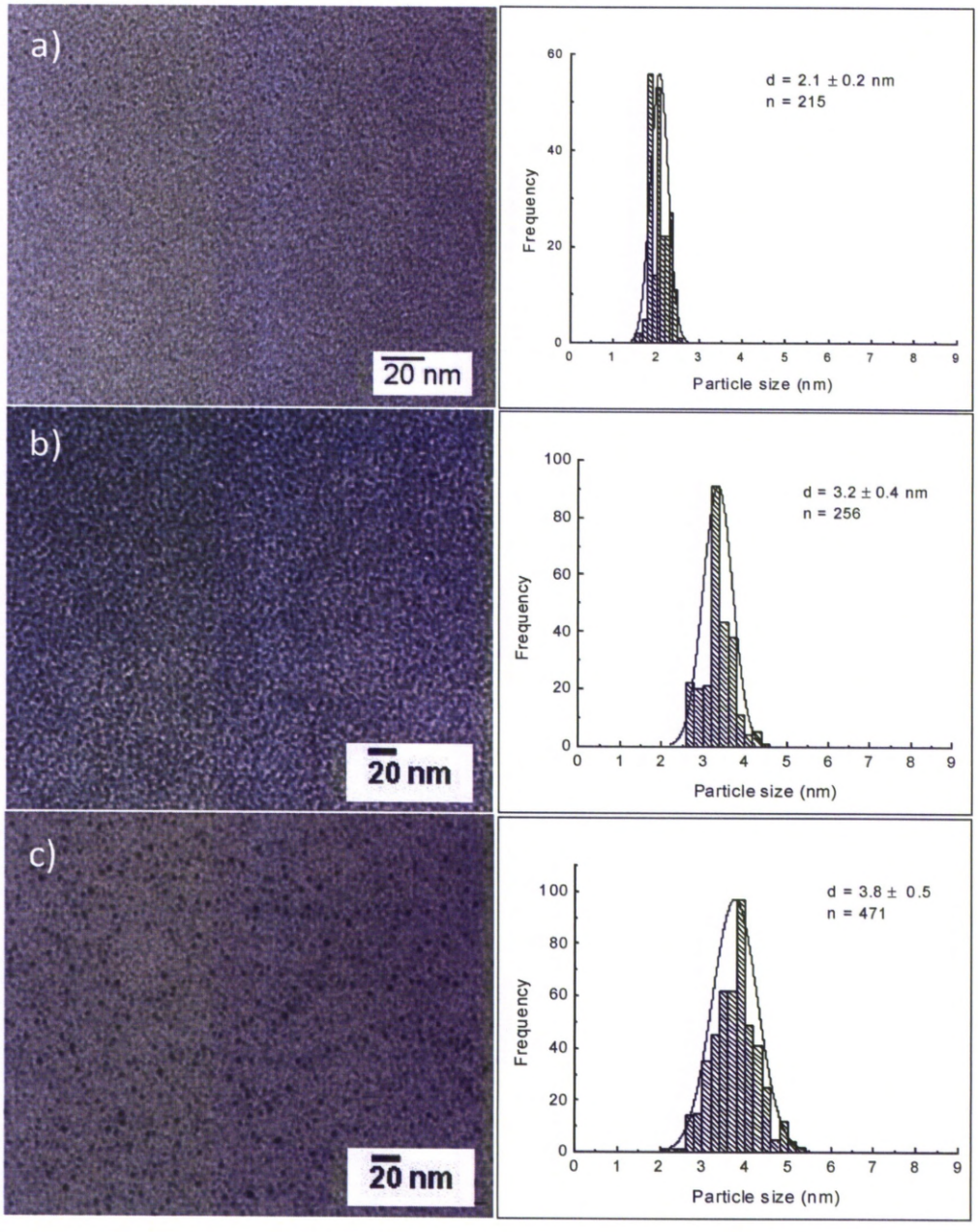

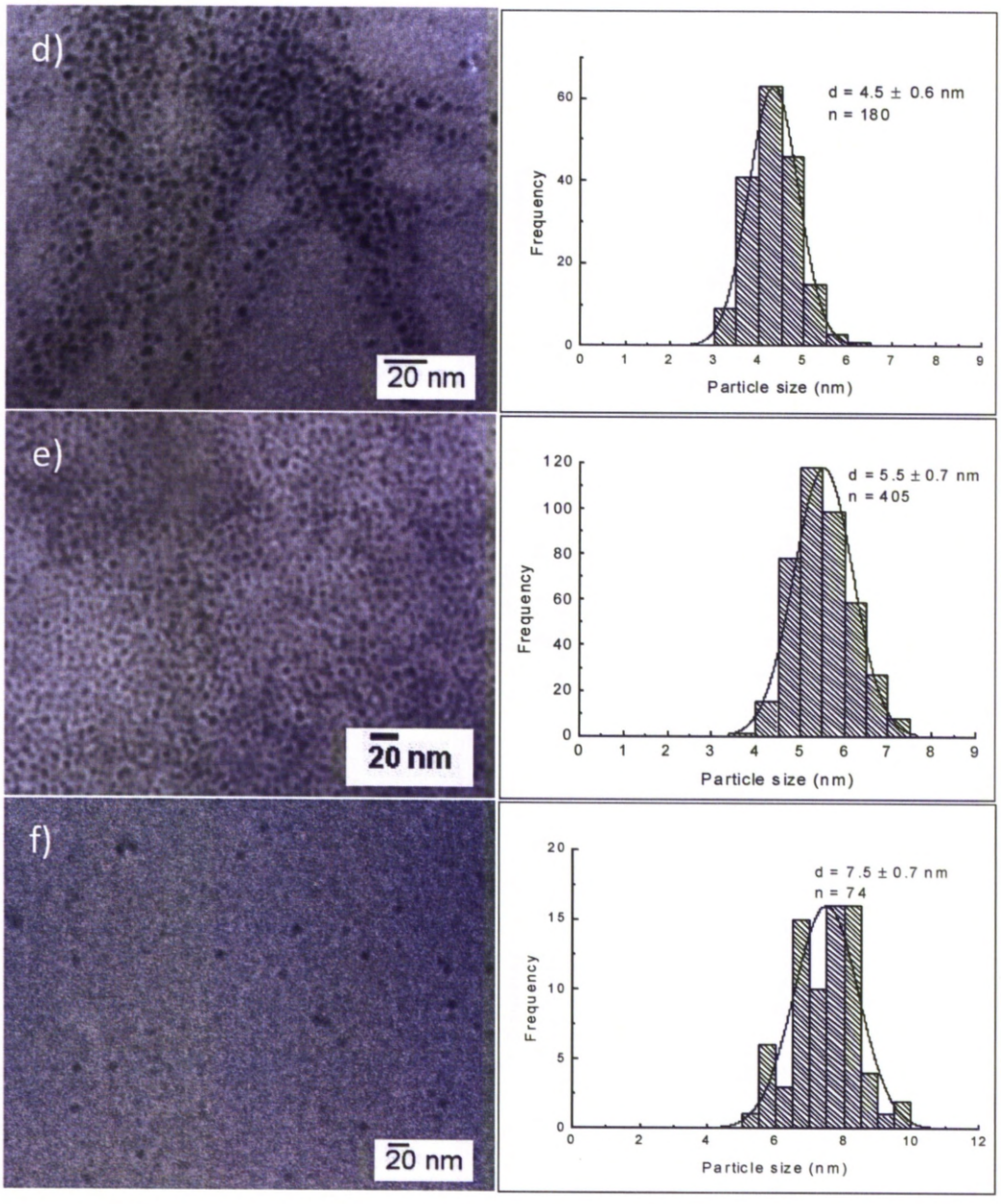

Figure 2.3: TEM images of the PMAA-DDT (M_w = 13,500) stabilised Co nanoparticles (left panels) and the corresponding histograms of the nanoparticle size distribution (right panels) obtained for polymer concentration of a) 0.48 mM; b) 0.24 mM; c) 0.12 mM; d) 0.03 mM; e) 0.01 mM and f) 0.006 mM; The corresponding particle sizes are 2 nm, 3.2 nm, 3.8 nm, 4.3 nm, 5.5 nm and 7.5 nm.

When the polymer concentration was reduced further (0.0048 mM), rod-shaped nanoparticles with an average length of 36 nm and an average width of 15 nm were obtained (Figure 2.4). Previously, Co nanorods were synthesised in organic solvent using the commercially unavailable organometallic complex $[Co(\eta^3\text{-}C_8H_{13})(\eta^4\text{-}C_8H_{12})$.[44] In contrast, here, Co nanorods have been obtained by simple reduction of inexpensive $CoCl_2$. To the best of my knowledge, this is the first example of Co nanorods synthesised in aqueous media. In spite of extensive studies on the formation of Au nanorods, the mechanism of their formation in aqueous media remains unclear.[45] In the case of the Co nanoparticles, one possibility is that the Co^{2+} cations complex with the carboxylate anions of the polymer ligand. Thus, when the polymer concentration is below a certain threshold, this causes the preferential growth at specific crystallographic faces of the nanoparticles, due to preferential adsorption of the polymer-Co complex to particular crystal faces during the growth of the nanoparticles.

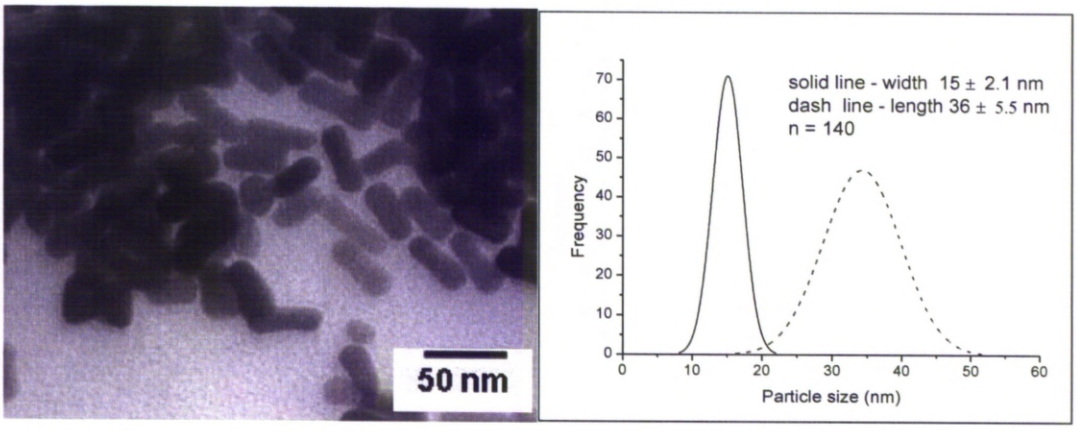

Figure 2.4: TEM image and the corresponding histograms of 36 x 15 nm Co nanorods synthesised in the presence of the PMAA-DDT polymer at a molecular weight M_w = 13,500 g mol^{-1} and a concentration of 0.0048 mM.

2.3.2.3 Effect of the order of addition of the reactants and their injection speed on the particle size

To further increase the range of nanoparticle sizes and morphologies, the effect of changing the order of addition of the reductant ($NaBH_4$ solution) and of the $CoCl_2$ precursor solution was investigated using the polymer with M_w = 13,500 g mol^{-1}. Here, the concentration of all starting materials was kept the same, but the reductant $NaBH_4$ was introduced after dissolving both the $CoCl_2$ precursor and the polymer together in water. In this case, it was found that the speed of adding the solution containing the reductant has a profound effect on the nucleation and growth processes of the Co nanoparticles, resulting in very different average particle sizes. When the reductant was rapidly injected, large Co nanoparticles of about 81 nm (Figure 2.5a,b) were obtained in comparison with 4.4 ± 0.6 nm when the reductant was introduced drop-wise (Figure 2.5c). The reaction under the condition of making 81 nm nanoparticles was repeated twice to test reproducibility. Large nanoparticles were also obtained. However, the results show that the size of nanoparticles is varied for each experiment (between 40 and 160 nm) and difficult to control. Figure 2.5b shows a higher magnification image of the 81 nm nanoparticles. It can be seen that large nanoparticles are composed of much smaller aggregated ones. There are two possible main factors leading to the aggregation to form secondary large nanoparticles. The first factor may relate to the solubility of the polymer. PMAA-DDT is relatively difficult to dissolve in water.[34] Under strong sonication and in the absence of $NaBH_4$, we observed that PMAA-DDT with a molecular weight of 13,500 g mol^{-1} is totally dissolved after about 30 min of sonication (the shorter the polymer, the less sonication time). However, in the presence of $NaBH_4$ (both PMAA-DDT and $NaBH_4$ are dissolved together) we observed that the polymer takes only about 3 min to dissolve completely. For all the reactions in this work, the sonication time is kept at the range of 7 - 12 min. Therefore, PMAA-DDT is only partly dissolved in the case of the reaction condition that $NaBH_4$ is injected in the mixture

solution of polymer and $CoCl_2$, and thus the actual polymer concentration in the reaction solution is low. The low polymer concentration is possibly resulting in the aggregation of small nanoparticles because of the less compact ligand shell surrounding the Co cores. The second parameter that may affect the formation of secondary aggregated nanoparticles is the adding speed of the reductant. $NaBH_4$ is a powerful reductant, it can reduce Co^{+2} to Co metal almost instantly. A rapid injection of $NaBH_4$ into the $CoCl_2$ solution will generate a high supersaturation level of Co atoms in a short time, which results in a large number of small critical nuclei and thus small nanoparticles would be formed. As discussed in Section 1.4.1, fast nucleation and growth of nuclei as well as high surface energy of small nanoparticles favour for the aggregation growth to form large nanoparticles. In addition, the charge of the PMAA-DDT polymer probably affects the aggregation. As mentioned before, dissolving $NaBH_4$ in water resulted in increasing the pH of the solution. It will be seen in Section 2.3.2.8 that the absolute value of charge of the polymer is increased with the increase of pH due to the deprotonation of carboxylic acid group in the polymer. Under studying condition, $NaBH_4$ is dissolved separately with PMAA-DDT, the pH value of the mixture PMAA-DDT and $CoCl_2$ is around 7. This value is lower than that of most reactions ($pH \geq 9.6$) where PMAA-DDT and $NaBH_4$ are dissolved together. The lower charge of PMAA-DDT (weak electrostatic repulsion between nanoparticles) is a possible reason that could lead to the aggregation that forms large nanoparticles.

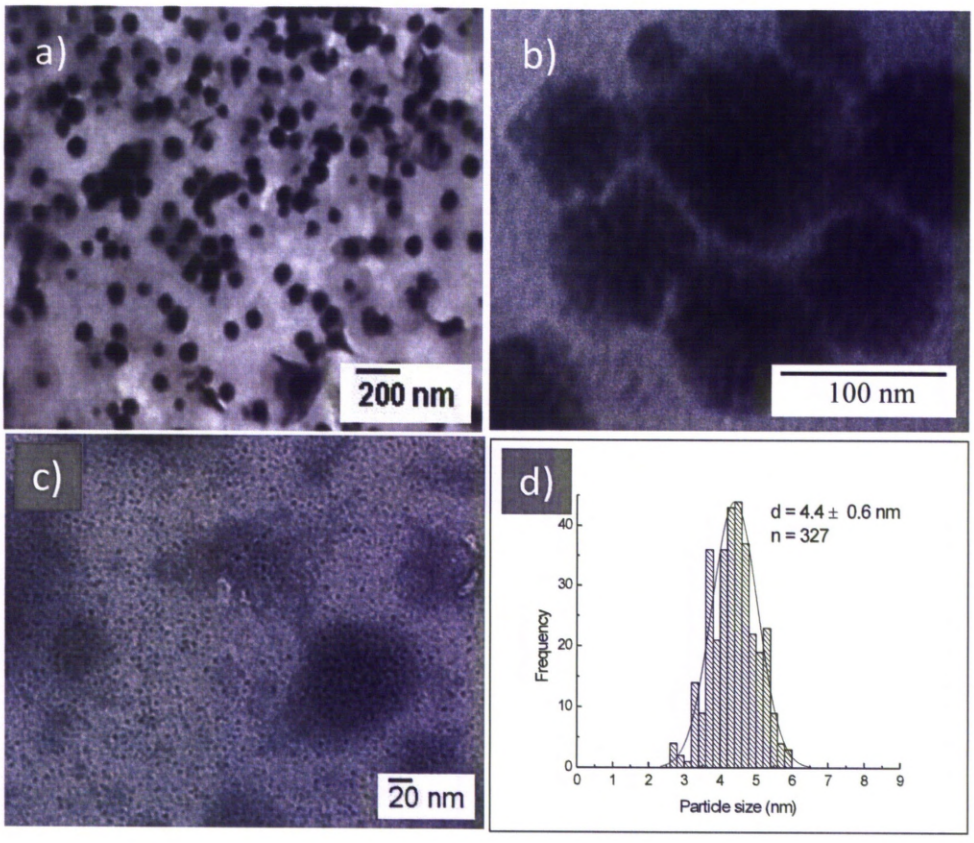

Figure 2.5: TEM images and size distribution histogram of the Co nanoparticles synthesised at different adding speed of $NaBH_4$ into solution of polymer and $CoCl_2$: a,b) rapid injection (different magnification), c) drop-wise adding and d) histogram of size distribution of sample (c). Polymer molecular weight M_w = 13,500 g mol^{-1}.

PMAA-DDT with a molecular weight M_w = 8,610 g mol^{-1} was also investigated. In this case, the speed of $NaBH_4$ addition had little effect on the particle size. The size of the nanoparticles was almost unchanged (4.1 nm in the case of rapid injection and 3.8 nm in the case of drop-wise addition) when varying the speed of addition of reductant (Figure 2.6).

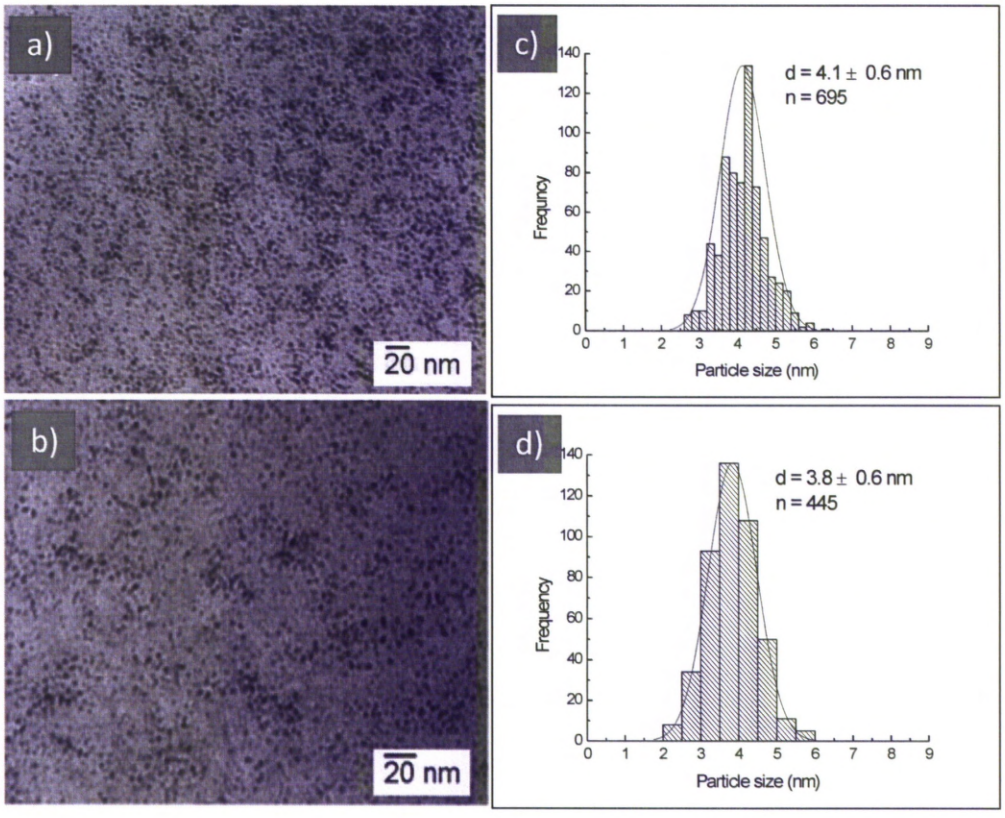

Figure 2.6: TEM images and size distribution histogram of the Co nanoparticles synthesised at different adding speed of $NaBH_4$ into solution of polymer and $CoCl_2$: a) rapid injection, b) drop-wise adding; c and d) corresponding histogram of size distributions of samples (a) and (b). Polymer molecular weight M_w = 8,610 g mol^{-1}.

2.3.2.4 Magnetic properties of the PMAA-DDT stabilised Co nanoparticles

The magnetic properties of the Co nanoparticles were determined by measurements in the SQUID magnetometer of the zero-field-cooled (ZFC) and field-cooled (FC) magnetisations of different Co nanoparticles with particle sizes from 3.2 nm to 7.5 nm (Figure 2.7, left panel). It can be seen that the blocking temperature T_B, determined from the peak in the ZFC curve, increased with increasing particle size (Figure 2.7, right panel). The splitting between the ZFC and FC magnetisation curves occurs fairly close to the peak observed in the ZFC curve, which would indicate that the samples are quite uniform and

monodisperse,[46,47] in agreement with the measurements made from the TEM images (Figure 2.3).

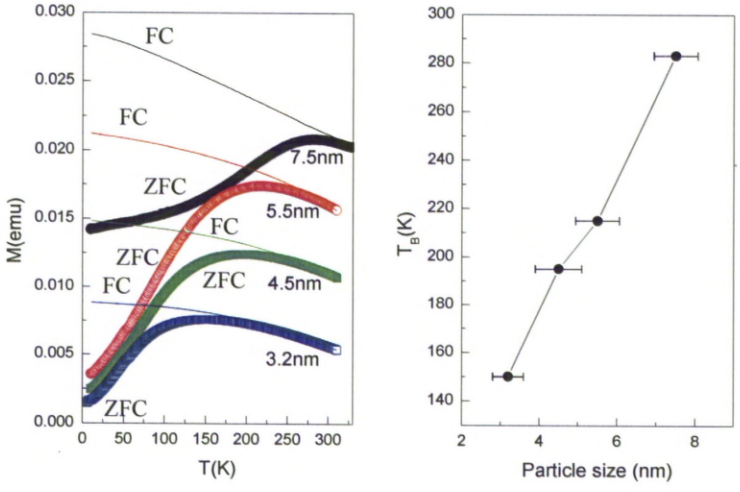

Figure 2.7: The zero-field-cooled (ZFC) and field-cooled (FC) magnetisation of the PMAA-DDT (13,500 g mol^{-1}) stabilised Co nanoparticles with different sizes (left panel) and the blocking temperature T_B as a function of the particle size (right panel).

The ZFC and FC magnetisation curves of the Co nanorods (Figure 2.8) indicate an absence of the peak on the ZFC curve until 350 K. This suggests that the nanoparticles are ferromagnetic at room temperature.

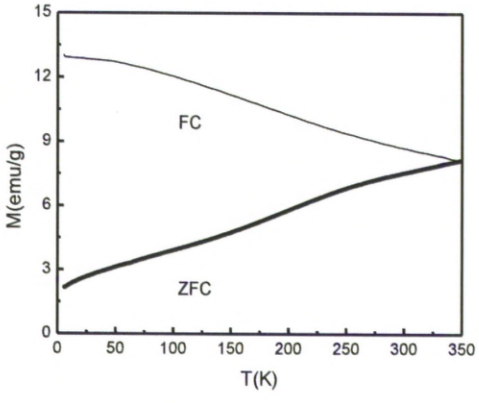

Figure 2.8: The zero-field-cooled (ZFC), field-cooled (FC) magnetisation of the Co nanorods with sizes of (36 ± 5.5) x (15 ± 2.1) nm.

2.3.2.5 Stability of the PMAA-DDT stabilised Co nanoparticles in aqueous solution

The polymer ligand, PMAA, is a weak polyelectrolyte and can provide both steric and electrostatic repulsion between the nanoparticles to prevent them from aggregating.[48] On the other hand, since the standard reduction potential of Co^{2+}/Co is low (-0.28 V), Co is very susceptible to oxidation, especially at the nanoscale. The formation of a layer of oxidised Co might disrupt the coordinative bonding between the Co core and the coating polymer layer, which could then compromise the stabilising repulsion between the nanoparticles. It was observed that, over certain time periods, the as-prepared nanoparticles become aggregated and precipitated from the aqueous solution and, thus the stability time for these aqueous solutions could be monitored visually. There also appeared to be a chemical reaction taking place inside the sediments on a longer timescale. In all likelihood, this resulted in the formation of complexes containing Co^{2+} ions, since the solution was observed to become pale green in colour (Figure 2.9, inset). Figure 2.9 shows the stability over time of the aqueous solutions containing the Co nanoparticles coated with PMAA-DDT of different molecular weights and at two polymer concentrations, 0.06 and 0.12 mM. It can be seen that the stability is improved by increasing the polymer concentration from 0.06 mM to 0.12 mM. However, a further increase in the polymer concentration beyond 0.12 mM did not improve the stability of the nanoparticles (result not shown). Increasing the polymer molecular weight also improved the stability of the nanoparticles quite markedly for a given concentration. The greatest stability was observed with a polymer molecular weight of 13,500 g mol^{-1} and the Co nanoparticles remained well dispersed in aqueous solution for up to eight weeks after the synthesis. As mentioned above, it was observed that the particle size increased with the polymer molecular weight. Therefore, it may be that the smaller nanoparticles are more susceptible to oxidation, perhaps because of their greater surface area/volume ratio and the polymer coat not shielding the metal core from the environment sufficiently. It is also possible that, as a

result of increasing the polymer molecular weight, a thicker/denser polymer layer forms, which then better protects the Co core from oxidation, as well as increasing the steric and electrostatic repulsion between the nanoparticles.

The thioether DDT end-group was also found to play an important role in determining the stability of the nanoparticles. The nanoparticles coated only with PMAA (M_w = 13,000 g mol^{-1}, no thioether DDT end group) began to precipitate from the aqueous solution after just 11 days. This may be due to a stronger adsorption of the DDT and its thioether onto the surface of the nanoparticles, which would enhance the attachment of the polymer ligand to the metal core and hence increase the stability of the nanoparticles.[34]

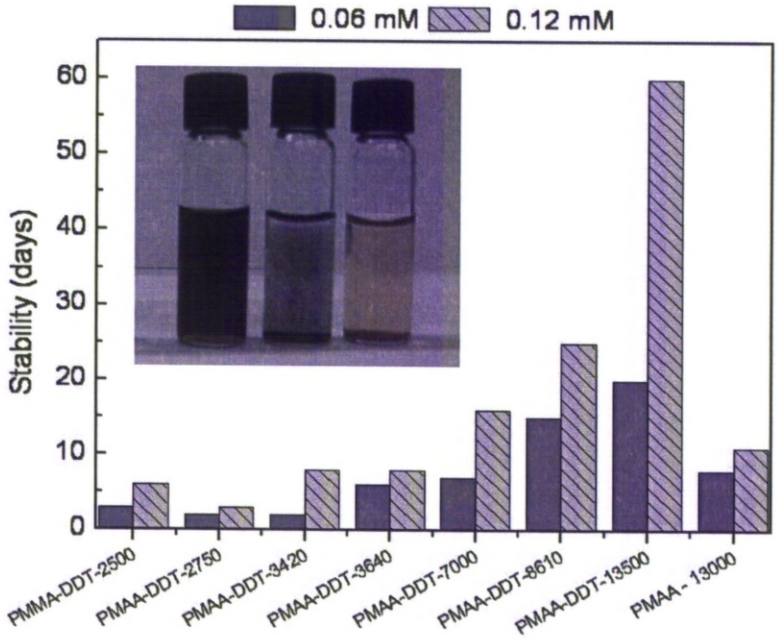

Figure 2.9: The stability of the PMAA-DDT stabilised Co nanoparticles with different molecular weights (M_w = 2,500, 2,750, 3,420, 3,640, 7,000, 8,610, 13,500 g mol^{-1}) and PMAA (M_n = 13,000 g mol^{-1}) at concentrations of 0.06 (grey bars) and 0.12 mM (hatched bars).

2.3.2.6 Stability of PMAA-DDT stabilised Co nanoparticles in different salt concentrations

To be used in biomedical applications it is required that the particles be stable under physiological condition. A first approximation of such conditions is afforded by increasing the concentration of electrolytes, particularly NaCl to determine if the colloidal stability of the nanoparticles is retained (Figure 2.10). It can be seen that the PMAA-DDT stabilised Co nanoparticles are stable below 230 mM NaCl (Figure 2.10a, b), which is slightly higher than that attained *in vivo* (the equivalent of 160 mM NaCl). At these NaCl concentrations, the nanoparticles can be collected by centrifugation and easily re-dispersed in water by sonication. At higher NaCl concentrations the nanoparticles were aggregated and began to precipitate about 30 min to 1 h after adding the NaCl (Figure 2.10c, d and e). In these cases, the nanoparticles cannot be re-dispersed in water by sonication.

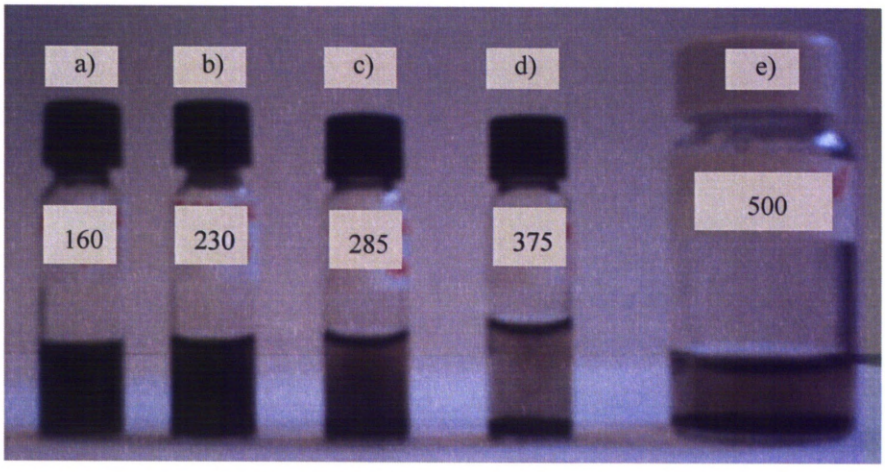

Figure 2.10: Stability of the PMAA-DDT (13,500 g mol^{-1}) stabilised Co nanoparticles at different NaCl concentrations: 160 mM (a), 230 mM (b), 285 mM (c), 375 mM (d) and 500 mM (e) in the presence of phosphate buffer (10 mM).

2.3.2.7 Stability of the sample in air

The oxidation of the Co nanoparticles in the presence of air can be monitored by SQUID measurements. When the Co superparamagnetic Co nanoparticles are oxidised, usually it forms an antiferromagnetic CoO phase on the surface of the nanoparticles. The oxidation of Co results in a reduction in the saturation magnetisation. In addition the exchange bias coupling between antiferromagnetic CoO and ferromagnetic Co phase will lead to a shift of the field cooled hysteresis loop, i.e., the hysteresis loop becomes asymmetric.[49, 50] The hysteresis loop of the Co nanoparticles stabilised by 0.12 mM PMAA-DDT (M_w = 13,500 g mol^{-1}) was examined after exposure to air for different times (Figure 2.11). Neither reduction in the saturation magnetisation nor shift in the field cooled hysteresis loop was observed after 22 days. These suggest that PMAA-DDT polymer protects effectively the Co core from oxidation.

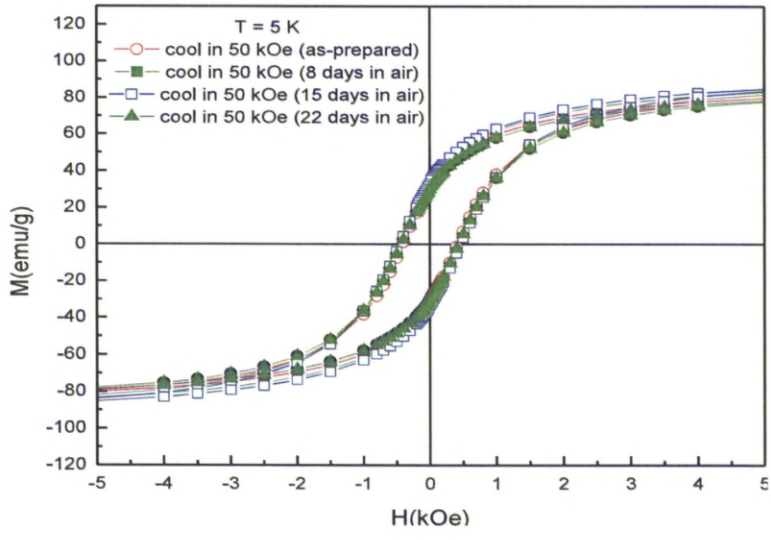

Figure 2.11: Field cooled hysteresis loop of the Co nanoparticles stabilised by 0.12 mM PMAA-DDT (13,500 g mol^{-1}) before and after exposure to air. A powder sample is cooled from room temperature to 5 K under magnetic field H = 50 kOe (5 Tesla). At 5 K, the magnetisation values of the sample were measured as a function of applied field H.

2.3.2.8 Surface properties of the PMAA-DDT stabilised Co nanoparticles

It is well known that an important factor determining the colloidal stability of the nanoparticles in solutions of electrolytes is the surface charge, which can be measured through the zeta potential (ζ). A high (absolute) value of the ζ-potential indicates a high surface charge, strong particle repulsion, and high stability of the nanoparticles in solution. At a fixed pH, the exposure of charged domains increases, as the molecular weight of the coating polymer layer increases, resulting in an increase of the absolute value of the ζ-potential (see, for example, Figure 2.12a). Similarly, when the molecular weight of the coating polymer layer is fixed, we observed that increasing the pH also results in an increase of the absolute value of the ζ-potential (Figure 2.12b). In this case, the dependence of the ζ-potential upon pH could be attributed to an increase in the particle surface ionisation of which a contribution is most likely due to the deprotonation of the carboxylic acid groups in the polymer ligand chains under increasingly alkaline conditions.

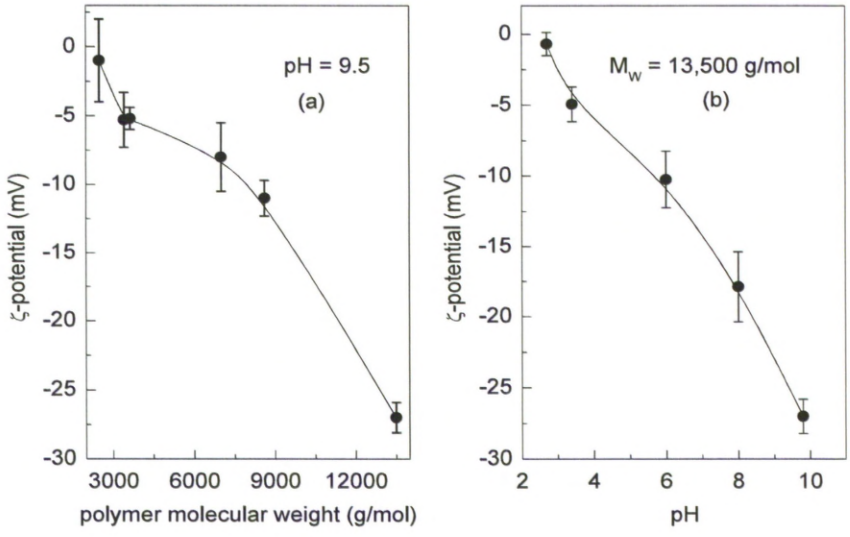

Figure 2.12: The ζ- potential as a function of the PMAA-DDT polymer molecular weight (a) and of pH (b).

2.3.2.9 MRI signal of PMAA-DDT coated Co nanoparticles

The possibility of using Co nanoparticles as MRI contrast enhancers was investigated. The Co nanoparticles were dispersed in either 2% (w/v) agarose gels at different concentrations from 0 to 0.5 mM (mmoles of Co atom per litre of water) or in water at concentrations from 0 to 0.8 mM. No significant difference were obtained between relaxivities of the samples in water and in agarose. Table 2.3 shows relaxivities of two samples of nanoparticles of size of 3.3 and 3.9 nm, coated by PMAA-DDT of molecular weight of 3,420 g mol^{-1} and 13,500 g mol^{-1} dispersed in agarose gels, respectively. It can be seen that the larger nanoparticles had higher relaxivities. There was insignificant change in r_1 or r_2 relaxivities with temperature but r_1 at 1.5 Tesla was approximately double the value at 3 Tesla. The highest relaxivities obtained were 7.4 ± 2 mM^{-1} s^{-1} for r_1 at 1.5 T and 105 ± 3.5 mM^{-1} s^{-1} for r_2 at 3 T. These values are higher than those of $r_1 = 3.2 \pm 0.9$ mM^{-1} s^{-1} and $r_2 = 72 \pm 12$ mM^{-1} s^{-1} reported for commercial iron oxide nanoparticles (Ferumoxsil) with larger core size of 9.5 nm,[51,52] and the high r_2 value of the samples suggests the potential of the Co nanoparticles for development and future use as negative contrast agent.

Table 2 3: Relaxivity values of PMAA-DDT coated Co nanoparticles

Relaxivity values *					
Sample	3.3 nm	3.9 nm	3.9 nm	3.9 nm	3.9 nm
Temperature (^{o}C)	37	37	40	25	25
Field strength (T)	3	3	3	3	1.5
r_1 (mM^{-1} s^{-1})	2.2 ± 0.7	4.3 ± 1.1	4.2 ± 1.1	3.9 ± 1.0	7.4 ± 2.0
r_2 (mM^{-1} s^{-1})	94 ± 2.6	99 ± 3.6	98 ± 2.7	105 ± 3.5	88 ± 3.2
r_2/r_1	43	23	23	27	12

*The samples were dispersed in agarose gel.

2.3.2.10 Other analytical techniques

So far, in this work, the synthesised nanoparticles have been characterised mainly in the aspects of morphology and magnetic property using TEM and SQUID techniques. Oxidative stability of the sample under air is indirectly evaluated via SQUID measurements and visual observation. Information on the interaction between polymer ligands and particle surface is lacking. For example, it is important to know whether the carboxylic acid or the thioether functional group binds to the particles, and if the hydrophobic tail DDT of the polymer is actually absorbed to the particle surface to enhance the attachment of the ligand. In addition, it is also necessary to carry out analyses to gain direct evidence about the oxidation stability of the sample. Thus, other analytical methods such as FTIR, TGA, DSC, XPS, etc. should be used.

Wu *et al.* have studied the interaction of oleic acid (OA) monolayers with Co nanoparticles using FTIR.[53] The authors indicated a noticeable variation between the FTIR spectrum of pure OA and that of OA coated Co nanoparticles (Figure 2.13). In the OA spectrum (Figure 2.13a), there were several important bands associated with free carboxylic acid. The broad feature between 2500 and 3500 cm^{-1} was due to the O-H stretching of the carboxylic group. The intense peak at 1710 cm^{-1} was assigned to C=O stretching. The two peaks at 1462 and 937 cm^{-1} were attributed to O-H in-plane and out-of-plane bendings, respectively. In the OA coated Co nanoparticles FTIR spectrum (Figure 2.13b), the intense C=O stretching band of carboxyl group at 1710 cm^{-1} and the broad band of O-H stretching at between 2500 and 3500 cm^{-1}, which presented in FTIR spectrum of neat oleic acid, were absent. Instead, there were two new peaks at 1556 and at 1410 cm^{-1} which have been assigned to the asymmetric $\nu_{as}(COO^-)$ and the symmetric $\nu_s(COO^-)$ stretching, respectively. The difference between $\nu_{as}(COO^-)$ and $\nu_s(COO^-)$, Δ = 1556 cm^{-1} - 1410 cm^{-1} = 145 cm^{-1}, suggested that OA molecule attaches to the particle surfaces via chemically symmetric coordination between two oxygen atoms in the carboxylate and Co

atoms at the surface of the nanoparticles. The authors also pointed out that the shift of the two sharp peaks from 2924 cm^{-1} (the asymmetric CH_2 stretching) and 2854 cm^{-1} (the symmetric CH_2 stretching) in the FTIR spectrum of OA to 2919 and 2850 cm^{-1} in the spectrum of the OA coated Co nanoparticles is due to a well ordered packing of the hydrocarbon chains of the OA molecules surrounding the Co cores.

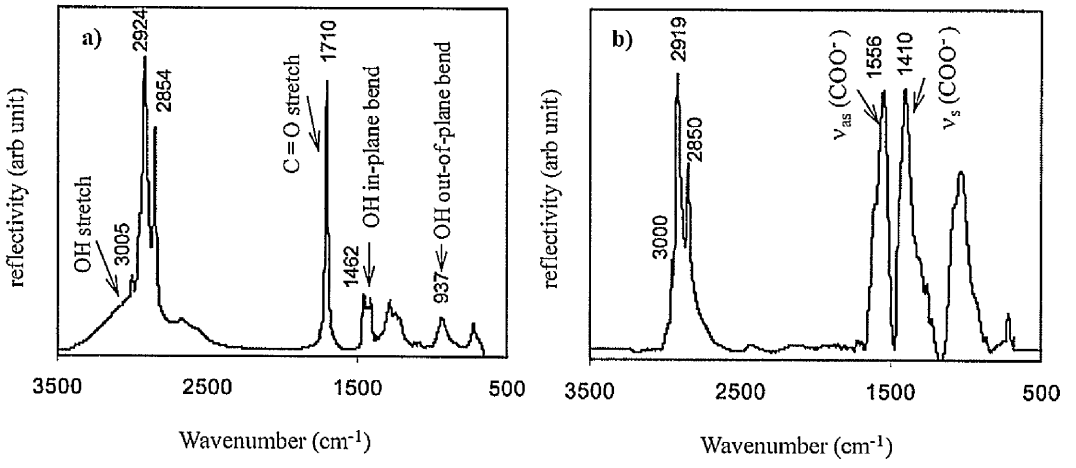

Figure 2.13: FTIR spectra of pure OA (a) and OA coated Co nanoparticles (b). (Reprinted from ref.[53]).

In the present study, PMAA-DDT is expected to anchor to the surfaces of Co nanoparticles both via its thioether group and its hydrophobic dodecane tail. The hydrophilic carboxylic groups in the polymer are pointed out to the solution. Thus, the characteristic bands of carboxylic group in the FTIR spectra of pure PMAA-DDT and the polymer coated Co nanoparticles are expected to be the same. An analysis of these two spectra would reveal information about the interaction between the polymer ligand and the particle surfaces.

The presence and content of polymer on particles can be also confirmed by thermal analyses. Li *et al.* have used TGA to investigate the thermal composition of Fe_3O_4 nanoparticles coated by PMAA polymer with multi thiol functional groups.[54] It were

indicated that there were two steps of weight loss of the sample. The weight loss at between 180 to 220 °C, about 10 %, was due to the elimination of free thiol groups, which supported for the authors' suggestion that the polymer decomposition started at the free thiol terminal groups. The main weight loss in the temperature range of 230 and 420 °C, approximately 53%, was attributed to the decomposition of carboxylic group (at 240 – 360 °C) and decomposition of polymer backbone.

In our study, PMAA-DDT with higher molecular weight (13.500 g mol^{-1}) in comparison with that of 4537 g mol^{-1} of the polymer in the above work[54] was used. Therefore, we expect a larger weight loss is observed in the TGA curves. Additionally, it has been presumed that PMAA-DDT is attached to the Co nanoparticles through binding of thioether groups and Co metals, and the adsorption of dodecane tail on the particle surfaces. So it is not to expect to see a loss weigh at the temperature below 220 °C in the TGA as the absence of free thiol groups, instead, it is possible to observe endothermic peak(s) in the DSC curves due to the desorption of dodecane tail and/or thioether group of the polymer.

Concerning the oxidative stability of the Co sample, XPS has been demonstrated to be a useful and important technique for the characterisation of surface oxidation of the sample. In XPS spectra of Co samples, two $2p_{1/2}$ and $2p_{3/2}$ lines are usually used to indentify or distinguish the oxidation state of the Co. At zero-valence state, Co XPS spectra show sharp peaks with typical binding energies of 777.9 eV ($Co2p_{3/2}$) and 793.0 eV ($Co2p_{1/2}$).[53, 55] However, if Co is oxidised, a shift of these peaks is generally observed.[56, 57]

Yang *et al.* used XPS to inspect the oxidative stability of Co nanoparticles coated by oleic acid and triphenyl phosphine.[55] The authors indicated that the nanoparticles exposing to air exhibits no change in the XPS spectrum after 90 days. Two sharp peaks at 778.5 and 793.6 eV which correspond to binding energies of $Co2p_{3/2}$ and $Co2p_{1/2}$ of the Co metal were observed. After 120 days, a shift of the peaks from 778.5 eV and 793.6 eV to 779.5

eV (for $Co2p_{3/2}$) and 795.4 eV (for $Co2p_{1/2}$), respectively, which are characteristic of Co^{2+} oxidation state was recorded. In addition, a broadening of the peaks and the appearance of satellite peaks also indicated evidence of the formation of CoO.[55]

2.4 Conclusion

Water-dispersible magnetic Co nanoparticles have been directly synthesized directly in water using a simple method. Peptide ligands could not protect efficiently the Co core from aggregation and oxidation. PMAA-DDT polymer was demonstrated to be a suitable stabilizing ligand for Co nanoparticles. The size of the PMAA-DDT stabilised Co nanoparticles could be tuned between 2-7.5 nm by changing the concentration of the polymer. These nanoparticles are superparamagnetic and stable in aqueous solution. The stability of the PMAA-DDT stabilised Co nanoparticles in different electrolyte concentrations was also tested. The results show that the nanoparticles are stable up to NaCl concentration of 230 μM, slightly higher than value required for bio-applications (about 160 μM). Visual observation and SQUID measurements indicated that PMAA-DDT coated Co nanoparticles are relatively stable in air. However, more characterisation such as XPS, FTIR, Raman, TGA and DSC should be carried out to provide comprehensive evidence on the oxidative stability of the sample as well as information about the interaction between polymer ligand and surfaces of the Co nanoparticles.

This synthesis method is simple and it also allows to apply to other systems such as CoPt alloy with controlled morphology, which will be described in chapter 3. The preliminary use of the Co nanoparticles as a MRI contrast enhancer was tested and provided evidence that these materials have considerable potential in this application.

Reference

1. Safarik, I.; Safarikova, M. *J. Chromatography B* **1999,** 722, (1-2), 33-53.
2. Lee, K. B.; Park, S.; Mirkin, C. A. *Angew. Chemie-Inter. Ed.* **2004,** 43, (23), 3048-3050.
3. Gu, H. W.; Xu, K. M.; Xu, C. J.; Xu, B. *Chem. Commun.* **2006,** (9), 941-949.
4. Yavuz, C. T.; Mayo, J. T.; Yu, W. W.; Prakash, A.; Falkner, J. C.; Yean, S.; Cong, L. L.; Shipley, H. J.; Kan, A.; Tomson, M.; Natelson, D.; Colvin, V. L. *Science* **2006,** 314, (5801), 964-967.
5. Yavuz, C. T.; Prakash, A.; Mayo, J. T.; Colvin, V. L. *Chem. Eng. Sci.* **2009,** 64, (10), 2510-2521.
6. Kang, K.; Choi, J.; Nam, J. H.; Lee, S. C.; Kim, K. J.; Lee, S. W.; Chang, J. H. *J. Phys. Chem. B* **2009,** 113, (2), 536-543.
7. Lubbe, A. S.; Alexiou, C.; Bergemann, C. *J. Surg. Res.* **2001,** 95, (2), 200-206.
8. Pankhurst, Q. A.; Connolly, J.; Jones, S. K.; Dobson, J. *J. Phys. D-Appl. Phys.* **2003,** 36, (13), R167-R181.
9. Jun, Y. W.; Lee, J. H.; Cheon, J. *Angew. Chemie-Inter. Ed.* **2008,** 47, (28), 5122-5135.
10. Pankhurst, Q. A.; Thanh, N. K. T.; Jones, S. K.; Dobson, J. *J. Phys. D-Appl. Phys.* **2009,** 42, (22), 224001
11. Tartaj, P.; Morales, M. D.; Veintemillas-Verdaguer, S.; Gonzalez-Carreno, T.; Serna, C. J. *J. Phys. D-Appl. Phys.* **2003,** 36, (13), R182-R197.
12. Alexiou, C.; Arnold, W.; Klein, R. J.; Parak, F. G.; Hulin, P.; Bergemann, C.; Erhardt, W.; Wagenpfeil, S.; Lubbe, A. S. *Cancer Res.* **2000,** 60, (23), 6641-6648.
13. Ito, A.; Shinkai, M.; Honda, H.; Kobayashi, T. *J. Biosci.& Bioeng.* **2005,** 100, (1), 1-11.
14. Yu, S.; Chow, G. M. *J. Mater. Chem.* **2004,** 14, (18), 2781-2786.
15. Lee, S. J.; Jeong, J. R.; Shin, S. C.; Huh, Y. M.; Song, H. T.; Suh, J. S.; Chang, Y. H.; Jeon, B. S.; Kim, J. D. *J. Appl. Phys.* **2005,** 97, (10), 3512-3515.
16. Zhang, T. R.; Ge, J. P.; Hu, Y. P.; Yin, Y. D. *Nano Lett.* **2007,** 7, (10), 3203-3207.
17. Xia, H. B.; Yi, J. B.; Foo, P. S.; Liu, B. H. *Chem. Mater.* **2007,** 19, (16), 4087-4091.
18. Harris, L. A.; Goff, J. D.; Carmichael, A. Y.; Riffle, J. S.; Harburn, J. J.; St Pierre, T. G.; Saunders, M. *Chem. Mater.* **2003,** 15, (6), 1367-1377.
19. Yuan, J. J.; Armes, S. P.; Takabayashi, Y.; Prassides, K.; Leite, C. A. P.; Galembeck, F.; Lewis, A. L. *Langmuir* **2006,** 22, (26), 10989-10993.

20. Euliss, L. E.; Grancharov, S. G.; O'Brien, S.; Deming, T. J.; Stucky, G. D.; Murray, C. B.; Held, G. A. *Nano Lett.* **2003,** 3, (11), 1489-1493.
21. Wang, Y.; Wong, J. F.; Teng, X. W.; Lin, X. Z.; Yang, H. *Nano Lett.* **2003,** 3, (11), 1555-1559.
22. Pellegrino, T.; Manna, L.; Kudera, S.; Liedl, T.; Koktysh, D.; Rogach, A. L.; Keller, S.; Radler, J.; Natile, G.; Parak, W. J. *Nano Lett.* **2004,** 4, (4), 703-707.
23. Yu, W. W.; Chang, E.; Sayes, C. M.; Drezek, R.; Colvin, V. L. *Nanotech.* **2006,** 17, (17), 4483-4487.
24. Kim, M.; Chen, Y. F.; Liu, Y. C.; Peng, X. G. *Adv. Mater.* **2005,** 17, (11), 1429-1430.
25. Frankamp, B. L.; Fischer, N. O.; Hong, R.; Srivastava, S.; Rotello, V. M. *Chem. Mater.* **2006,** 18, (4), 956-959.
26. Robinson, D. B.; Persson, H. H. J.; Zeng, H.; Li, G. X.; Pourmand, N.; Sun, S. H.; Wang, S. X. *Langmuir* **2005,** 21, (7), 3096-3103.
27. Kim, D. H.; Nikles, D. E.; Johnson, D. T.; Brazel, C. S. *J. Mag. Mag. Mater.* **2008,** 320, (19), 2390-2396.
28. De Palma, R.; Peeters, S.; Van Bael, M. J.; Van den Rul, H.; Bonroy, K.; Laureyn, W.; Mullens, J.; Borghs, G.; Maes, G. *Chem. Mater.* **2007,** 19, (7), 1821-1831.
29. Tromsdorf, U. I.; Bigall, N. C.; Kaul, M. G.; Bruns, O. T.; Nikolic, M. S.; Mollwitz, B.; Sperling, R. A.; Reimer, R.; Hohenberg, H.; Parak, W. J.; Forster, S.; Beisiegel, U.; Adam, G.; Weller, H. *Nano Lett.* **2007,** 7, (8), 2422-2427.
30. Hong, R.; Fischer, N. O.; Emrick, T.; Rotello, V. M. *Chem. Mater.* **2005,** 17, (18), 4617-4621.
31. Bagaria, H. G.; Ada, E. T.; Shamsuzzoha, M.; Nikles, D. E.; Johnson, D. T. *Langmuir* **2006,** 22, (18), 7732-7737.
32. Xu, C. J.; Xu, K. M.; Gu, H. W.; Zhong, X. F.; Guo, Z. H.; Zheng, R. K.; Zhang, X. X.; Xu, B. *JACS* **2004,** 126, (11), 3392-3393.
33. Hussain, I.; Graham, S.; Wang, Z. X.; Tan, B.; Sherrington, D. C.; Rannard, S. P.; Cooper, A. I.; Brust, M. *JACS* **2005,** 127, (47), 16398-16399.
34. Wang, Z. X.; Tan, B. E.; Hussain, I.; Schaeffer, N.; Wyatt, M. F.; Brust, M.; Cooper, A. I. *Langmuir* **2007,** 23, (2), 885-895.
35. Levy, R.; Thanh, N. T. K.; Doty, R. C.; Hussain, I.; Nichols, R. J.; Schiffrin, D. J.; Brust, M.; Fernig, D. G. *JACS* **2004,** 126, (32), 10076-10084.
36. Pearson, R. G. *JACS* **1963,** 85, (22), 3533-3534.
37. Pearson, R. G. *JACS* **1968,** 45, (9), 581-582.

38. Shen, J. Y.; Li, Z. Y.; Yan, Q. J.; Chen, Y. *J. Phys. Chem.* **1993,** 97, (32), 8504-8511.
39. Glavee, G. N.; Klabunde, K. J.; Sorensen, C. M.; Hadjipanayis, G. C. *Langmuir* **1993,** 9, (1), 162-169.
40. Linderoth, S.; Morup, S. *J. Appl. Phys.* **1990,** 67, (9), 4472-4474.
41. Tong, G. X.; Guan, J. G.; Xiao, Z. D.; Mou, F. Z.; Wang, W.; Yan, G. Q. *Chem. Mater.* **2008,** 20, (10), 3535-3539.
42. Thanh, N. T. K.; Puntes, V. T.; Tung, L. D.; Fernig, D. G. *J. Phys.: Confer. Seri.* **2005,** 17, 70-76.
43. Shimmin, R. G.; Schoch, A. B.; Braun, P. V. *Langmuir* **2004,** 20, (13), 5613-5620.
44. Dumestre, F.; Chaudret, B.; Amiens, C.; Respaud, M.; Fejes, P.; Renaud, P.; Zurcher, P. *Angew. Chemie-Inter. Ed.* **2003,** 42, (42), 5213-5216.
45. Perez-Juste, J.; Pastoriza-Santos, I.; Liz-Marzan, L. M.; Mulvaney, P. *Coordin. Chem. Rev.* **2005,** 249, (17-18), 1870-1901.
46. Cannas, C.; Musinu, A.; Ardu, A.; Orru, F.; Peddis, D.; Casu, M.; Sanna, R.; Angius, F.; Diaz, G.; Piccaluga, G. *Chem. Mater.* **2010,** DOI:10.1021/cm903837g.
47. Hansen, M. F.; Morup, S. *J. Mag. Mag. Mater.* **1999,** 203, 214-216.
48. Shimmin, R. G.; Schoch, A. B.; Braun, P. V. *Langmuir* **2004,** 20, (13), 5613-5620.
49. Meiklejohn, W. H.; Bean, C. P. *Phys. Rev.* **1957,** 105, (3), 904-913.
50. Meiklejohn, W. H.; Bean, C. P. *Phys. Rev.* **1956,** 102, (5), 1413-1414.
51. Jung, C. W.; Jacobs, P. *Mag. Res. Imag.* **1995,** 13, (5), 661-674.
52. Li, W.; Tutton, S.; Vu, A. T.; Pierchala, L.; Li, B. S. Y.; Lewis, J. M.; Prasad, P. V.; Edelman, R. R. *J. Mag. Res. Imag.* **2005,** 21, (1), 46-52.
53. Wu, N. Q.; Fu, L.; Su, M.; Aslam, M.; Wong, K. C.; Dravid, V. P. *Nano Lett.* **2004,** 4, (2), 383-386.
54. Li, Z.; Tan, B.; Allix, M.; Cooper, A. I.; Rosseinsky, M. J. *Small* **2008,** 4, (2), 231-239.
55. Yang, H. T.; Shen, C. M.; Wang, Y. G.; Su, Y. K.; Yang, T. Z.; Gao, H. J. *Nanotech.* **2004,** 15, (1), 70-74.
56. He, T.; Chen, D. R.; Jiao, X. L.; Wang, Y. L.; Duan, Y. Z. *Chem. Mater.* **2005,** 17, (15), 4023-4030.
57. Nguyen, T. D.; Do, T. O. *J. Phys. Chem. C* **2009,** 113, (26), 11204-11214.

Chapter 3
Synthesis and characterisation of water-dispersible CoPt nanoparticles

3.1 Introduction

Hollow nanoparticles have received significant attention owing to their high surface area, lower density, saving of metal and the ability of tune their optical properties in the infrared, all of which are very useful for a variety of applications such as catalysis,[1-4] photothermal treatment,[5-7] optical imaging[7, 8] and drug delivery.[9-13]

There are a number of synthesis methods for hollow structures, such as those using hard templates, galvanic replacement and Kirkendall effect based reactions. Hollow nanoparticles are often prepared by using templates of silica and polymers.[14,15] The latter method allows the synthesis of hollow nanoparticles with good control over size and monodispersity. However, an extra step to remove the template is required, and this sometimes complicates the synthetic procedure. Galvanic replacement reactions, which are based on differences in the reduction potential of two or more metals are also used to synthesise hollow nanoparticles.[16,17] More recently, hollow nanoparticles have been synthesised using the Kirkendall effect,[18] in which pores form, because of the difference in diffusion rates between two components in a diffusion couple. A number of hollow nanoparticles of materials such as CoO, Co_2S_4, and iron oxide have been synthesised using this approach.[18,19] This method is relatively simple and can produce hollow nanoparticles with narrow size distribution. To obtain small sizes, however, the synthesis is commonly performed in an organic solvent.

Other methods to fabricate hollow nanoparticles have been reported including ones

using soft templates, e.g. emulsion droplets,[20-23] surfactants,[24] gas bubbles,[25-27] Ostwald ripening,[28-31] self-assembly[32] and oriented attachment.[33] These methods are simple, but it is difficult to control the size of the nanoparticles. An important challenge is to synthesise hollow nanoparticles suitable for biomedical applications, i.e., dispersible and stable in aqueous solutions and biofunctionalised. In addition, in many cases, such applications also require small hollow nanoparticles, e.g., with a diameter of less than 20 nm. These constraints are very difficult to meet using conventional synthesis methods in aqueous solution.

In terms of chemical stability, compared with a pure metal of Co or Fe, alloys of CoPt or FePt are much more stable. In addition, Pt sites on the nanoparticle surface are known to bond strongly to the thiol groups on ligands,[34,35] which provide a strategy for forming a robust ligand shell able to prevent the nanoparticles from aggregating. Moreover, CoPt alloy nanoparticles offer other advantages, such as enhanced catalytic activity and selectivity relative to the individual components.[36] By adjusting their composition, the magnetic and catalytic properties of the alloy nanoparticles could be tuned.[37,38]

In chapter 2, the synthesis of water-dispersible magnetic Co nanoparticles using polymer PMAA-DDT as stabiliser was described. The size, shape and the stability of the Co nanoparticles in aqueous solution could be tuned by varying the length and concentration of the polymer, as well as by changing the order of addition of the reactants.

In this chapter, using the same synthetic method, the synthesis of CoPt alloy nanoparticles was investigated by simultaneous reduction of Co and Pt salts in aqueous solution in the presence of polymers and/or peptide ligands. By varying concentration of the reactants and the type of ligand a range of nanoparticle morphologies were obtained, including solid, hollow and nanochains/wires. The nanoparticles obtained were characterised using TEM, HRTEM, SQUID, ICP-AES and DLS techniques. Other analytical methods, such as FTIR, XPS and Raman, which have been extensively used in

the literatures for the characterisation of the structure of organic molecules and of the interactions between stabilising ligands and the surface of nanoparticles are also discussed. The synthesised hollow nanoparticles were extremely stable in water over a broad range of different pH and at high concentrations of electrolytes. The hollow nanoparticles were successfully used by collaborators for tracking neural stem cells.

3.2 Experimental

3.2.1 Materials

Cobalt (II) chloride hydrate ($CoCl_2.2H_2O$) 97 %, and hexachloroplatinic (IV) acid hexahydrate ($H_2PtCl_6.6H_2O$) > 37 % Pt basis were purchased from (Sigma-Aldrich Ltd, UK), sodium borohydride ($NaBH_4$) 98 % was obtained from VWR Ltd, UK, peptides including CCALNN, CCVVVT, NNLACC, CALNN and TLVVN were received from Sigma-Genosys Ltd, UK. The structures of these peptides are given in the previous chapter. Methoxypolyethylene glycol acetic acid (PEG-COOH) (M_w = 5,000 g mol^{-1}), methoxypolyethylene glycol amine (PEG-NH_2) (M_w = 5,000 g mol^{-1}) and O-[-(3-mercapto-propionylamino)ethyl]-o'-methyl-polyethyleneglycol (PEG-SH) with M_w = 5,000 and 20,000 g mol^{-1} were purchased from Fluka Ltd, UK. Water-dispersible polymers including poly(methacrylic acid) dodecanethiol (PMAA-DDT) with M_w = 13,500 g mol^{-1}, and poly-(methacrylic acid) pentaerythritol tetrakis (3-mercaptopropionate) (PMAA-PTMP), M_w = 2,000 g mol^{-1} were synthesized at Liverpool.[39,40] The structures of these polymers are shown in Table 3.1.

Table 3.1: Structure of polymer ligands

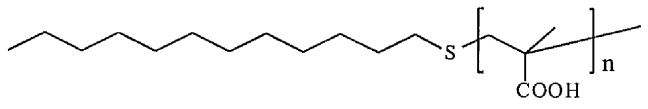 poly(methacrylic acid) dodecanethiolether (PMAA-DDT)
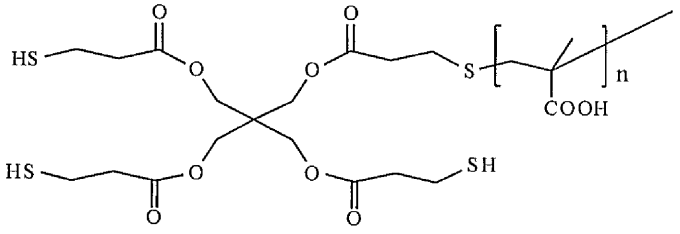 poly(methacrylic acid) pentaerythritol tetrakis (3-mercaptopropionate) (PMAA-PTMP)
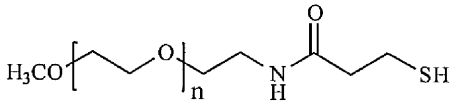 *O*-[2-(3-mercaptopropionylamino)ethyl]-*O'*-methylpolyethylene glycol (PEG-SH)
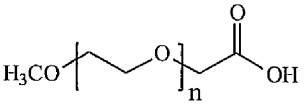 methoxypolyethylene glycol acetic acid (PEG-COOH)
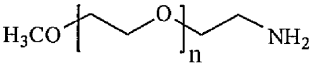 Methoxypolyethylene glycol amine (PEG-NH_2)

3.2.2 Synthesis of CoPt nanoparticles

CoPt alloy nanoparticles were prepared by simultaneous reduction of Co^{2+} and Pt^{+4} with $NaBH_4$ in water in the presence of the stabilising ligands. In a typical procedure, Co and Pt salts (precursors), and stabilising ligand(s) were added to a 100 mL two necked flask, which was then degassed by purging with N_2 for 30 min and placed under vacuum using a mechanical pump for at least 10 min. To this flask, degassed and de-ionised water (19 mL)

was added and the mixture was sonicated for 10-15 min in a U 300 Ultrawave sonic bath (Ultrawave Ltd, UK) to dissolve the stabilising ligand(s) and precursors. $NaBH_4$ solution was freshly prepared by dissolving 0.4 mmol (15.2 mg) of $NaBH_4$ in degassed water (1 mL). This solution was rapidly injected into the reaction flask under sonication. The final concentrations of $NaBH_4$, $CoCl_2$ and H_2PtCl_6 in the reaction flask were 20 mM, 1 mM and 2 mM. Sonication was continued for 5 min after the injection. During this time, the solution changed rapidly to a dark near black colour with some gas evolution. Variations in the synthesis involved changing the stabilising ligands, the length of the polymer ligands (molecular weight), their concentration and the end-functional groups, as well as by changing the concentration of precursors.

3.3 Results and discussion

A simultaneous reduction of Co^{2+} and Pt^{4+} in water in the presence of ligand(s) produced CoPt nanoparticles. In aqueous solution, there are possible chemical reactions:[41]

$$CoCl_2 + 2NaBH_4 + 6H_2O \rightarrow Co + 2NaH_2BO_3 + 2HCl + 7H_2\uparrow \quad (3.1)$$

$$H_2PtCl_6 + NaBH_4 + 3H_2O \rightarrow Pt + H_3BO_3 + 5HCl + NaCl + 2H_2\uparrow \quad (3.2)$$

$$Co + Pt \rightarrow CoPt \quad (3.3)$$

$$NaBH_4 + 2H_2O \rightarrow NaBO_2 + 4H_2\uparrow \quad (3.4)$$

$$NaBO_2 + H_2O \rightleftharpoons BO_2H + NaOH \quad (3.5)$$

At the initial stage of the experiment, Co^{2+} and Pt^{4+} are rapidly reduced to Co and Pt metals (reactions 3.1 and 3.2). These metals are combined to form CoPt alloy (reaction 3.3). Because of the excess of $NaBH_4$ in the solution, reactions 3.4 and 3.5 continue after reactions 3.1-3.3 are completed. The continuing of these reactions is indicated by small bubbling and gradual increase in pH from about 3.5 of the starting solution to 10 after 30 min of reaction. The low pH of the starting solution of Pt and Co salts is due to the acidic

3.3.1 The effect of structure and functional groups of stabilising ligands on morphology of CoPt nanoparticles

The different types of polymers with different functional groups used were PEG-COOH, PEG-SH, PMAA-DDT and PMAA-PTMP (Table 3.1). TEM images of CoPt nanoparticles synthesised in the presence of each of these polymers show that very different morphologies were obtained. Nanochains of about 3-5 nm in width and 50-160 nm in length were formed in the presence of PEG-SH (single thiol) (Figure 3.1a), small solid nanoparticles of around 3.5 nm for the synthesis in the presence of PEG-COOH (no-thiol) or PMAA-DDT (mono-thiolether) (Figure 3.1b,c) and hollow nanoparticles of 9.5 ± 1.5 nm in the case of PMAA- PTMP polymer (Figure 3.1d).

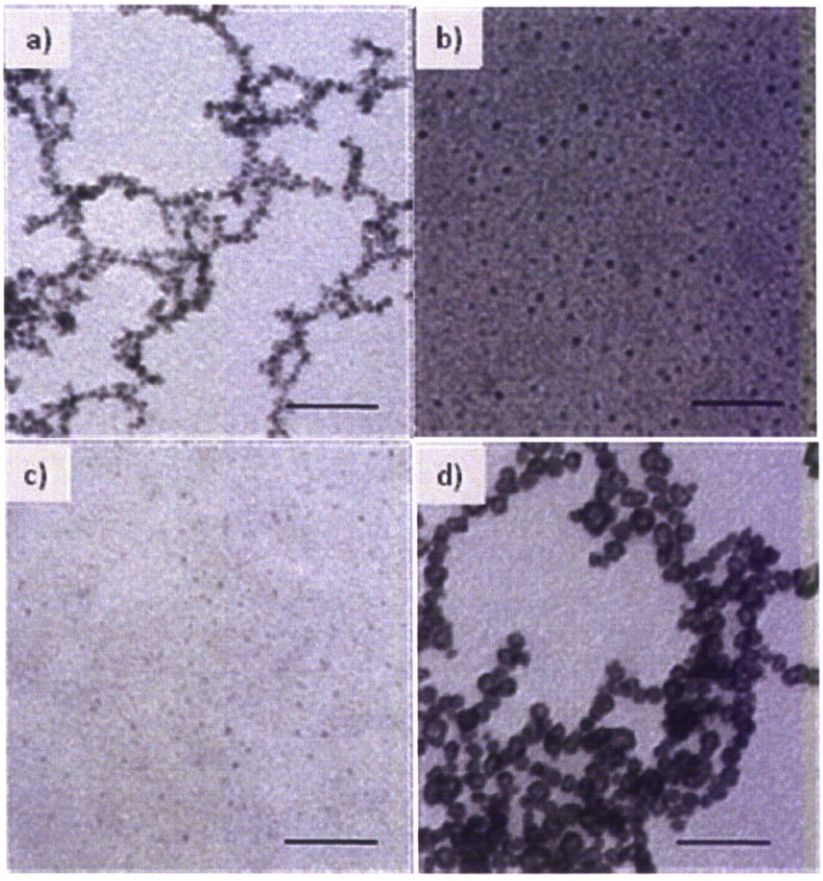

Figure 3.1: TEM images of the CoPt nanoparticles synthesised in the presence of 0.24 mM: a) PEG-SH, b) PEG-COOH, c) PMAA-DDT and PMAA-PTMP. Scale bar: 50 nm.

The formation of nanochains in the presence of PEG-SH may be the result of dipole-dipole interactions of the nanoparticles, whereby the nanoparticles self-assemble into nanochains on the TEM grid when the sample is dried. If these were the case, then increasing the concentration of PEG-SH would cause the ligand shell to become denser which would diminish the dipole-dipole interactions. Indeed, when the PEG-SH concentration was raised to 0.36 mM only isolated small solid nanoparticles were observed.

PMAA-DDT and PMAA-PTMP polymers have similar structure (Table 3.1) but possess different functional groups, thiolether in DDT and three thiols in PTMP. Therefore, it was hypothesised that the formation of hollow nanoparticles may relate to multi-thiol functional groups rather than the structure of the polymer.

To test the hypothesis that the presence of multi-thiol functional groups played an important role in the formation of the hollow nanoparticles, peptides with two thiols were used as ligands, CCALNN, CCVVVT and NNLACC and compared with CALNN, which has a single thiol and TLVVN that lacks a thiol (Table 2.1) using the indicated concentrations (Table 3.1). However, when the synthesis was carried out in the presence of these peptides, only aggregated nanoparticles were produced, which then precipitated. These peptides are short in length and possess multiple functional groups that may interact with the metal surface. As a result, when coating the nanoparticles, they may lie down on the surface and so not provide sufficient steric repulsion to stabilise the nanoparticles. Moreover, the other functional groups of the peptides (i.e. amine, amide and caboxyl) may have bridged nanoparticles and caused them to aggregate.

To try to overcome this problem, a mixture of peptide and polymer (e.g. PEG-SH, M_w = 5,000 g mol^{-1}) was investigated. When di-thiol peptide CCALNN, CCVVVT or NNLACC was used in conjunction with the polymer, CoPt hollow nanoparticles were

obtained (see Table 3.2).

Figure 3.2a shows an example of monodisperse hollow nanoparticles of 9.8 ± 1.3 nm obtained when using CCALNN. On the other hand, solid nanoparticles and nanochains were obtained in the presence of CALNN and TLVVN, which possess one and no thiol, respectively (Figure 3.2b, c). Thus, these results suggest that the presence of the multi-thiol functional group in the peptides is very important for the formation of the CoPt hollow nanoparticles, whereas the mono-thiol PEG-SH is critical in this instance for ensuring colloidal stability and to prevent the hollow nanoparticles from aggregating. In contrast, the presence of TLVVN in combination with PEG assisted in the formation of nanowires.

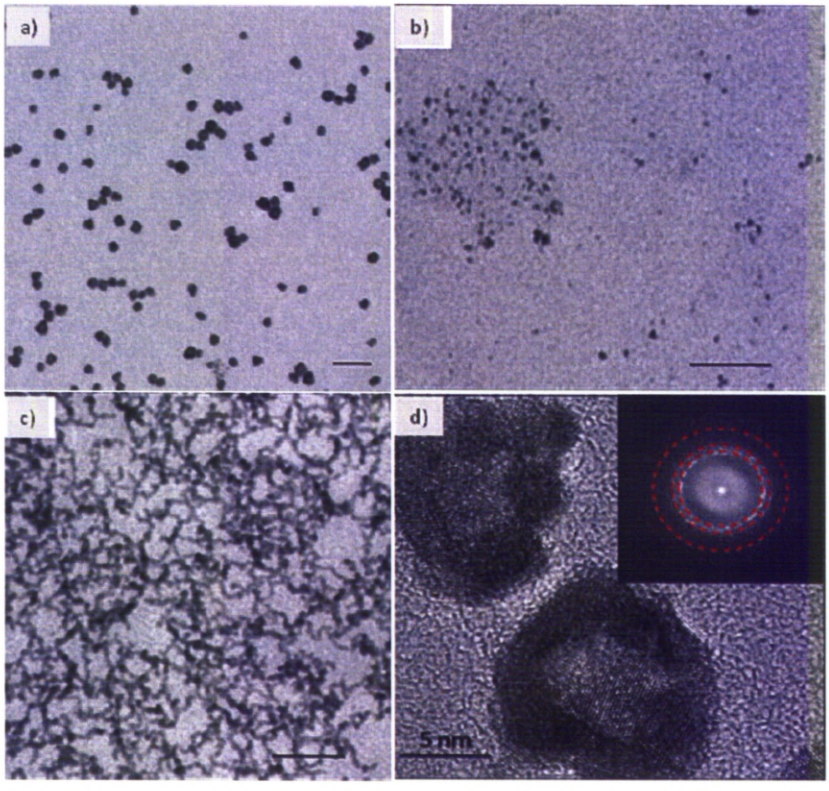

Figure 3.2: TEM images of the CoPt nanoparticles synthesised in the presence of 0.24 mM PEG-SH (5,000 g mol^{-1}) and 0.12 mM peptide: a) CCALNN, b) CALNN and c) TLVVN; and d) HRTEM image of (a). The inset shows the corresponding Fast Fourier Transform (FFT) image which shows 3 strongest rings with d-spacings of 2.213, 1.954 and 1.362 Å. Scale bar: 50 nm.

To study the nanoparticles in more detail, HRTEM was performed on the hollow nanoparticles synthesised in the presence of 0.12 mM CCALNN and 0.24 mM PEG-SH (Figure 3.2d). It can be seen that the hollow nanoparticles consist of crystallised small nanoparticles of a diameter of about 3 nm. At the edge of the hollow nanostructures, the mass contrast is darker than inside, which suggests the presence of small nanoparticles in the outer ring. From the FFT image of the electron diffraction pattern, one can observe 3 rings with d-spacings of 2.213, 1.954 and 1.362 Å, which are closely matched with the d spacings of the corresponding (100), (200) and (220) planes of the fcc $CoPt_3$ phase (pdf file N_o 29-0499).

To test further the idea that ligands with multiple thiols were essential for the formation of hollow nanoparticles, the combination of stabilising ligands was extended to include PMAA-PMTP + PEG (SH or NH_2), PMAA-DDT + CCALNN, PMAA-DDT + CALNN, PMAA-DDT + PEG-SH and PEG-NH_2 + TLVVN (Table 3.2). The results support the role of multiple thiol functional groups in the formation of hollow nanoparticles. Moreover, the results also show that the presence of TLVVN peptide determines the formation of nanowires, as illustrated by TEM (Figure 3.3).

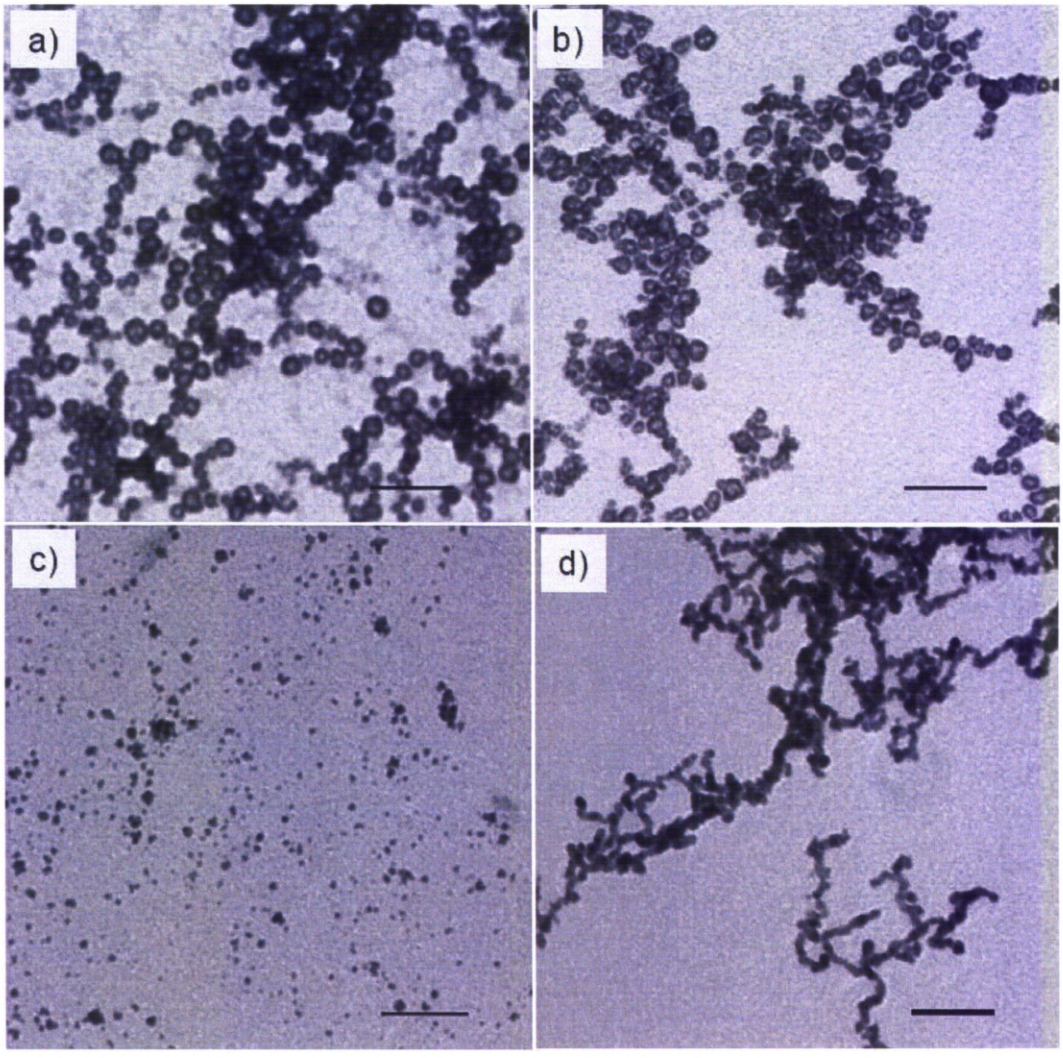

Figure 3.3: TEM images of the CoPt nanoparticles synthesised in the presence of a) PMAA-PTMP + PEG-SH, b) 0.24 mM PMAA-PTMP + 0.12 mM PEG-NH_2, c) 0.24 mM PMAA-DDT + 0.12 mM PEG-SH and d) 0.24 mM PEG-NH_2 + 0.12 mM TLVVN. Scale bar: 50 nm.

3.3.2 Effect of the ligands' concentrations and molecular weight on the size of hollow nanoparticles

The effect of the concentration of the stabilising ligands and the size of the polymers (molecular weight, M_w) on the morphology of CoPt hollow nanoparticles was investigated by synthesising nanoparticles in the presence of a mixture of PEG-SH polymer (single

thiol) and CCALNN peptide (di-thiol). For the PEG-SH polymer, the molecular weight could be varied between 5,000 and 20,000 g mol^{-1}.

Table 3.3: The effect of ligand's concentration and length on the size of hollow nanoparticles.

PEG (mM) M_w = 5,000 g mol^{-1}	PEG (mM) M_w = 5,000 g mol^{-1}	CCALNN (mM)	Perimeter (nm)
0.24		0.06	7.3 ± 1.5
0.24		0.12	9.8 ± 1.3
0.24		0.24	14.9 ± 3.0
0.24		0.60	30.5 ± 8.5
0.24		0.96	40.0 ± 7.9
0.12		0.12	8.3 ± 1.3
0.36		0.12	15.5 ± 2.2
0.40		0.12	18.5 ± 2.5
0.48		0.60	20 – 60
	0.24	0.12	14.6 ± 1.9
	0.24	0.14	18.8 ± 3.4
	0.24	0.60	42.6 ± 8.2
	0.24	0.96	54.0 ± 8.6

3.3.2.1 Effect of CCALNN concentration on the size of hollow nanoparticles

When the concentration of PEG-SH was fixed at 0.24 mM and the concentration of CCALNN was varied (Table 3.3), the particle size increased with increasing peptide concentration. At CCALNN concentrations of 0.06 mM, a mixture of small solid nanoparticles and hollow nanoparticles with an average outer diameter of 7.3 ± 1.5 nm was obtained (Figure 3.4a). In this case, the number of di-thiols is presumably too low and, as a

result, only part of the population of small nanoparticles in the solution can be bridged to produce hollow nanoparticles.

It was observed that hollow nanoparticles were formed rather homogenously when the concentration of CCALNN was between 0.12 to 0.24 mM and the average outer diameter of the hollow nanoparticles increased from 9.8 ± 1.3 nm to 14.9 ± 3 nm (Figures 3.2a and 3.4b), respectively. When the concentration of peptide was increased further, particle size also increased, however the nanoparticles were unstable. At CCALNN concentration of 0.6 and 0.96 mM, hollow porous-like nanoparticles with corresponding average perimeter size of 30.5 ± 8.5 nm and 40 ± 7.9 nm were obtained (Figure 3.4c, d).

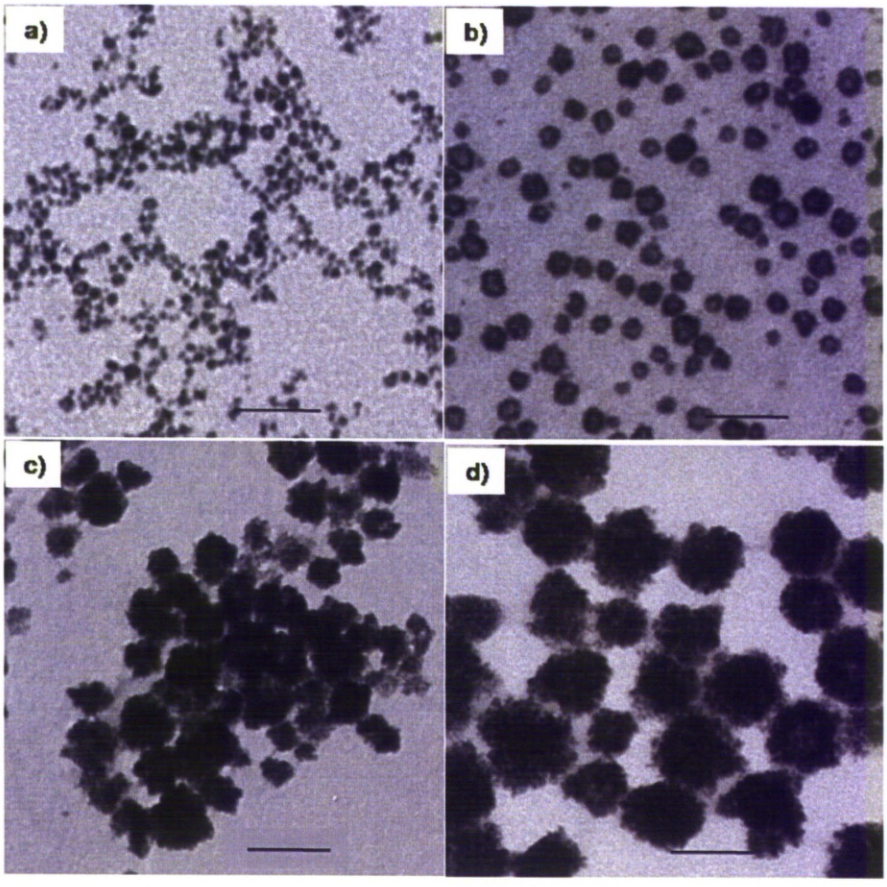

Figure 3.4: TEM images of the CoPt hollow nanoparticles synthesised in the presence of a mixture of 0.24 mM PEG-SH (5,000 g mol^{-1}) and CCALNN peptide of: a) 0.06 mM, b) 0.24 mM, c); 0.60 mM and d) 0.96 mM. Scale bar: 50 nm.

3.3.2.2 Effect of PEG-SH concentration on nanoparticle size

The effect of the concentration of PEG-SH (5,000 g mol^{-1}) on the size of the CoPt hollow nanoparticles was also investigated. Here, the concentration of CCALNN was fixed at 0.12 mM and that of PEG-SH was varied. It was found that the outer diameter of the hollow nanoparticles increased as the concentration of PEG-SH increased. This latter parameter can tune the size of the nanoparticles from 8.3 to 18.5 nm when it is varied between 0.12 nm to 0.6 mM (see Table 3.3 for more details).

When both PEG-SH (5,000 g mol^{-1}) and CCALNN concentrations were increased, the nanoparticles were larger and polydisperse. Figure 3.5 shows hollow CoPt nanoparticles of 20 - 60 nm synthesised in the presence of 0.48 mM PEG-SH and 0.6 mM CCALNN.

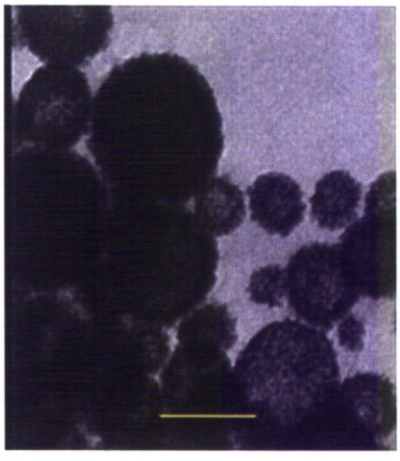

Figure 3.5: TEM image of the CoPt hollow nanoparticles synthesised in the presence of a mixture of 0.48 mM PEG-SH (5,000 g mol^{-1}) and 0.6 mM CCALNN. Scale bar: 50 nm.

In addition to varying the concentration of ligands, the effect of molecular weight (length) of the polymer was also explored. Figure 3.6 shows TEM images of hollow nanoparticles synthesised using 0.24 mM PEG-SH (20,000 g mol^{-1}) in combination with different CCALNN concentrations. The outer diameter of the hollow nanoparticles increased from 14.6 ± 1.9 to 54 ± 8.6 nm when peptide concentration was increased from

0.12 to 0.96 mM. These values are substantially larger than the outer diameter of nanoparticles synthesized using a mixture of PEG-SH (5000 g mol^{-1}) and CCALNN under the same conditions (Table 3.3).

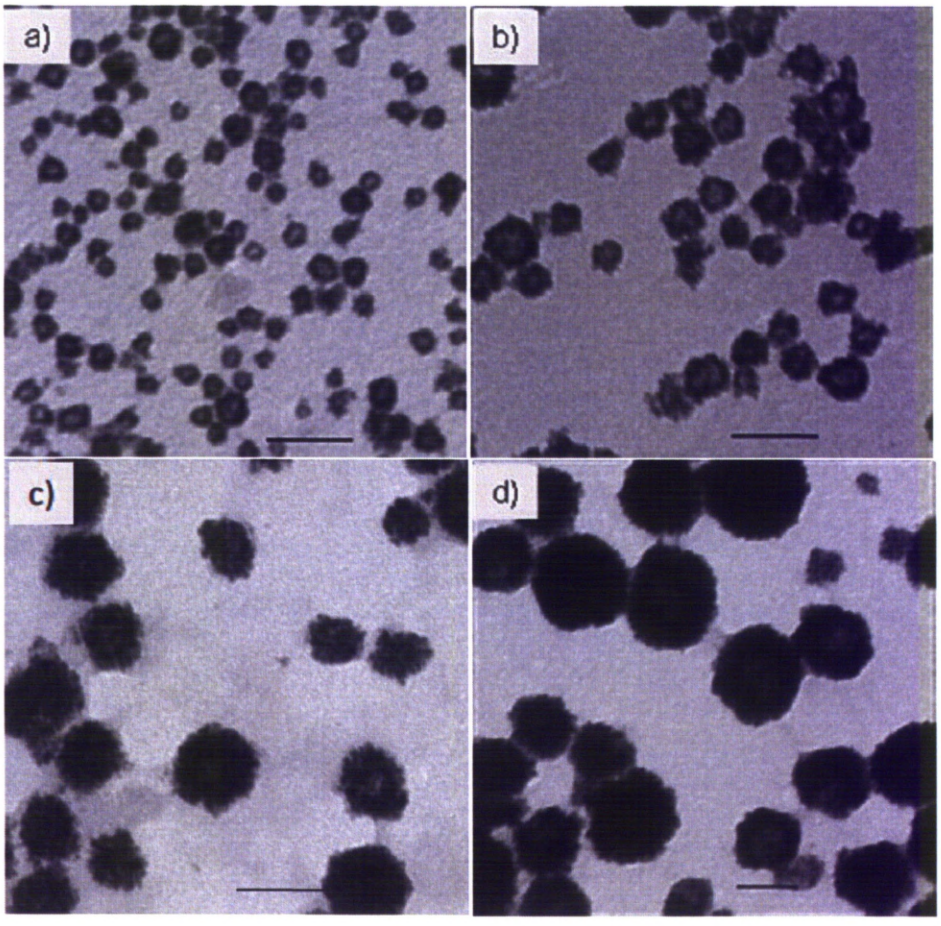

Figure 3.6: TEM images of the CoPt hollow nanoparticles synthesised in the presence of a mixture of 0.24 mM PEG-SH (20,000 g mol^{-1}) and CCALNN peptide of: a) 0.12 mM, b) 0.24 mM, c); 0.60 mM and d) 0.96 mM. Scale bar: 50 nm.

3.3.3 Effect of precursor concentration on the morphology of nanoparticles

The effect of the concentration of Co^{+2} and Pt^{4+} on the morphology of the nanoparticles was also investigated. Here, concentration of PEG-SH (5,000 g mol^{-1}) and CCALNN were fixed at 0.24 mM and 0.12 mM and the concentrations of the precursors varied whilst the

ratio of Co^{2+}/Pt^{4+} was maintained at 0.5 (Table 3.4). It was found that no hollow nanoparticles were obtained at low or high precursor concentrations.

Table 3.4: The effect of precursor concentration on the morphology of CoPt nanoparticles

$CoCl_2$ concentration (mM)	H_2PtCl_6 concentration (mM)	Perimeter size (nm)	Morphology
0.2	0.4	19.3 ± 3.4	porous spheres
1	2	9.8 ± 1.3	hollow
3	6	17.2 ± 3.1	clusters

TEM images show that small nanoparticles were formed and assembled into 19.3 nm ''porous spheres'' at low concentrations of precursors (Figure 4.7a) while 17.2 nm ''clusters'' formed at high concentrations (Figure 4.7b).

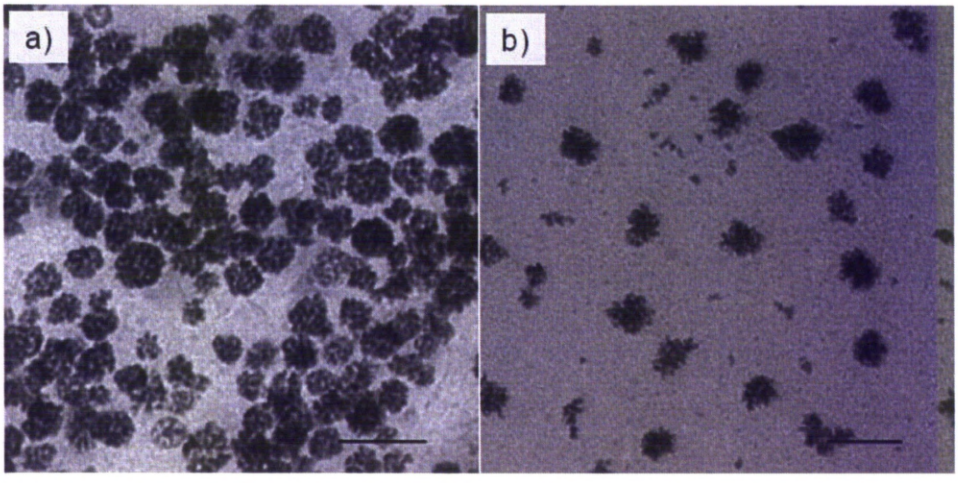

Figure 3.7: TEM images of the CoPt nanoparticles synthesised in the presence of a mixture of 0.24 mM PEG-SH (5,000 g mol^{-1}) and 0.12 mM CCALNN at different concentrations of precursors: a) 0.2 mM $CoCl_2$ and 0.4 mM H_2PtCl_6 and b) 3 mM $CoCl_2$ and 6 mM H_2PtCl_6. Scale bar: 50 nm.

3.3.4 Effect of Co^{2+}/Pt^{4+} precursor ratio on the composition of CoPt nanoparticles

The effect of the ratio of metal salt precursors on the morphology and composition was investigated using a mixture of CCALNN (0.12 mM) and PEG-SH (0.24 mM, M_w = 5,000 g mol^{-1}). It was found that hollow nanoparticles were formed rather homogeneously when

the ratio of Co/Pt salts was 1:2 (Figure 3.2a) and 3:1 (Figure 3.8a). At a higher ratio (9:1) there were no hollow nanoparticles and the sample contained only small nanoparticles (Figure 3.8b). When only Pt salt was used, a large network of small nanoparticle aggregates was formed (Figure 3.8c). Thus, it is also clear that hollow nanoparticles are formed only in the presence of both Co and Pt salts and in a certain range of their concentrations.

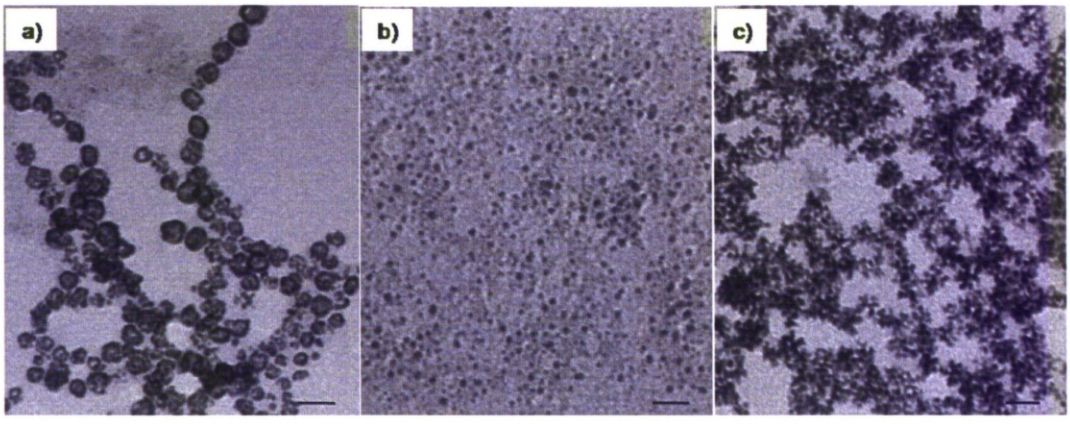

Figure 3.8: TEM images of nanoparticles synthesised in the presence of 0.24 mM PEG-SH (5000 g mol^{-1}) and 0.12 mM CCALNN at different ratios of Co^{2+}/Pt^{4+} : a) 3:1, b) 9:1 and c) only Pt salt. Scale bar: 20 nm.

It was expected that the final composition of the CoPt alloys could be tuned by changing the concentrations of the Co/Pt precursors, since the reductant was added in excess the reduction reaction should have gone to completion very rapidly. The composition of the nanoparticles obtained was determined by using inductively coupled plasma atomic emission spectrometry (ICP-AES). Samples for elemental analysis were thoroughly washed by a combination of centrifugation and magnetic washing. Typically, a specimen of CoPt nanoparticles is purified by centrifugation at 7000 rpm for about 5 min. When agglomeration of nanoparticles starts to appear, a magnetic bar is approached to collect the sample (without centrifugation, it takes several hours to collect the CoPt nanoparticles with the magnetic bar). The supernatant was discarded, and the sediment was

redispersed in water by sonication. The procedure was repeated at least twice to eliminate unreacted reagents or by-products. The experimental measurement of the CoPt alloy composition matched very closely the expected value based on the initial concentrations of the respective metal ions (Table 3.5). This is interesting and demonstrates that the composition of CoPt alloys can be controlled, regardless of the size and shape of the materials obtained. Thus the present method of synthesis retains this property, which has been observed previously in another system of forming FePt alloys, the thermodecomposition of iron pentacarbonyl ($Fe(CO)_5$) and reduction of platinum (II) acetylacetonate ($Pt(acac)_2$).[43] It was also found that no B content was detected in the analysised samples. This suggests that no cobalt borides are present in the synthesised nanoparticles.

Table 3.5: Composition and morphology dependence of CoPt nanoparticles on the precursor ratio

Co salt conc. (mM)	Pt salt conc. (mM)	Starting Co:Pt ratio	Composition of obtained NPs*	Morphology
0	3	0:3	Pt	small NPs, large network
1	2	1:2	$Co_{36}Pt_{64}$	hollow
1.5	1.5	1:1	$Co_{55}Pt_{45}$	hollow
2.25	0.75	3:1	$Co_{78}Pt_{22}$	hollow
2.7	0.3	9:1	$Co_{95}Pt_5$	solid

* As no B was detected in the analysed samples, the composition of synthesised nanoparticles was calculated based on the assumption of 100 % of Co and Pt content in the sample (in fact, S, N, C and O of the coating ligands are present in the samples).

Preliminary experiments were conducted to determine whether the present method of synthesis for hollow nanoparticles using multi-thiol functional ligands could be extended to other materials, namely the isostructural FePt and NiPt systems. With a mixture of CCALNN (0.12 mM) and PEG-SH (0.24 mM, M_w = 5,000 g mol^{-1}), hollow

nanoparticles were also formed with both FePt and NiPt (Figure 3.9). Although the nanoparticles are not as monodisperse and there are also small nanoparticles present in the samples, the results indicate that this simple approach may be more generally applicable.

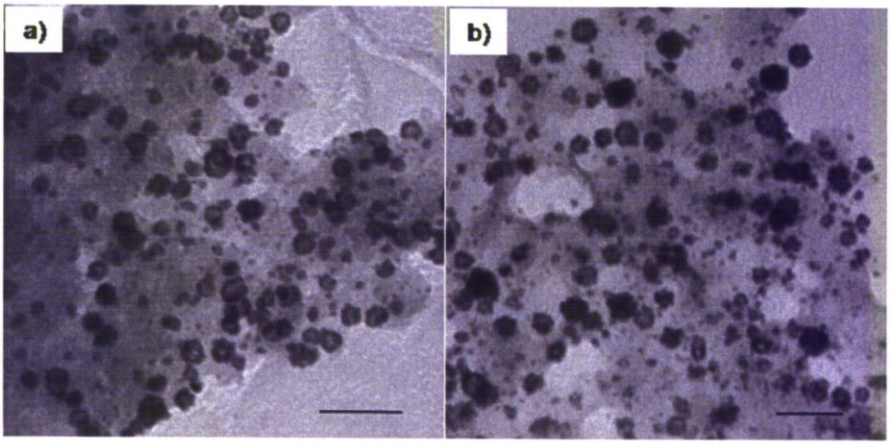

Figure 3.9: TEM images of: a) FePt and b) NiPt hollow nanoparticles synthesised in the presence of 0.24 mM PEG-SH (5000 g mol^{-1}) and 0.12 mM CCALNN. Scale bar: 20 nm.

3.3.5 Proposed mechanism of formation of hollow nanoparticles

Hollow nanoparticles were formed only with the polymer PMAA-PTMP or peptides that contained multiple thiols. This suggests that the presence of multiple thiols in these ligands plays a very important role in the formation of hollow structures. The thiol functional group is well known to bind strongly to noble metals like Au or Pt.[35] In the present synthesis, it was found that the hollow nanoparticles consist of small nanoparticles. Since each small nanoparticle was coated by the ligand, the multiple thiol functional groups may act as a "glue" in the process of forming the hollow structures. The long ligand (e.g. PMAA or PEG), on the other hand, may have two distinct roles. Firstly, it can act as a soft template to assist the formation of the hollow nanoparticles. Secondly, by coating on the nanoparticles it can also give steric and/or electrostatic repulsion sufficiently strong to protect the hollow nanoparticles from aggregation. This mechanism, involving multiple

thiol functional groups in the formation of the hollow nanoparticles, is presented in Figure 3.10. Accordingly, to realize the formation of the hollow nanoparticles, there should be a sufficient content of Pt with respect to Co. When the Pt content was too low (e.g. 10 % by mole), the number of thiols bound to each individual nanoparticle would be too low to allow the small solid nanoparticles to be held together, and only small nanoparticles were formed (Figure 3.8a). On the other hand, when the Pt content was high (e.g., 100 %), too many thiols would be bound to the surface of the small nanoparticles and the result would be the formation of a large aggregated network of nanoparticles (Figure 3.8b).

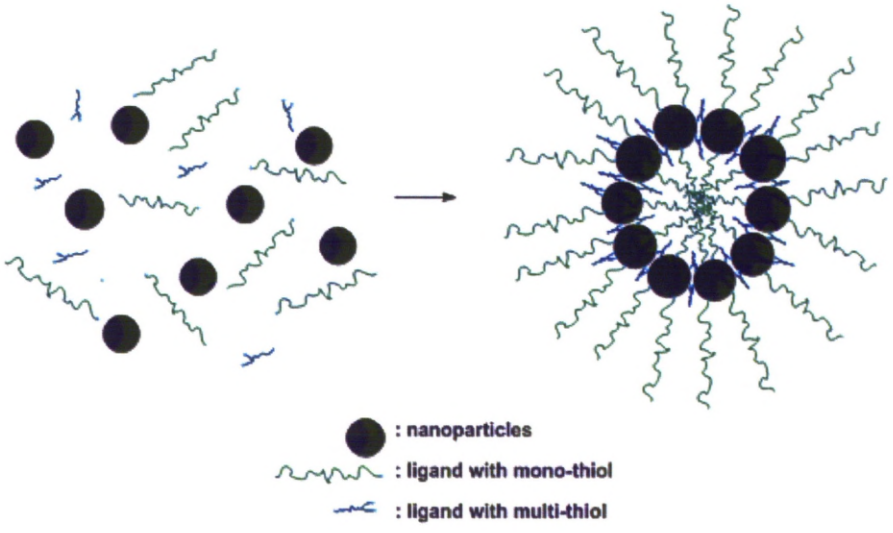

Figure 3.10: Proposed mechanism of formation of hollow nanoparticles.

3.4.6 Magnetic properties of CoPt nanoparticles

The magnetic properties of the CoPt nanoparticles were determined by measurements in a SQUID magnetometer. The zero-field-cooled (ZFC) and the field-cooled (FC) magnetisation of the CoPt nanoparticles with different morphologies were measured (Figure 3.11). All samples have a peak in the ZFC curve, which is due to the transition of the nanoparticles from the superparamagnetic to the ferromagnetic blocked state with

decreasing temperature. The blocking temperature, T_B, as determined from the peak in the ZFC curves is relatively low with values of 11, 22 and 33 K for nanochains, solid nanoparticles and nanowires (Figure 3.11a, c and d), respectively.

Figure 3.11b shows a peak at 14 K followed by a small shoulder at around 50 K in the ZFC, which indicates that the sample contains small nanoparticles and is inhomogeneous. This is supported by TEM, which confirms that the sample consists of mainly small nanoparticles and 7.3 ± 1.5 nm hollow nanoparticles (Figure 3.4a).

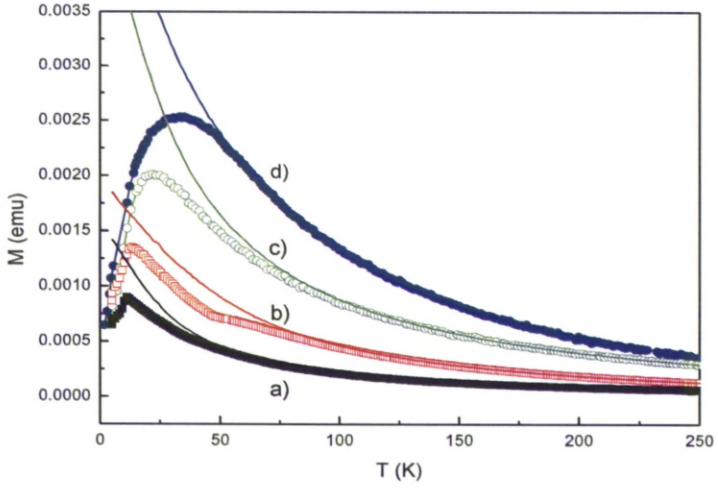

Figure 3.11: The zero-field-cooled (ZFC), field-cooled (FC) magnetisation of CoPt nanoparticles with different morphologies: a) nanochains (0.24 mM PEG-SH), b) hollow nanoparticles (0.24 mM PEG-SH + 0.06 mM CCALNN) c) solid nanoparticles (0.12 mM PEG-SH and 0.24 mM PMAA-DDT) and d) nanowires (0.24 mM PEG-SH and 0.12 mM TLVVN).

The magnetic properties of CoPt hollow nanoparticles of different sizes were also investigated. All samples exhibited a peak in the ZFC curve (Figure 3.12). The blocking temperature, T_B, increased from 14 K to 175 K, as the size of the hollow nanoparticles increased from 7.3 to 40 nm. For two samples synthesised with CCALNN concentrations of 0.12 mM and 0.24 mM, the splitting between the ZFC and FC curves occurs at temperatures quite close to T_B, suggesting that the hollow nanoparticles are of good

homogeneity and monodispersity, consistent with the corresponding TEM images (Figures 3.2a and 3.4b).

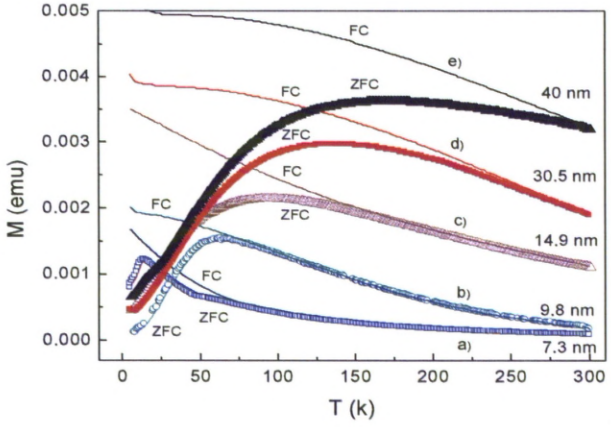

Figure 3.12: The zero-field-cooled (ZFC), field-cooled (FC) magnetisation of CoPt hollow nanoparticles synthesised in the presence of 0.24 mM PEG-SH and different CCALNN concentrations: a) 0.06 mM, b) 0.12 mM, c) 0.24 mM, d) 0.6 mM and e) 0.96 mM.

3.3.7 Stability of the CoPt nanoparticles in aqueous solution

To assess the potential usefulness of the CoPt nanoparticles for biomedical applications, their stability under simple, standard conditions was measured. The CoPt hollow nanoparticles synthesised in the presence of a mixture of 0.24 mM PEG-SH (5,000 g mol^{-1}) and 0.12 mM CCALNN were observed to be colloidally stable in aqueous solution for at least five months after synthesis. Even after removal of excess free ligands by three centrifugations (12,000 rpm, 10 min), the CoPt hollow nanoparticles were still very well dispersed and stable in solution (pure water), whereas with Co nanoparticles synthesised in water using PMAA-DDT (Section 2.2.2), this step would cause them to aggregate.

At different electrolyte (NaCl) concentrations and pH values, the hydrodynamic size of the hollow nanoparticles, i.e., the core plus the coating shell, was measured by dynamic light scattering (Figure 3.13a). As the concentration of NaCl was increased up to 2 M, the hydrodynamic size remained almost unchanged at 20 nm, supporting the observation that

the hollow nanoparticles did not aggregate and were well dispersed and stable. Similarly, when the pH increases from 1 to 8.5, the hydrodynamic size also remained constant at 20 nm. However, above 8.5 the hydrodynamic radius increased to 25 nm at pH of 11.5 and 38 nm at pH of 12.5 (Figure 3.13b).

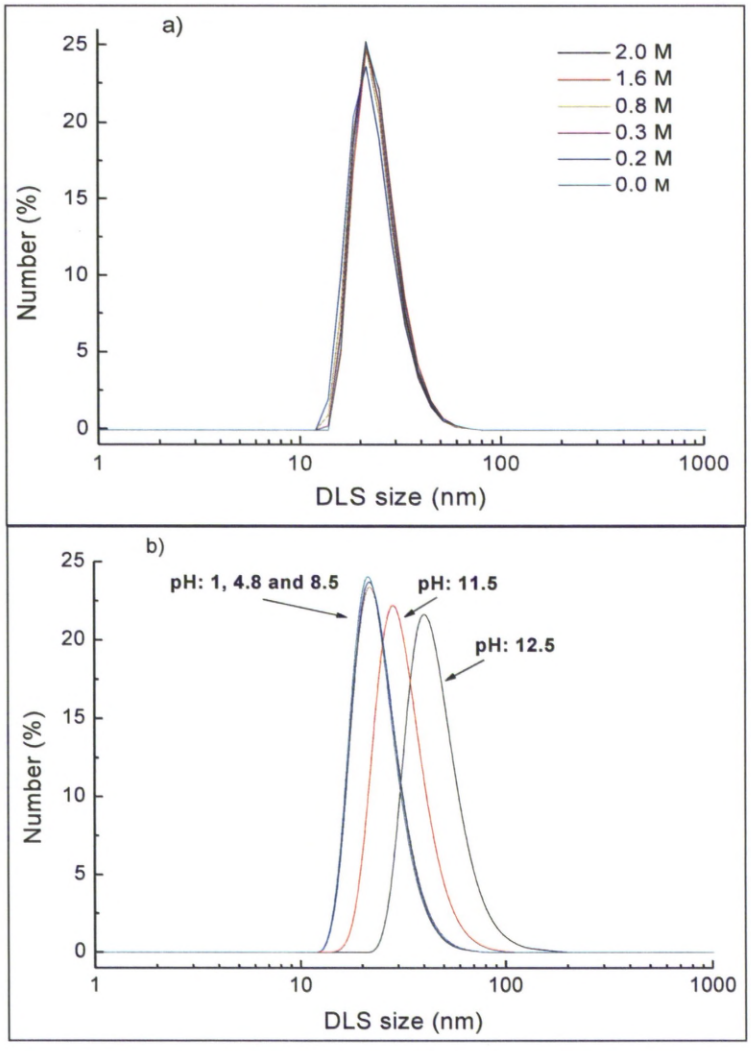

Figure 3.13: DLS size distribution of CoPt hollow nanoparticles at: a) different NaCl concentrations of 0, 0.2, 0.3, 0.8, 1.6 and 2 M; and b) different pH: 1, 4.8, 8.5, 11.5 and 12.5.

At pH > 11.5, all terminal carboxylic groups of the peptides are negatively charged, which would cause repulsion of neighbouring molecules. This could destabilise the highly

compacted self assembled monolayer of ligands which is required for the stabilisation of the nanoparticles.[44,45] Since no precipitation was observed in the solution the large increases in the hydrodynamic size may also be that the PEG ligand shell extended in straight conformation rather curling up in a shorter form.

The stability of the sample in cell culture medium Dulbecco's Modified Eagles Medium (DMEM) was also studied. DLS measurements were carried out, but the cell culture medium has very complex composition that obscured the nanoparticle peaks. However, no precipitation or aggregate of the nanoparticles was visually observed, which may suggest that the hollow nanoparticles remained stable and dispersible in the medium.

3.3.8 Other characterisation techniques

In this chapter, the morphology, magnetic property and colloidal stability of synthesised nanoparticles have been characterised using TEM, SQUID and DLS techniques. However, it is necessary to elucidate the interactions of polymer and peptide ligands and CoPt nanoparticles. Co and Pt have different affinity to SH, NH_2 and COOH functional groups. Thiol is known to have high affinity to Pt. There was no doubt that peptide or/and polymer molecules attach on particles via Pt-thiol bonding. The attachment of these ligands to the particle surfaces can also be achieved possibly through Pt-amine linkage due to the relatively high affinity of amine to Pt.[46] The interactions of SH, NH_2 or COOH functional groups with Co need to be studied because of the differences in affinity of these functional group to Co. According to the acid-base concept and their classification in hard and soft acids and bases (HSAB) proposed by Pearson[47,48] discussed in Section 1.4.2, Co metal is considered as relatively soft acid and it prefers to bind to SH than to COOH or NH_2. When CoPt nanoparticles are coated with peptide (e.g. CCALNN) and PEG-SH polymer ligands, accompanied with the bindings of thiol and possibly amine to Pt, it is probable that these ligands also anchor to CoPt nanoparticles via thiol-Co linkage. These interactions could be

feasibly identified by spectroscopy methods such as Raman, FTIR or XPS. Free thiol functional groups exhibit vibrational bands at around 2550 cm^{-1} in Raman and FTIR spectra.[49-52] However, this peak will disappear when thiol interacts with the particle surface. This phenomenon has been verified for various nanoparticles, such as Pt, Fe, Cu, Au, Ag or CdS, etc.[49,51-55] It has also been pointed out that the characteristic peak of the stretching mode at around 3300 cm^{-1} of the amine group could be shifted to 3440 cm^{-1} if the amine coordinates to the particle.[46,53] Moreover, the interactions of thiol or amine with the particle surface could be effectively evaluated through the changes in the binding energies of the elements involved, usually based on the features of the S2p for sulfur and N1s for nitrogen.[34,56] Differences in the core-level binding energies of an unmodified metal, for example Pt4f, and the thiol or amine-modified metal are seldom observed.[34,51]

Using different analytical techniques to study the nature of the interactions between the cysteine ligand and Fe_3O_4 nanoparticles, Cohen *et al.* found that cysteine molecules are strongly attached to the particle surface via chemical Fe-S bonding.[52] Raman spectra of pure cysteine sample show a characteristic peak of thiol at 2557 cm^{-1}. This peak is absent in the spectra of cysteine coated Fe_3O_4 nanoparticles. XPS spectra of S2p in thiol group recorded for two samples indicated significant difference in binding energy. Pure cysteine sample shows two peaks at 163 and 164 eV, while for cysteine coated Fe_3O_4, two additional new peaks at 161 and 162 eV, suggesting the formation of Fe-S bondings, were recorded. The authors also observed that the binding energy of C1s for carbon in COOH (≈ 288 eV) and N1s for nitrogen in NH_2 (≈ 400 eV) was unchanged in both samples which indicated that there were no chemical bondings of Fe to COOH or NH_2.[52]

In the current study, if PEG-SH polymer and CCALNN peptide ligands are attached to CoPt nanoparticles. The characteristic peaks related to vibrations of amide I (at ≈ 1630 cm^{-1}) of peptide backbone and the vibrations of C-O-C bonds of the PEG at 1106 and 1349

cm^{-1} in the FTIR spectra[57,58] are also considered as evidence for the presence of these ligands on the nanoparticles surface.

3.3.9 CoPt nanoparticles as contrast agent for tracking neural stem cells

(This work was done in collaboration with Professor Bing Song and Dr Xiaoting Meng)

The hollow CoPt nanoparticles (Section 3.3.2) were used by collaborators to examine their potential as MRI contrast reagents for tracking neural stem cells (NSCs). Loading NSCs with the nanoparticles was carried out by growing the cells in well plates in the Dulbecco's modified eagle medium (DMEM/F-12) containing fibroblast growth factor (FGF-2) and epidermal growth factor (EGF) and in the presence of different concentrations of the nanoparticles. The concentration of the nanoparticles and incubation time were varied to find out the optimised conditions in order to limit the effect of nanoparticles on the cells. No influence was detected on the cell viability and proliferation at concentrations of CoPt nanoparticles up to 16 $\mu g\ mL^{-1}$. To confirm whether nanoparticles entered into the cells, the sample was characterised by TEM. Figure 3.14 shows TEM image of the cell labelled with the nanoparticles. It can be seen that the nanoparticles presented in various compartments of the cells.

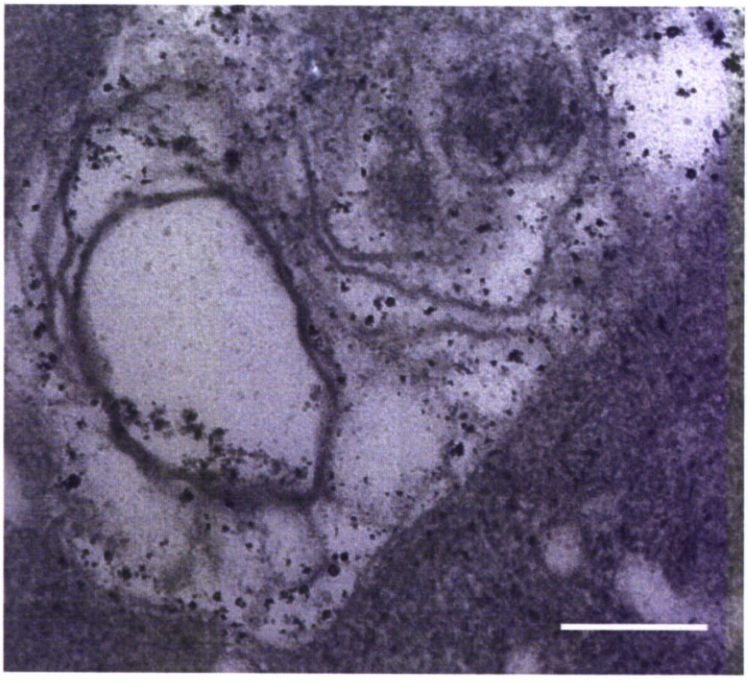

Figure 3.14: TEM image of the CoPt hollow nanoparticles loaded neural stem cells. Scale bar: 200 nm.

To evaluate the potential of CoPt nanoparticles for tracking stem cells, CoPt nanoparticles labelled NSCs were scanned by MRI. Figure 3.15A shows T_2-weighted MRI images of NSCs loaded with the different concentration of the nanoparticles. It can be seen that CoPt nanoparticles reduced efficiently transverse relaxation time, T_2, in labelled NSCs giving greater contrast on MRI images (at the tip of effendorf tubes). Analytical results find that relaxation time T_2 were reduced from 150 ms (unlabelled cells) to 50 ms (8 μg mL^{-1} labelled cells) and 30 ms (16 μg mL^{-1} labelled cells). Figure 3.15B shows MRI images of labelled NSCs at different cell numbers. The result indicates that MRI can efficiently detect low numbers of labelled cells with the enhanced contrast depending on the numbers of labelled cells.

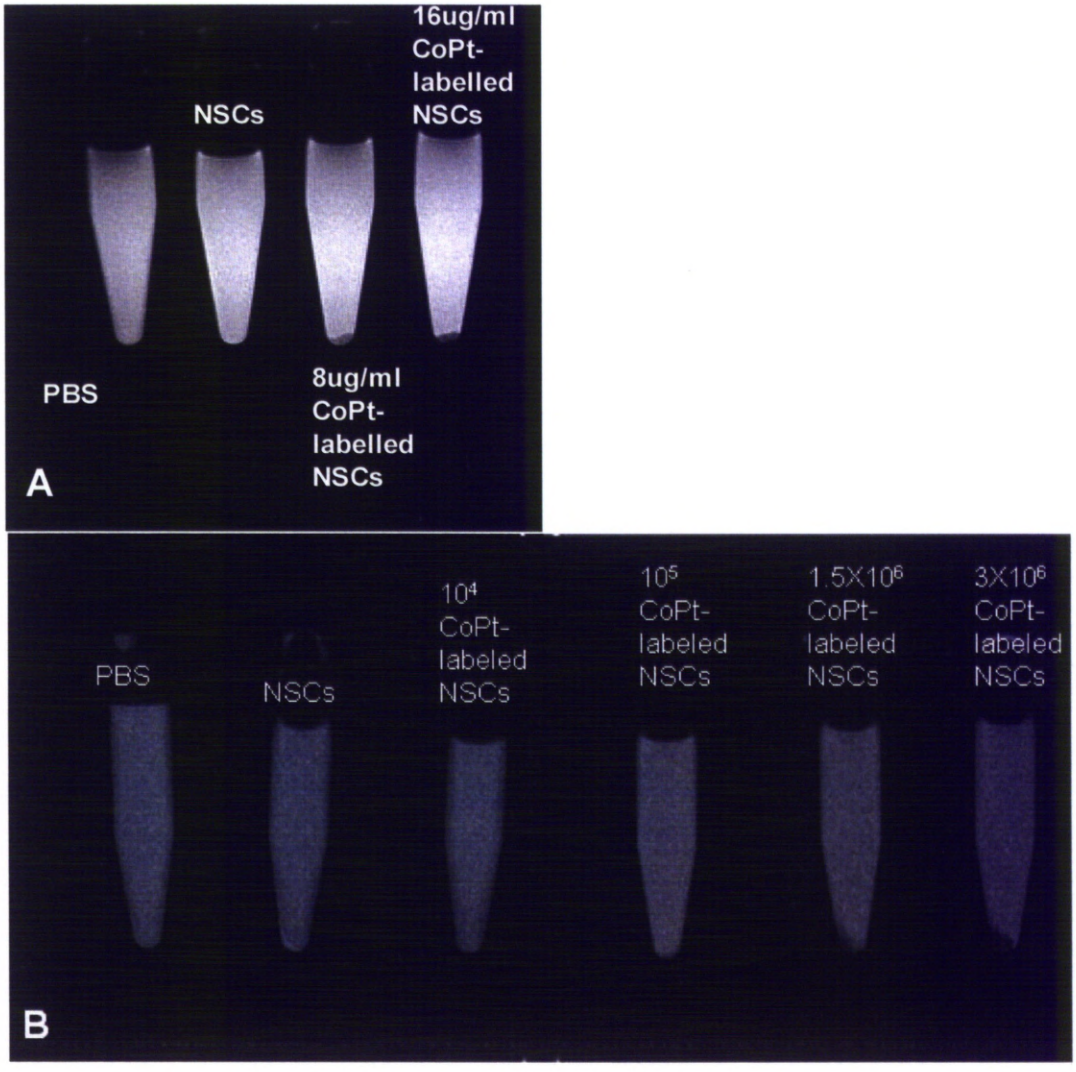

Figure 3.15: A) T_2-weighted MRI images of NSCs labelled with different concentrations of nanoparticles, from left to right the tubes were PBS, nonlabelling NSCs and NSCs labelled at 8 μg mL^{-1} and 16 μg mL^{-1} CoPt nanoparticles, respectively. B) T_2-weighted MRI images of CoPt-labelled NSCs at the different cell numbers, from left to right the tubes were PBS solution, nonlabelled NSCs, 10^4 labelled NSCs, 10^5 labelled NSCs, 1.5 x 10^6 labelled NSCs and 3 x 10^6 labelled NSCs.

3.4 Conclusions

Water-dispersible CoPt nanoparticles with different morphologies were directly synthesised in water by simultaneous reduction of Co^{2+} and Pt^{4+} in the presence of stabilising ligands. The morphology could be changed by varying the structure, end functional group and the combination of stabilising ligands. It was found that multiple thiol groups of the ligands played a crucial role in the formation of hollow nanoparticles. In contrast, the peptide TLVVN led to the formation of nanowires.

The size of PEG-SH and CCALNN coated hollow CoPt nanoparticles could be tuned by varying both the concentration and length of the ligands. SQUID measurements show that the nanoparticles (solids, hollows and nanochains/nanowires) are superparamagnetic at room temperature.

The hollow nanoparticles are stable at different pH values and high salt concentrations. They have been successfully used as MRI contrast enhancers by collaborators for transplanted neural stem cells (NSCs) detection. The experimental data of the effect on cell viability and proliferation of CoPt concentration showed that viability and proliferation of cells were insignificantly affected at concentrations of the nanoparticles up to 16 $\mu g\ mL^{-1}$. At this nanoparticle concentration, the results indicated that T_2 relaxation time in labeled NSCs was substantially reduced and MRI could effectively detect low number of CoPt labeled NSCs with the enhanced image contrast.

Reference

1. Chen, G.; Xia, D. G.; Nie, Z. R.; Wang, Z. Y.; Wang, L.; Zhang, L.; Zhang, J. J. *Chem. Mater.* **2007,** 19, (7), 1840-1844.
2. Kim, S. W.; Kim, M.; Lee, W. Y.; Hyeon, T. *JACS* **2002,** 124, (26), 7642-7643.
3. Li, B. X.; Xie, Y.; Jing, M.; Rong, G. X.; Tang, Y. C.; Zhang, G. Z. *Langmuir* **2006,** 22, (22), 9380-9385.
4. Li, Y. G.; Zhou, P.; Dai, Z. H.; Hu, Z. X.; Sun, P. P.; Bao, J. C. *New J. Chem.* **2006,** 30, (6), 832-837.
5. Chen, J. Y.; Wang, D. L.; Xi, J. F.; Au, L.; Siekkinen, A.; Warsen, A.; Li, Z. Y.; Zhang, H.; Xia, Y. N.; Li, X. D. *Nano Lett.* **2007,** 7, (5), 1318-1322.
6. Skrabalak, S. E.; Au, L.; Lu, X. M.; Li, X. D.; Xia, Y. N. *Nanomed.* **2007,** 2, (5), 657-668.
7. Son, S. J.; Bai, X.; Lee, S. *Drug Discov. Today* **2007,** 12, (15-16), 657-663.
8. Chen, J.; Saeki, F.; Wiley, B. J.; Cang, H.; Cobb, M. J.; Li, Z. Y.; Au, L.; Zhang, H.; Kimmey, M. B.; Li, X. D.; Xia, Y. *Nano Lett.* **2005,** 5, (3), 473-477.
9. Bergbreiter, D. E. *Angew. Chemie-Inter. Ed.* **1999,** 38, (19), 2870-2872.
10. An, K.; Hyeon, T. *Nano Today* **2009,** 4, (4), 359-373.
11. Son, S. J.; Bai, X.; Lee, S. B. *Drug Discov. Today* **2007,** 12, (15-16), 650-656.
12. Cai, Y. R.; Pan, H. H.; Xu, X. R.; Hu, Q. H.; Li, L.; Tang, R. K. *Chem. Mater.* **2007,** 19, (13), 3081-3083.
13. Cheng, K.; Peng, S.; Xu, C. J.; Sun, S. H. *JACS* **2009,** 131, (30), 10637-10644.
14. Jeong, U.; Teng, X. W.; Wang, Y.; Yang, H.; Xia, Y. N. *Adv. Mater.* **2007,** 19, (1), 33-60.
15. Deng, Z. W.; Chen, M.; Gu, G. X.; Wu, L. M. *J. Phys. Chem. B* **2008,** 112, (1), 16-22.
16. Vasquez, Y.; Sra, A. K.; Schaak, R. E. *JACS* **2005,** 127, (36), 12504-12505.
17. Liang, H. P.; Wan, L. J.; Bai, C. L.; Jiang, L. *J. Phys. Chem. B* **2005,** 109, (16), 7795-7800.
18. Yin, Y. D.; Rioux, R. M.; Erdonmez, C. K.; Hughes, S.; Somorjai, G. A.; Alivisatos, A. P. *Science* **2004,** 304, (5671), 711-714.
19. Cabot, A.; Puntes, V. F.; Shevchenko, E.; Yin, Y.; Balcells, L.; Marcus, M. A.; Hughes, S. M.; Alivisatos, A. P. *JACS* **2007,** 129, (34), 10358-10360.
20. Wang, Z. X.; Chen, M.; Wu, L. M. *Chem. Mater.* **2008,** 20, (10), 3251-3253.
21. Liu, Q.; Liu, H. J.; Han, M.; Zhu, J. M.; Liang, Y. Y.; Xu, Z.; Song, Y. *Adv. Mater.* **2005,** 17, (16), 1995-1999.

22. Jiang, Z. Y.; Xie, Z. X.; Zhang, X. H.; Lin, S. C.; Xu, T.; Xie, S. Y.; Huang, R. B.; Zheng, L. S. *Adv. Mater.* **2004,** 16, (11), 904-907.
23. Zhang, X. J.; Li, D. *Angew. Chemie-Inter. Ed.* **2006,** 45, (36), 5971-5974.
24. Zhang, D. B.; Qi, L. M.; Ma, J. M.; Cheng, H. M. *Adv. Mater.* **2002,** 14, (20), 1499-1502.
25. Guo, L.; Liang, F.; Wen, X. G.; Yang, S. H.; He, L.; Zheng, W. Z.; Chen, C. P.; Zhong, Q. P. *Adv. Funct. Mater.* **2007,** 17, (3), 425-430.
26. Hou, H. W.; Peng, Q.; Zhang, S. Y.; Guo, Q. X.; Xie, Y. *Europ. J. Inorg. Chem.* **2005,** (13), 2625-2630.
27. Peng, Q.; Dong, Y. J.; Li, Y. D. *Angew. Chemie-Inter. Ed.* **2003,** 42, (26), 3027-3030.
28. Yang, H. G.; Zeng, H. C. *J. Phys. Chem. B* **2004,** 108, (11), 3492-3495.
29. Wang, W. S.; Zhen, L.; Xu, C. Y.; Zhang, B. Y.; Shao, W. Z. *J. Phys. Chem. B* **2006,** 110, (46), 23154-23158.
30. Wang, X.; Yuan, F. L.; Hu, P.; Yu, L. J.; Bai, L. Y. *J. Phys. Chem. C* **2008,** 112, (24), 8773-8778.
31. Liu, B.; Zeng, H. C. *Small* **2005,** 1, (5), 566-571.
32. Cao, A. M.; Hu, J. S.; Liang, H. P.; Wan, L. J. *Angew. Chemie-Inter. Ed.* **2005,** 44, (28), 4391-4395.
33. He, T.; Chen, D. R.; Jiao, X. L.; Xu, Y. Y.; Gu, Y. X. *Langmuir* **2004,** 20, (19), 8404-8408.
34. Fu, X. Y.; Wang, Y.; Wu, N. Z.; Gui, L. L.; Tang, Y. Q. *J. Colloid & Interface Sci.* **2001,** 243, (2), 326-330.
35. Brust, M.; Walker, M.; Bethell, D.; Schiffrin, D. J.; Whyman, R. *J. Chem. Soc.-Chem. Commun.* **1994,** (7), 801-802.
36. Scott, R. W. J.; Wilson, O. M.; Oh, S. K.; Kenik, E. A.; Crooks, R. M. *JACS* **2004,** 126, (47), 15583-15591.
37. Mulvaney, P. *Langmuir* **1996,** 12, (3), 788-800.
38. Sun, S. H.; Murray, C. B.; Weller, D.; Folks, L.; Moser, A. *Science* **2000,** 287, (5460), 1989-1992.
39. Hussain, I.; Graham, S.; Wang, Z. X.; Tan, B.; Sherrington, D. C.; Rannard, S. P.; Cooper, A. I.; Brust, M. *JACS* **2005,** 127, (47), 16398-16399.
40. Wang, Z. X.; Tan, B. E.; Hussain, I.; Schaeffer, N.; Wyatt, M. F.; Brust, M.; Cooper, A. I. *Langmuir* **2007,** 23, (2), 885-895.

41. Vanrheenen, P. R.; Mckelvy, M. J.; Glaunsinger, W. S. *J. Solid State Chem.* **1987,** 67, (1), 151-169.
42. Linderoth, S.; Morup, S. *J. Appl. Phys.* **1990,** 67, (9), 4472-4474.
43. Ung, D.; Tung, L.; Caruntu, G.; Delapotas, D.; Alexandreu, I.; Prior, I.; Thanh, N. Cryst. Eng. Commun. **2009,** 11, 1309-1316.
44. Duchesne, L.; Gentili, D.; Comes-Franchini, M.; Fernig, D. G. *Langmuir* **2008,** 24, (23), 13572-13580.
45. Levy, R.; Thanh, N. T. K.; Doty, R. C.; Hussain, I.; Nichols, R. J.; Schiffrin, D. J.; Brust, M.; Fernig, D. G. *JACS* **2004,** 126, (32), 10076-10084.
46. Tzitzios, V.; Niarchos, D.; Margariti, G.; Fidler, J.; Petridis, D. *Nanotech.* **2005,** 16, (2), 287-291.
47. Pearson, R. G. *JACS* **1963,** 85, (22), 3533-3539.
48. Pearson, R. G. *J. Chem. Edu.* **1968,** 45, (9), 581-587.
49. Aryal, S.; Remant, B. K. C.; Dharmaraj, N.; Bhattarai, N.; Kim, C. H.; Kim, H. Y. *Spectrochim. Acta Part a-Molec. & Biomolec. Spectr.* **2006,** 63, (1), 160-163.
50. Hostetler, M. J.; Stokes, J. J.; Murray, R. W. *Langmuir* **1996,** 12, (15), 3604-3612.
51. Bagaria, H. G.; Ada, E. T.; Shamsuzzoha, M.; Nikles, D. E.; Johnson, D. T. *Langmuir* **2006,** 22, (18), 7732-7737.
52. Cohen, H.; Gedanken, A.; Zhong, Z. Y. *J. Phys. Chem. C* **2008,** 112, (39), 15429-15438.
53. Panigrahi, S.; Kundu, S.; Basu, S.; Praharaj, S.; Jana, S.; Pande, S.; Ghosh, S. K.; Pal, A.; Pal, T. *Nanotech.* **2006,** 17, (21), 5461-5468.
54. Mandal, S.; Gole, A.; Lala, N.; Gonnade, R.; Ganvir, V.; Sastry, M. *Langmuir* **2001,** 17, (20), 6262-6268.
55. Priyam, A.; Chatterjee, A.; Das, S. K.; Saha, A. *Res. Chem. Intermed.* **2005,** 31, (7-8), 691-702.
56. Ma, Z.; Han, H. *Colloids & surface A: Physicochem. Eng. Aspects* **2008,** 317, 229-233.
57. Gupta, A. K.; Wells, S. *IEEE Trans. Nanobiosci.* **2004,** 3, (1), 66-73.
58. De Palma, R.; Peeters, S.; Van Bael, M. J.; Van den Rul, H.; Bonroy, K.; Laureyn, W.; Mullens, J.; Borghs, G.; Maes, G. *Chem. Mater.* **2007,** 19, (7), 1821-1831.

Chapter 4

Synthesis and characterisations of water-dispersible CoFe alloy and CoFe@Pt core/shell nanoparticles

4.1 Introduction

Amongst various magnetic nanoparticles, CoFe materials exhibit ultra-high saturation magnetisation (245 emu g^{-1} for bulk value). This gives CoFe nanoparticles advantages in many proposed biomedical applications (Section 1.3), such as magnetic separation,[1] MRI imaging[2-5] and hyperthermia cancer treatment.[6] However, this material is unstable and is easily oxidised, resulting in decreased response to an external magnetic field. To avoid oxidation, nanoparticles have been coated with an additional inorganic layer. Moreover, a key remaining challenge in the biomedical applications of CoFe nanoparticle is how to make them dispersible and stable in water medium.

Thus far, a lot of effort in the preparation of water-dispersible core/shell structures of Fe_2O_3@Au,[7-9] Fe_3O_4@Au,[10-19] Fe_3O_4@silica,[20-26] $CoFe_2O_4$@Au,[27,28] FePt@silica,[29,30] Co@silica,[31,32] Co@Au,[33,34] Co@Ag[35] and Fe@Au[36] have been reported. In these syntheses, the coatings are usually carried out through reverse micelle methods or seeding techniques. In the reverse micelle methods, magnetic cores and a reductant (for metal coating) or ammonia (for silica coating) are usually loaded into micelles, and the coating is achieved by adding of metal salt(s) or tetraethylorthosilicate (TEOS) precursors to the micelle suspension.[17,20,23,24,26,29,30,37-40] For seeding techniques, pre-formed magnetic nanoparticles are used as seeds for the deposition of a shell layer. To prevent the homogenous nucleation, which results in the formation of separated nanoparticles of the

shell materials, a mild reductant (e.g. hydroxylamine or hexadecanediol) is generally used.[8-11,15,18,19,27]

In the case of CoFe, to date, there have been limited reports on the synthesis of core/shell structures including CoFe@C,[2, 5, 41-44] CoFe@Au[45-47] or CoFe@Ag[46] and only a few reports on the synthesis of the water-dispersible nanoparticles.[2,4,5,42] To coat CoFe nanoparticles with carbon[2] or noble metal shells,[46] the syntheses are mainly based on gas phase or physical techniques. For noble metal coating, nanoparticles, which are formed in gas phase, are flowed through a shell formation chamber. The coating is achieved by sputtering or evaporating the shell material during their flight.[46] The shell thickness is controlled via varying flying velocity of nanoparticles. In the case of carbon coating, acetylene or methane is usually used as carbon source for the shell material and the coating is performed by introducing these gases into the reaction chamber at high temperature during the formation of particles.[2,41,43] Core/shell structures prepared by these methods are generally polydisperse and an extra step is needed to reduce their size distribution.[2,42]

Amongst the inorganic shells, Au coating of magnetic nanoparticles is especially interesting, as Au is inert, at least in terms of oxidation under ambient conditions, it is biocompatible and has a very well understood surface chemistry. However, in some cases it was found that the direct coating of magnetic nanoparticles with Au is difficult due to the mismatch of crystal lattices of two surfaces.[36,48]

In this chapter, the syntheses of monodisperse and high saturation magnetisation CoFe alloy and novel CoFe@Pt core/shell nanoparticles in 1,2-dichlorobenzene (DCB) solvent are described. The hydrophobic CoFe and CoFe@Pt core/shell nanoparticles were transferred into water by exchange of OA/OLA molecules on the surface of the nanoparticles with alkoxysilane or combination of silane and poly (ethylene glycol) (PEG). The morphology, structure and magnetic properties of the prepared nanoparticles were characterised by TEM, HRTEM, STEM, XRD and SQUID. Some other experimental

techniques, such as EDS, EELS, FTIR or NMR spectroscopy, which have been widely used in the literatures for the investigation of core/shell nanoparticles as well as the interactions between stabilising ligands and the particle surface, are also discussed.

4.2 Experimental

4.2.1 Materials

The specialised reagents listed below were all purchased from Sigma-Aldrich Ltd, UK. The precursors: cobalt carbonyl ($Co_2(CO)_8$) 99.9 %, iron pentacarbonyl ($Fe(CO)_5$) 99.5 %, platinum (II) acetylacetonate ($Pt(acac)_2$) 99.9 %. The solvents: 1,2-dichlorobenzene (DCB) anhydrous 99 %, octyl ether 99 %, chloroform, toluene, hexane, acetonate and absolute ethanol. The surfactants, ligands and other reagents including: oleic acid (OA) 99 %, oleylamine (OLA) 70 %, N-[3-(trimethoxysilyl)-propyl]ethylenediamine (silane-NH_2) 97 %, poly (ethylene glycol) (PEG) with different functional group (SH, NH_2 and COOH) and tetramethylammonium hydroxide (TMAOH). All the reagents were used without further purification.

4.2.2 Synthesis of CoFe nanoparticles

Syntheses were carried out under nitrogen atmosphere in a Schlenk line. In detail, the precursors, 0.25 g (0.75 mmol) $Co_2(CO)_8$ and 0.2 mL (1.50 mmol) $Fe(CO)_5$, were dissolved in 2.5 mL DCB. In a two necked round bottom flask, in the presence of 0.62 mmol OA and 0.62 mmol OLA surfactants, 17.5 mL DCB solvent was added. The reaction mixture was degassed at room temperature for 40 min and then heated to 172 ^{o}C. At this temperature, 2.5 mL DCB containing precursors was injected into the solution and the reaction was continued for 60 min. Samples were removed after 5 min, 30 min and 45 min 60 min to see the evolution of nanoparticle morphology.

4.2.3 Synthesis of CoFe@Pt core/shell nanoparticles

To 5 mL of as-synthesised CoFe sample (Section 4.2.2*)* and at 170 °C, three mL of degassed DCB solution containing 100 mg $Pt(acac)_2$ (0.25 mmol) and 1 mmol OLA was added drop-wised over 5 min. The mixture was maintained at this temperature for 60 min before cooling down to room temperature. During this time, 3 mL of the sample was also removed to prepare for TEM and SQUID characterizations.

4.2.4 Transferring CoFe alloy and CoFe@Pt core/shell nanoparticles into water

4.2.4.1 Ligand exchange of OA/OLA coated CoFe nanoparticles using alkoxysilanes

As-synthesised CoFe alloy nanoparticles were purified from free excess surfactants before ligand exchange. In a typical purification process 0.5 mL of the nanoparticle solution was mixed with 1 mL of toluene and 2 mL of acetone. The mixture was sonicated for 1-2 min and the nanoparticles were collected using a magnetic bar. After discarding the supernatant, the nanoparticles were dissolved in 1 mL of toluene and further precipitated by adding 2 mL of ethanol. The precipitation-redispersion procedure was repeated two more times, and the nanoparticles were finally dissolved in 5 mL of toluene prior to ligand exchange. The ligand exchange of hydrophobic CoFe nanoparticles using alkoxysilane was carried out following the literature[49] with some modifications. To the solution of the purified nanoparticles, 1 mL of toluene containing 0.05 mL of N-[3-(trimethoxysilyl)-propyl]ethylenediamine (silane-NH_2) was added under sonication. After 60 min, 1 mL TMAOH (0.01 M) in methanol was added. The sonication was continued for another 60 min and precipitated nanoparticles were washed repeatedly in toluene/ethanol and then were dispersed in 5 mL of water.

4.2.4.2 Ligand exchange of OA/OLA coated CoFe nanoparticles using mixture of PEG polymer and silane

As-synthesised CoFe nanoparticles (0.5 mL in DCB, 2.5 mg) was purified as above and was dispersed in 5 mL of chloroform. To this, 1 mL of chloroform containing 0.05 mL of silane-NH_2 and 50 mg of PEG-NH_2 (M_w = 20,000 g mol^{-1}) was added under sonication. After 60 min, 1 mL TMAOH (0.01 M) in methanol was added. The sonication was continued for another 60 min and precipitated nanoparticles were washed repeatedly in chloroform/ethanol to remove free excess ligands and were then dispersed in 5 mL of water.

4.2.4.3 Ligand exchange of CoFe@Pt core/shell nanoparticles using PEG polymer

As-synthesis CoFe@Pt core/shell nanoparticles (1 mL in DCB) were purified as above and dispersed in 1 mL of chloroform. Two mL of chloroform containing 60 mg of PEG-NH_2 (M_w = 5,000 g mol^{-1}) was added under sonication. After 30 min, nanoparticles were washed repeatedly in chloroform/ethanol to remove free excess ligands and were then dispersed in 5 mL of water. PEG polymer with other functional groups (SH, COOH) was also used to evaluate the effectiveness of different functional groups in the ligand exchange process.

4.3 Results and discussion

4.3.1 CoFe nanoparticles

CoFe alloy nanoparticles were synthesised by simultaneously thermal decomposition of cobalt and iron carbonyls in the presence of OA and OLA as stabilising agents. Thermal decomposition process of cobalt and iron carbonyls can occur via several steps and

generate some intermediate products such as $Co_4(CO)_{12}$ and $Co_6(CO)_{16}$.[50,51] However, the overall decomposition reaction is described as follow:

$$Co_2(CO)_8 + 2Fe(CO)_5 \rightarrow 2CoFe + 18CO\uparrow \qquad (4.1)$$

Figure 4.1 shows TEM images and their corresponding size distribution histograms of CoFe nanoparticles synthesised by decomposition of $Co_2(CO)_8$ and $Fe(CO)_5$ mixture in the presence of OA/OLA (OA : OLA = 1: 1) at different reaction times. It can be seen that spherical and monodisperse nanoparticles were produced and their size increased slightly from 7.2 ± 0.7 nm to 8.9 ± 0.7 nm as reaction time increased from 5 min to 60 min.

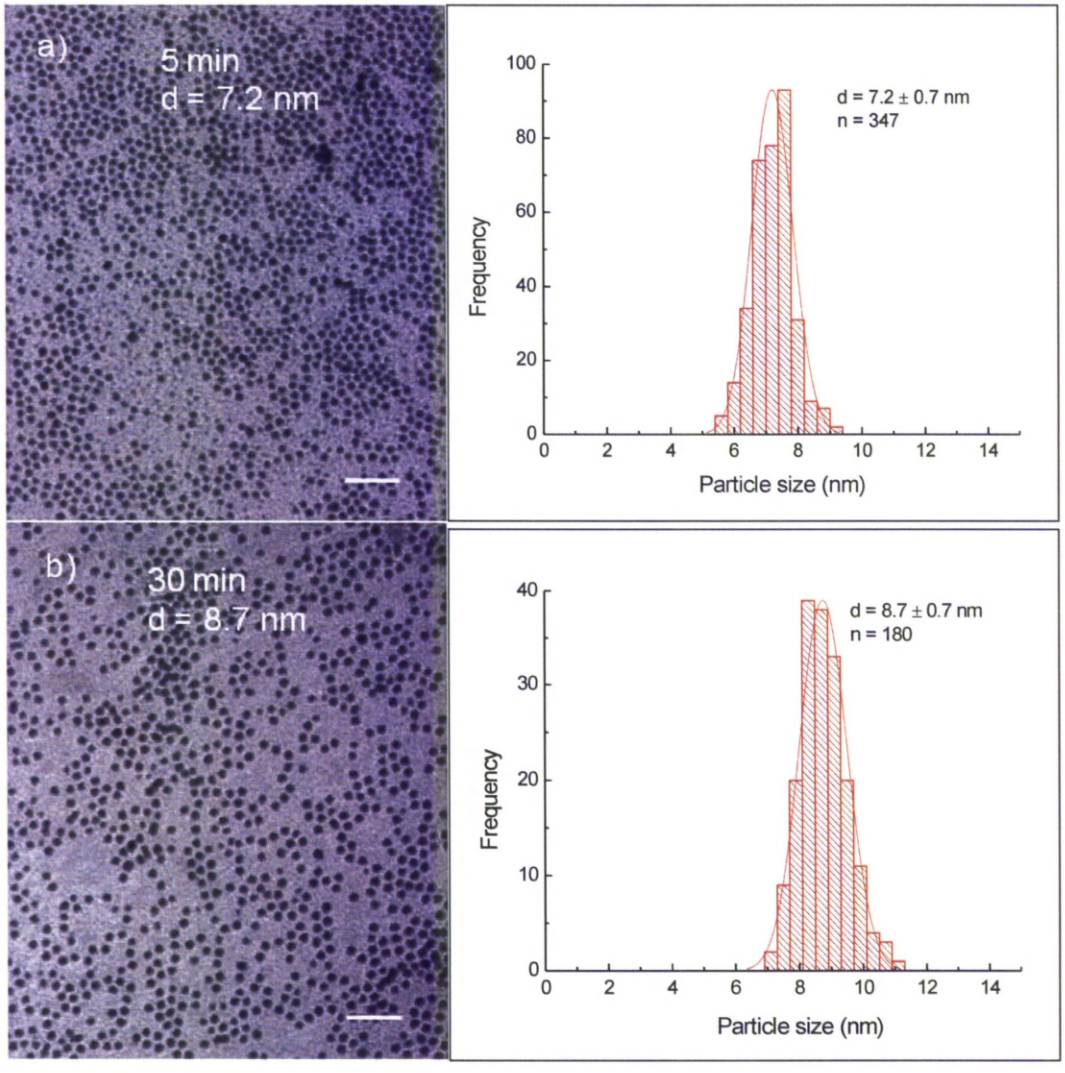

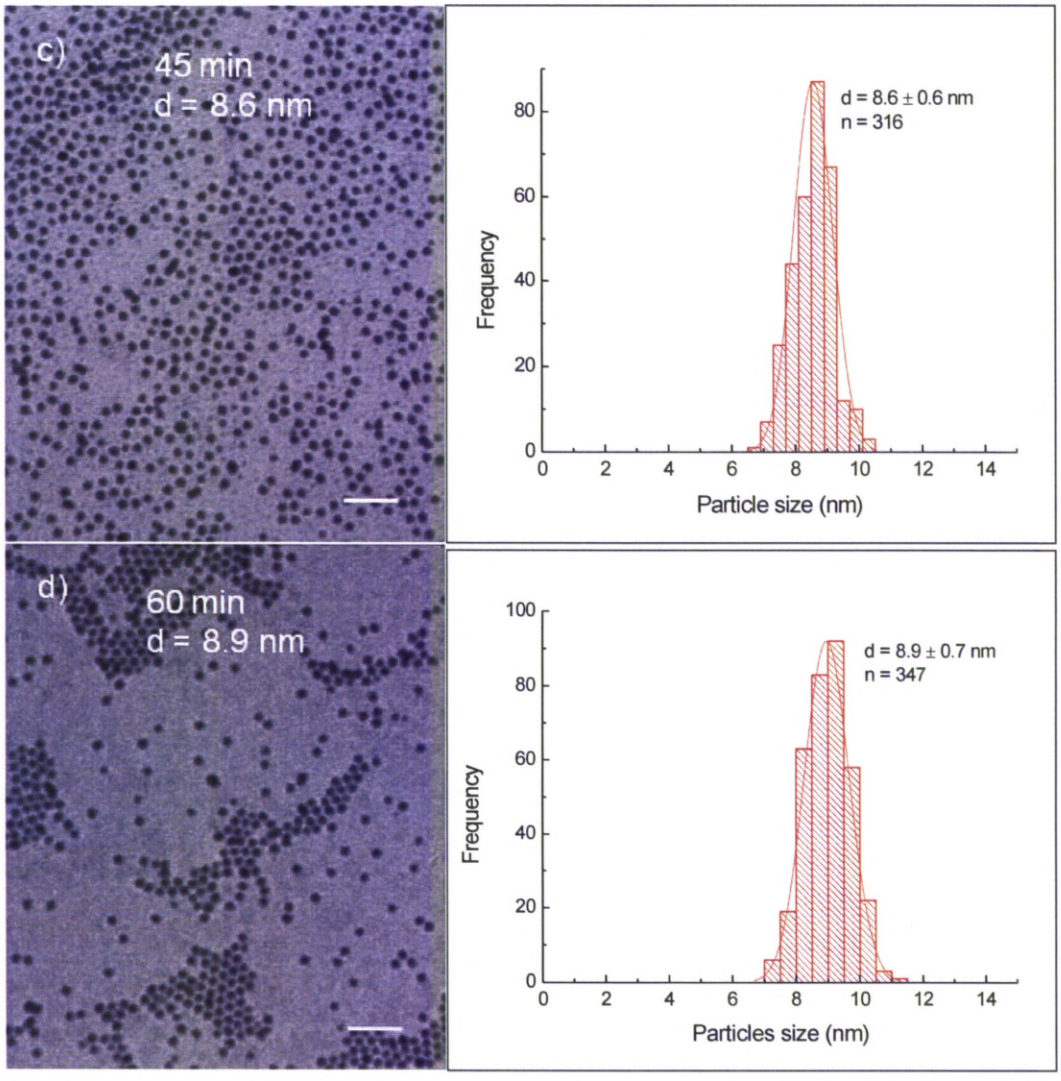

Figure 4.1: TEM images and their corresponding size distribution histograms of CoFe alloy nanoparticles synthesised at different reaction times: a) 5 min, b) 30min, c) 45 nm and d) 60 min. Scale bar: 50 nm.

4.3.2 Platinum coated CoFe nanoparticles

Pt coating was formed by reduction of Pt^{2+} ions onto the surfaces of CoFe nanoparticles in the presence of capping agents and in organic solvents. The coating was carried out in the presence of a mixture of OA and OLA with OLA used as a reductant.

Figure 4.2 shows TEM images of the Pt coated CoFe nanoparticles synthesised after 45 min and 60 min of reaction. It can be seen that the size of nanoparticles was almost unchanged after the coating (Figures 4.1 and 4.2).

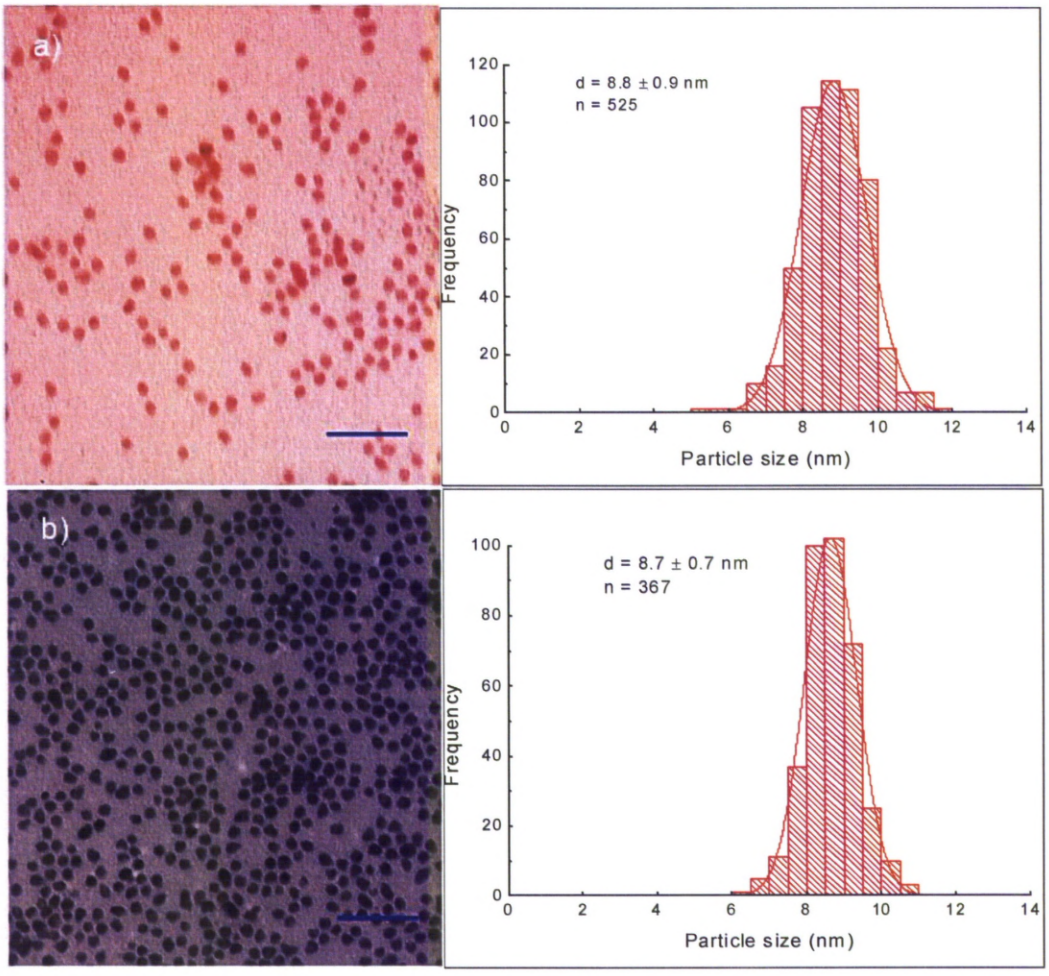

Figure 4.2: TEM images and their corresponding size distribution histograms of CoFe@Pt nanoparticles synthesised at different reaction time: a) 45 min and b) 60 min. Scale bar: 50 nm.

To investigate the core/shell structures, the sample was characterised using HRTEM. The HRTEM images of CoFe@Pt nanoparticles synthesised after 60 min reaction shows clearly core/shell structures with a bright and about 2 nm thick shell around a dark core, 4.5 nm (Figure 4.3a, b). This feature is opposite to what is expected (i.e. a dark shell

surrounded a bright core) and is possible because of the mass contrast dominated over diffraction contrast resulting the shell lighter even though Pt has a higher electron density than CoFe. Analogous results have recently been observed for Co@Ag,[35,52] Ni@Au[53] and Fe@Au[54] core/shell nanoparticles by several authors. In the current study, it is possible to eliminate the formation of Pt@CoFe core/shell structures with CoFe shell coating over Pt core as Pt was reduced after CoFe cores formed.

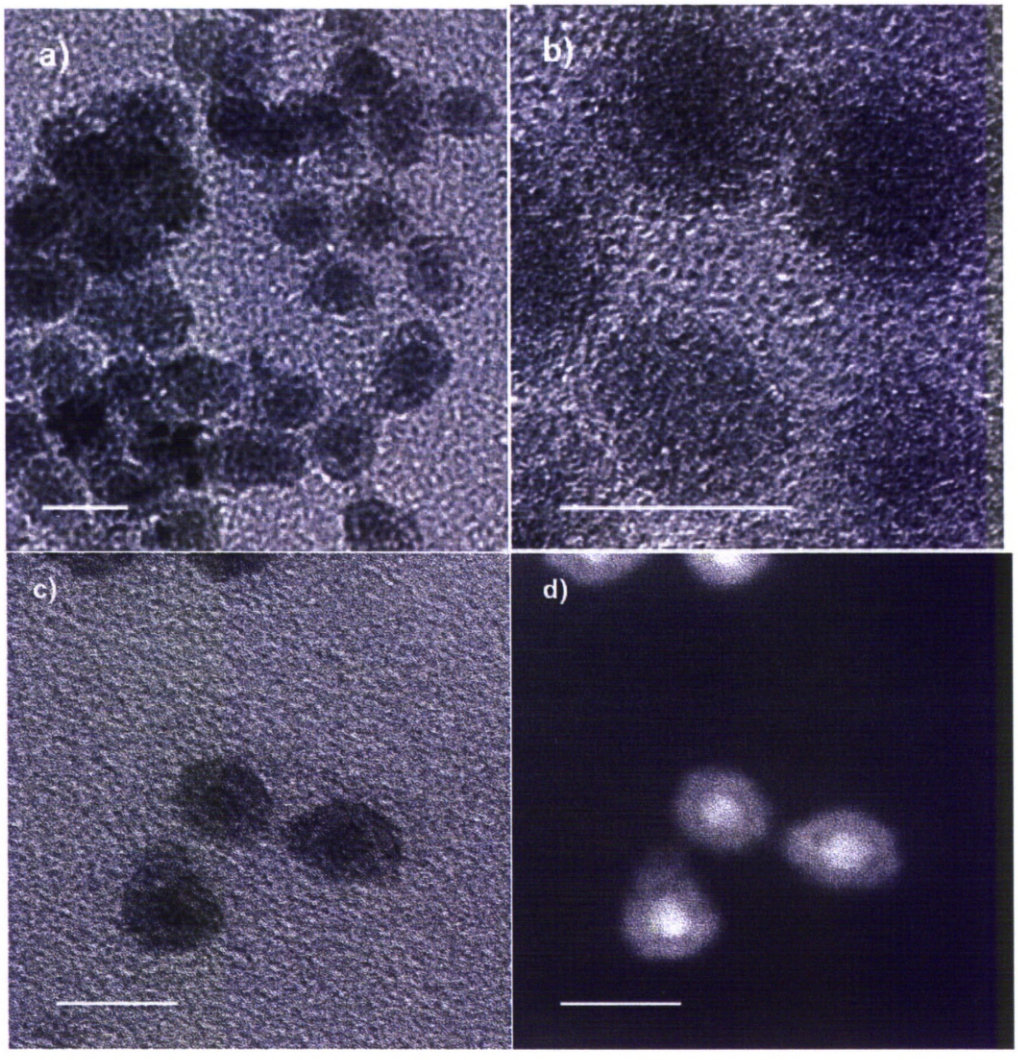

Figure 4.3 : Different magnification HRTEM images (a,b) and STEM images in bright field c) and dark field d) of Pt coated CoFe nanoparticles synthesised after 60 min reaction. Scale bar: 10 nm.

To confirm the core/shell structures, the sample was further characterised by utilising STEM and Z contrast images were presented in Figure 4.3c, d. The images show clearly the core/shell structures. From the dark field image (Figure 4.3d), it should be noted a dark area existing between bright core and grey shell, which indicates the existence of a gap between the CoFe core and the Pt shell. In the current study, OLA was used as a reductant to reduced Pt^{2+} to Pt metal with the expectation that the size of magnetic cores would be preserved. It was known that Fe and Co metal can reduce Au^{3+} and Pt^{2+} to Au and Pt metals through a process known as redox-transmetalation/galvanic replacement (a metal with more negative redox potential can reduce ions of more positive redox-potential metal into metal state). The reduction potential for Pt^{2+} is +1.2 V, whereas for Co^{2+} and Fe^{2+} are -0.28 and -0.44 V, respectively. Therefore, the decrease of magnetic cores and formation of the gap between the core and Pt shell suggests that redox-transmetalation/galvanic replacement reactions were mainly involved in the reduction of Pt^{2+} to Pt metal in the coating process. The possible replacement reactions can be expressed as follow:

$$Pt(acac)_2 + Fe \rightarrow Pt + Fe(acac)_2 \qquad (4.2)$$

$$Pt(acac)_2 + Co \rightarrow Pt + Co(acac)_2 \qquad (4.3)$$

The phase structure of the CoFe@Pt core/shell nanoparticles was determined by using XRD (Figure 4.4). A strong and broad peak was observed at 2 theta $\approx$ 39 degrees, suggesting that the Pt shell of the sample is amorphous. This is consistent with observation from HRTEM image that no clear crystalline was noted on the core/shell structures (Figure 4.3b). There were no peaks of oxides or cobalt ferrite observed.

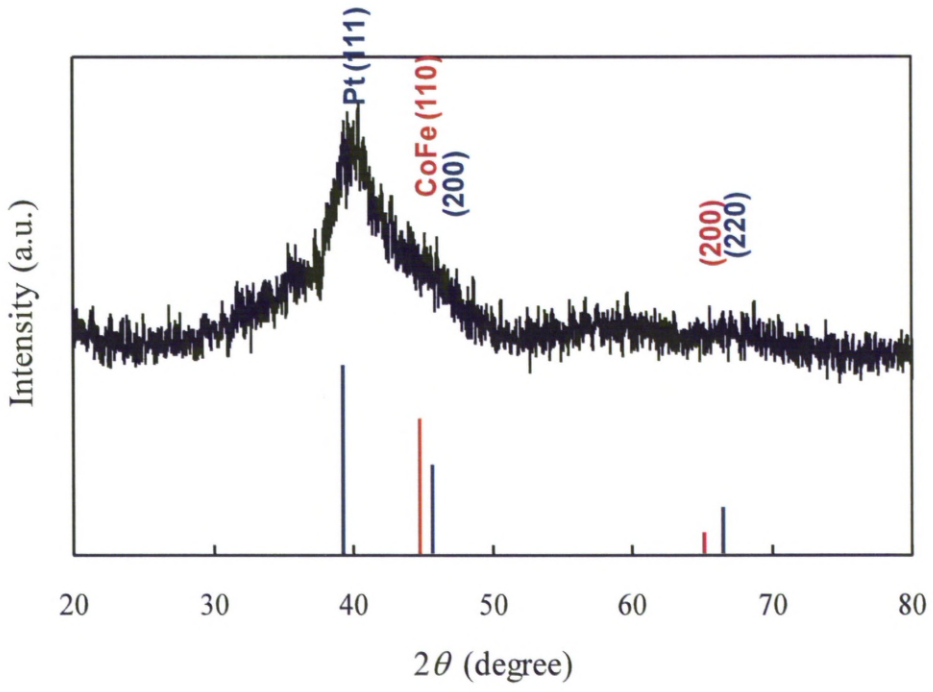

Figure 4.4: XRD pattern of the CoFe@Pt core/shell nanoparticles synthesised after 60 min reaction.

4.3.3 Magnetic properties of nanoparticles

The magnetic properties including blocking temperature (T_b) and coercivity (H_c) of CoFe@Pt core/shell nanoparticles were investigated and compared with the magnetic properties of uncoated CoFe nanoparticles. The ZFC and FC magnetisation curves as a function of temperature of the CoFe and CoFe@Pt core/shell nanoparticles prepared at different times are shown in Figure 4.5. It can be seen that the blocking temperature, T_b (i.e. the temperature at which the nanoparticles become magnetically blocked) of these nanoparticles decreases significantly from 150 K for uncoated CoFe nanoparticles to 66 K for CoFe@Pt core/shell nanoparticles after 60 min reaction.

The reduction in the blocking temperature has been observed in FePt@Au, FePt@SiO_2 and Fe_3O_4@Au core/shell nanoparticles.[29,55,56] In these works it should be noted that the

size of magnetic cores is unchanged after the coating, the small shift of T_b (5 K for Fe_3O_4@Au, 12 K for FePt@Au and 55 K for FePt@SiO_2) observed was believed to be the result of the reduction of the magnetic dipole-dipole interaction due to the increased interparticle spacing of the magnetic cores.[57,58] In the current study, the large shift of T_b, 84 K, is more likely to relate to the decrease in the size of the magnetic core, which was shown in HRTEM and STEM images (Figures 4.3), as the blocking temperature is proportional to volume or 3rd power of dimension of magnetic cores.

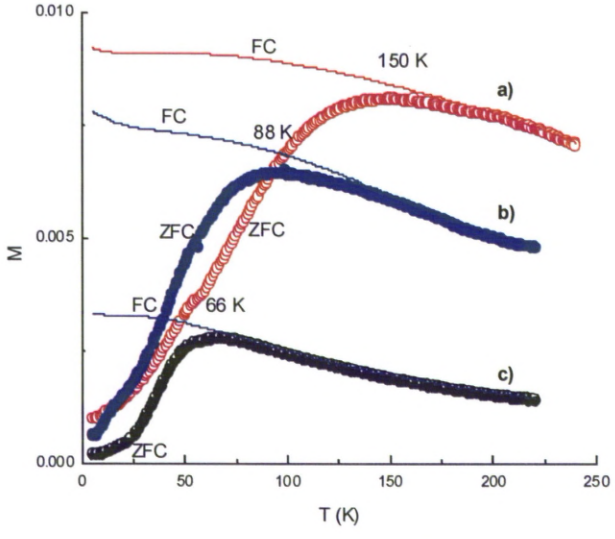

Figure 4.5: ZFC-FC curves of uncoated CoFe nanoparticles (a) and Pt coated CoFe nanoparticles after 45 min (b) and 60 min (c).

Hysteresis loops of the CoFe and CoFe@Pt core/shell nanoparticles were measured at 5K (Figure 4.6). It can be seen that the nanoparticles are ferromagnetic and their coercivity, H_c, increases from 0.81 kOe for uncoated nanoparticles to 1.41 kOe for CoFe@Pt core/shell nanoparticles synthesised after 45 min of reaction and then decreases slightly to 1.24 kOe by prolonging the reaction time. The enhanced coercivity of core/shell

nanoparticles has previously observed for Co@Ag,[52] Fe_3O_4@Au.[56] This behaviour is generally explained by the enhanced effective anisotropy introduced either by increasing of surface anisotropy after the coating,[59,60] or due to the less-effective coupling of the magnetic dipole moments of the core/shell nanoparticles.[56] In the present study, even though the size of magnetic cores decreases, which may result in the decrease of H_c, the increase in coercivity for CoFe@Pt nanoparticles actually observed suggests that surface anisotropy of CoFe magnetic cores has profound effect on the H_c. The slight decrease in the coercivity with prolonging the reaction time consists with that observed by Mandal *et al.* for Co@Au nanoparticles.[61] Using displacement reaction to coat Co nanoparticles with Au shell, the authors indicated that coercivity of Co@Au nanoparticles was constantly decreased with reaction time (values of 300, 247 and 91 Oe were obtained for 30, 60 and 90 min, respectively).[61]

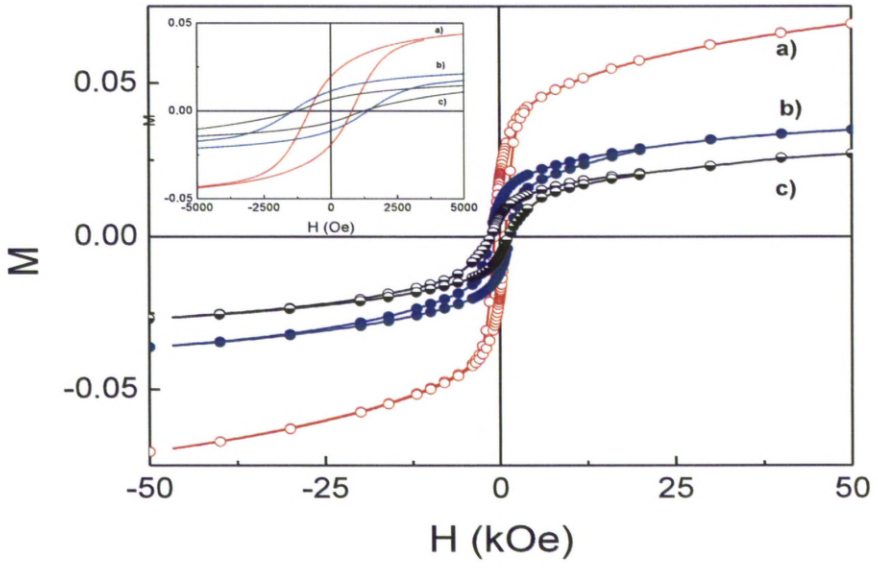

Figure 4.6: Hysteresis loops of uncoated CoFe nanoparticles (a) and Pt coated CoFe nanoparticles after 45 min (b) and 60 min (c). The H_c values was 0.81 kOe for uncoated nanoparticles and were 1.41 kOe and 1.24 kOe for Pt coated CoFe nanoparticles after 45 and 60 min, respectively (inset).

4.3.4 Transferring nanoparticles into water

In the current study, both uncoated CoFe and CoFe@Pt core/shell nanoparticles were made water-dispersible by utilising ligand exchange reactions to replace the hydrophobic OA/OLA molecules on the surface of nanoparticles with hydrophilic ligands. With uncoated CoFe nanoparticles, alkoxysilanes were chosen, as they have been used successfully to transfer various hydrophobic nanoparticles such as cobalt ferrite,[62] iron oxide,[49] noble metals[49] and QDs[49] into water. It has also been shown that alkoxysilanes can self-assemble and form a dense layer on the surface of nanoparticles, which can keep the nanoparticles chemical stable and protect them from aggregation.[62]

The phase transfer was conducted by sonicating the toluene solution of the purified nanoparticles and silane-NH_2. The proposed reaction scheme is that silane conjugation is involved in the ligand exchange of OA/OLA molecules on the surface of nanoparticles by silane molecules (reaction I, Figure 4.7a). The attachment of these molecules to particle surfaces is attained via their NH_2 group. Under basic and heating (by sonication) condition, these silane molecules are cross-linked via silanisation or condensation process to form a robust silica shell (reaction II, Figure 4.7a). During the silanisation process, dimethyl ether, $(CH_3)_2O$, is probably released as by-product.

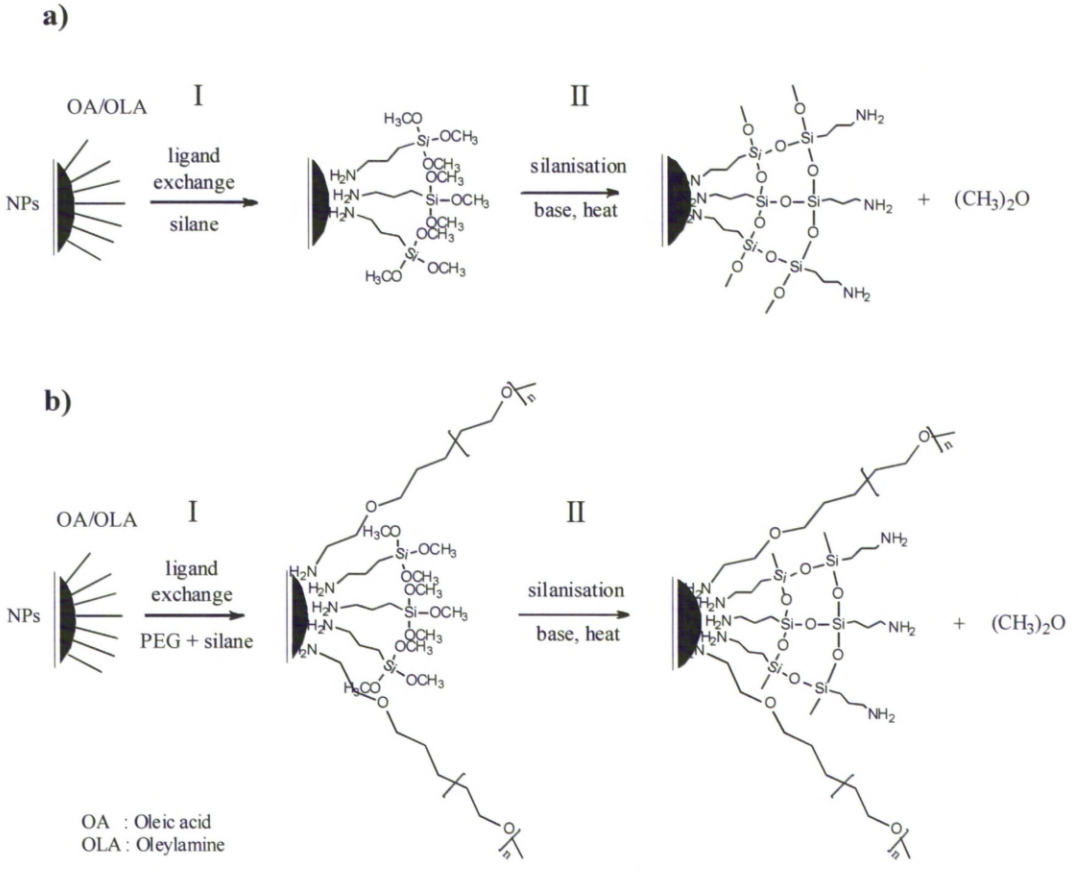

Figure 4.7: Ligand exchange and silanisation of OA/OLA coated CoFe nanoparticles using silane (a) and a mixture of silane-NH_2 and PEG-NH_2 polymer (b).

TEM images of the silica coated CoFe nanoparticles dispersed in different solvents are shown in Figure 4.8. The silane modified nanoparticles are not dispersible in toluene and aggregated into 100-200 nm clusters on the TEM grid (Figure 4.8a). The TEM images of the samples prepared from ethanol and water suspensions show isolated nanoparticles and no significant aggregates were observed (Figure 4.8b, c). These are in agreement with visual observations that silica coated CoFe nanoparticles are well dispersed in ethanol and water. However, the visual observation of the silica coated nanoparticles also indicated that the nanoparticles are not stable in water and ethanol. They began to aggregate resulting in precipitation after just 2-3 days. It was supposed that silane ligands were too short to

protect the nanoparticles from aggregation. To overcome this problem, a mixture of silane and a longer ligand (PEG-NH_2) was used, in an attempt to improve the stability of the nanoparticles. The ligand exchange and silanisation processes are shown in Figure 4.7b. TEM image of the sample prepared from water suspension of the CoFe nanoparticles stabilised by mixture of silane-NH_2 and PEG-NH_2 (M_w = 20,000 g mol^{-1}) indicates well isolated nanoparticles (Figure 4.8d). The nanoparticles are fairly stable in water (up to a week). DLS measurements performed on the sample after 5 days of the synthesis showed one peak at around 35 nm, which suggests the good dispersity of the nanoparticles in water (data no shown).

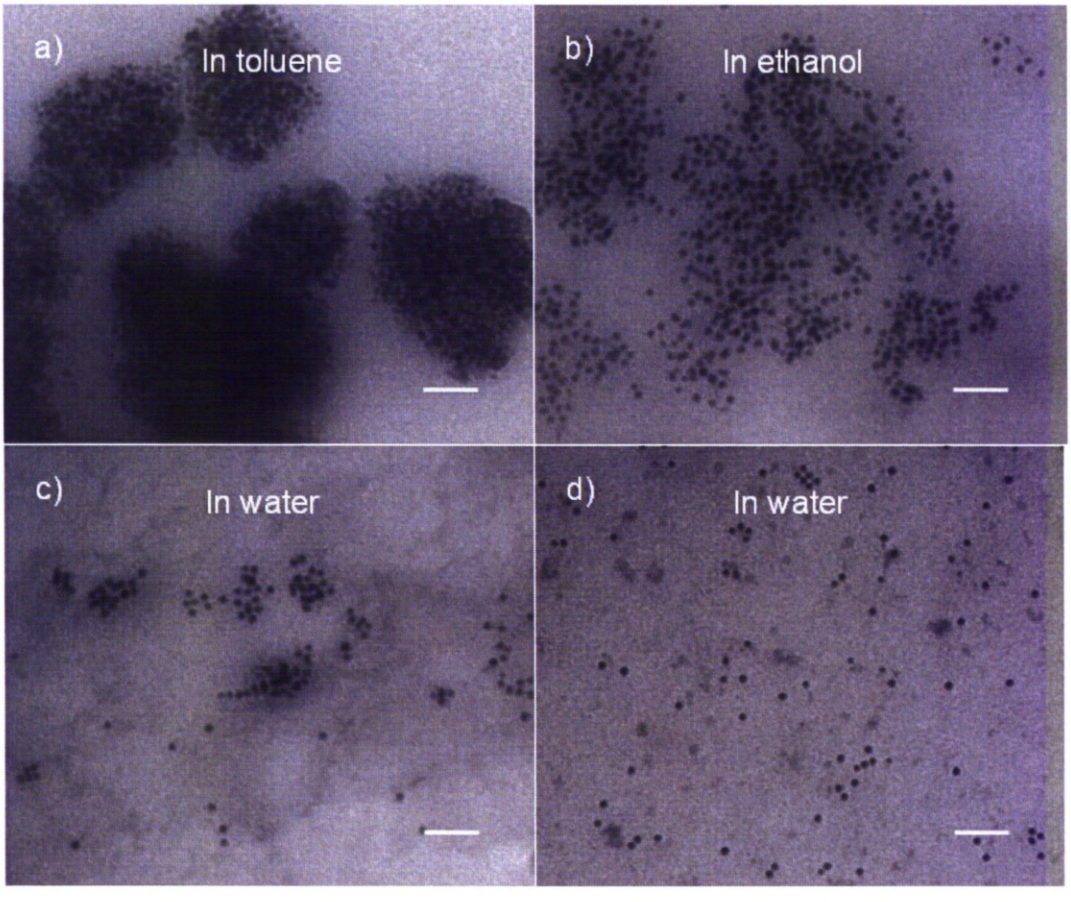

Figure 4.8: TEM images of CoFe nanoparticles stabilised by: silane-NH_2 in different solvents (a-c) and mixture of silane-NH_2 and PEG-NH_2 in water (d). Scale bar: 50 nm.

Hydrophobic CoFe@Pt core/shell nanoparticles were transferred into water by sonicating a chloroform solution of the purified nanoparticles and PEG-SH polymer. After the OA/OLA ligands were exchanged, the CoFe@Pt core/shell nanoparticles are well dispersed in water. TEM image of water dispersed nanoparticles shows that the nanoparticles are well separated (Figure 4.9a).

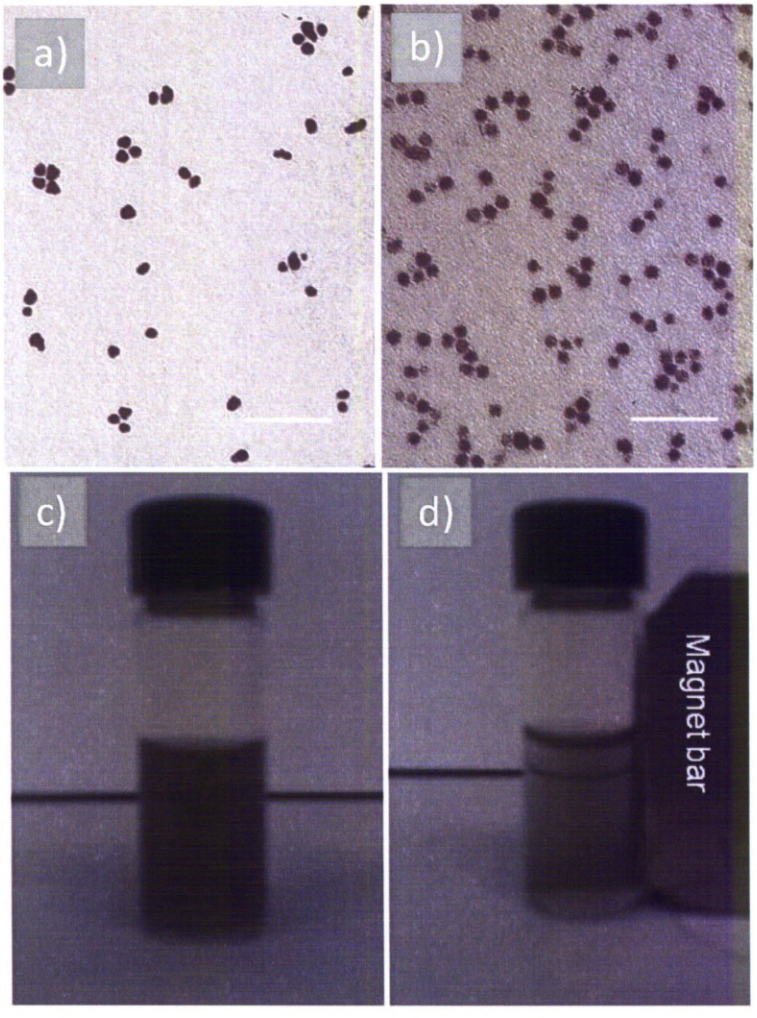

Figure 4.9: TEM images of CoFe@Pt nanoparticles stabilised by: a) PEG-SH and b) PEG-NH_2 in water. c,d) photographs of the PEG-NH_2 stabilised CoFe@Pt nanoparticles dispersed in water without and with a magnetic bar approach (after 1 min), respectively. Scale bar: 50 nm.

PEG polymers with other functional groups such as NH_2 and COOH were also explored for the ligand exchange. TEM image of the sample prepared from water suspension of PEG-NH_2 stabilised CoFe@Pt core/shell nanoparticles is presented in Figure 4.9b. It can be seen that the nanoparticles are monodisperse and well isolated. Visual observations indicate that PEG-NH_2 stabilised CoFe@Pt nanoparticles are well dispersed and fairly stable in water. There was no significant difference of the colloidal stability of the nanoparticles stabilised by PEG-SH and PEG-NH_2 (stable in water for about 2 weeks). The nanoparticles stabilised by PEG (SH or NH_2) can be collected using a magnetic bar and are then easily redispersed in water by gently shaking. Figures 4.9c, d show an example of water suspension of CoFe@Pt nanoparticles stabilised by PEG-NH_2 in the absence and in the presence of a magnetic bar.

When PEG polymer with a COOH functional group was used for ligand exchange, however, nanoparticles were aggregated and precipitated in water shortly after the synthesis (within 1 h). Once the nanoparticles are collected by magnetic bar, they were difficult to redisperse in water (using sonication). It has been known that SH and NH_2 functional groups have high affinities for Pt surfaces, whilst COOH has a high affinity for Fe, Co or their oxides.[63, 64] Therefore, the obtained results for ligand exchange of CoFe@Pt nanoparticles provide further, though indirect, evidence for the successful Pt coating of the nanoparticles.

4.3.5 Other characterisation techniques

HRTEM, STEM and SQUID analyses on Pt coated CoFe samples indicated the core/shell structure. However, as poor crystalline of the sample, HRTEM result could not confirm if the shell is pure Pt or CoFePt alloy. In order to have better evidence to clarify the core/shell structures, other analytical methods are required. Energy dispersive X-ray spectroscopy (EDS) and electron energy loss spectroscopy (EELS) have been proved to be

very useful techniques in the characterisation of various Fe@Au,[36] Au@Ag,[65] Rh@Pt,[66,67] Ag@Co,[68] Pt@Fe_2O_3[69] or Fe@Fe_3O_4,[70,71] core/shell structures due to the ability to provide local information on the composition of the sample (in combination with STEM) with very high spatial resolution. These techniques feasibly not only give direct images of elemental distribution within a particle (mapping) but also provide information about the oxidation states of each element. To assess the success of ligand exchange processes, characterisation techniques such as FTIR or NMR should be performed to verify the coating of CoFe with silane/PEG or CoFe@Pt with PEG ligands after OA/OLA exchange.

In the current case, pure Pt shell coated over CoFe core is expected. Thus, EDS or EELS elemental analyses carried out at the edges or the shell of the core/shell structures give strong Pt signal and very weak or no Co and Fe signals would be detected. If Co and Fe presented at the shell, their composition can be calculated from the EDS or EELS spectra. Figure 4.10 show an example of STEM-EDS analysis in the characterisation of Rh@Pt core/shell structures performed by Alayoglu.[66] EDS spectra acquired at different locations on a single particle indicate a significant variation in the intensity of Rh signal (centre panel). Calculation of elemental composition from EDS show the highest atomic Pt (99.42 %) at the edge with more Rh (85.37 %) at the centre suggested the Rh@Pt core/shell structure.

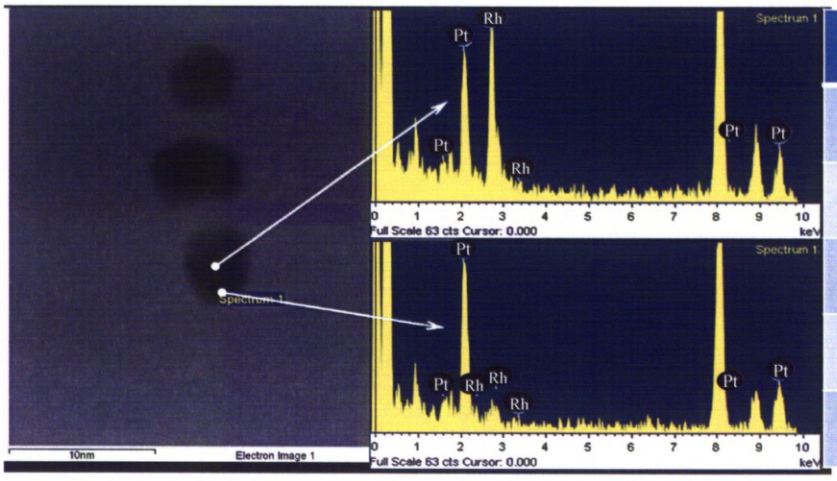

Elements (at centre)	Atomic (%)
Pt	14.63
Rh	85.37
Elements (at edge)	**Atomic (%)**
Pt	99.42
Rh	0.58

Figure 4.10: A) STEM image (left panel) and EDS spectra of Rh@Pt core/shell structure (centre panel); and the elemental composition from the analysing points (right panel). (Reprinted from ref.[66]).

Related to the ligand exchange reactions, the coating of PEG polymer on CoFe@Pt or PEG/silane ligands on CoFe nanoparticles after surface modification could be identified by FTIR or NMR. The presence of PEG is feasibly confirmed through two characteristic peaks at around 1106 and 1349 cm^{-1} on the FTIR spectra due to the vibrations of C-O-C bonds.[28,72] The existence of the silica shell on CoFe@Pt can also be verified by sharp peaks at 1079.5 and 1197.3 cm^{-1} of asymmetry stretching modes of siloxane bonds (Si-O-Si).[29,73] Additionally, the formation of silica shell could be elucidated through ^{29}Si NMR spectra. Wu *et al.* indicated that silicon (chemical environment, $-CH_2CH_2-Si(OSi)_3$) in Ormosil exhibited a strong peak at 69 ppm in ^{29}Si NMR spectra.[74] A similar peak would be expected to be recorded in the current case. However, a broadening of the peak and decrease in intensity of the signal could possibly be observed due to the dipolar interaction between ^{29}Si nuclei and magnetic nanoparticles.[74,75]

As above mentioned, the coating of CoFe with Pt and the formation of silica shell after ligand exchange are related to replacement reactions and silanisation processes. Cobalt and

iron acetylacetonate complexes or dimethyl ether are supposed to be produced as by-products of replacement reactions or silanisation process, respectively. Characterisation of these compounds by analytical techniques, such as UV-vis or FTIR, would provide supplementary evidence for the formation of Pt and silica shells.

4.4 Conclusion

In summary, monodisperse CoFe alloy and CoFe@Pt core/shell nanoparticles have been successfully prepared in organic medium. HRTEM, STEM and SQUID analyses confirmed CoFe@Pt core/shell structures. The results also revealed that the size of CoFe cores decreased significantly after Pt coating and this suggests that a galvanic replacement/ transmetalation process mainly involved. These nanoparticles, CoFe and CoFe@Pt core/shell, were successfully transferred into water by ligand exchange OA/OLA molecules on the surface of nanoparticles with hydrophilic PEG polymers or a mixture of silane/PEG. The core/shell nanoparticles are well dispersed and stable in water up to 2 weeks. HRTEM, STEM and SQUID results were not able to eliminate the formation of CoFePt alloy shell, Although the successful transferring of the CoFe@Pt core/shell structure into water using PEG polymers with SH or NH_2 functional groups suggests the presence of a rich Pt shell. More characterisation techniques, such as EDS, EELS, FTIR or NMR should be used to provide better evidence of the existence of the CoFe@Pt core/shell structures as well as the presence of hydrophilic ligands of silane and PEG on the particles. Furthermore, to elucidate the occurrence of galvanic replacement/transmetalation reactions during the Pt coating or silanisation reaction in the ligand exchange processes, by-products of these processes should be characterised, for example by UV-vis or FTIR techniques, to identify the presence of cobalt and iron acetylacetonate complexes (for galvanic replacement/transmetalation reaction) or dimethyl ether (for silanisation process).

Reference

1. Gu, H. W.; Xu, K. M.; Xu, C. J.; Xu, B. *Chem. Commun.* **2006**, (9), 941-949.
2. Seo, W. S.; Lee, J. H.; Sun, X. M.; Suzuki, Y.; Mann, D.; Liu, Z.; Terashima, M.; Yang, P. C.; McConnell, M. V.; Nishimura, D. G.; Dai, H. J. *Nature Mater.* **2006,** 5, (12), 971-976.
3. Lee, J. H.; Huh, Y. M.; Jun, Y.; Seo, J.; Jang, J.; Song, H. T.; Kim, S.; Cho, E. J.; Yoon, H. G.; Suh, J. S.; Cheon, J. *Nature Med.* **2007,** 13, (1), 95-99.
4. Kosuge, H.; Sherlock, S. P.; Kitagawa, T.; Terashima, M.; Barral, J. K.; Nishimura, D. G.; Dai, H. J.; McConnell, M. V. *Plos One* **2011,** 6, (1), e14523.
5. Lee, J. H.; Sherlock, S. P.; Terashima, M.; Kosuge, H.; Suzuki, Y.; Goodwin, A.; Robinson, J.; Seo, W. S.; Liu, Z.; Luong, R.; McConnell, M. V.; Nishimura, D. G.; Dai, H. J. *Mag. Res. Med.* **2009,** 62, (6), 1497-1509.
6. Hergt, R.; Dutz, S.; Muller, R.; Zeisberger, M. *J. Phys.-Condens. Matter* **2006,** 18, (38), S2919-S2934.
7. Park, H. Y.; Schadt, M. J.; Wang, L.; Lim, I. I. S.; Njoki, P. N.; Kim, S. H.; Jang, M. Y.; Luo, J.; Zhong, C. J. *Langmuir* **2007,** 23, (17), 9050-9056.
8. Lyon, J. L.; Fleming, D. A.; Stone, M. B.; Schiffer, P.; Williams, M. E. *Nano Lett.* **2004,** 4, (4), 719-723.
9. Jeong, J.; Ha, T. H.; Chung, B. H. *Analyt. Chim. Acta* **2006,** 569, (1-2), 203-209.
10. Zhao, X. L.; Cai, Y. Q.; Wang, T.; Shi, Y. L.; Jiang, G. B. *Analyt. Chem.* **2008,** 80, (23), 9091-9096.
11. Wang, L. Y.; Luo, J.; Maye, M. M.; Fan, Q.; Qiang, R. D.; Engelhard, M. H.; Wang, C. M.; Lin, Y. H.; Zhong, C. J. *J. Mater. Chem.* **2005,** 15, (18), 1821-1832.
12. Zhang, H.; Zhong, X.; Xu, J. J.; Chen, H. Y. *Langmuir* **2008,** 24, (23), 13748-13752.
13. Kouassi, G. K.; Wang, P.; Sreevatan, S.; Irudayaraj, J. *Biotech. Progress* **2007,** 23, (5), 1239-1244.
14. Kim, J.; Park, S.; Lee, J. E.; Jin, S. M.; Lee, J. H.; Lee, I. S.; Yang, I.; Kim, J. S.; Kim, S. K.; Cho, M. H.; Hyeon, T. *Angew. Chemie-Inter. Ed.* **2006,** 45, (46), 7754-7758.
15. Lo, C. K.; Xiao, D.; Choi, M. M. F. *J. Mater. Chem.* **2007,** 17, (23), 2418-2427.
16. Zhang, H.; Zhong, X.; Xu, J. J.; Chen, H. Y. *Langmuir* **2008,** 24, (23), 13748-13752.
17. Kouassi, G. K.; Irudayaraj, J. *Analyt. Chem.* **2006,** 78, (10), 3234-3241.
18. Xu, Z. C.; Hou, Y. L.; Sun, S. H. *JACS* **2007,** 129, (28), 8698-8699.

19. Liu, H. L.; Sonn, C. H.; Wu, J. H.; Lee, K. M.; Kim, Y. K. *Biomater.* **2008,** 29, (29), 4003-4011.
20. Lee, J.; Lee, Y.; Youn, J. K.; Bin Na, H.; Yu, T.; Kim, H.; Lee, S. M.; Koo, Y. M.; Kwak, J. H.; Park, H. G.; Chang, H. N.; Hwang, M.; Park, J. G.; Kim, J.; Hyeon, T. *Small* **2008,** 4, (1), 143-152.
21. Chen, L. Y.; Xu, Z. X.; Dai, H.; Zhang, S. T. *J. Alloys & Compounds* **2010,** 497, (1-2), 221-227.
22. Hu, H. B.; Wang, Z. H.; Pan, L. *J. Alloys & Compounds* **2010,** 492, (1-2), 656-661.
23. Lu, C. W.; Huang, D. M.; Hung, Y.; Hsiao, J. K.; Yao, M.; Chung, T. H.; Lin, Y. S.; Wu, S. H.; Hsu, S. C.; Liu, H. M.; Mou, C. Y.; Yang, C. S.; Chen, Y. C. *Nano Lett.* **2007,** 7, (1), 149-154.
24. Palani, A.; Lee, J. S.; Huh, J.; Kim, M.; Lee, Y. J.; Chang, J. H.; Lee, K.; Lee, S. W. *J. Proteome Res.* **2008,** 7, (8), 3591-3596.
25. Lai, C. W.; Wang, Y. H.; Lai, C. H.; Yang, M. J.; Chen, C. Y.; Chou, P. T.; Chan, C. S.; Chi, Y.; Chen, Y. C.; Hsiao, J. K. *Small* **2008,** 4, (2), 218-224.
26. Kang, K.; Choi, J.; Nam, J. H.; Lee, S. C.; Kim, K. J.; Lee, S. W.; Chang, J. H. *J. Phys. Chem. B* **2009,** 113, (2), 536-543.
27. Pita, M.; Abad, J. M.; Vaz-Dominguez, C.; Briones, C.; Mateo-Marti, E.; Martin-Gago, J. A.; Morales, M. D. P.; Fernandez, V. M. *J. Colloid & Interface Sci.* **2008,** 321, (2), 484-492.
28. De Palma, R.; Peeters, S.; Van Bael, M. J.; Van den Rul, H.; Bonroy, K.; Laureyn, W.; Mullens, J.; Borghs, G.; Maes, G. *Chem. Mater.* **2007,** 19, (7), 1821-1831.
29. Aslam, M.; Fu, L.; Li, S.; Dravid, V. P. *J. Colloid & Interface Sci.* **2005,** 290, (2), 444-449.
30. Lee, D. C.; Mikulec, F. V.; Pelaez, J. M.; Koo, B.; Korgel, B. A. *J. Phys. Chem. B* **2006,** 110, (23), 11160-11166.
31. Kobayashi, Y.; Horie, M.; Konno, M.; Rodriguez-Gonzalez, B.; Liz-Marzan, L. M. *J.f Phys. Chem. B* **2003,** 107, (30), 7420-7425.
32. Aslam, M.; Li, S.; Dravid, V. P. *J. Am. Ceram. Soc.* **2007,** 90, (3), 950-956.
33. Bao, Y. P.; Calderon, H.; Krishnan, K. M. *J. Phys. Chem. C* **2007,** 111, (5), 1941-1944.
34. Lee, W. R.; Kim, M. G.; Choi, J. R.; Park, J. I.; Ko, S. J.; Oh, S. J.; Cheon, J. *JACS* **2005,** 127, (46), 16090-16097.

35. Bala, T.; Arumugam, S. K.; Pasricha, R.; Prasad, B. L. V.; Sastry, M. *J. Mater. Chem.* **2004,** 14, (6), 1057-1061.
36. Cho, S. J.; Idrobo, J. C.; Olamit, J.; Liu, K.; Browning, N. D.; Kauzlarich, S. M. *Chem. Mater.* **2005,** 17, (12), 3181-3186.
37. Vestal, C. R.; Zhang, Z. J. *Nano Lett.* **2003,** 3, (12), 1739-1743.
38. Yi, D. K.; Selvan, S. T.; Lee, S. S.; Papaefthymiou, G. C.; Kundaliya, D.; Ying, J. Y. *JACS* **2005,** 127, (14), 4990-4991.
39. Yi, D. K.; Lee, S. S.; Papaefthymiou, G. C.; Ying, J. Y. *Chem. Mater.* **2006,** 18, (3), 614-619.
40. Lu, A. H.; Salabas, E. L.; Schuth, F. *Angew. Chemie-Inter. Ed.* **2007,** 46, (8), 1222-1244.
41. Turgut, Z.; Scott, J. H.; Huang, M. Q.; Majetich, S. A.; McHenry, M. E. *J. Appl. Phys.* **1998,** 83, (11), 6468-6470.
42. Sun, X. M.; Tabakman, S. M.; Seo, W. S.; Zhang, L.; Zhang, G. Y.; Sherlock, S.; Bai, L.; Dai, H. J. *Angew. Chemie-Inter. Ed.* **2009,** 48, (5), 939-942.
43. Turgut, Z.; Huang, M. Q.; Gallagher, K.; McHenry, M. E.; Majetich, S. A. *J. Appl. Phys.* **1997,** 81, (8), 4039-4041.
44. Desvaux, C.; Amiens, C.; Fejes, P.; Renaud, P.; Respaud, M.; Lecante, P.; Snoeck, E.; Chaudret, B. *Nature Mater.* **2005,** 4, (10), 750-753.
45. Kline, T. L.; Xu, Y. H.; Jing, Y.; Wang, J. P. *J. Mag. Mag. Mater.* **2009,** 321, (10), 1525-1528.
46. Bai, J. M.; Wang, J. P. *Appl. Phys. Lett.* **2005,** 87, (15), 5414-5416.
47. Xu, Y. H.; Wang, J. P. Applied Physics Letters **2007,** 91, (23).
48. Yu, H.; Chen, M.; Rice, P. M.; Wang, S. X.; White, R. L.; Sun, S. H. *Nano Lett.* **2005,** 5, (2), 379-382.
49. Jana, N. R.; Earhart, C.; Ying, J. Y. *Chem. Mater.* **2007,** 19, (21), 5074-5082.
50. Zubris, M.; King, R. B.; Garmestani, H.; Tannenbaum, R. *J. Mater. Chem.* **2005,** 15, (12), 1277-1285.
51. Wen, J. Z.; Goldsmith, C. F.; Ashcraft, R. W.; Green, W. H. *J. Phys. Chem. C* **2007,** 111, (15), 5677-5688.
52. Poddar, P.; Srinath, S.; Gass, J.; Prasad, B. L. V.; Srikanth, H. *J. Phys. Chem. C* **2007,** 111, (38), 14060-14066.
53. Chen, D.; Li, J. J.; Shi, C. S.; Du, X. W.; Zhao, N. Q.; Sheng, J.; Liu, S. *Chem. Mater.* **2007,** 19, (14), 3399-3405.

54. Ban, Z. H.; Barnakov, Y. A.; Golub, V. O.; O'Connor, C. J. *J. Mater. Chem.* **2005,** 15, (43), 4660-4662.
55. de la Presa, P.; Multigner, M.; Morales, M. P.; Rueda, T.; Fernandez-Pinel, E.; Hernando, A. *J. Mag. Mag. Mater.* **2007,** 316, (2), E753-E755.
56. Wang, L. Y.; Luo, J.; Fan, Q.; Suzuki, M.; Suzuki, I. S.; Engelhard, M. H.; Lin, Y. H.; Kim, N.; Wang, J. Q.; Zhong, C. J. *J. Phys. Chem. B* **2005,** 109, (46), 21593-21601.
57. Garcia-Otero, J.; Porto, M.; Rivas, J.; Bunde, A. *Phys. Rev. Lett.* **2000,** 84, (1), 167-170.
58. Boal, A. K.; Frankamp, B. L.; Uzun, O.; Tuominen, M. T.; Rotello, V. M. *Chem. Mater.* **2004,** 16, (17), 3252-3256.
59. Zeng, H.; Sun, S. H. *Adv. Funct. Mater.* **2008,** 18, (3), 391-400.
60. Luis, F.; Torres, J. M.; Garcia, L. M.; Bartolome, J.; Stankiewicz, J.; Petroff, F.; Fettar, F.; Maurice, J. L.; Vaures, A. *Phys. Rev. B* **2002,** 65, (9), 6341-6345.
61. Mandal, S.; Krishnan, K. M. *J. Mater. Chem.* **2007,** 17, (4), 372-376.
62. Palma, R.; Laureyn, W.; Frederix, F.; Bonroy, K.; Pireaux, J. J.; Borghs, G.; Maes, G. *Langmuir* **2007,** 23, (2), 443-451.
63. Sun, S. H. *Adv. Mater.* **2006,** 18, (4), 393-403.
64. Shukla, N.; Liu, C.; Jones, P. M.; Weller, D. *J. Mag. Mag. Mater.* **2003,** 266, (1-2), 178-184.
65. Jiang, H. L.; Akita, T.; Ishida, T.; Haruta, M.; Xu, Q. A. *JACS* **2011,** 133, (5), 1304-1306.
66. Alayoglu, S.; Eichhorn, B. *JACS* **2008,** 130, (51), 17479-17486.
67. Alayoglu, S.; Zavalij, P.; Eichhorn, B.; Wang, Q.; Frenkel, A. I.; Chupas, P. *ACS Nano* **2009,** 3, (10), 3127-3137.
68. Sobal, N. S.; Hilgendorff, M.; Mohwald, H.; Giersig, M.; Spasova, M.; Radetic, T.; Farle, M. *Nano Lett.* **2002,** 2, (6), 621-624.
69. Teng, X. W.; Yang, H. *Nanotech.* **2005,** 16, (7), S554-S561.
70. Wang, C. M.; Baer, D. R.; Amonette, J. E.; Engelhard, M. H.; Antony, J.; Qiang, Y. *JACS* **2009,** 131, (25), 8824-8832.
71. Ong, Q. K.; Wei, A.; Lin, X. M. *Phys. Rev. B* **2009,** 80, (13), 5418-5422.
72. Gupta, A. K.; Wells, S. *IEEE Trans. Nanobiosci.* **2004,** 3, (1), 66-73.
73. Yamaura, M.; Camilo, R. L.; Sampaio, L. C.; Macedo, M. A.; Nakamura, M.; Toma, H. E. *J. Mag. Mag. Mater.* **2004,** 279, (2-3), 210-217.

74. Wu, K. H.; Chao, C. M.; Liu, C. H.; Chang, T. C. *Corros. Sci.* **2007,** 49, (7), 3001-3014.
75. Rouessac, F.; Rouessac, A., *Chemical Analysis: Modern Instrumetation Methods and Techniques*. John Wiley & Son Inc.: NY, 2000; p 464.
76. Park, J. I.; Cheon, J. *JACS* **2001,** 123, (24), 5743-5746.
77. Park, J. I.; Kim, M. G.; Jun, Y. W.; Lee, J. S.; Lee, W. R.; Cheon, J. *JACS* **2004,** 126, (29), 9072-9078.

Chapter 5

Synthesis of monodisperse magnetic cobalt ferrite nanoparticles with controlled morphology and composition

5.1 Introduction

Controlling monodispersity, morphology and composition of magnetic nanoparticles is important since their magnetic and catalytic properties strongly depend on these parameters. Recently, various wet chemical techniques including solvothermal,[1-3] electro-chemical,[4] reverse micelle[5] and organic phase syntheses have extensively been used to prepare magnetic nanoparticles with different sizes and shapes. Of these methods, the organic phase synthesis has proved to be the most successful methods for the preparation of the nanoparticles, giving a good control over the size and shape of the nanoparticles. Using the organic phase synthesis, non-spherical shape of cube, rod, tetrapod, wire or star of various magnetic nanoparticles such as Fe_3O_4,[6-9] Fe_2O_3,[10-13] $MnFe_2O_4$,[14-16] $CoFe_2O_4$,[17-19] FePt,[20-24] CoPt,[20] NiPt,[20] Co[25,26] and Fe[27] have been made. In this method, the size of magnetic nanoparticles is controlled by adjusting the boiling temperature of solvent mixture,[6] the reaction time,[7] the reagent concentration,[8,14,28] or by seeding growth process.[9,17] The particle shape is usually controlled by varying the heating rate,[17] the ratio of precursor to surfactant,[10,14] or the reaction time or concentration of reagent.[11,19] Generally, high temperature and long reaction time produced large particles whilst low heating rate or low ratio of precursor to surfactant generated non-spherical shape.[6,7,14,17]

Among magnetic oxides, cobalt ferrite with a normal formula $CoFe_2O_4$ has drawn a lot of attention because of its high magnetic anisotropy (~$2x10^6$ erg cm^{-3} at 300 K)[29] which is

advantages in applications of high density magnetic recording media.[30-32] At present, many synthetic techniques for the preparation of $CoFe_2O_4$ nanoparticles with controllable size have been reported, including co-precipitation,[33-43] hydro/solvothermal,[44-48] sol-gel,[49-54] reverse micelle[55-59] and organic phase syntheses.[16-19 60-65] However, there are limited works on the synthesis of the shape-controlled $CoFe_2O_4$ nanoparticles.[17-19,48,53] In these works, $CoFe_2O_4$ nanoparticles were produced by decomposition of iron (III) acetylacetonate, $Fe(acac)_3$, and cobalt (II) acetylacetonate, $Co(acac)_2$,[66] or metal oleate complexes at high temperature in organic solvents.[18,19,53] The control of particle shape was made possible by a seeding growth process[17] or by varying the concentration of precursors and heating rate of the reaction.[18,19,53]

This chapter describes the elaboration of a general and one step synthetic method for cobalt ferrite nanoparticles, which control over morphology and composition. The size, shape and composition of the nanoparticles are simply tuned by varying concentration of oleic acid (OA) and oleylamine (OLA), the reaction time and ratio of precursors. The obtained nanoparticles were characterised by TEM, HRTEM, SQUID, XRD and ICP-AES techniques. Analytical methods such as FTIR, DSC, TGA or mass spectroscopy, which have been commonly used to study the decomposition process of precursors, are also mentioned. Cobalt ferrite nanoparticles with sizes in a broad range from 4 to over 30 nm and diverse shapes, including spherical, cubic and star-like and different compositions were produced. The nanoparticles were monodisperse and in some cases self-assembled into micrometer scale two dimensional superlattices. Water-dispersible cobalt ferrite nanoparticles are also produced by ligand exchange reaction utilising water-dispersible poly(methacrylic acid) dodecanethiol (PMAA-DDT) polymer.

5.2 Experimental

5.2.1 Mareials

Chemicals using for the synthesis are commercially available. All chemicals, including precursors: iron (III) acetylacetonate ($Fe(acac)_3$) 99.99 % and cobalt (II) acetylacetonate ($Co(acac)_2$) 99 %; solvents: octyl ether 99 %, chloroform, absolute ethanol, toluene and hexane; surfactants and reductant: oleic acid (OA) 99 %, oleylamine (OLA) 70 %, 1,2-hexadecanediol (HDD) 90 % were purchased from Sigma-Aldrich Ltd, UK. All the chemicals were used as received without further purification. PMAA-DDT polymer (M_w = 3,420 g mol^{-1}) were synthesised at the University of Liverpool.[67,68]

5.2.2 Synthesis of cobalt ferrite nanoparticles

The syntheses were carried out under oxygen-free conditions in a Schlenk line. In a typical synthesis, 20.75 mM $Co(acac)_2$ (0.107 g, 0.415 mmol) and 41.5 mM $Fe(acac)_3$ (0.293 g, 0.83 mmol) were stored in a 50 mL three necked round bottom flask in the presence of a mixture of equimolar OA and OLA at the total concentration of 496 mM (1.6 mL, for each), and 75 mM HDD (0.387 g, 1.5 mmol). The volume of octyl ether solvent used was 20 mL. The reaction mixture was degassed at room temperature for at least 30 min and then heated to 100 °C and kept at this temperature for another 30 min before increasing the temperature to 295 °C (heating rate of 25 °C min^{-1}) under continuous nitrogen flow. Samples were removed at various times up to 120 min to investigate the morphological evolution of the nanoparticles. The effects of the surfactant concentration, the ratio of metal precursors and surfactants on the size, shape, composition and magnetic properties of the nanoparticles were also investigated. The synthesis conditions are shown in Table 5.1.

5.2.3 Transferring cobalt ferrite nanoparticles into water

Cobalt ferrite nanoparticles synthesised in the presence of 372 mM OA/OLA (OA : OLA = 1 : 1) and precursor ratio of $Co(acac)_2$: $Fe(acac)_3$ = 1 : 2 were used for ligand exchange. The as-synthesised nanoparticles were purified from free excess ligands before ligand exchange. In a typical purification, 1 mL of a solution of nanoparticles (≈ 3.5 mg) was mixed with 1 mL of ethanol. The nanoparticles were collected using a magnetic bar and the supernatant was discarded. The nanoparticles were then dispersed in 1 mL hexane and precipitated by adding 1 mL of ethanol. The precipitation-redispersion procedure was repeated 2 more times and the nanoparticles were finally dispersed in 2 mL chloroform prior to ligand exchange. To this solution, 45 mg PMAA-DDT polymer (M_w = 3,420 g mol^{-1}) dissolving in 1 mL ethanol was added under sonication for 60 min. The nanoparticles were collected using a magnetic bar and dispersed in ethanol before transfer into water.

5.3 Results and discussion

5.3.1 Cobalt ferrite nanoparticles with controllable morphology and composition

Cobalt ferrite ($CoFe_2O_4$) nanoparticles were synthesised by thermal decomposition of $Co(acac)_2$ and $Fe(acac)_3$ in the presence of OA, OLA and HDD. Thermal decomposition of $Co(acac)_2$ and $Fe(acac)_3$ produced cobalt ferrite nanoparticles, and acetone and carbon dioxide were released as by-products of the reaction:[69,70]

$$Co(acac)_2 + Fe(acac)_3 \rightarrow CoFe_2O_4 + CH_3COCH_3 + CO_2$$

The size, shape and composition of the as-synthesised nanoparticles were controlled by varying the reaction parameters (Table 5.1).

Table 5.1: Synthesis conditions and the morphology of the cobalt ferrite nanoparticles

Precursor concentration (mM)		Surfactant concentration (mM)		Reaction time	Size	Shape	Synthesised temperature
Co^{2+}	Fe^{3+}	OA	OLA	(min)	(nm)		°C
20.75	41.5	124	124	5	4.7 ± 0.6	Spherical	295
				30	8 ± 1.1	spherical	
				60	10.5 ± 0.9	spherical	
				120	12 ± 2.2	spherical	
20.75	41.5	186	186	30	9.2 ± 0.8	cubic	295
				60	11.0 ± 0.9	cubic	
20.75	41.5	248	248	30	15.2 ± 1.3	cubic	295
				60	17.9 ± 1.5	cubic	
20.75	41.5	310	310	5	13.2 ± 2.0	cubic	295
				30	22.3 ± 2.9	cubic + star	
				60	29.7 ± 2.7	star	
25.0	37.5	64	64	5	5.7 ± 0.5	spherical	295
				30	6.4 ± 0.9	spherical	
				60	7.6 ± 0.9	spherical	
25.0	37.5	124	124	30	8.9 ± 1.0	spherical	295
				60	11 ± 0.9	spherical	
				120	10 ± 1.8	spherical	
25.0	37.5	186	186	30	10.7 ± 0.7	round cubic	295
				60	12.4 ± 0.8	cubic	
				120	12.9 ± 0.9	cubic+faced	
25.0	37.5	248	248	30	13.7 ± 0.8	cubic	295
				60	16.7 ± 1.3	cubic	
				120	16.3 ± 2.5	faceted+spherical	
25.0	37.5	310	310	1	4.3 ± 0.4	spherical	287
				10	16.1 ± 2.0	cubic	
				30	18.3 ± 2.2	cubic	
				60	24.9 ± 4.6	cubic + star	
				120	28.1 ± 2.8	star	
25.0	37.5	310	310	1 30 60	6.4 ± 0.5 19.8 ± 2.0 27.9 ± 2.8	spherical cubic + star star	295
25.0	37.5	620	620	30	24.4 ± 3.0	star	287
				120	≈ 100	aggregate	
25.0	37.5	1,200	1,200	5	10-16	irregular	295
				30	12-17	irregular	
				60	12-20	more spherical	
25.0	37.5		620	30	8.2 ± 1.6	spherical + cubic	287
				60	9.8 ± 1.2	spherical + cubic	
				120	11.2 ± 0.8	rounded cubic	
25.0	37.5	620		30	≈ 3-4	spherical	287
				180	15.2 ± 1.3	cubic + faceted	
31.0	31.0	186	186	30	12.2 ± 1.3	rounded cubic	295
				60	14.4 ± 1.2	rounded cubic	

				120	13.9 ± 1.7	faceted	
31.0	31.0	248	248	30	19.9 ± 2.1	cubic	295
				60	26.3 ± 3.0	cubic+star	
				120	29.0 ± 3.0	star	
31.0	31.0	310	310	5	≈ 4-6	spherical	287
				60	17.7 ± 3.0	cubic+star	
				120	30.0 ± 3.7	star	
37.5	25.0	186	186	30	15.4 ± 1.2	cubic	295
				60	17.9 ± 1.3	cubic	
				120	21.0 ± 2.3	spherical	
37.5	25.0	248	248	30	18.4 ± 2.5	star	295
				60	20.2 ± 2.9	star	
37.5	25.0	310	310	120	28.3 ± 3.9	star	287

It was well known that the morphology of the synthesised nanoparticles can be controlled by the nucleation and growth progresses which are in turn strongly influenced by the synthetic conditions, such as the concentration of reagents, reaction time and its temperature.[71] Figure 5.1 shows the TEM images of the cobalt ferrite nanoparticles in which the shape can be varied between the sphere, cube and star-like with the equimolar amount of OA and OLA at total concentration of 248 mM, 496 mM, and 620 mM, respectively. Here, the concentrations of $Co(acac)_2$ and $Fe(acac)_3$ were kept at 20.75 and 41.5 mM, respectively and the time of the reaction varies between 30-60 min. The longer the reaction time, the larger nanoparticles are obtained, but the shape of the nanoparticles remains almost the same. For spherical nanoparticles the size of 8.0-10.5 nm can be obtained, and it is 15.0-17.9 nm for cubic nanoparticles and 22.3-29.7 nm for stars.

Previously, the use of OA and OLA mixture as surfactants to synthesise magnetic nanocubes has been reported by several authors.[20,23,24] The carboxylic group on OA and the amine group on OLA have different strength and selective binding energy to the surfaces of the nanoparticle and are necessary for controlling the nanoparticles' shape. Sun *et al.* have shown that nanocubes can be obtained when the ratio of OA surfactant to iron precursor is more than 3 : 1.[14] In the current study, it was observed the formation of the

cubic nanoparticles at 372 mM OA/OLA corresponding with a ratio of OA surfactant to Fe precursor of ≈ 4.4.

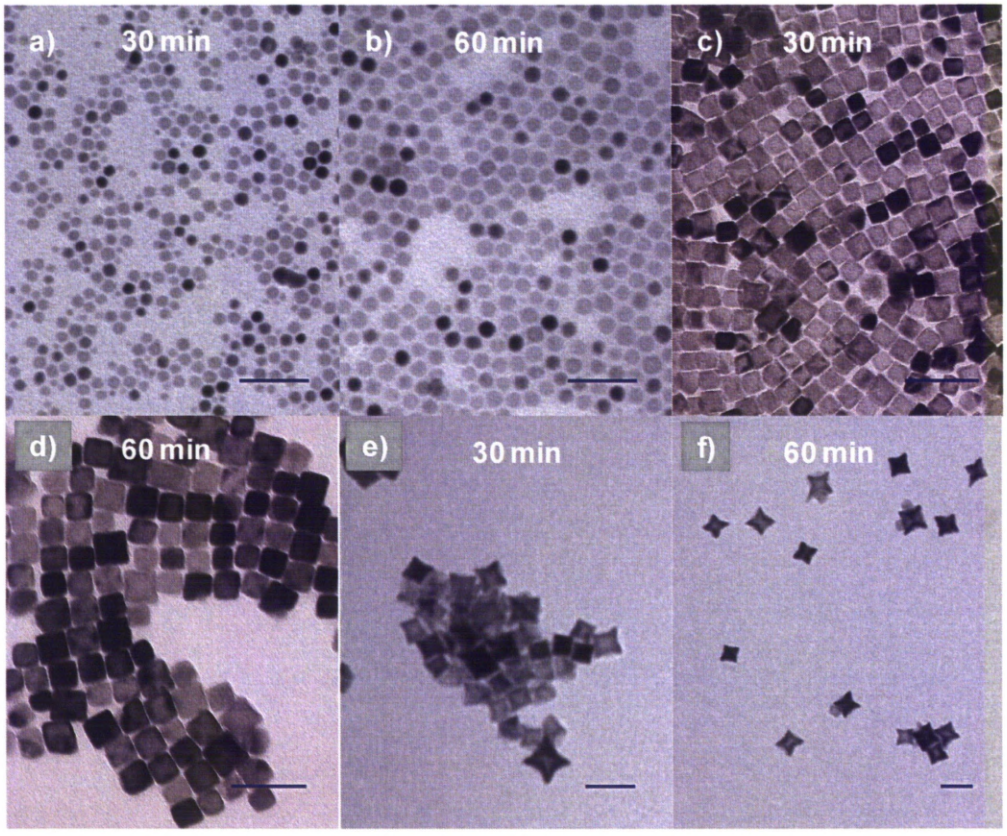

Figure 5.1: TEM images of cobalt ferrite nanoparticles synthesised with the precursor ratio Co^{2+} : Fe^{3+} = 1 : 2, in the presence of equimolar amount of OA/OLA at total concentration of 248 mM (a,b); 496 mM (c,d) and 620 mM (e,f) and different reaction times as indicated. Scale bar: 50 nm.

The influence of the starting ratio of $Co(acac)_2$: $Fe(acac)_3$ on the morphology and phase structure of the as-synthesised nanoparticles was also investigated in experiments where the total concentration of precursors was fixed at 62.25 mM. It was observed that with different ratios of $Co(acac)_2$: $Fe(acac)_3$ = 1 : 1.5, 1 : 1 and 1.5 : 1, there is only change in the size but the shape of the nanoparticles remains very much similar. With the total equimolar OA/OLA concentration in between 372-496 mM, nanocubes were obtained (Table 5.1 and Figure 5.2a, b). Higher concentration of 1.2 M of equimolar OA/OLA

resulted in the production of star-like shapes (Figure 5.2c). At the concentrations of 2.4 M equimolar OA/OLA there are neither cubes nor stars to be observed but only the irregular shape nanoparticles with size ranging from 10 to 17 nm (Table 5.1) which may come as a result of the inhibitation of the growth process by the presence of abundant OA/OLA in the solution and it was similarly observed previously in the synthesis of the FePt nanoparticles.[24]

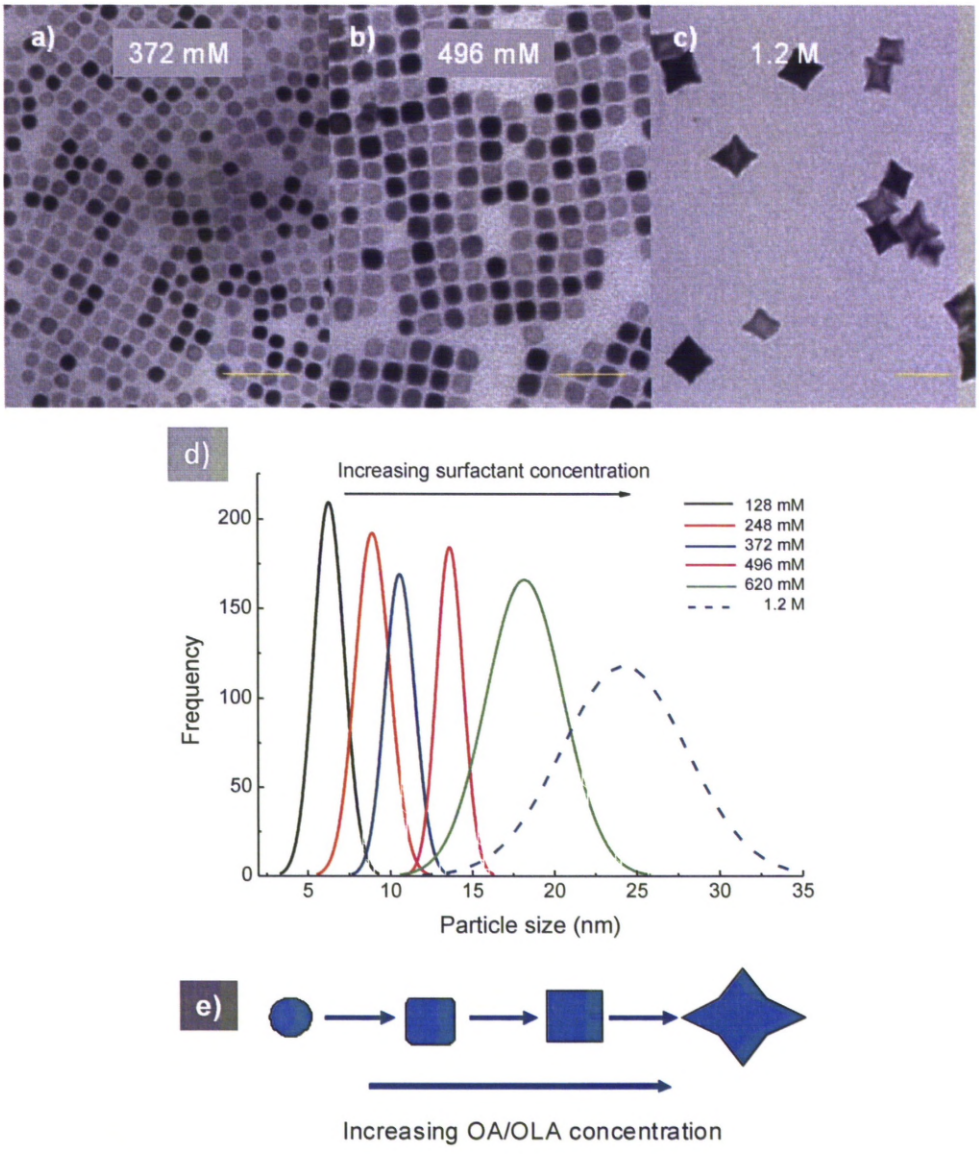

Figure 5.2: TEM images of the cobalt ferrite nanoparticles synthesised in the presence of equimolar amount of OA/OLA at the total concentration of a) 372 mM, b) 496 mM, c) 1.2 M. Size distribution histogram of the nanoparticles with different surfactant concentrations

(d) and schematic of shape evolution of nanoparticles (e) are also shown. The starting precursor ratio Co^{2+} : Fe^{3+} = 1 : 1.5 and the reaction time is 30 min. Scale bar: 50 nm.

The role of the individual surfactant, OA and OLA, on the morphology of the synthesised nanoparticles was also explored. In the presence of solely OA at concentration of 620 mM, only small spherical nanoparticles of about 3 nm were formed after 30 min of reaction whereas for OLA, there was mainly a mixture of spherical and cubic nanoparticles. However, with prolonging the reaction time to 120 min for OLA and 180 nm for OA, it resulted in the formation of nanocubes and faceted nanoparticles, respectively (Table 5.1, and Figure 5.3). This fact, therefore indicates that in the presence of only OA or OLA, longer reaction time would be required for the growth of the nanoparticles.

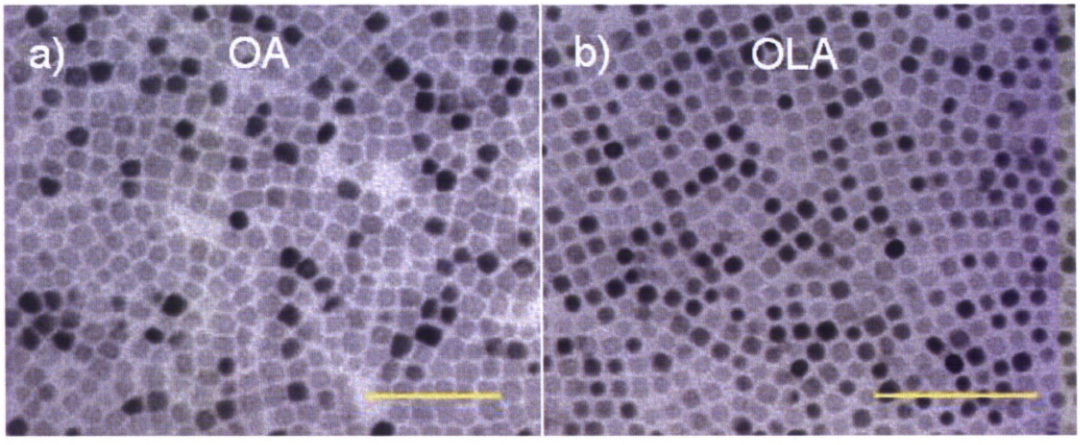

Figure 5.3: TEM image of cobalt ferrite nanoparticles synthesised in the present of 620 mM surfactant: a) OA at 180 min and b) OLA at 120 min. Scale bar: 100 nm.

To investigate the effect of reaction time on the morphology of the nanoparticles further, the syntheses were carried out under different concentrations or ratio of reagents and at each synthesis the sample was removed from the reaction at different times. The results consistently show that small spherical nanoparticles were initially formed and then

by prolonging the reaction time, these small nanoparticles developed into larger spheres, cubes or stars depending on the surfactant concentration. For example, at a ratio of Co^{2+} : Fe^{3+} = 1 : 2 and in the presence of 248 mM equimolar OA/OLA, 4.7 nm spherical nanoparticles were obtained after 5 min and the size of the nanoparticles increased to 12.5 nm after 120 min (Table 5.1). At higher surfactant OA/OLA concentration of 620 mM, the 13.2 nm cubes were formed after 5 min of reaction but they then developed quickly into 29.7 nm stars after 60 min of reaction (Table 5.1, Figure 5.1f). By further extending reaction time to 120 min, aggregated nanoparticles were formed (data not shown).

To investigate the effect of reaction time on the morphology of nanoparticles in more details, we reduce both the growth rate of the nanoparticles by decreasing the reaction temperature from 295 to 287 °C and the sampling interval. As an example, Figure 5.4 shows TEM images and the histograms of size distributions of nanoparticles synthesised at a ratio of Co^{2+} : Fe^{3+} = 1 : 1.5 after different reaction times. It can be seen that 4.3 nm spheres were formed within 1 min of reaction and these then developed into 16.1 nm nanocubes after 10 min and 28.1 nm stars after 120 min.

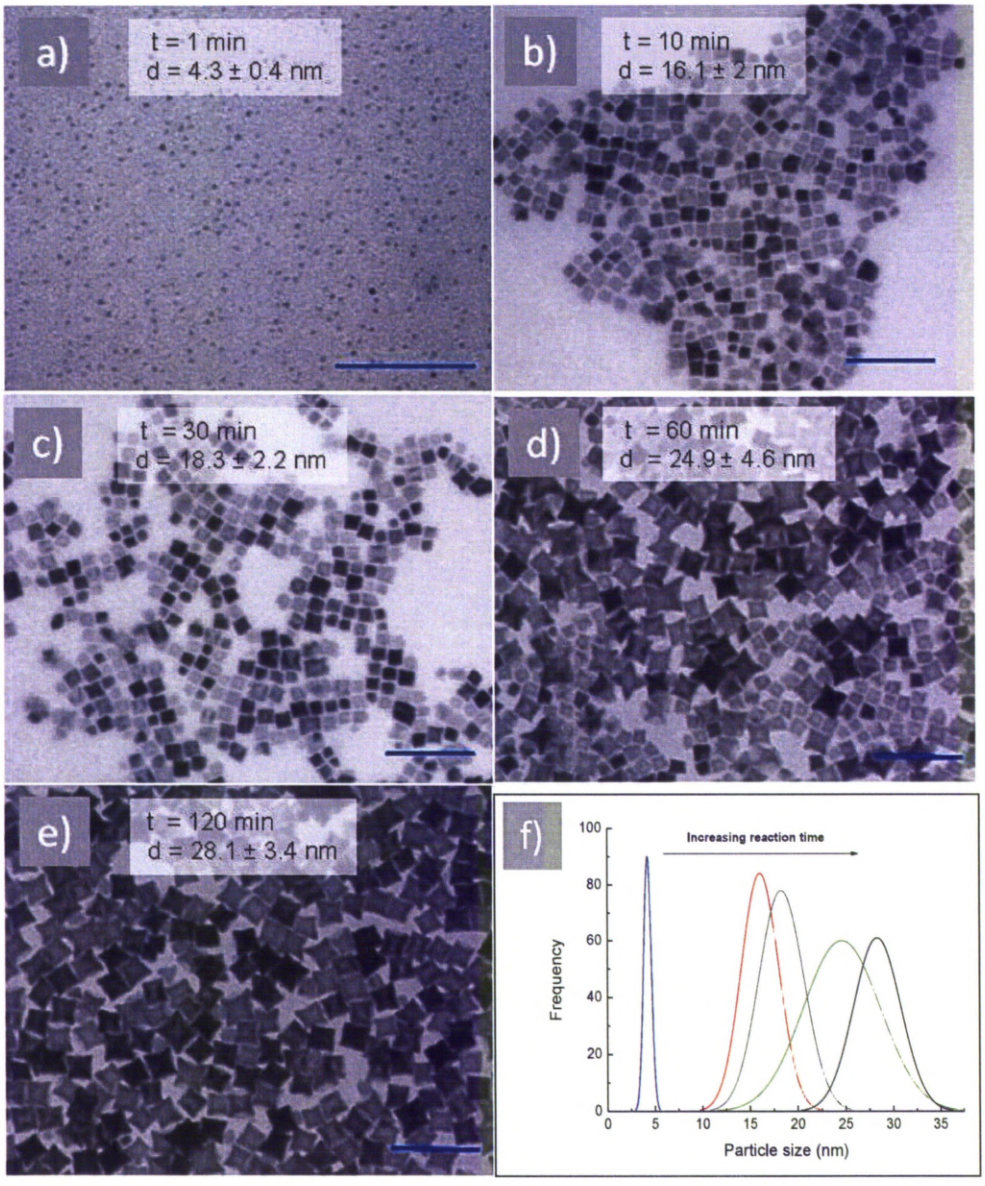

Figure 5.4: TEM images of nanoparticles synthesised in the presence of 620 mM of equimolar amount of OA and OLA at different reaction times: a) 1 min, b) 10 min, c) 30 min, d) 60 min, e) 120 min; The corresponding size distribution histograms are shown in (f). The samples were synthesised at 287 °C and the precursor ratio Co^{2+} : Fe^{3+} = 1 : 1.5. Scale bar: 100 nm.

.

It is widely accepted that tuning the size and shape of the nanoparticles is enabled by controlling the relative surfactant concentrations. OA is known to selectively and strongly bonded to the crystalline facets such as a (100) plane whilst OLA weakly and isotropically

binds to the surface of nanoparticles.[7] In the current study, it is believed that small faceted nanoparticles were formed in the solution at the initial stage of the synthesis. By extending the reaction time, the nanoparticles grow and become bigger. In high surfactant concentrations, OA molecules were assumed to quickly attach to the lowest energy {100} facets and inhibit the growth of nanoparticles in [100] direction by forming a dense surfactant layer, resulting in the formation of cubic nanoparticles.[8,17,72] As this crystal plane is blocked, metal ions are absorbed on the faster growing {111} or {110} planes and lead to the formation of star-like nanoparticles given the available precursors in the solution. However, at low surfactant concentration, the surfactant layer is not dense enough to reduce the growth in the particular direction, thus leading to spherical shape.

In the present study, it is observed that the size of nanoparticles significantly increased with increasing reaction time. Surprisingly, at the same time, it is also found that the size was dramatically changed with varying OA/OLA concentrations for example from few nm for spheres to around 25 nm for stars, as OA/OLA concentration increased from 0.124 to 1.2 M in contrast with previous reported works, where the size of nanoparticles decreased with increasing of ratio of surfactant/precursor concentration.[73,74] In the current study, regardless of the shape, it is observed that size of nanoparticles increased (see Table 5.1). Here the mechanism leading to increasing the size of nanoparticles could possibly be due to the partial formation of stable cobalt and iron oleate complexes during the synthesis. Cobalt and iron acetylacetonates were known to be decomposed at around 190 °C,[70,75] however, if they complexed with OA resulting in metal oleates, it was indicated that the decomposition temperature of these complexes increased to around 300 °C.[18] In the presence of low OA/OLA concentration, iron and cobalt sources in form of acetylacetonate complexes are quickly decomposed at around 230-250 °C leading to the formation of many small nucleus and reduced cobalt and iron sources to feed up for the growth stage of nanoparticles and thus smaller nanoparticles were obtained. On the contrary, at high

OA/OLA concentration, cobalt and iron ions mainly form complexes with OA resulting in oleate complexes. As the high decomposition temperature of oleate complexes, cobalt and iron sources are available in the solution for the further growth of nanoparticles.

In the present study, the formation of cubic and star-like nanoparticles occurred at temperatures of 287 and 295 °C which is lower in comparison with those reported by Gupta and co-workers.[18] When the synthesis was carried out in the presence of HDD. It was reported that HDD could act as an accelerating agent for the formation of nanoparticles.[66,76] Therefore, the presence of HDD in the reaction may have reduced the temperature for forming of cubic and star-like shapes.

In addition to controlling the size, the formation of *in-situ* cobalt and iron oleate complexes also plays an important role in the monodispersity of the nanoparticles. It was observed that nanoparticles became polydisperse at longer reaction times (120 min) in the presence of low OA/OLA concentration (Figure 5.1d). Due to the quick decomposition of acetylacetonate complexes, after about 60 min almost metal ions were consumed. By further extending reaction time nanoparticles became polydisperse as a result of the Ostward ripening process.[71] In the case the nanoparticles synthesised in the presence of high OA/OLA concentration, cobalt and iron ions are available in the solution in a form of oleate complexes. It will therefore require longer reaction time to reach the focusing regime[71] (Figure 5.3e).

From the observations, we proposed the schematic diagram for morphology evolution of nanoparticles in relation with OA/OLA surfactants concentrations and reaction time as shown in Figure 5.5. It can be seen that small spherical (faceted) nanoparticles with few nm in size were formed in the solution at the initial stage within few minutes of the reaction. At low OA/OLA concentration, only nanoparticles with spherical shape were obtained in the whole process of reaction (Figure 5.5a). However, the initial spheres developed into different morphologies including rounded cubes, cubes and faceted

nanoparticles (Figure 5.5b) or cubes and stars at higher surfactant concentrations (Figure 5.5c).

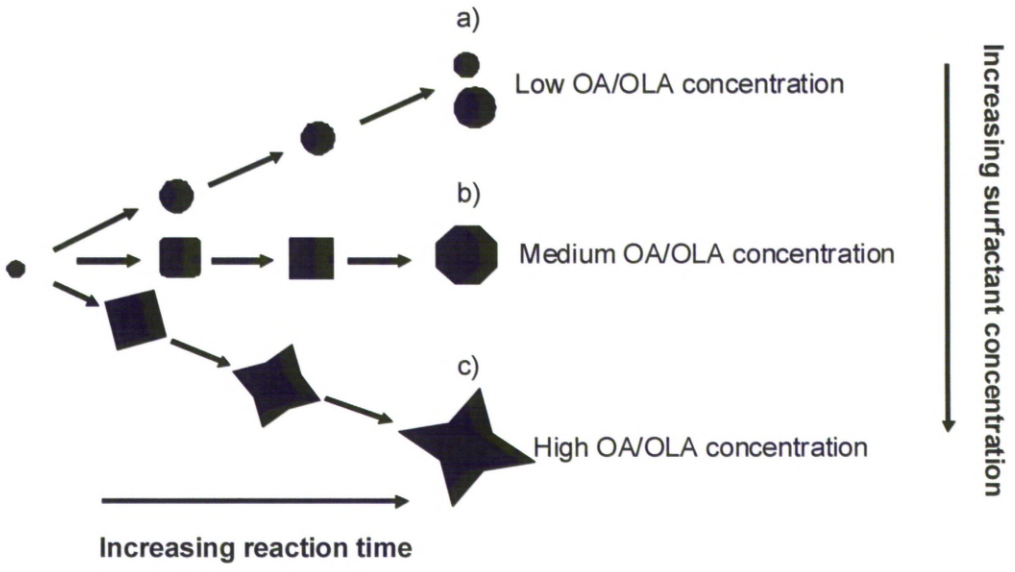

Figure 5.5: Schematic diagram of size and shape evolution of nanoparticles with surfactant OA/OLA concentration and reaction time.

To study the nanoparticles in more detail, HRTEM was performed on some selected samples, including rounded cubes (Figure 5.6a), cubes (Figure 5.6b) and stars (Figure 5.6c, d). It can be seen that the shape of the nanoparticles is clearly defined and the images showed the high degree of crystallinity in the samples. All samples showed clear lattice fringes corresponding to group of atomic planes. The HRTEM images also indicated that the growth of the nanoparticles was terminated at {100} planes which agreed with the above assumption of the formation of the cubes and stars that OA molecules attached to the lowest energy {100} faces and inhibited the growth of nanoparticles in [100] direction by forming a dense surfactant layer, resulting in the formation of cubic shape nanoparticles. The star-shape was created by the continuing development of higher energy planes of {110}. FFT analyses (insets) reveal that these particles are single crystals with lattices parameters corresponding to those of the bulk $CoFe_2O_4$ material.

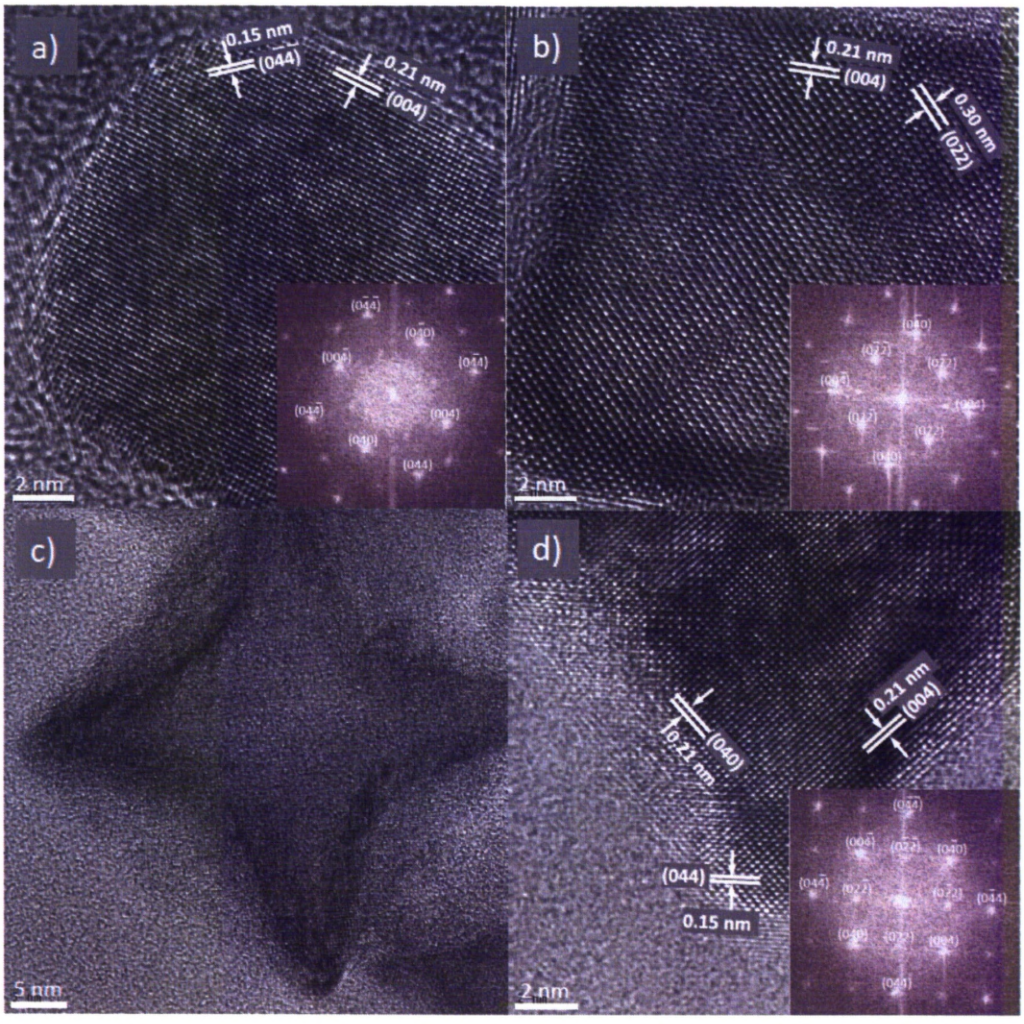

Figure 5.6: HRTEM and the corresponding fast fourier transform (FFT) images of nanoparticles synthesised in the presence of different OA/OLA concentration and at different reaction times: a) 372 mM at 30 min; b) 620 mM at 30 min and c, d) 620 mM at 120 min (different magnifications). The precursor ratio Co^{2+} : Fe^{3+} = 1 : 1.5. Zone axis of all images is [100].

Self-assembly of the nanoparticles

Nanoparticles have been used as building blocks to produce multifunctional nanocomposites.[77,78] In the current study, under certain synthesis conditions the cobalt ferrite nanoparticles were observed to self-assemble into micrometer scale two dimension

superlattices on the TEM grid (see Figure 5.7a for spherical nanoparticles and Figure 5.7b the nanocubes).

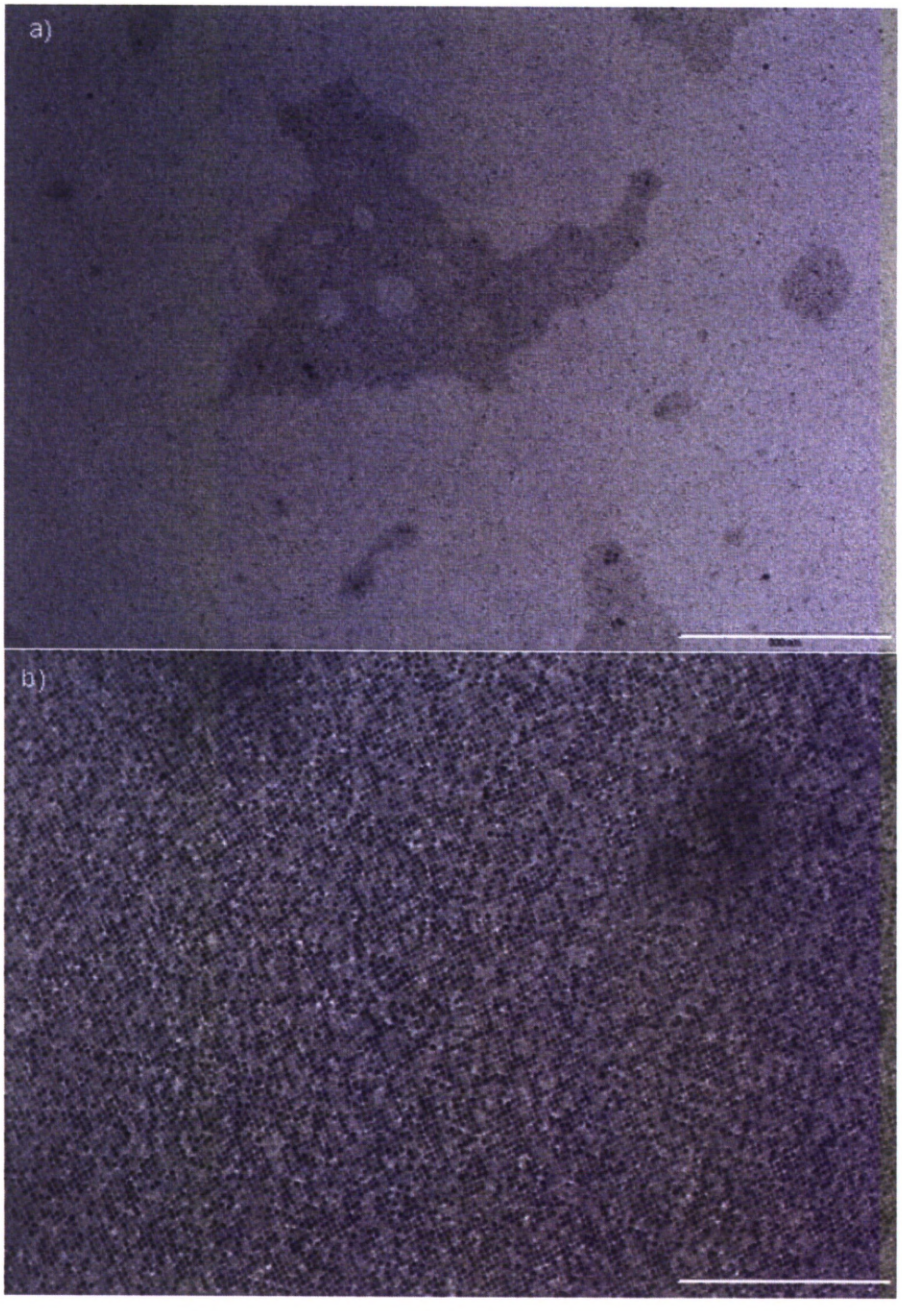

Figure 5.7: Self-assembly of cobalt ferrite nanoparticles: a) 6.4 nm spheres synthesised at 295 °C after 1 min reaction in the presence of 620 mM OA/OLA and b) 13.7 nm nanocubes synthesised at 295 °C after 30 min reaction in the presence of 496 mM OA/OLA. Scale bar: 500 nm.

Phase identification and degree of crystallinity of the nanoparticles were investigated and the typical XRD patterns of some samples are shown in Figure 5.8. At a precursor ratio of Co^{2+} : Fe^{3+} = 1 : 2 the nanoparticles had a single phase and the XRD pattern can be indexed with the spinel cobalt ferrite $CoFe_2O_4$ (Figure 5.8a). At precursor ratios of Co^{2+} : Fe^{3+} = 1 : 1 or 1.5 : 1, the sample is consisted of multiple phases of $CoFe_2O_4$ and CoO (Figure 5.8b, c). The mean size of nanoparticles was calculated from the broadening of X-ray peaks using Scherrer formula:[79]

$$d = \frac{K\lambda}{B\cos\theta}$$

where d is particle size, λ is the wavelength of X-ray radiation, K is a constant in range of 0.89 to 1.39 depending on the geometry of the crystallites (particle shape). Generally, K value of 0.94 for cubic crystallites or 1.33 for spherical shape was used for the calculation.[79] In the current study, the K value of 0.94 and the wavelength λ of 0.154 nm (Cu K_α radiation) were used in the calculation of the crystallite size. With the samples prepared at the ratios of Co^{2+}/Fe^{3+} = 1/2 and 1/1 (Figure 5.8a,b), the crystallite sizes estimated from the broadening of peak 311 were 28.5 nm and 19.2 nm, which are in good agreement with the particle sizes of 29.7 ± 2.7 nm and 19.9 ± 2.1 nm, respectively, determined by TEM. In the case of the sample prepared at the ratio of Co^{2+}/Fe^{3+} = 1.5/1, the crystallite size evaluated by XRD was 15.2 nm (Figure 5.8c) and was smaller than the particle size determined by TEM (18.4 ± 2.5 nm). The decrease in the particle size calculated by XRD compared with those determined by TEM was possible due to the presence of significant amount of CoO phase in the sample.

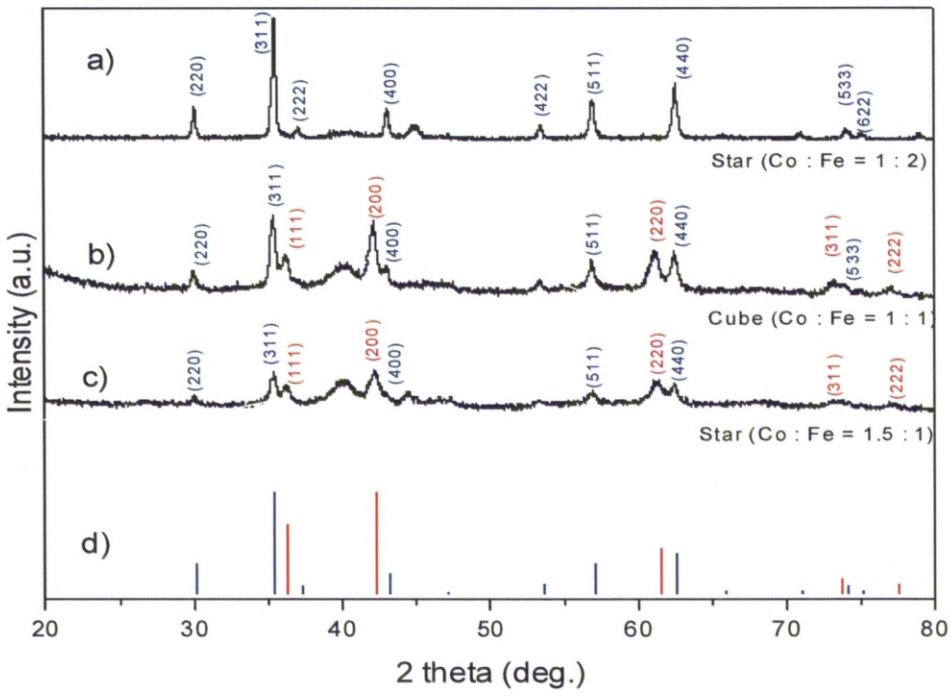

Figure 5.8: XRD patterns of cobalt ferrite nanoparticles with different shapes synthesised at different precursor ratio of Co^{2+} : Fe^{3+} at a) 1:2; b) 1: 1 and c) 1.5 : 1; The reference XRD patterns of $CoFe_2O_4$ (blue) and CoO (red) are shown in (d).

The elemental analysis results performed on some samples indicated that the compositions of Co and Fe in the nanoparticles matched well with ratio of starting $Co(acac)_2$: $Fe(acac)_3$ used in the synthesis (Table 5.2).

Table 5.2: The dependence of composition of cobalt ferrite nanoparticles on the ratio of precursors

Sample	Starting Co : Fe ratio	Surfactant concentration (mM)		Reaction time	Composition of synthesis nanoparticles	Morphology
		OA	OLA	(min)	(Co : Fe)	
1	1 : 2	124	124	5	32.8 : 67.2	sphere
2	1 : 2	310	310	60	33.1 : 66.9	star
3	1 : 1.5	248	248	30	39.5 : 60.5	cube
4	1 : 1.5		620	120	39.1 : 60.9	rounded cube
5	1 : 1	248	248	30	50.4 : 49.6	cube
6	1.5 : 1	186	186	60	58.7 : 41.3	cube

5.3.2 Magnetic properties of cobalt ferrite nanoparticles

The magnetic properties of the cobalt ferrite nanoparticles were determined by measurements of the zero-field-cooled (ZFC) and the field-cooled (FC) magnetisation and the results obtained for some samples are presented in Figure 5.9. For different samples, it was observed the peak in the ZFC curve which is associated with the transition of the nanoparticles from the superparamagnetic to ferromagnetic blocked states with decreasing temperature.

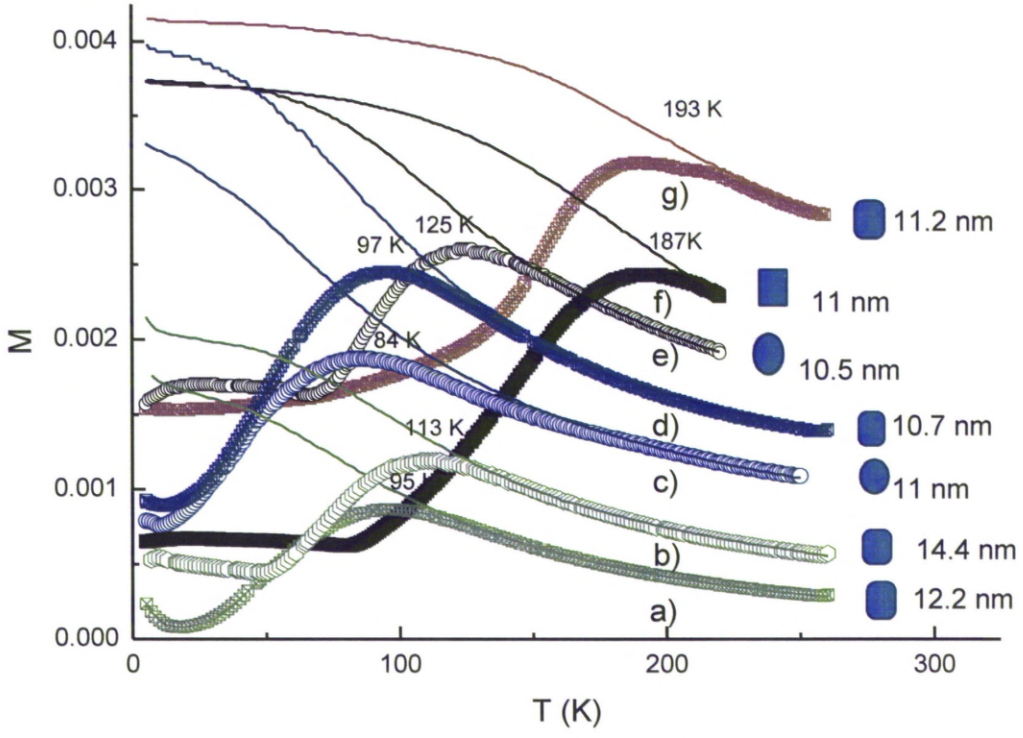

Figure 5.9: The zero-field-cooled (ZFC), field-cooled (FC) magnetisation of cobalt ferrite nanoparticles with different morphologies and prepared at different precursor ratios: a,b) OA/OLA coated 12.2 nm and 14.4 nm rounded cubes (Co^{2+} : Fe^{3+} = 1 : 1); c) OA/OLA coated 11 nm spheres (Co^{2+} : Fe^{3+} = 1 : 1.5, d) OA/OLA coated 10.7 nm rounded cubes (Co^{2+} : Fe^{3+} = 1 : 1.5); e) OA/OLA coated 10.5 nm spheres (Co^{2+} : Fe^{3+} = 1 : 2); f) OA/OLA coated 11 nm cubes (Co^{2+} : Fe^{3+} = 1 : 2) and g) OLA coated 11.2 nm rounded cubes (Co^{2+} : Fe^{3+} = 1 : 1.5).

For the nanoparticles synthesised with the same starting precursor ratio, we observed that the values of the blocking temperature T_b obtained at the peak of the ZFC curves of the nanoparticles increased with increasing particle volume regardless of the shape of the nanoparticles. For the rounded cubes, the 12.2 nm and 14.4 nm nanoparticles synthesized at a ratio of Co : Fe = 1 : 1 have T_b values of 95 K and 113 K, respectively (Figure 5.9a, b). When nanoparticles were synthesised at a ratio of Co : Fe = 1 : 2, the blocking temperature became 125 K for 10.5 nm spheres and then increased to 187 K for 11 nm nanocubes (Figure 5.9e, f).

Surfactants were also found to have significant effect on the blocking temperature T_b. For example, 11.2 nm rounded nanocubes coated with solely OLA had T_b value of 193 K (Figure 5.9g). However, 10.7 nm rounded nanocubes coated with mixture of OA/OLA showed a significant lower T_b value of 97 K (Figure 5.9d). These nanoparticles are similar in shape and size and synthesised at the same ratio of Co : Fe = 1 : 1.5. Therefore the large difference in their T_b temperatures is possible allocated to the difference of surfactants used in the synthesis.

5.3.3 Transferring nanoparticles into water

Hydrophobic cobalt ferrite nanoparticles can also be transferred into water by replacing OA/OLA molecules on the particle surface with hydrophilic polymer. In this study, PMAA-DDT polymer is chosen as it has been demonstrated being a suitable stabilising ligand for cobalt (Chapter 2) and iron oxide nanoparticles.[80] Phase transfer was conducted by sonicating the mixture of 1 mL chloroform suspension of the purified nanoparticles (3.5 mg) and 45 mg PMAA-DDT (3420 g mol^{-1}) polymer dissolved in 1 mL ethanol (Section 5.2.3). Figure 5.10 shows TEM images of the nanoparticles prepared from toluene suspension before ligand exchange and those from an aqueous suspension after ligand

exchange. There is no obvious agglomeration and no significant morphological differences are apparent between the samples.

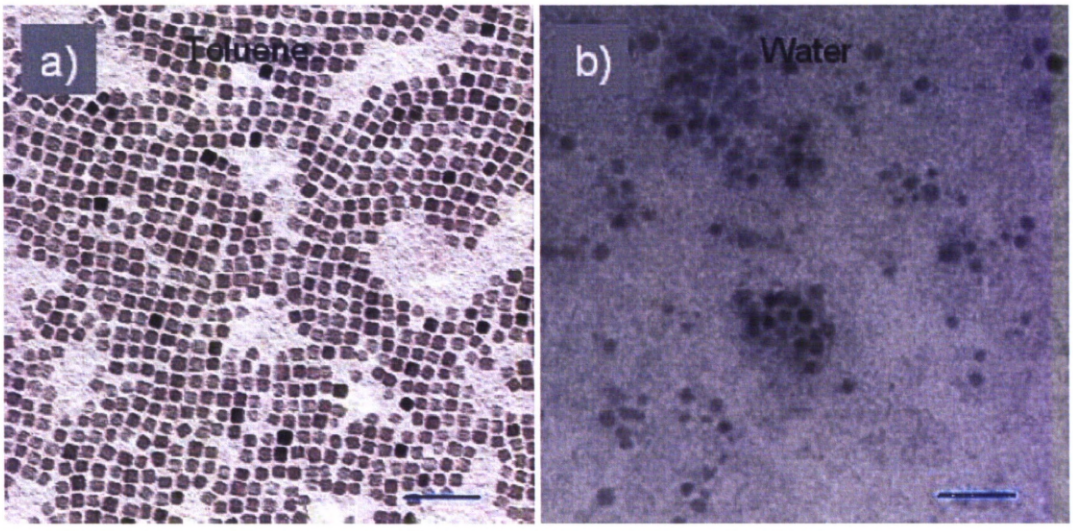

Figure 5.10: TEM image of $CoFe_2O_4$ nanocubes prepared in the presence of 372 mM OA/OLA (OA : OLA = 1 : 1) at reaction time of 30 min a) before and b) after ligand exchange with PMAA-DDT polymer. Scale bar: 50 nm.

Visual examination of the aqueous solution of PMAA polymer coated cobalt ferrite nanoparticles indicates that the nanoparticles are well dispersed and fairly stable for few weeks in solution in the absence of external magnetic field (Figure 5.11a). However, they can be easily collected with a magnetic bar (Figure 5.11b).

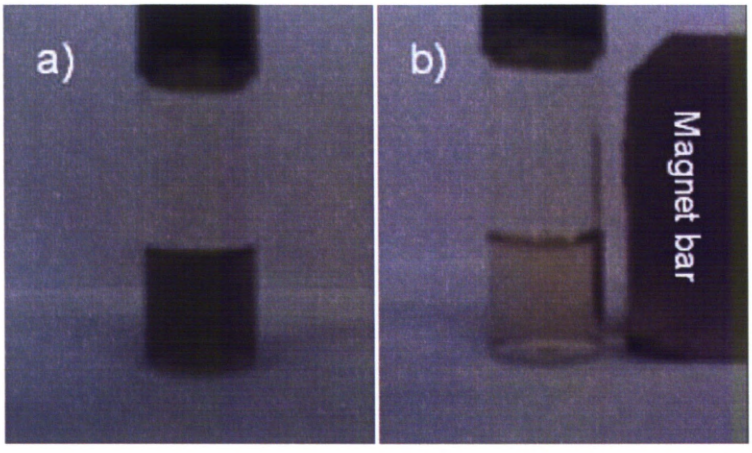

Figure 5.11: Photographs of cobalt ferrite nanocubes dispersed in water: a) without and b) with a magnetic bar, respectively.

5.3.4 Other characterisation

As discussed above, the reaction time and concentration of OA/OLA surfactants are the important parameters in the control of the size, shape and monodispersity of nanoparticles. It was also observed that particle size is dramatically increased with the increase of OA/OLA concentration. This is in contrast with previously reported works, where the size of nanoparticles usually decreased with the increase of surfactant concentration.[73,74] In the present case, OA was assumed to react with cobalt and iron acetylacetonates resulting in more stable metal oleate complexes during the heating process, and as mentioned before, the more metal oleate complexes (higher OA concentration) are available, the larger nanoparticles are obtained. Previously, the *in-situ* formation of iron oleate complex when heated a mixture of OA and iron pentacarbonyl was observed by Hyeon and coworkers.[81] In that work, UV-vis absorption spectrum of metal complex obtained by mixing OA with $Fe(CO)_5$ at 100 °C showed a single intense peak at 330 nm, and FTIR spectrum of the complex exhibited no C=O stretching peak of free OA, suggested the formation of Fe oleate complex.[81] Here, if metal oleate complexes are actually formed during the heating process, the decomposition temperature of the oleate complexes would be increased significantly in comparison with those of the metal acetylacetonates, and the presence of the metal oleates could be feasibly identified by thermal analytic techniques such as DSC or TGA.[18,82] Additionally, other spectral methods, e.g. FTIR or mass spectroscopy, should be utilised for the identification of the oleate complexes.[18,82,83]

Using thermal analyses (DTA and TGA), Rautiainen *et al.* indicated that the temperature of decomposition of cobalt and iron acetylacetonates is in the range of 190-250 °C.[84] At the temperature of 225 °C, a strong endothermic peak in DTA curve corresponding to a major weight loss of 40 % sample mass in TGA was observed.

Bao *et al.* have combined thermal analysis (TGA) and magnetic measurements to quantitatively investigate the process of the thermal decomposition of mixed-metal

($Co^{+2}Fe^{3+}$)-oleate complex.[16,18] The authors were observed an insignificant weight loss, less than 10 % sample mass, at the temperature up to 300 °C in the TGA curve. A small magnetic moment was measured for the corresponding sample. With increasing the temperature to the range of 300-350 °C, a massive weight loss of about 60 % sample mass in the TGA curve and a large magnetic moment were recorded, which suggested the formation of nanoparticles due to the decomposition of the oleate complex at the high temperature.

In the current work, thermal analyses are necessary to be made on the pure metal acetylacetonates and the pre-mixed mixture of these acetylacetonate compounds and OA. It is expected that a significant increase in the decomposition temperature of the later due to the formation of metal oleate complexes would be observed. Here, the formation of metal oleate complexes is also possibly characterised by other analytical techniques such as FTIR or mass spectroscopy. As discussed in previous chapter, free carboxylate group of OA exhibited a strong peak of C=O stretching at around 1710 cm^{-1}. If metal oleates are formed, the sample (after washing free excess OA) usually showed two peaks at 1519 and 1450 cm^{-1} due to the interaction of the carboxylate group with the metal ions[83] (a bidentate coordination is expected as its low energy and high group symmetry[18]). Other strong peaks characteristic of the oleyl group in OA at 2850-3000 cm^{-1} region should be observed. Additionally, the formation of cobalt and iron oleate complexes could be evidenced by utilising mass spectroscopy.

5.4 Conclusion

In summary, monodisperse cobalt ferrite nanoparticles of diverse size, shape and composition have been successfully prepared in organic medium using one pot synthesis. The observations show that synthesis conditions such as surfactant concentration and reaction time play critical roles in controlling the size, shape and monodispersity of the

nanoparticles. Although the role of individual surfactants in the synthesis is still need to be clarified, the results suggest that OA and OLA surfactants have more complicated roles than that of simply imparting colloidal stability to the nanoparticles. It was believed that OA interacts with cobalt and iron acetylacetonate precursors to yield stable metal oleate complexes during the heating. Therefore, more characterisation techniques, such as TGA, DSC, FTIR or mass spectroscopy should be used to identify the formation of metal oleates as well as to investigate the decomposition of acetylacetonate and oleate complexes. The data of composition analysis and XRD indicate that composition and phase structure of the nanoparticles can be tuned by varying ratio of starting precursors. Results obtained from SQUID show that T_b temperature of the nanoparticles depends strongly on composition, volume and stabilising ligand of the nanoparticles.

Ligand exchange to transfer hydrophobic nanoparticles into water using PMAA-DDT polymer demonstrates to work well on nanocubes. There was no significant aggregation observed on TEM image. The nanoparticles were well disperse and fairly stable in water.

Reference

1. Wang, S. B.; Min, Y. L.; Yu, S. H. *J. Phys. Chem. C* **2007,** 111, (9), 3551-3554.
2. Liu, X. H.; Qiu, G. Z.; Li, X. G. *Nanotech.* **2005,** 16, (12), 3035-3040.
3. Xiong, Y.; Ye, J.; Gu, X. Y.; Chen, Q. W. *J. Phys. Chem. C* **2007,** 111, (19), 6998-7003.
4. Chen, Y. X.; Chen, S. P.; Zhou, Z. Y.; Tian, N.; Jiang, Y. X.; Sun, S. G.; Ding, Y.; Wang, Z. L. *JACS* **2009,** 131, (31), 10860-10861.
5. Duxin, N.; Brun, N.; Colliex, C.; Pileni, M. P. *Langmuir* **1998,** 14, (8), 1984-1989.
6. Kovalenko, M. V.; Bodnarchuk, M. I.; Lechner, R. T.; Hesser, G.; Schaffler, F.; Heiss, W. *JACS* **2007,** 129, (20), 6352-6352.
7. Yang, H. T.; Ogawa, T.; Hasegawa, D.; Takahashi, M. *J. Appl. Phys.* **2008,** 103, (7), D526.1-3.
8. Kim, D.; Lee, N.; Park, M.; Kim, B. H.; An, K.; Hyeon, T. *JACS* **2009,** 131, (2), 454-455.
9. Song, Q.; Ding, Y.; Wang, Z. L.; Zhang, Z. J. *J. Phys Chem. B* **2006,** 110, (50), 25547-25550.
10. Ahniyaz, A.; Sakamoto, Y.; Bergstrom, L. *PNAS* **2007,** 104, (45), 17570-17574.
11. Salazar-Alvarez, G.; Qin, J.; Sepelak, V.; Bergmann, I.; Vasilakaki, M.; Trohidou, K. N.; Ardisson, J. D.; Macedo, W. A. A.; Mikhaylova, M.; Muhammed, M.; Baro, M. D.; Nogues, J. *JACS* **2008,** 130, (40), 13234-13239.
12. Redl, F. X.; Black, C. T.; Papaefthymiou, G. C.; Sandstrom, R. L.; Yin, M.; Zeng, H.; Murray, C. B.; O'Brien, S. P. *JACS* **2004,** 126, (44), 14583-14599.
13. An, K.; Kwon, S. G.; Park, M.; Bin Na, H.; Baik, S. I.; Yu, J. H.; Kim, D.; Son, J. S.; Kim, Y. W.; Song, I. C.; Moon, W. K.; Park, H. M.; Hyeon, T. *Nano Lett.* **2008,** 8, (12), 4252-4258.
14. Zeng, H.; Rice, P. M.; Wang, S. X.; Sun, S. H. *JACS* **2004,** 126, (37), 11458-11459.
15. Song, Q.; Ding, Y.; Wang, Z. L.; Zhang, Z. J. *Chem. Mater.* **2007,** 19, (19), 4633-4638.
16. Bao, N. Z.; Shen, L. M.; Wang, Y. H.; Padhan, P.; Gupta, A. *JACS* **2007,** 129, (41), 12374-12375.
17. Song, O.; Zhang, Z. J. *JACS* **2004,** 126, (19), 6164-6168.
18. Bao, N. Z.; Shen, L. M.; An, W.; Padhan, P.; Turner, C. H.; Gupta, A. *Chem. Mater.* **2009,** 21, (14), 3458-3468.

19. Bao, N. Z.; Shen, L. M.; Padhan, P.; Gupta, A. *Appl. Phys. Lett.* **2008,** 92, (17), 173101.1-3.
20. Zhang, J.; Fang, J. Y. *JACS* **2009,** 131, (51), 18543-18547.
21. Poudyal, N.; Chaubey, G. S.; Nandwana, V.; Rong, C. B.; Yano, K.; Liu, J. P. *Nanotech.* **2008,** 19, (35), 355601.
22. Chou, S. W.; Zhu, C. L.; Neeleshwar, S.; Chen, C. L.; Chen, Y. Y.; Chen, C. C. *Chem. Mater.* **2009,** 21, (20), 4955-4961.
23. Chen, M.; Kim, J.; Liu, J. P.; Fan, H. Y.; Sun, S. H. *JACS* **2006,** 128, (22), 7132-7133.
24. Ung, D.; Tung, L. D.; Caruntu, G.; Delaportas, D.; Alexandrou, I.; Prior, I. A.; Thanh, N. T. K. *Cryst. Eng. Commun.* **2009,** 11, (7), 1309-1316.
25. Graf, C. P.; Birringer, R.; Michels, A. *Phys. Rev. B* **2006,** 73, (21), 212401.
26. Scariot, M.; Silva, D. O.; Scholten, J. D.; Machado, G.; Teixeira, S. R.; Novak, M. A.; Ebeling, G.; Dupont, J. *Angew. Chemie-Inter. Ed.* **2008,** 47, (47), 9075-9078.
27. Lacroix, L. M.; Lachaize, S.; Falqui, A.; Respaud, M.; Chaudret, B. *JACS* **2009,** 131, (2), 549-557.
28. Jana, N. R.; Chen, Y. F.; Peng, X. G. *Chem. Mater.* **2004,** 16, (20), 3931-3935.
29. Valenzuela, R., *Magnetic Ceramics*. Cambrid. Uni. Press,: Cambrid., 1994; p 312.
30. Weller, D.; Moser, A.; Folks, L.; Best, M. E.; Lee, W.; Toney, M. F.; Schwickert, M.; Thiele, J. U.; Doerner, M. F. *IEEE Trans. Mag.* **2000,** 36, (1), 10-15.
31. Weller, D.; Moser, A. *IEEE Trans. Mag.* **1999,** 35, (6), 4423-4439.
32. Pillai, V.; Shah, D. O. *J. Mag. Mag. Mater.* **1996,** 163, (1-2), 243-248.
33. Ayyappan, S.; Philip, J.; Raj, B. *Mater. Chem. & Phys.* **2009,** 115, (2-3), 712-717.
34. Olsson, R. T.; Salazar-Alvarez, G.; Hedenqvist, M. S.; Gedde, U. W.; Lindberg, F.; Savage, S. J. *Chem. Mater.* **2005,** 17, (20), 5109-5118.
35. Kim, Y. I.; Kim, D.; Lee, C. S. *Phys. B-Condens. Matter* **2003,** 337, (1-4), 42-51.
36. Gu, Z. J.; Xiang, X.; Fan, G. L.; Li, F. *J. Phys. Chem. C* **2008,** 112, (47), 18459-18466.
37. Limaye, M. V.; Singh, S. B.; Date, S. K.; Kothari, D.; Reddy, V. R.; Gupta, A.; Sathe, V.; Choudhary, R. J.; Kulkarni, S. K. *J. Phys. Chem. B* **2009,** 113, (27), 9070-9076.
38. Ayyappan, S.; Mahadevan, S.; Chandramohan, P.; Srinivasan, M. P.; Philip, J.; Raj, B. *J. Phys. Chem. C* **2010,** 114, (14), 6334-6341.
39. Zhao, S. Y.; Qiao, R.; Zhang, X. L.; Kang, Y. S. *J. Phys. Chem. C* **2007,** 111, (22), 7875-7878.

40. Zhang, X. J.; Jiang, W.; Song, D.; Sun, H. J.; Sun, Z. D.; Li, F. S. *J. Alloys & Compounds* **2009,** 475, (1-2), L34-L37.
41. Culita, D. C.; Patron, L.; Teodorescu, V. S.; Balint, L. *J. Alloys & Compounds* **2007,** 432, (1-2), 211-216.
42. Maaz, K.; Mumtaz, A.; Hasanain, S. K.; Ceylan, A. *J. Mag. & Mag. Mater.* **2007,** 308, (2), 289-295.
43. Chen, Y.; Ruan, M.; Jiang, Y. F.; Cheng, S. G.; Li, W. *J. Alloys & Compounds* **2010,** 493, (1-2), L36-L38.
44. Yanez-Vilar, S.; Sanchez-Andujar, M.; Gomez-Aguirre, C.; Mira, J.; Senaris-Rodriguez, M. A.; Castro-Garcia, S. *J. Solid State Chem.* **2009,** 182, (10), 2685-2690.
45. Liu, Q.; Sun, J. H.; Long, H. R.; Sun, X. Q.; Zhong, X. J.; Xu, Z. *Mater. Chem. & Phys.* **2008,** 108, (2-3), 269-273.
46. Thimmaiah, S.; Rajamathi, M.; Singh, N.; Bera, P.; Meldrum, F.; Chandrasekhar, N.; Seshadri, R. *J. Mater. Chem.* **2001,** 11, (12), 3215-3221.
47. Zhao, L. J.; Zhang, H. J.; Xing, Y.; Song, S. Y.; Yu, S. Y.; Shi, W. D.; Guo, X. M.; Yang, J. H.; Lei, Y. Q.; Cao, F. *J. Solid State Chem.* **2008,** 181, (2), 245-252.
48. Liu, X. M.; Fu, S. Y.; Zhu, L. P. *J. Solid State Chem.* **2007,** 180, (2), 461-466.
49. Wang, Z. L.; Liu, X. J.; Lv, M. F.; Chai, P.; Liu, Y.; Meng, J. *J. Phys. Chem. B* **2008,** 112, (36), 11292-11297.
50. Cannas, C.; Musinu, A.; Peddis, D.; Piccaluga, G. *Chem. Mater.* **2006,** 18, (16), 3835-3842.
51. Ji, G. B.; Tang, S. L.; Xu, B. L.; Gu, B. X.; Du, Y. W. *Chem. Phys. Lett.* **2003,** 379, (5-6), 484-489.
52. Lavela, P.; Tirado, J. L. *J. Power Sources* **2007,** 172, (1), 379-387.
53. Bao, N. Z.; Shen, L. M.; Wang, Y. H. A.; Ma, J. X.; Mazumdar, D.; Gupta, A. *JACS* **2009,** 131, (36), 12900-12901.
54. Wang, Z. L.; Liu, X. J.; Lv, M. F.; Chai, P.; Liu, Y.; Zhou, X. F.; Meng, J. *J. Phys. Chem. C* **2008,** 112, (39), 15171-15175.
55. Cannas, C.; Ardu, A.; Musinu, A.; Peddis, D.; Piccaluga, G. *Chem. Mater.* **2008,** 20, (20), 6364-6371.
56. Rondinone, A. J.; Samia, A. C. S.; Zhang, Z. J. *J. Phys. Chem. B* **1999,** 103, (33), 6876-6880.
57. Chiu, W. S.; Radiman, S.; Abd-Shukor, R.; Abdullah, M. H.; Khiew, P. S. *J. Alloys & Compounds* **2008,** 459, (1-2), 291-297.

58. Liu, C.; Zou, B. S.; Rondinone, A. J.; Zhang, J. *JACS* **2000,** 122, (26), 6263-6267.
59. Zhang, Z. T.; Rondinone, A. J.; Ma, J. X.; Shen, J.; Dai, S. *Adv. Mater.* **2005,** 17, (11), 1415-1419.
60. Sun, S. H.; Zeng, H.; Robinson, D. B.; Raoux, S.; Rice, P. M.; Wang, S. X.; Li, G. X. *JACS* **2004,** 126, (1), 273-279.
61. Hyeon, T.; Chung, Y.; Park, J.; Lee, S. S.; Kim, Y. W.; Park, B. H. *J. Phys. Chem. B* **2002,** 106, (27), 6831-6833.
62. Cannas, C.; Musinu, A.; Ardu, A.; Orru, F.; Peddis, D.; Casu, M.; Sanna, R.; Angius, F.; Diaz, G.; Piccaluga, G. *Chem. Mater.* **2010,** 22, (11), 3353-3361.
63. Vestal, C. R.; Song, Q.; Zhang, Z. J. *J. Phys. Chem. B* **2004,** 108, (47), 18222-18227.
64. Arelaro, A. D.; Lima, E.; Rossi, L. M.; Kiyohara, P. K.; Rechenberg, H. R. *J. Mag. Mag. Mater.* **2008,** 320, (14), E335-E338.
65. Kim, D. H.; Nikles, D. E.; Johnson, D. T.; Brazel, C. S. *J. Mag. Mag. Mater.* **2008,** 320, (19), 2390-2396.
66. Crouse, C. A.; Barron, A. R. *J. Mater. Chem.* **2008,** 18, (35), 4146-4153.
67. Hussain, I.; Graham, S.; Wang, Z. X.; Tan, B.; Sherrington, D. C.; Rannard, S. P.; Cooper, A. I.; Brust, M. *JACS* **2005,** 127, (47), 16398-16399.
68. Wang, Z. X.; Tan, B. E.; Hussain, I.; Schaeffer, N.; Wyatt, M. F.; Brust, M.; Cooper, A. I. *Langmuir* **2007,** 23, (2), 885-895.
69. Hoene, J. V.; Charles, R. G.; Hickam, W. M. *J. Phys. Chem.* **1958,** 62, 1098-1101.
70. Charles, R. G.; Pawlikowski, M. A. *J. Phys. Chem.* **1958,** 62, (4), 440-444.
71. Yin, Y.; Alivisatos, A. P. *Nature* **2005,** 437, (7059), 664-670.
72. Davies, M. J.; Parker, S. C.; Watson, G. W. *J. Mater. Chem.* **1994,** 4, (6), 813-816.
73. Carenco, S.; Boissiere, C.; Nicole, L.; Sanchez, C.; Le Floch, P.; Mezailles, N. *Chem. Mater.* **2010,** 22, (4), 1340-1349.
74. Xu, Z. C.; Shen, C. M.; Hou, Y. L.; Gao, H. J.; Sun, S. S. *Chem. Mater.* **2009,** 21, (9), 1778-1780.
75. Vonhoene, J.; Charles, R. G.; Hickam, W. M. *J. Phys. Chem.* **1958,** 62, (9), 1098-1101.
76. Shevchenko, E. V.; Talapin, D. V.; Schnablegger, H.; Kornowski, A.; Festin, O.; Svedlindh, P.; Haase, M.; Weller, H. *JACS* **2003,** 125, (30), 9090-9101.
77. Shevchenko, E. V.; Talapin, D. V.; Kotov, N. A.; O'Brien, S.; Murray, C. B. *Nature* **2006,** 439, (7072), 55-59.

78. Shevchenko, E. V.; Talapin, D. V.; Murray, C. B.; O'Brien, S. *JACS* **2006,** 128, (11), 3620-3637.
79. Borchert, H.; Shevehenko, E. V.; Robert, A.; Mekis, I.; Kornowski, A.; Grubel, G.; Weller, H. *Langmuir* **2005,** 21, (5), 1931-1936.
80. Li, Z.; Tan, B.; Allix, M.; Cooper, A. I.; Rosseinsky, M. J. *Small* **2008,** 4, (2), 231-239.
81. Hyeon, T.; Lee, S. S.; Park, J.; Chung, Y.; Bin Na, H. *JACS* **2001,** 123, (51), 12798-12801.
82. Lee, Y. J.; Jun, K. W.; Park, J. Y.; Potdar, H. S.; Chikate, R. C. *J. Indust. & Eng. Chem.* **2008,** 14, 38-44.
83. Bronstein, L. M.; Huang, X. L.; Retrum, J.; Schmucker, A.; Pink, M.; Stein, B. D.; Dragnea, B. *Chem. Mater.* **2007,** 19, (15), 3624-3632.
84. Rautiainen, A.; Lindblad, M.; Backman, L. B.; Puurunen, R. L. *Phys. Chem. Chem. Phys.* **2002,** 4, (11), 2466-2472.

Chapter 6
Conclusions and further work

This thesis presents a detailed investigation of synthesis methods for water-dispersible magnetic nanoparticles of Co, CoPt, CoFe, $CoFe_2O_4$ and CoFe@Pt. The syntheses were carried out either in water (for Co and CoPt) or in organic solvents (for CoFe, cobalt ferrite and CoFe@Pt core/shell nanoparticles). Direct synthesis in water had some clear advantages, which included environmental friendliness and simplicity. The use of hydrophilic peptide and polymer ligands enabled the synthesis of nanoparticles that were readily dispersible in water without any further surface modification. Furthermore, in case of CoPt nanoparticles, by combining peptides and polymers, as well as varying the ratio of these ligands, it should be possible to control the number of sites on the particle surface for subsequent conjugation of biomolecules. The synthesis in organic solvents, however, has its own advantages such as superior control over the size and shape of the nanoparticles.
The achievements of the work can be summarised as follows:

- Water-dispersible and colloidal stable Co nanoparticles were successfully prepared by a reduction method in the presence of PMAA-DDT polymer. The colloidal stability and size of Co nanoparticles were controlled by varying the molecular weight and the concentration of PMAA-DDT. It was observed that the stability of the nanoparticles increased with increasing polymer molecular weight, which is likely due to the increase of both steric and electric charge repulsions. In all likelihood a factor contributing to the stability of PMAA-DDT coated Co nanoparticles was the adsorption of hydrophobic DDT and its thiolether in the PMAA-DDT polymer to the surface of the nanoparticles. This would enhance the attachment of the polymer to the Co core. PMAA-DDT coated Co nanoparticles were found to be stable in

electrolyte solution up to 0.23 M NaCl, which is slightly higher than that attained *in vivo* (0.16 M NaCl). Co nanorods were produced at diluted PMAA-DDT concentration, which to the best of my knowledge is the first report of such structures.

- Water-dispersible CoPt nanoparticles were successfully synthesised using a simple one step method. The effect of structure, functional groups and the combination of stabilizing ligands on the morphology of the nanoparticles were investigated. It was found that multiple-thiol functional groups of the ligands played a critical role in the formation of hollow nanoparticles. The mechanism of formation of the hollow nanoparticles was also suggested. The CoPt hollow nanoparticles were found to be stable in a wide range of pH and in electrolyte solution up to 2 M NaCl. The experiment on tracking stem cells using the CoPt hollow nanoparticles indicated that MRI can effectively detect low numbers of labelled cells due to the enhanced contrast provided by the nanoparticles. CoPt hollow nanoparticles may, thus, have potential applications in MRI, targeted drug delivery and, because of the alloy, in catalysis. The solid and nanochain/wires may also be appropriate for exploring the potential of these materials in catalysis.
- CoFe and CoFe@Pt core/shell nanoparticles were synthesised in organic solvent. The results from HRTEM, STEM and SQUID indicated the existing of core/shell structures. Water-dispersible and fairly stable CoFe and CoFe@Pt core/shell nanoparticles were prepared by ligand exchange using hydrophilic silane and/or PEG polymer. The observations indicated that CoFe nanoparticles stabilised by mixture of silane-NH_2 and PEG-NH_2 were well dispersed in water and stable for up to one week. The CoFe@Pt core/shell nanoparticles coated by PEG (NH_2 or SH) exhibited a slight improved stability.

- The synthesis of cobalt ferrite nanoparticles by thermal decomposition in organic solvent showed that both the size and shape of the nanoparticles could be tuned by varying the concentration of surfactants and reaction time. The relationship between size, shape and monodispersity of the nanoparticles and reaction conditions was also proposed. HRTEM results showed that nanoparticles were of high crystallinity. XRD and composition analyses indicated that the phase structure and the composition of nanoparticles might be varied by changing the ratio of the precursors. These materials may possibly have potential applications in catalysis.

The development of successful methods to make the above nanoparticles, alongside an exploration of the parameters that can be varied to tune the shape and size of the product represents an important step in the field. In particular, these methods are reasonably scalable, which will allow others to test their potential in the proposed applications. However, there is scope for improvement in the syntheses and characterisation of the materials. Moreover, whilst considerable effort was expended on making the nanoparticles water-dispersible, it is likely that to be used in biomedical applications that the current generation of materials is not sufficiently performing.

Further work

- For PMAA-DDT coated Co nanoparticles and peptide/PEG coated CoPt nanoparticles, visual observation and SQUID data indicated that PMAA-DDT polymer could protect Co cores from aggregation and oxidation. However, in order to have better evidence on the oxidative stability of the nanoparticles as well as detailed information about the interaction between polymer ligand and Co nanoparticle surface, more characterisation such as XPS, FTIR or Raman should be made. With peptide/PEG coated CoPt nanoparticles, similar characterisation techniques need to be carried out to have deeper understanding about the interactions

between the functional groups (COOH, SH or NH_2) of the peptide and polymer molecules and surface of CoPt nanoparticles.

- In the case of CoFe and Pt coated CoFe nanoparticles, more characterisation techniques, such as EDS or EELS in combination with STEM analysis to confirm the CoFe@Pt core/shell structures. Additionally, the presence of hydrophilic ligands of silane and PEG on the particles after ligand exchange needs to be characterized by analytical techniques such as FTIR and NMR. Furthermore, to elucidate the existences of galvanic replacement/transmetalation reactions during the Pt coating or silanisation reaction in the ligand exchange processes, by-products of these processes should be characterised, for example by FTIR or UV-vis techniques. The CoFe coated by mixture of silane and PEG and CoFe@Pt core/shell nanoparticles would also benefit from more comprehensive SQUID measurements to evaluate the protecting effectiveness of Pt coating and ligand shells against oxidation. In addition, the galvanic replacement process of the magnetic core of the CoFe@Pt core/shell nanoparticles may result in an undesired decrease in size, which would in turn result in a decrease of blocking temperature and saturation magnetization. It would, therefore, be essential to perform the Pt coating using either a more stable platinum complex or a stronger reductant. Krishnan *et al.* pointed out that using $[(C_6H_5)_3P]AuCl$ complex for Au coating on Co nanoparticles could prevent the occurrence of the galvanic replacement process during synthesis.[1] In case of Pt coated CoFe nanoparticles such a $[(C_6H_5)_3P]PtCl$ precursor would need to be explored for Pt coating. Preliminary experiments suggest that the synthesis of CoFe@Pt core/shell or solid nanoparticles can be achieved using metal carbonyls, such as $Fe(CO)_5$ or $W(CO)_6$ as metal sources to reduce Pt^{2+} (not shown). Moreover, SQUID measurements on CoFe@Pt nanoparticles produced in this way suggest that

by using $Fe(CO)_5$ as an *in situ* metal source for reducing Pt results in a blocking temperature of the nanoparticles that is slightly increased after Pt coating.

- With cobalt ferrite nanoparticles, TGA, DSC, FTIR and mass spectroscopy analyses should be made to identify the formation of cobalt and iron oleates as well as to investigate the thermal decomposition process of the metal complexes.

A theme in this thesis is the use of magnetic nanoparticles in biology and medicine. A degree of stability in water was achieved for the materials synthesised. However, the stability achieved is at the very least, not demonstrated to be sufficient for biomedicine. This is a major problem in the nanoparticle field. Chemists have a far simpler view of nanoparticle stability than biologists. For example a demonstration of colloidal stability in water with electrolyte is sufficient to claim a degree of biological compatibility.[2] Indeed such materials were used by collaborators to demonstrate MRI contrast enhancement. However, recent papers from the gold nanoparticle field demonstrate that a far more sophisticated set of measurements are necessary to established biocompatibility.

In 2008 Duchesne *et al.*[3] demonstrated unequivocally that colloidal stability in solution of electrolytes failed to predict biological stability. Thus, very stable peptide-coated Au nanoparticles were shown to bind non-specifically to proteins and protein mimetic substances. Moreover, the authors demonstrated that such ''stable'' nanoparticles readily undergo ligand exchange. They go on to design a new ligand shell of thiolalkane ethylene glycol and penta peptidol which is truly stable. This work clearly shows that stability of magnetic nanoparticles needs to be tested to the same standard.

In 2009 See and co-workers[4] showed that the ''stable'' peptide capped Au nanoparticles demonstrated by Duchesne *et al.*[3] to be rather unstable were subject to enzymatic transformation in living cells. Thus See *et al.* demonstrated that cellular proteases would cleave the peptides of the ligand shell.

Taken together, these two papers show that chemists need to test their nanoparticles in new ways such tests could include:

- ligand exchange
- non-specific binding to bio-molecules
- chemical transformation of ligand shells by living systems.

Thus one very important future work is likely to be the design of new ligand shells for the nanomaterials synthesised by methods described in this thesis.

Reference

1. Bao, Y. P.; Calderon, H.; Krishnan, K. M. *J. Phys. Chem. C* **2007,** 111, (5), 1941-1944.
2. Lu, L. T.; ung, L. D.; Long, J.; Fernig, D. G.; Thanh, N. T. K. *J. Mater. Chem.* **2009,** 19, 6023-6028.
3. Duchesne, L.; Gentili, D.; Comes-Franchini, M.; Fernig, D. G. *Langmuir* **2008,** 24, (23), 13572-13580.
4. See, V.; Free, P.; Cesbron, Y.; Nativo, P.; Shaheen, U.; Rigden, D. J.; Spiller, D. G.; Fernig, D. G.; White, M. R. H.; Prior, I. A.; Brust, M.; Lounis, B.; Levy, R. *ACS Nano* **2009,** 3, (9), 2461-2468.

H_2PtCl_6. Here, morphology (size and shape) of CoPt nanoparticles were controlled by varying the structure and functional groups of the stabilising ligands as well as the combination of stabilising ligands (Table 3.2).

Table 3.2: The effect of stabilising ligands and functional groups on the morphology of CoPt nanoparticles.

Ligand(s)	Concentration (mM)	Perimeter size (nm)	Morphplogy
PMAA-PMTP	0.24	9.5 ± 1.5	Hollow
PMAA-DDT	0.24	3.1 ± 0.6	Solid
PEG-SH	0.24 → 0.36	assembly of 3 nm	Chains→solid
PEG-COOH	0.24	3.5 ± 0.5	Solid
CCALNN	0.24-0.48	-	Aggregates
CALNN	0.24-0.60	-	Aggregates
NNLACC	0.24-0.48	-	Aggregates
CCVVVT	0.46-0.6	-	Aggregates
TLVVN	0.36	-	Aggregates
PEG-SH + CCALNN	0.36	9.8 ± 1.3	Hollow
PEG-SH + CCVVVT	0.36	10-20	Hollow
PEG-SH + NNLACC	0.36	9.1	Hollow
PEG-SH + CALNN	0.36	~ 4	Solid
PEG-SH + TLVVN	0.36	~ 3 x 70	Wires
PMAA-PMTP + PEG-SH	0.36	12.5 ± 2.5	Hollow
PMAA-PMTP + PEG-NH_2	0.36	11.5 ± 2.3	Hollow
PMAA-DDT + CCALNN	0.36	12.9 ±1.7	Hollow
PMAA-DDT + PEG-SH	0.36	3.3	Solid
PEG-NH_2+TLVVN	0.36	~ 5 x 70	Wires
PMAA-DDT + CALNN	0.36	~ 3	Solid